CALEDONIAN STRUCTURE, METAMORPHISM, GEOCHRONOLOGY, AND TECTONICS OF THE SITAS-SINGIS AREA, SWEDEN

VOL. 1

by

Peter Gerhard Tilke

B.S., University of California, Los Angeles
(1982)

SUBMITTED TO THE DEPARTMENT OF
EARTH, ATMOSPHERIC, AND PLANETARY SCIENCES
IN PARTIAL FULFILLMENT OF
THE REQUIREMENTS FOR THE
DEGREE OF

DOCTOR OF PHILOSOPHY

at the

MASSACHUSETTS INSTITUTE OF TECHNOLOGY
September 1986

Signature of Author _____
Department of Earth, Atmospheric, and Planetary Sciences
July 14, 1986

Certified by _____
B.C. Burchfiel
Thesis Supervisor

Accepted by _____
Chairman, Departmental Graduate Committee

CALEDONIAN STRUCTURE, METAMORPHISM, GEOCHRONOLOGY, AND TECTONICS OF THE SITAS-SINGIS AREA, SWEDEN

by

PETER GERHARD TILKE

Submitted to the Department of Earth, Atmospheric, and Planetary Sciences on July 14, 1986 in partial fulfillment of the requirements for the Degree of Doctor of Philosophy

ABSTRACT

Rocks of the Sitas-Singis area of north Sweden form the southeastern margin of the Rombak-Sjangeli Window. The three principal lithotectonic elements of the northern Scandinavian Caledonides are exposed in this area: 1) gabbroic, amphibolitic, and sedimentary rocks of the Proterozoic basement with its autochthonous Vendian to Middle Cambrian sedimentary cover sequence correlative with units exposed in the Baltic Shield foreland to the east; 2) the allochthonous upper nappe complex consisting of a heterogeneous assemblage of gneiss, amphibolite, schist and psammite; 3) a complex shear zone ranging from 50 to 500 m in thickness consisting of highly strained basement rocks separates the basement from the overlying upper nappe complex. The upper nappe complex was derived from west of the present day Norwegian west coast during the Late Silurian to Early Devonian underthrusting of the Baltic Shield associated with final closure of the Iapetus Ocean.

Deformation and metamorphism in the area is subdivided into eight temporally distinct events: D1 to D8. D1 is the Late Cambrian or Early Ordovician deformation and asssociated high-grade metamorphism of some elements within the upper nappe complex. Phase relations within a meta-gabbro lens indicate peak metamorphic conditions during this event approached 750^{o}C, 1500 MPa. D2 led to the Late Ordovician to Early Silurian deformation and associated metamorphism of the remaining elements in the upper nappe complex. Metamorphic conditions during this event ranged from middle greenschist to upper amphibolite. D3 is the Silurian greenschist to lower amphibolite facies imbrication of all the elements in the upper nappe complex. Relations within shear zone rocks to the west of the study area indicate initial obduction of the upper nappe complex onto the Baltic Shield also occurred during this event. D4 through D6 are related to the Late Silurian to Early Devonian S60E directed emplacement of the amalgamated upper nappe complex onto the Baltic Shield and associated deformation of basement rocks in the Sitas-Singis area. D7 resulted in an Early to Middle(?) Devonian post-thrusting event that warped and backfolded the entire sequence along N-S trending axes. D8 is the Late Devonian to Early Carboniferous gravitational collapse of the orogen recorded by N70W vergent extensional structures within the upper nappe complex.

The timing of deformation and metamorphism in the study area is constrained by ^{40}Ar-^{39}Ar hornblende, muscovite, and biotite ages from units between the west coast of Norway and the eastern margin of the study area. Excess argon is a major problem in the Scandinavian Caledonides, although

modification of the isotope correlation technique allowed reasonable data to be obtained. Between 430 Ma and 390 Ma, rocks in the upper nappe complex cooled at a relatively slow rate of 1-2 ^{o}C/Ma. Following D3 to D6 imbrication of the upper nappe complex and final obduction onto the Baltic Shield during this period, the cooling rate increased to 9 ^{o}C/Ma and is thought to be related to the post-tectonic gravitational collapse of the orogen.

During final en bloc underthrusting of the Baltic Shield basement, slivers up to 1 km thick became detached from the basement. These laterally discontinuous lozenge-shaped slivers of the crystalline basement have warped the overlying upper nappe complex leading to the characteristic dome and basin outcrop pattern of the Scandinavian Caledonides. The Rombak-Sjangeli Window is such a lozenge, bounded by frontal, trailing, and lateral ramps, and appears to have been translated at least 60 km to S60E.

Thesis Supervisor: Dr. B.C. Burchfiel
Title: Professor of Geology

TABLE OF CONTENTS

LIST OF FIGURES

LIST OF TABLES

LIST OF PLATES

ACKNOWLEDGEMENTS

In the four years spent working on this project, I have learned a great deal about science, life, and the interaction between the two. It is impossible to thank all the people who have contributed to this education and to acknowledge the manner in which they did.

I must particularly thank Clark Burchfiel and Kip Hodges for spending a great deal of time and effort trying to teach me the principles of structural geology and continental tectonics. Frank Spear was an inspiring teacher who made thermodynamics marginally comprehensible. Dan Lux put up with me in his lab at the University of Maine while I floundered with the basics of ^{40}Ar-^{39}Ar dating. Phil England kept me thinking about geodynamics, while Stan Hart frustrated me with kinetics.

The tectonics graduate students have become dear friends while keeping me honest about geology. If I were to list all their names and influences upon me this section would be the longest in the thesis.

Thanks must also go to Cynthia Ebinger and Leigh Royden for providing the lure of a summer in Africa which inspired me to finish. Lyle Hodgson was also of enormous help during the final weeks of the project.

CHAPTER 1: INTRODUCTION

Many of the world's younger orogens have received much study, such as the North American Cordillera (Price and Mountjoy, 1970; Burchfiel and Davis, 1975) the Western Alps (e.g. Ramsay, 1981) and the Himalayas (e.g. Le Fort, 1975). Unfortunately, only the shallowest crustal levels of these young orogens are available for direct study; deeper structural levels can only be accessed remotely (e.g. Fitch, 1970). Some of these geophysical studies have indicated the possibility of continental subduction to deep levels (e.g. Roecker, 1982).

The Scandinavian Caledonides is an early to middle Paleozoic orogen resulting from closure of the Iapetus Ocean and consequent collision of the Baltic and Greenland cratons. East-directed obduction of a variety of rocks of both continental and oceanic affinities onto the Baltic Shield, and subsequent deep-seated erosion has resulted in the present lithologic distributions (Fig. 1-1). While the polarity of subduction is a matter of some controversy, most workers agree that immediately prior to and during final collision, subduction was west-directed. The strongest evidence for this polarity is the absence of Late Ordovician to Early Devonian intrusive rocks within the Proterozoic basement of Baltica, but their common occurrence within the East Greenland Caledonides (Henriksen and Higgins, 1976).

Well-exposed, deeply eroded Phanerozoic orogenic belts resulting from a continental collision are extremely rare on our planet. As such, the Scandinavian Caledonides are unique in having been eroded to mid-crustal levels, yet retaining much of their obducted sequences. The excellently exposed northern Caledonides are thus an ideal region to study the mid-crustal effects of continental collision.

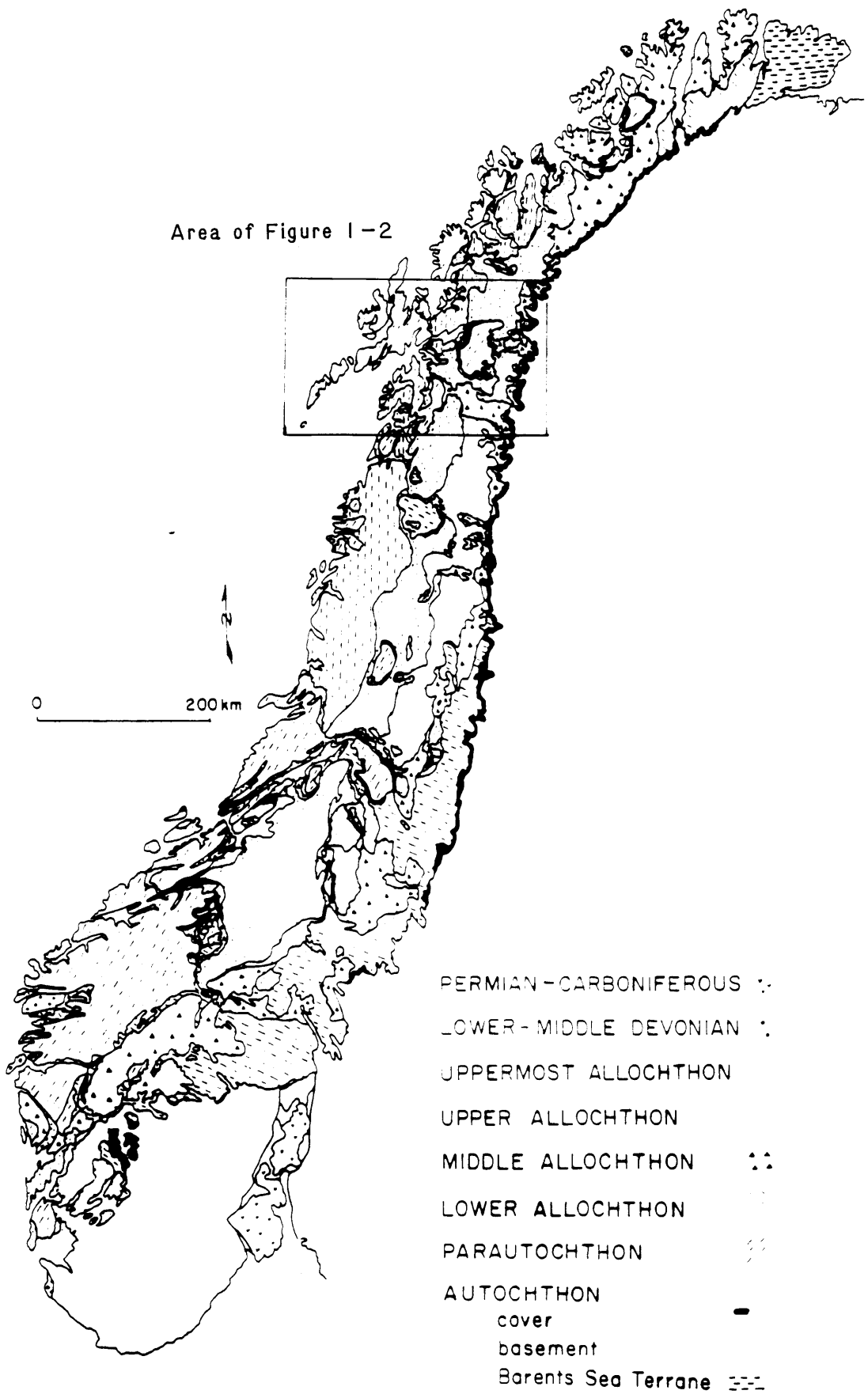

Figure I-1: The Scandinavian Caledonides

GEOLOGICAL SETTING

The Scandinavian Caledonides extend 1500 km from northernmost to southernmost Norway (Fig. 1-1). The southern part of the orogen is completely within Norway, whereas the central and northern parts evenly straddle the Norwegian-Swedish border. In central and northern Scandinavia the orogen is dominated by generally flat-lying thrust sheets which have been transported eastward onto the Baltoscandian platform.

Gee (1975, 1978), Gee and Zachrisson (1979), and Oftedahl (1980) have presented reviews of the Scandinavian Caledonides, while the most recent summary of the north-central Caledonides is by Stephens et al. (1985). Regional syntheses of northern Scandinavia have been presented by Kulling (1964, 1972) and Gustavson (1978).

The orogen may be subdivided into three tectonic elements: 1) the autochthon-parautochthon, 2) an upper nappe complex, and separating these two domains, 3) variably deformed basement rocks of the main Caledonian shear zone.

The autochthon-parautochthon is the structurally lowest domain in the orogen. This element includes Precambrian crystalline basement rocks and a thin sedimentary cover of Vendian to Early Ordovician age. The autochthon -parautochthon is exposed within three areally distinct areas in the orogen: 1) the Baltic Shield east of the present erosional front, 2) the basement cored windows which straddle the Norwegian-Swedish border, and 3) the west coast of Norway. The term parautochthon has been used to describe sedimentary cover sequences along the thrust front which show minor tectonic disturbance (Gee and Zachrisson, 1979). The same authors have used the term to describe similar basement and cover rocks exposed within tectonic windows farther west.

In northern and central Scandinavia, the upper nappe complex (a.k.a. Upper Allochthon) is a heterogeneous sequence of rocks metamorphosed from greenschist to eclogite facies. These rocks include Precambrian crystalline basement rocks (e.g. Emmett, 1982), ophiolitic rocks (Minsas and Sturt, 1981; Furnes et al., 1982), and Proterozoic to Silurian metasedimentary rocks (e.g. Gee 1975). The upper nappe complex can be divided into three sequences, separated by tectonic boundaries: 1) a lower sequence of schist, amphibolite and gneiss metamorphosed under medium- to high-grade conditions, 2) an intermediate sequence of low- to medium-grade sparsely fossiliferous metasedimentary and volcanic rocks and 3) an uppermost sequence of psammitic, pelitic and calcareous schists, and subordinate gneiss and amphibolite which locally contain synorogenic gabbro and granitoid intrusions (Stephens et al., 1985). These units have been termed the Seve, Koli, and Rodingsfjallet nappes respectively. Work in the Lofoten-Kebnekaise area (Bartley, 1981; Hodges, 1982; Crowley, 1985; Steltenpohl, 1985; Tilke, this work) has shown that, while this classification is useful in the broad sense, in detail it breaks down. For example, within the "Koli", metamorphism ranges from chlorite grade up to rocks metamorphosed at 1400 MPa and 850°C (see chapter 4). In the Efjord area (Fig. 1-2) the contact between the "Koli" and overlying "Rodingsfjallet" nappe has been shown to be a depositional contact (Hodges, 1985; Steltenpohl, 1985), further breaking down the simple classification scheme.

It was within units of the upper nappe complex that Tornebohm (1888) originally developed the concept of far-travelled thrust sheets. Paleogeographic and palinspastic reconstructions require the upper nappe complex to have been derived from west of the present Norwegian west coast (e.g. Gee, 1975). These rocks appear to be an assemblage of obducted units

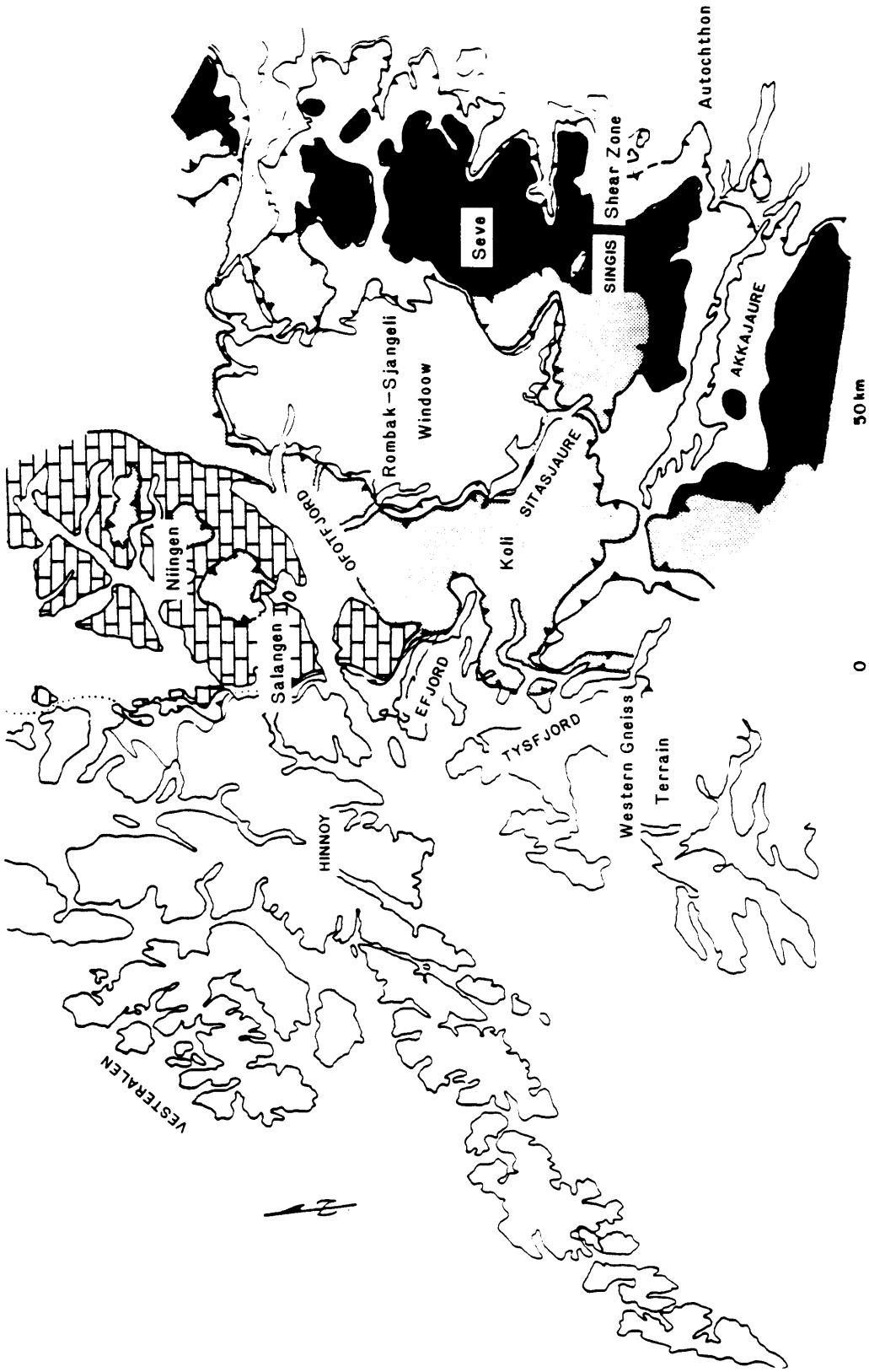

Figure 1-2: Lofoten - Kebnekaise transect

formed marginal to the Baltic and Greenland cratons, and oceanic crust, island arc, accretionary prism and overlap assemblages formed within the intervening pre-Caledonian Iapetus Ocean.

Rocks within the shear zone shear zone separate the autochthon -parautochthon from rocks in the overlying upper nappe complex. The rocks of the shear zone have been subdivided into two groups: 1) the Lower Allochthon, a sequence of low-grade moderately deformed thrust sheets predominantly composed of late Proterozoic to early Paleozoic sedimentary rocks locally unconformably overlying Precambrian crystalline basement, and 2) the Middle Allochthon, a sequence of greenschist (and occasionally higher) grade penetratively deformed mylonitic rocks containing both Proterozoic crystalline rocks and their sedimentary cover.

In the type area of the Lower Allochthon in the central Caledonides of Jamtland and Vasterbotten Counties, Sweden, these units are interpreted to represent part of the imbricated miogeoclinal wedge of Baltica (e.g. Gee, 1975). Palinspastic restoration of this sequence indicates a predeformational thickness of c. 1800 m (Kumpulainen, 1982).

North of the Nassafjell Window (Fig. 1-1) the distinction between Lower and Middle Allochthon breaks down, mainly due to the dramatic decrease in thickness of the Lower Allochthon. For this reason, in the study area, I consider all units between the autochthon-parautochthon and the upper nappe complex as part of the Caledonian shear zone, with only locally preserved rocks that can be assigned to the Lower Allochthon.

The scarcity of fossils in the Caledonian metamorphic rocks, and the paucity of reliable radiometric dates has resulted in a relatively poor understanding of the relationships between different deformational and

metamorphic events. However, there is good evidence for at least two phases of Paleozoic deformation within the Scandinavian Caledonides. Throughout much of the orogen, the Late Silurian to Early Devonian Scandian Orogeny has been well documented (e.g. Gee and Wilson, 1979; Roberts, 1981). In recent years, however, an earlier event beginning in the Late Cambrian was first documented in northernmost Norway (Sturt et al., 1975, 1978). This event, termed the "Finnmarkian Orogeny" is associated with south-directed thrusting and syntectonic intrusion of plutons which yield Rb-Sr whole rock crystallization ages of 530 to 490 Ma. Broadly coeval events appear to be associated with ophiolite obduction in the Bergen area (Henriksen, 1981) and the Trondheim region (Roberts and Wolff, 1981). Claesson (1980a, 1980b), Dallmeyer et al. (1985) and Dallmeyer and Gee (1986) have obtained Rb-Sr and K-Ar mineral ages ranging from 455 to 510 Ma from the upper nappe complex within the central Caledonides. The exact temporal and structural relationships of these events to the Scandian and Finnmarkian Orogenies is at present poorly understood.

PURPOSE

The primary objective of this study was to investigate part of the Caledonian collisional orogen now exposed at a level that was in the middle crust during orogenesis. A second objective was to integrate the results of this work with earlier studies in the northern Scandinavian Caledonides. The ultimate goal of this study was to understand better the processes involved in collisional orogenesis in general.

With these goals in mind, the selected study area was at the southeastern margin of the Rombak-Sjangeli Window in northwestern Sweden between 68° and 69°N (Fig. 1-3). The area includes parautochthonous Precambrian crystalline basement and its Vendian to Middle Cambrian

autochthonous cover exposed within the Window. Overlying this basement complex, and separated by the main Caledonian shear zone, is a heterogeneous sequence of low- to high-grade rocks of the upper nappe complex. These structural relations allow the following four principal questions to be addressed:

1) What is the tectonostratigraphy of the units within the window and the upper nappe complex, and how do these units correlate with surrounding areas?

2) What is the nature and degree of basement involvement during emplacement of the upper nappe complex?

3) What is the nature of deformation and metamorphism within the upper nappe complex, and how does it relate to deformation within the basement?

4) What are the spatial and temporal relationships of this deformation and metamorphism, and how does the thermal evolution of the area relate to these events?

PREVIOUS WORK

This thesis is part of a project by B.C. Burchfiel and his students to map a structural-stratigraphic transect from west to east across the Scandinavian Caledonides between 68°N and 69°N. The field work has been augmented by metamorphic and geochronologic studies focussed on gaining a more complete understanding of the structural and thermal evolution of the area. The initial work on the "Lofoten-Kebnekaise transect" was focussed on the extent of Caledonian deformation within the pre-Caledonian basement of Vestvagoy (Tull, 1972, 1977) and of West Hinnoy (Hakkinen, 1977). On East Hinnoy, Bartley (1980, 1981, 1982) examined the nature of the contact between the Lofoten crystalline basement and the overlying upper nappe complex. To the south on the Norwegian mainland, Hodges (1982, 1985)

compared the nature of the basement-cover contact on the coast near Efjord with the same contact to the east at the southwestern margin of the Rombak-Sjangeli Window (Fig. 1-2). He concluded that these thrusts were active at different times (e.g. Hodges et al., 1982). Hodges and Royden (1984), and Royden and Hodges (1984) attempted to integrate petrologic and thermochronologic data to understand the uplift and cooling history of the area. Crowley (1985), working along the southwestern margin of the Rombak-Sjangeli Window extended and expanded the tectonostratigraphy established by Hodges (1982). Crowley (1985) also examined the nature of the shear zone rocks in this area, as well as examining the metamorphic grade of the basement, shear zone and upper nappe complex. This study continues the transect to the east between the Sitasjaure and Singis areas. Page (in progress) is further extending the transect and will hopefully reach the present erosional front to the southwest of Nikkaluokta (Fig. 1-2).

Several workers have completed or are involved in detailed structural studies in areas adjacent to the "transect". A large area north of Akkajaure has been mapped by Bjorklund (1985), from the Caledonian front to the Norwegian west coast (Fig. 1-2). This study focussed on the nature and development of the thick (c. 2 km) sequence of shear zone rocks within the Akkajaure Window. Burchfiel and Royden (in progress) are continuing work to the northwest of Akkajaure within the Tysfjord culmination. Steltenpohl (1985) completed a structural-metamorphic study of upper nappe complex units to the north of Ofotfjord (Fig. 1-2).

Early reconnaissance mapping in the Swedish portion of the transect area was completed by Kulling (1964). The map, published at a scale of 1:400,000 is useful as a general guide to the distribution of rock types

but proved relatively poor in detail, and virtually useless with regard to structural relations. A portion of the Rombak-Sjangeli basement north of Sitasjaure was mapped by Birkeland (1976) at a scale of 1:100,000. The Norwegian mainland portion of the transect area was mapped by Foslie (1941) at a scale of 1:100,000. The lithologic control of the study was excellent, as were many of the structural relations. Gustavson (1974) reinterpreted Foslie's map and included it in his 1:250,000 Narvik sheet.

PHYSIOGRAPHY OF THE STUDY AREA

Sitasjaure, the 35 km long lake which straddles the Norwegian-Swedish border marks the western boundary of the study area (Plate 7). Singis, a very small Lapp community within the north-south trending Tjaktjavagge Valley marks the eastern boundary of the area. Elevation ranges from 610 m.a.s.l. at Sitasjaure to 1710 m.a.s.l. on the peak Salka at the northeastern boundary of the study area. Kebnekaise, the highest peak in Sweden (2123 m.a.s.l.) lies 10 km northeast of Singis. The entire area is above tree line. The physiography is dominated by the effects of glaciation; U-shaped valleys, eskers, drumlins and kettles are ubiquitous. While exposure on ridges and peaks approaches 100%, valleys are commonly swamps or filled by glacial debris. Wildlife in the area is dominated by reindeer, all of which are owned by Lapps who periodially herd them with helicopters. Lemmings dominate the small end of the mammal scale, while moose, red fox and wolverine have been seen. Birdlife includes ptarmigan, raven and flocks of mosquitoes.

ACCESS

The study area is within a remote area of arctic Sweden. While there are no permanent residents within this area, parts are relatively popular

with backpackers and fishermen. Snow prevents work from beginning before late June, while the first snow in late August or early September ends the field season. Rain is often successful in preventing work during the remaining two months of "summer". The nearest roads to the study area are at the northern end of Sitasjaure in Norway, at the southern end of Sitasjaure in Sweden, and 40 km east of Singis in Nikkaluokta. Access from each of these locations was utilized at various stages of the project. The western half of the area was accessed on foot, the central part by floatplane from Stora Sjofjallet (south of the study area), and the eastern part by helicopter from Nikkaluokta. Between one to three weeks were spent in the field for a given period, depending on the form of access, complexity of the area, weather, and motivation.

METHODS

Mapping was accomplished during the summers of 1983 to 1985. Field maps were on a 1:25,000 base enlarged from the 1:100,000 BD7 sheet made by Allmanna Kartverk in 1966. The contour interval on this map is 20 m, and proved to be relatively accurate. The field maps were compiled on a 1:50,000 base (Plate 1), while the complex area north of Kaisejaure was also compiled on a 1:10,000 base (Plate 4). Although a more recent series of 1:100,000 maps have been published by Allmanna Kartverk in 1984, with numerous location name changes to follow Lappish culture and tradition, names from the earlier version were retained for this study.

CHAPTER 2: TECTONOSTRATIGRAPHY OF THE SITAS - SINGIS AREA

INTRODUCTION

The rocks of the Sitas-Singis area are subdivided into two lithologically and structurally distinct packages, a lower basement complex and an overlying nappe complex. The lower of these two packages is exposed within the Rombak-Sjangeli and Singis windows. These basement rocks are composed of Proterozoic intrusive and extrusive rocks, and metasedimentary roof pendants unconformably overlain by highly deformed autochthonous sedimentary rocks. A complex shear zone separates the footwall rocks from the overlying nappe complex. The nappe complex consists of an assemblage of gneissic, metaigneous and metasedimentary rocks that were derived from west of the present Norwegian coast. The nappe complex was emplaced during a protracted series of events during early and middle Paleozoic time.

An inverted metamorphic gradient characterizes this sequence of units. Basement rocks were metamorphosed to greenschist grade during emplacement of the upper nappe complex, and units of the upper nappe complex have experienced a wide range of metamorphic conditions from greenschist to eclogite facies. The metamorphism of these units will be discussed below, and in chapter 4.

BASEMENT COMPLEX

ROMBAK-SJANGELI BASEMENT

Proterozoic intrusive, metavolcanic and metasedimentary rocks crop out in the Rombak-Sjangeli and Singis windows. These rocks are overlain unconformably by clastic sedimentary rocks correlative with the Vendian to Cambrian Dividal Group of the Baltic Shield foreland.

While no comprehensive study has previously been done of the Proterozoic rocks within the Windows, numerous reconnaissance studies have

been made (e.g. Vogt, 1950; Kulling, 1964; Birkeland, 1976; Gunner, 1981). These workers subdivided the Proterozoic units into two groups: granitic to gabbroic intrusive rocks, and metasedimentary rocks of the Supracrustal Series. Mapping by Vogt (1950) and Birkeland (1976) has shown that intrusive rocks in the Rombak-Sjangeli Window are dominantly granitic to syenitic in composition (Fig. 2-1). Units of the Supracrustal Series occur as pendants within the intrusive rocks that range in size from a few meters, to long sinuous NS trending bands more than 30 km long and 5 km wide. Proterozoic rocks within the Windows were not the main focus of this study, and although the lithologic distribution of the rocks was noted, contacts were not mapped. In the study area, the lithologies were subdivided into three assemblages: granite (includes granitic to granodioritic intrusive rocks), greenstone, and sedimentary rocks. Following Birkeland (1976) these three lithologies are considered to be part of the Grunfjell Group.

Grunfjell granite

The Grunfjell granite crops out extensively in the northwestern part of the study area. Good outcrops are present along the southern and eastern slopes of Patnakaive, on Mattjeramatjakka, and along the northeastern shore of Tutturjaure (Plate 1). Grunfjell greenstone and schist increasingly dominate the Rombak-Sjangeli basement lithology to the east of Tutturjaure, such that granite crops out only locally.

Contact relationships between the Grunfjell granite and the other basement lithologies show the granite to be the youngest unit. No chill margins were found at contacts with other basement units, and large greenstone pendants are commonly cut by aplite (Fig. 2-2). A set of greenstone dikes that strike approximately NS and dip 80E do however appear to intrude the granite northwest of Tutturjaure.

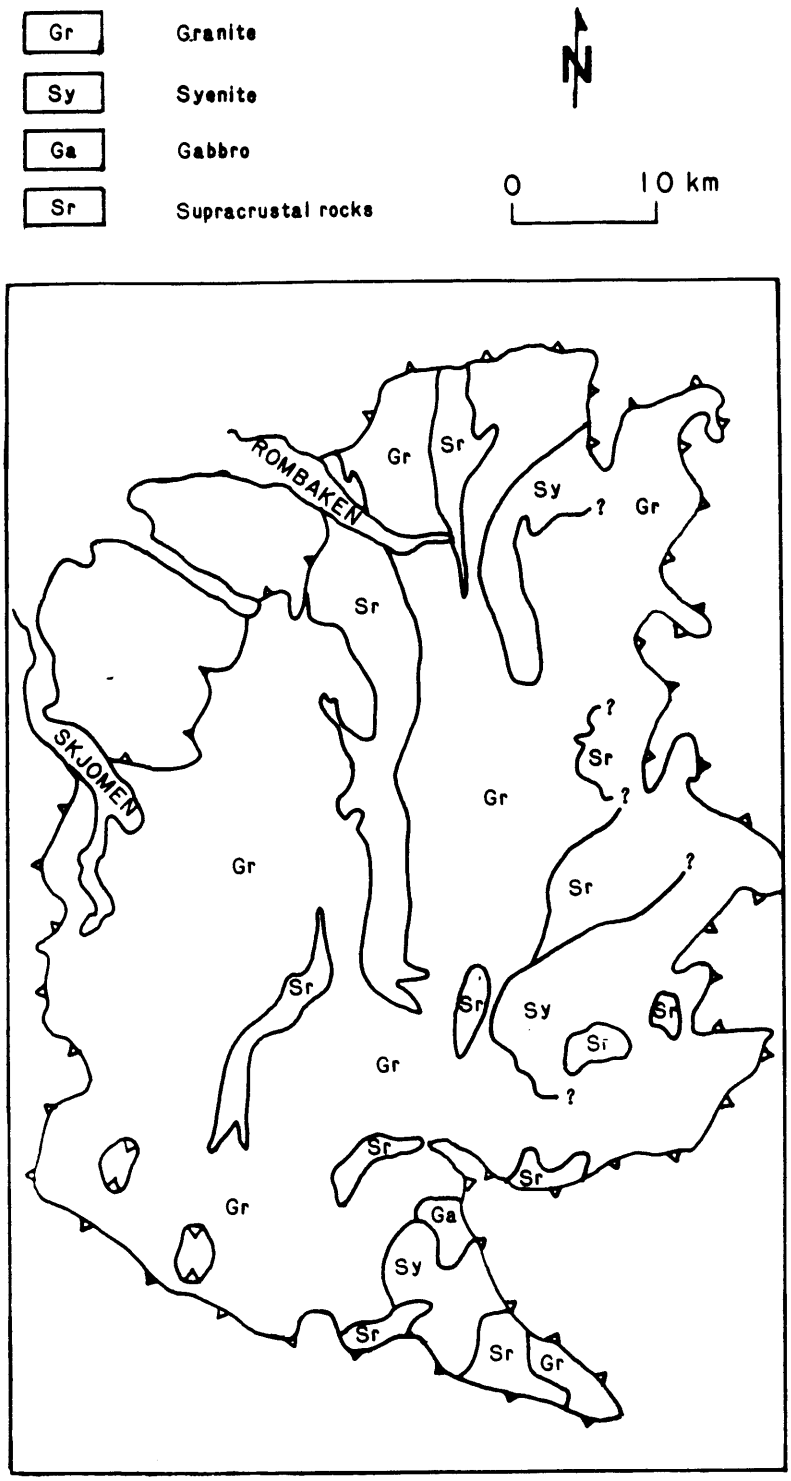

Figure 2–1: Rombak – Sjaangeli Window basement lithologies (after Gunner, 1981)

Figure 2-2 Grunfjell greenstone intruded by aplite dike. Located 1 km north of northern tip of Tutturjaure.

Figure 2-3: Basal contact of Tornetrask Formation with underlying Grunfjell sedimentary rocks. Note angular discordance between flat-lying pebble conglomerate of the lower sandstone member of the Tornetrask Formation and pre-Caledonian foliation of the Grunfjell metasedimentary rocks. Located 1 km west of the northern end of Tutturjaure.

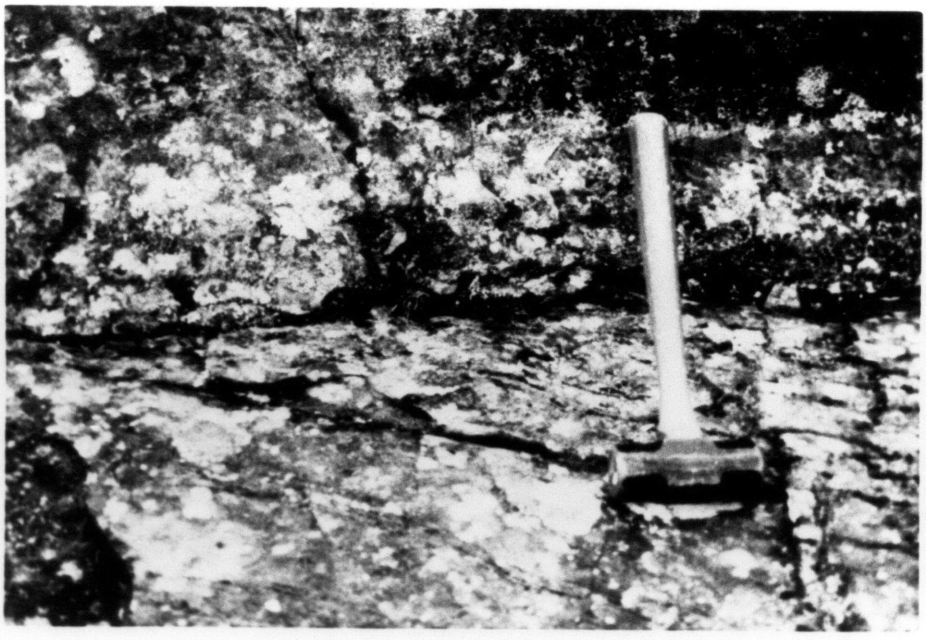

The contact between the Grunfjell granite and the overlying Tornetrask Formation is an unconformity with little or no displacement. The irregular nature of this contact and presence of a basal conglomerate in many localities precludes any movement between the two units. The upper 1-3 m of the granite commonly contains a weathered zone and a regolith is commonly present.

In the study area, the Grunfjell granite is an unfoliated medium-grained (0.5-1 cm) pink microcline granite to white granodiorite. The granodiorite is often difficult to distinguish from the massive Grunfjell quartzite, althougn euhedral phenocrysts are characteristic of the granodiorite. Basement involved thrust faults are associated with a foliation in the granite for up to 5 m away from the faults, with the development of blastomylonite at the fault.

In thin section, the mineral paragenesis of the Grunfjell granite is: plagioclase + microcline + quartz + epidote ± biotite ± chlorite ± hornblende ± rutile ± sphene ± tourmaline. Greenschist grade alteration of the granite is characteristic of the field area. Fine-grained (0.1 mm) anhedral to medium-grained (5-8 mm) subhedral igneous feldspar typically makes up 65% of the rock. Plagioclase is ubiquitously saussuritized with coarser (0.1 mm) epidote idioblasts common. Fine-grained (0.5 to 0.1 mm) anhedral quartz makes up 20-25% of the rock. Fine-grained (0.1 mm) olive-green biotite is the igneous mafic phase, and is typically altered to green amphibole and pale-green chlorite.

While the Grunfjell granite is generally unfoliated, evidence of strain at greenschist grade is ubiquitous. Relict quartz grains are always highly strained and commonly surrounded by fine neoblasts. Coarse-grained feldspar grains typically have deformation lamellae and kink bands.

Grunfjell greenstone

The Grunfjell greenstone forms the dominant basement lithology on Juovvatjaros, from east of Tutturjaure to north of Kaisejaure, and on Raktas northeast of Kaisejaure (Plate 1). Smaller pendants up to 500 m wide are also present in the basement rocks dominated by granite north of Tutturjaure.

As mentioned above, the Grunfjell greenstone appears to predate the granite since it is intruded by aplitic dikes. This interpretation agrees with that of Adamek (1975) and Gunner (1981), who studied similar 'supracrustal' rocks in neighboring areas.

In the area north and northwest of Kaisejaure, the Grunfjell greenstone is generally a massive unfoliated olive to dark green amphibolite. Locally, the greenstone contains coarse-grained (0.5-2 cm) white prismatic plagioclase pseudomorphs.

While the Grunfjell granite is characterized by relict igneous phases and textures, the greenstone has been completely metamorphosed to epidote-amphibolite facies locally retrograded to greenschist facies. The mineral paragenesis of the Grunfjell greenstone is: plagioclase + hornblende + epidote ± quartz ± rutile ± chlorite ± biotite ± calcite ± sphene ± tourmaline. In thin section the plagioclase pseudomorphs are composed of fine-grained (0.1 to 0.2 mm) subidioblastic albitic plagioclase. The pseudomorphs also contain abundant very fine-grained (0.02-0.04 mm) pale green acicular zoisite grains (saussurite). These relationships suggest the epidote amphibolite reaction: anorthite + H_2O → albite + zoisite. Pale green epidote and blue-green hornblende within the pseudomorphs also requires infiltration of FeMg-rich fluids during the metamorphism.

Medium-grained (0.1 to 2 mm) acicular to prismatic sub-idioblastic

twinned hornblende occurs throughout the matrix. Green to brown fine-grained (0.05 to 0.1 mm) idioblastic biotite is locally abundant, and is most common near late saussuritized veins.

The greenstone is generally unfoliated, although within 'dikes' there is a strong foliaton. This may be due to flow banding, chill margins or shearing. Where greenstone crops out in the footwall of normal faults, the unit is chloritized and dissected by saussuritic veins.

Grunfjell sedimentary rocks

Outcrops of Grunfjell sedimentary rocks are present throughout the Rombak-Sjangeli basement in the study area. Locally, these Grunfjell clastic and calcareous rocks dominate the lithology; notably north of Kaisejaure and in the basement sliver north and east of Rautasjaure. A variety of other lithologies are present within the Grunfjell sedimentary rocks, they include: orange to blue-grey psammitic schist, brown marble, and white massive quartzite.

The sedimentary rocks are generally foliated, and the foliation is demonstrably of pre-Caledonian age. On the southwestern shore of the northern end of Tutturjaure, there is a clear angular discordance between Grunfjell foliated sedimentary rocks and the overlying Tornetrask Formation (Fig. 2-3). Also, north-northwest of Kaisejaure, sub-horizontal Grunfjell sedimentary rocks intruded by vertical greenstone dikes are unconformably overlain by the Tornetrask Formation (Fig. 2-4).

AGE OF INTRUSIVE ROCKS

Preliminary isotopic dating suggests a Svecofennian age for the Rombak-Sjangeli granite. Heier and Compston (1969) obtained an Rb-Sr whole rock isochron of 1690±90 Ma. In a relatively extensive study of the Rombak-Sjangeli Window, Gunner (1981) obtained an 11-point Rb-Sr errorchron

Figure 2-4: Grunfjell sedimentary rocks intruded by vertical greenstone dikes. Note that sub-horizontal pre-Caledonian foliation of Grunfjell sedimentary rocks is truncated by greenstone dikes. View north on Juovvatjaros approximately 4 km north-northwest of Kaisejaure.

that yielded an age of 1780±85 Ma.

REGIONAL CORRELATIONS

Vogt (1942) and Hodges (1982) argued that the Rombak-Sjangeli granite gneiss is correlative with the Tysfjord granite gneiss exposed along the Norwegian coast, west of the study area. Gustavson (1966) presented major element analyses suggesting the two gneisses are correlative. Nearly half the exposed area in Lofoten-Vesteralen islands consists of granitic to gabbroic intrusive rocks that yield Svecofennian ages (1800-1700 Ma) (Griffin et al., 1978). On east Hinnoy these granites appear to intrude a sequence of terrigeneous-metasedimentary rocks (Bartley, 1981).

Comparison of the Vendian-Cambrian cover (see below) and basement lithologies, and Rb-Sr systematics (Gunner, 1981), allow correlation of the Proterozoic rocks of the Rombak-Sjangeli Window with rocks of the Baltic foreland to the east. Thus, although disturbed by Caledonian tectonism, the Proterozoic rocks of Lofoten-Vesteralen, Tysfjord and Rombak-Sjangeli areas all appear correlative with the Baltic Shield to the east.

DIVIDAL GROUP

INTRODUCTION

A sequence of conglomerate, sandstone and siltstone was deposited unconformably on the Proterozoic basement of the Rombak-Sjangeli and Singis windows. This sequence can be correlated with the Vendian-Cambrian Dividal Group, that forms the autochthonous cover of the Baltic Shield foreland east of the study area.

In the study area, the Dividal Group was subdivided into two formations, the Tornetrask Formation, and the overlying Alum Shale. In its type area 70 km NE of the study area, the Tornetrask Formation has been

subdivided into six members (Thelander, 1982). Although the Formation thins to the south, and is characterized by the lateral disappearance of these six members, three correlative units were present in the study area (Fig. 2-5). The lower sandstone member is composed of conglomerate, feldspathic sandstone and quartzite. Red siltstone and quartzite of the red and green siltstone member is a characteristic marker horizon of the Tornetrask Formation in the study area. Blue-gray siltstone and blue quartzite of the upper sandstone member is the highest member of the formation in the study area. Overlying the Tornetrask Formation are brown to black graphitic siltstones of the Alum Shale.

AGE

Although no fossils were found in the study area, the Dividal Group has yielded fossils. In its type area, Kulling (1960a, 1964, 1972) found *Kullingia concentrica* in the lower sandstone member of the Tornetrask Formation, that dates this part of the formation as very latest Proterozoic (upper Vendian). In the upper part of the Tornetrask Formation numerous workers have found Lower Cambrian fossils (Moberg 1908, Kulling 1960a, 1964, 1972, Vogt 1967, Ahlberg and Bergstrom 1978, Ahlberg 1979, 1980). In Norbotten County, the Alum Shale is Middle Cambrian (Andersson et al., 1985). As the Alum Shale provides a detachment horizon for the allochthonous thrust sheets, the Upper Cambrian part of the formation is only locally preserved.

NOMENCLATURE

The name "Dividal Group" was originally introduced by Pettersen (1878) and included what is presently defined as the Tornetrask Formation, Alum Shale, and some overlying metamorphic rocks. As such, the name

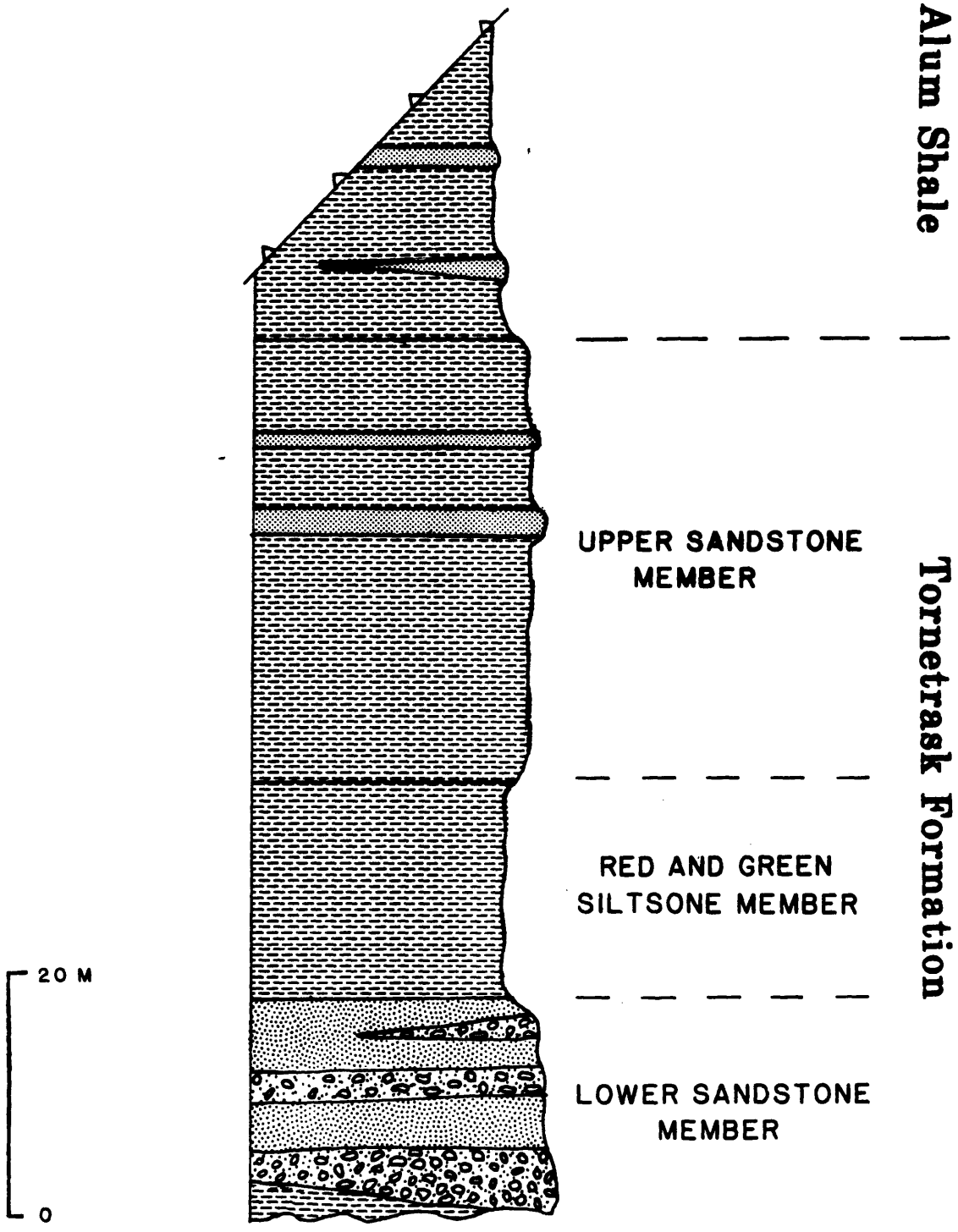

Figure 2-5: Dividal Group in the Kaisejaure area

"Hyolithus-series" (Sveonnius, 1892) was used in preference to Dividal Group for the sequence of sedimentary rocks. Foyn (1967) re-introduced the name "Dividal Group" to describe "an autochthonous group of sedimentary rocks, that consists mainly of shale, siltstone and sandstone, resting with erosional unconformity on the Precambrian crystalline basement, and is terminated at the top by thrust phases of Caledonian age. The thrust planes cut the group within the Alum Shale or at stratigraphically lower levels. The Group occurs along the margin of the Caledonian mountain range in Norbotten (Sweden), Enontekis (Finland), Troms and Finnmark (Norway)."

Thelander (1982) suggested the name Tornetrask Formation for the sedimentary sequence overlying the Proterozoic basement and underlying the Alum Shale in northern Norbotten.

The name Alum Shale is used for the entire sequence of Middle and Upper Cambrian black shales throughout Scandinavia (Andersson et al., 1985). No type section has been defined, although formation names have been proposed locally.

TORNETRASK FORMATION

The Tornetrask Formation is the basal unit of the autochthonous sedimentary cover of the Proterozoic basement in both the Rombak-Sjangeli and Singis windows. Locally the formation has been completely tectonically removed from the basement such as west of Rassepakte, and northeast of Rautasjaure (Plate 1). In some places, only the lower sandstone member is present (such as southwest of Tsutsajaure), whereas elsewhere the entire Dividal Group has been preserved (such as northwest of Kaisejaure). As noted earlier, three of the six formal members of the Tornetrask Formation are present in the study area.

Lower sandstone member

The lower sandstone member typically crops out as a resistant white ledge and ranges from 0 to approximately 20 meters thick. The variation in thickness is both stratigraphic and tectonic. The minimum stratigraphic thickness is approximately 5 meters; sections thinner than this are typically highly strained.

The lower sandstone member unconformably overlies the Grunfjell Group (Fig. 2-3). As noted earlier, in some places little or no slip has occurred along the contact, while in others it is a zone of high strain. The upper contact with the overlying red and green siltstone member is sharp but considered conformable (Fig. 2-6).

The internal stratigraphy of the lower sandstone member is complex. The unit is dominated by arkosic conglomerate and quartzitic to arkosic sandstone. The base of the member is characterized by a clast supported arkosic pebble (4-15 mm) conglomerate (Fig. 2-7). An arkosic siltstone up to 3 m thick with thin quartzite sandstone beds is however locally present at the base of the unit. The conglomerate and sandstone beds are typically 0.1 to 1 m thick and laterally continuous over 10 to 20 m.

Planar cross-beds are common in the lower sandstone member (Fig. 2-8) and were used as a facing indicator. Although deformation has complicated the study of the provenance of this unit, measurements on five sets of cross-beds indicate current directions were from the northeast and east.

The siltstone units above, and the basement rocks below typically contain an axial planar cleavage near the hinge area of folds, but the lower sandstone member rarely contains a foliation (Fig. 2-6).

Figure 2-6: Vertical contact between lower sandstone member (left) and red and green siltstone member (right) of Tornetrask Formation. View looking northeast approximately 2 km north-northwest of Tutturjaure. Note the west-dipping RSd1 axial surface foliation developed within the red and green silstone member but absent in the lower sandstone member.

Figure 2-7: Undeformed pebble conglomerate within lower sandstone member of the Tornetrask Formation. Located 1 km northeast of Tutturjaure.

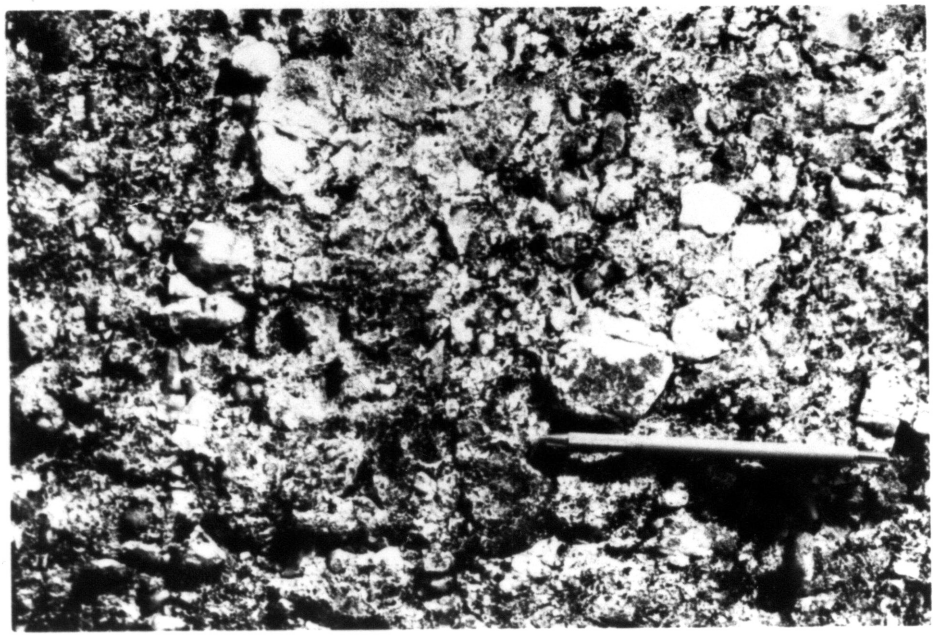

Figure 2-8: Cross-bedded sandstone of lower sandstone member of the Tornetrask Formation. Located 2 km east of Tutturjaure.

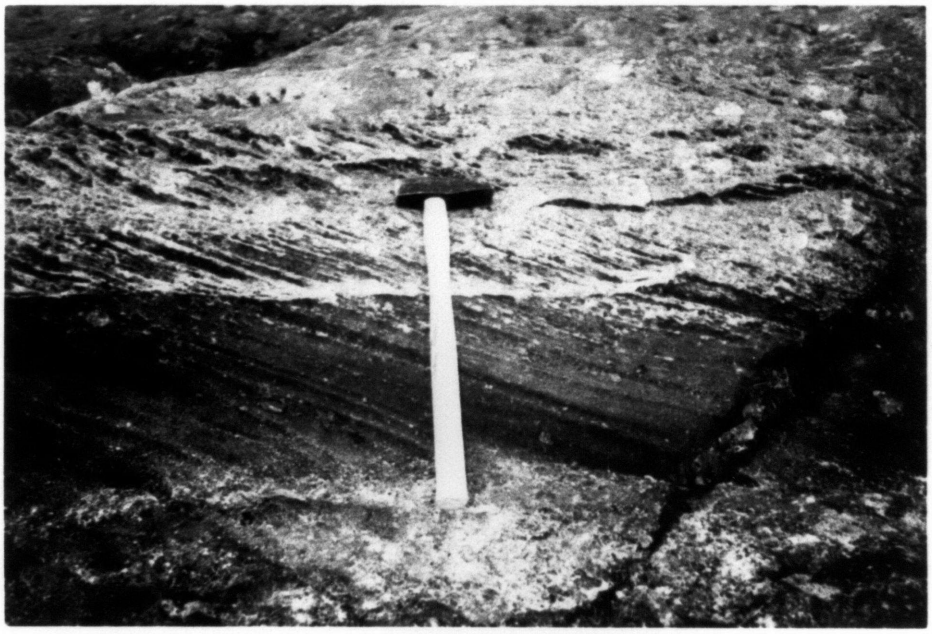

Red and green siltstone member

The red and green siltstone member lies in sharp conformable contact above the lower sandstone member. Although there has been much tectonic thickening and thinning, the stratigraphic thickness appears to range between 10 and 20 meters. The upper contact of this unit with the upper sandstone member is also sharp and considered conformable.

In the Rombak-Sjangeli Window, this member crops out as a rust-colored fissile siltstone, that is commonly crenulated. In thin section, the mineralogy is quartz (70%) + biotite (20%) + fine-grained muscovite (10%) + trace amounts of opaques. The rust color of this unit is due to dark-brown biotite (cf. upper sandstone member).

Bedding is often difficult to distinguish in the field, as it is readily transposed by an axial planar foliation. In thin section bedding is defined by the parallel alignment of biotite grains. Axial planar foliation generally develops as a spaced cleavage, with pressure solution of quartz along the cleavage planes. Pressure solution often is so intense, that quartz pods several centimeters in length have commonly segregated from the biotite rich "restite".

In the Singis Window at the eastern end of the study area, the red and green sandstone member also crops out. Here, however, the member is a massive rust to yellow-green quartzitic sandstone with medium (1 m) siltstone interbeds. This lithology is in sharp contrast to the monotonous siltstone present in this member that crops out 9 km to the west. Structural arguments presented later suggest the juxtaposition of distal and proximal facies of this member is due to the eastward translation of the Rombak-Sjangeli Window rocks with respect to underlying Singis Window rocks.

Upper sandstone member

The upper sandstone member in both the Rombak-Sjangeli and Singis windows is predominantly a blue-grey siltstone. In the upper 10 meters of the member, discontinuous blue 1-2 m thick quartzitic sandstone beds are relatively common. Locally, the uppermost 2-5 m of the upper sandstone member is a pale-green vitreous quartzite. This part of the unit may be a thin southerly equivalent of the upper siltstone member of the type Tornetrask Formation in the Tornetrask area (Kulling, 1964; Thelander, 1984).

In thin section, the upper sandstone member is texturally very similar to the red and green sandstone member. Mineralogically, it consists of quartz (50%) + chlorite (40%) + biotite (5%) + opaques (5%). The abundance of chlorite is responsible for its blue-grey color.

Like the red and green siltstone member, the thickness of this unit is complicated by tectonic thickening and thinning, although it appears to be approximately 30 to 40 m thick. In the western and eastern parts of the study area, only the lower 10 meters of the member are exposed, the remainder having been removed below the overlying thrust sheets. Where mylonitized siltstone of higher tectonic units such as the Storrit Complex and Matert Shear Zone overlie the upper sandstone member, the upper contact is generally difficult to locate in the field. However, close examination of rocks from these units reveals a variety of mylonitic features not present in the upper sandstone member such as porphyroclasts with asymmetric pressure shadows, mica fish, and S-C fabrics.

East of Tutturjaure and northwest of Kaisejaure, the entire upper sandstone member is exposed. This member forms the top of the Tornetrask Formation in the area, its upper contact with the Alum Shale is sharp and

conformable.

ALUM SHALE

The Alum Shale crops out extensively northwest of Kaisejaure, and is the highest exposed unit of the Dividal Group present in the study area. The formation is 0 to 30 m thick. The variation in thickness is due to deformation.

The formation crops out as a very fissile dark brown to black graphitic siltstone. In thin section it consists of quartz (50%) + muscovite (25%) + graphite (25%). The unit is commonly crenulated, and isoclinally folded on a small scale.

SHEAR ZONE ROCKS

The Grunfjell and Dividal Group rocks of the Rombak-Sjangeli and Singis windows are separated from the overlying high-grade rocks of the upper nappe complex by a complex ductile shear zone. In the Rombak -Sjangeli Window, this shear zone was named the Storrit Complex, after outcrops on the mountain Storrit to the north of Sitasjaure (Hodges, 1982). In the Singis Window, the shear zone is much thinner than the Storrit Complex, and is associated with a different thrust. It is here named the Matert Shear Zone after the mountain Matertjakka, north of the window.

STORRIT COMPLEX

The Storrit Complex is well exposed along much of the northeast margin of the study area. West of Tutturjaure, the complex is approximately 500 meters thick, decreasing to 200 meters northwest of Kaisejaure, to 40 meters at the southeastern end of the Rombak-Sjangeli Window.

Lithologically, the Storrit Complex is a complex, heterogeneous assemblage of highly strained slivers of rock derived from the basement and

autochthonous cover. Probable protoliths include granite to gabbro, quartzite, arkosic conglomerate, quartzofeldspathic siltstone, and graphitic siltstone. In the field, highly strained granite is virtually impossible to distinguish from similarly strained quartzofeldspathic siltstone. The Storrit Complex was therefore mapped by tracing lithologic breaks and careful sampling for petrographic analysis. It was subdivided into three units: a) granitic (to granodioritic) mylonite, b) quartzite mylonite, and c) quartzitic to graphitic siltstone that forms a matrix to the mylonitic slivers of the shear zone.

Granitic mylonite

Two major slivers of granitic mylonite 150 to 200 meters thick crop out in the western end of the study area between Sitasjaure and Tutturjaure (Plate 1). Northwest of Kaisejaure, another highly strained granitic slice 100 to 150 meters thick dominates the Storrit Complex. On the northern margin of the Tsutsajaure culmination, the entire complex is a 60 meter thick granitic slice.

In hand sample, the slices of granitic mylonite range from mylonite to ultra mylonite (Sibson, 1977). Mylonitic granite is often characterized by a strong L-S fabric (Bell and Etheridge, 1973). More typically, the granite mylonite of the study area is light-grey, very fine-grained and weakly lineated.

Petrographic examination reveals that feldspar porphyroclasts (200-500μ in diameter) constitute 2-15% of the sample, and sit in a quartz + plagioclase + muscovite + chlorite neoblast (10-50μ) matrix (Fig. 2-9). This strongly bimodal grain size distribution is typical of mylonites (Sibson, 1977). The more homogenized samples (2-5% porphyroblasts) have a very weak lineation, while samples with a higher porphyroclast-neoblast

Figure 2-9: Storrit Complex granite mylonite thin section. Field of view is 4 mm. Note 200-500 feldspar porphyroclasts in 10-50 neoblast matrix.

Figure 2-10: Storrit Complex matrix schist thin section. Field of view is 3mm. Note floating graphite-muscovite fold hinge in quartz matrix with weakly developed comb texture.

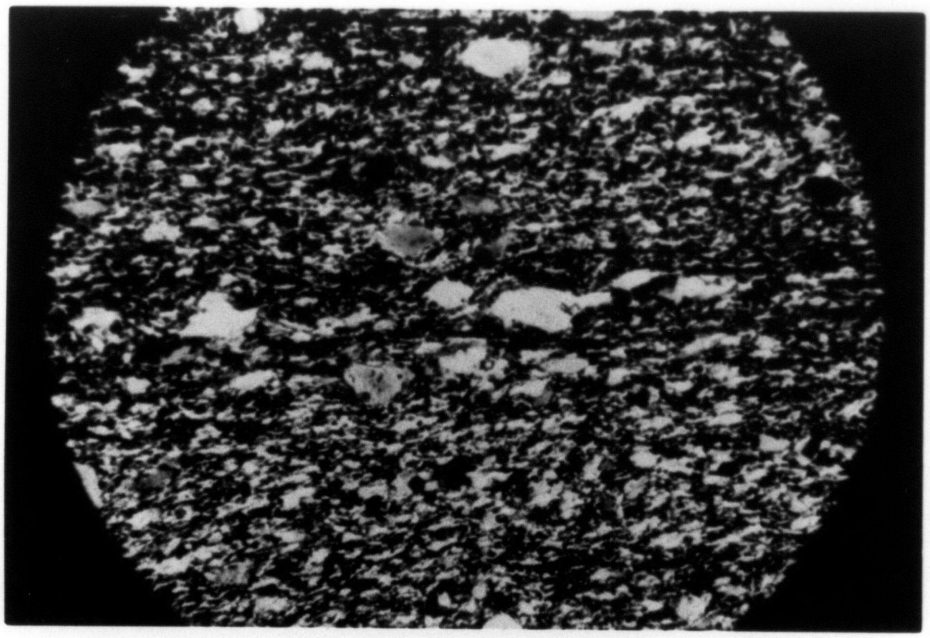

ratio (10-15%) are strongly lineated. In some samples, leucocratic lineations over 5 cm in length can be associated with a single feldspar porphyroclast.

The strong N60W lineations developed in the granitic mylonite unit as well as in the other Storrit units are of three types:

1) Stretching lineation formed by the recrystallization of feldspar neoblasts in the x-direction of the finite strain ellipse (see chapter 3).

2) Mineral lineation formed by the crystallization of acicular grains (e.g. epidote) with their long axes parallel to the x-direction.

3) Intersection lineation formed by the intersection of mylonitic cisaillement (C) surfaces (Berthe et al., 1979) and axial surfaces of a-type folds (see chapter 3).

The stretching and mineral lineations dominate in the granitic mylonite unit while the intersection lineation predominates the other Storrit lithologies.

Quartzite Mylonite

Several moderate size quartzite mylonite slivers crop out west of Tutturjaure. They range in size from 1-2 km in length and 40-100 m in thickness. Small slivers on the order of 10-50 m in length also crop out throughout the study area, but were too small to map.

In hand sample, the quartzite mylonite is white to blue-grey, weakly lineated, and in many cases difficult to distinguish from granitic ultramylonite (see above).

Thin section examination shows this unit to consist of up to 20% biotite + epidote + graphite + muscovite + plagioclase. The quartz grains have equiangular boundaries, are generally dislocation free, and are 100-200μ in diameter. Platy minerals are commonly discordant to the

mylonitic foliation, defining a later axial surface foliation.

Matrix schist

Approximately one-third of the Storrit Complex may be included in the matrix schist. The lithology ranges from graphite + quartz + muscovite to quartz + muscovite schist. Chlorite, epidote, calcite and apatite are subordinate phases. In hand sample, the schists are blue-grey to brown to black with increasing graphite content. Contacts between the various lithologies may be abrupt or gradational.

Thin sections reveal the matrix schist to be strongly folded and sheared. Floating mica hinges distinguish this unit from relatively undeformed siltstone of the Dividal Group below (Fig. 2-10).

MATERT SHEAR ZONE

The rocks of the Matert Shear Zone are similar to those of the Storrit Complex. The western and southwestern margins of the Singis Window are predominantly matrix schist, while shear zone rocks in the north-central part of the window consist of a sliver of granitic basement with a well-developed east-southeast vergent S-C fabric (see chapter 3). Immediately above the sliver is a strained (3:1) quartz pebble conglomerate.

CONTACT RELATIONS

While often difficult to locate in the field, the sole thrust of the Storrit Complex is very sharp. As noted above, shear zone schist is distinguished from Dividal Group siltstone on the basis of microshear zones and floating mica hinges.

The roof thrust is generally much easier to identify because there is commonly a sharp lithologic break (Fig. 2-11), or discordance at the contact. Retrogression and transposition of the metamorphic allochthon up

Figure 2-11: Roof thrust of Matert Shear Zone. View looking northeast at north-central margin of Singis Window. The hanging wall consists of chloritized Vidja Gneiss, while the footwall consists of mylonitic siltstone. Note weakly developed S-C fabric within mylonite.

Figure 2-12: Singis Window. View looking northeast across Singis Window. Matertjakka is at western edge of field of view. Valley floor is predominantly rhyolitic basement and Tornetrask Formation. Note west-dipping units of upper nappe complex truncated by flat-lying Matert Shear Zone below. Rusjka Fault is east of the saddle in the center of the field.

to 50 m above the shear zone does however often make the roof thrust difficult to locate exactly. In the western half of the Singis Window, the roof and sole thrusts of the Matert Shear Zone form a sharp topographic bench (Fig. 2-12).

Lithologic contacts within the Storrit Complex and the Matert Shear Zone are always concordant with no apparent concentration of strain. As such, the contacts are either tectonic contacts, highly strained stratigraphic contacts, or both. As noted by Crowley (1985), the common association of granitic and quartzitic mylonite suggests a possible stratigraphic association between these two rock types.

CORRELATION AND THICKNESS

At its type locality on Storriten at the southwestern end of the Rombak-Sjangeli Window (Plate 7), the Storrit Complex is 1 km thick. Approximately 30 km to the southeast on the east shore of Sitasjaure, the Complex is only 500 m thick. In the Tsutsajaure culmination at the southeast end of the Window, the Storrit Complex has decreased in thickness to approximately 40 m. Thus, over a distance of about 55 km, the Complex is wedge-shaped in cross-section with a 1° taper.

The highly strained matrix of the Storrit Complex and Matert Shear Zone preclude direct correlation with the basement. However, the gross lithologies bear a striking resemblance to undeformed Grunfjell and Dividal Group rocks. I agree with Crowley (1985) and Hodges (1982) on stratigraphic and structural (see below) grounds that all the shear zone rocks were derived by imbrication and deformation of the basement.

Within the Rombak-Sjangeli Window, Kulling (1964) called these shear zone rocks the Middle Allochthon. This name has been used by numerous workers elsewhere in the Caledonides (e.g. Gee and Zachrisson, 1979) for

mylonitic rocks of greenschist grade which separate the high-grade allochthonous units above from presumed autochthonous basement or Lower Allochthon units below. Working north of Storriten on the west side of the Rombak-Sjangeli Window, Gustavson (1966, 1974) named similar shear zone rocks the Storfjell Group. This name is not suitable, as the shear zone is not a continuous stratigraphic sequence, but rather a complex schuppen zone.

UPPER NAPPE COMPLEX

INTRODUCTION

The upper nappe complex consists of a sequence of flat lying to moderately west-dipping greenschist to eclogite grade metamorphic rocks. In the study area, the complex may be subdivided into four distinct packages:

1) The Aurek Assemblage - named for exposures on the peak Stuor Aurek at the southeast margin of the study area (Plate 1). This unit is composed of a sequence of kyanite bearing paragneiss containing discontinuous lenses of meta-gabbro.

2) The Salka Group - named for exposures on the 1910 m peak Salka, 2 km northeast of the study area (Plate 1). This package is composed of a sequence of greenschist grade calc-schist, graphitic schist, and chloritic pasammite.

3) The Litte Group - named for the 1000 m ridge in the central part of the study area. This group is a series of calcareous schists with the typical assemblage: biotite + muscovite + quartz + plagioclase + epidote ± clacite ± garnet ± hornblende. Lithologic contacts within this group are gradational and are presumed stratigraphic.

4) The Maitat Complex - named for the 1473 m peak Maitahatjakka at the south-central margin of the study area. This is the structurally highest

unit in the study area and is characterized by a distictive pale green chlorite + biotite + muscovite + quartz + albite + garnet ± hornblende ± ankerite schist with discontinuous mafic lenses.

The Litte Group and Maitat Complex are correlative with units in the Langvatn Assemblage exposed to the west of Sitasjaure (Crowley, 1985). The Langvatn Assemblage correlates with the Narvik Group of Gustavson (1964, 1966, 1974), Hodges (1982, 1985) and Steltenpohl (1985). Crowley (1985) chose to name this association the Langvatn Assemblage because the Narvik Group is not a continuous depositional sequence, but rather a series of tectonic slices. Lithologically the assemblage is composed of a sequence of amphibolite to kyanite grade calcareous schist and metavolcanic rocks.

Over 40 km northwest of the study area, along the west coast of Norway, the Langvatn Assemblage is overlain by marbles, calc-schists, pelites and amphibolites of the Salangen Group (Hodges, 1982, 1985, Steltenpohl, 1985). The contact between these two units is considered to be upright, because the Elvenes Conglomerate which contains clasts of Langvatn Assemblage (Narvik Group) lithologies occurs at the base of the Salangen Group (Hodges, 1982, 1985, Tull et al., 1985, Steltenpohl, 1985).

Workers in the central Scandinavian Caledonides more than 250 km to the south have subdivided the upper nappe complex into a series of thin laterally continuous tectonostratigraphic packages (e.g. Gee 1975; Gee and Zachrisson, 1979; Dyrelius et al., 1980; Stephens et al., 1985). In this area, the lower sequence of schist, amphibolite and gneiss, called the Seve nappe, is overlain by locally fossiliferous Ashgillian to Llandoverian graphitic phyllite and quartzitic wacke, called the Lower Koli. These rocks are in turn overlain by a sequence of calcareous phyllites and epidote amphibolite, called the Middle Koli. Arguments to be presented in

Chapter 6, tentatively correlate the Aurek Assemblage, Salka Group and Langvatn Assemblage of the study area with the Seve, Lower Koli and Middle Koli respectively of the central Caledonides.

Much of the deformation within the upper nappe complex predates deformation in the underlying basement and shear zone rocks. Only the latest stages of folding, faulting and retrogressive metamorphism in the upper nappe complex can be correlated with development of the shear zone (see Chapter 3).

Because the upper nappe sequence consists of gently west-dipping units, the structurally lowest unit, the Aurek Assemblage is exposed at the southeastern margin of the study area (Plate 1). The overlying Salka Group is exposed in the east-central portion of the area, while the structurally highest Litte Group and Maitat Complex forms its western half.

While the upper nappe complex has been disrupted by faulting, a more or less continuous tectonostratigraphic section is present in the study area (Plate 5). The westerly dip of the Aurek Assemblage and Salka Group with respect to the underlying shear zone has resulted in the westward wedging out of these units. However, the more flat-lying Litte Group crops out above the shear zone rocks of the Storrit Complex for more than 25 km to the northwest.

No stratigraphic facing indicators were found in the upper nappe complex of the study area. Based on structural relationships between the Langvatn Assemblage and overlying upright Elvenes Conglomerate (Hodges, 1982), Crowley (1985) argued that the Langvatn Assemblage west of Sitasjaure (and therefore in the study area east of Sitasjaure) is overturned. The argument is based on the following observations:

1) Below the Elvenes Conglomerate, the Langvatn Assemblage has been folded into a major isocline (Hodges, 1982, 1985),

2) The northern limb of the isocline crops out below the Elvenes Conglomerate,

3) The southern limb projects south across Langvatnet to the west shore of Sitasjaure.

Hodges (1982) argued that the structurally highest northern limb directly beneath the upright unconformable contact with the overlying Elvenes conglomerate is the upright limb. This implies that the southern limb and therefore the entire Langvatn Assemblage southwest of Sitasjaure is overturned (Crowley, 1985).

While this interpretation is appealing, it is not unique:

1) Assuming the northern limb of the isocline to be upright is only the simplest interpretation. If the isocline developed prior to deposition of the Elvenes Conglomerate, a structurally higher limb may have been removed by erosion during the depositional hiatus.

2) The isocline may not exist. While Hodges (1982) presents compelling evidence for the existence of this structure, no fold closure crops out.

3) Structural complexities southwest of Sitasjaure may prohibit straightforward projection of the overturned limb from the Efjord area to Maitahatjakka, 60 km to the southeast.

Because the facing direction of the Langvatn Assemblage, and indeed the other units of the upper nappe complex in the study area, is equivocal, references to top and bottom, etc. are with respect to the present orientation of the units.

AUREK ASSEMBLAGE

INTRODUCTION

The Aurek Assemblage is a sequence of kyanite bearing paragneiss with discontinuous lenses of amphibolite and meta-gabbro. This assemblage is the highest grade unit in the study area, with eclogite parageneses in the meta-gabbro body. The Aurek Assemblage has been overprinted by a biotite grade metamorphism and a variable mylonitization of the unit. In the study area, the Aurek Assemblage is subdivided into four distinctive lithologies which are discussed below.

AUREK GABBRO

The Aurek Gabbro is named for exposures of this unit on the peak Stuor Aurek about 3 km southwest of Singistugorna in the Tjaktjavagge Valley (Plate 1). This unit consists of a lens of gabbro approximately 6 km in length and up to 1500 m thick. Composed of very resistant eclogitic gabbro, the Aurek Gabbro forms the two peaks Stuor Aurek and Unna Aurek at the southeast border of the study area. The gabbro strikes approximately N30E and dips 30-40W, similar to other units in the eastern part of the area. It does not crop out north of of the Singis Window (Plate 1), although a thin amphibolite body is present (see below). Reconnaissance mapping indicates the Aurek Gabbro pinches out south of Unna Aurek.

In the field, the Aurek Gabbro crops out as resistant white, olive-green to rust-brown ridges. The color variations are due to variations in protolith compositions, and degree of eclogitization and amphibolitization. The unit has been variably sheared and deformed, although the internal portions of the lens are typically massive and unfoliated.

The protolith and predominant rock type of the Aurek gabbro is a medium-grained (1-5 mm) granoblastic plagioclase + olivine + augite +

magnetite gabbro. The gabbro has been variably metamorphosed at eclogite facies. Igneous olivine commonly has multiple corona structures: an internal corona of enstatite and an external one of garnet (Fig. 4-2). Fine needles and prisms of kyanite and zoisite respectively are ubiquitous in the labradoritic plagioclase. Brown barroisitic amphibole is commonly associated with relict magnesio-augite. Augite is also typically riddled with a fine mesh of opaques, possibly rutile exsolution lamellae. A thin rust-weathering sliver of olivine - gabbro crops out on the north slope of Stuor Aurek.

The eclogite metamorphic assemblages have been variably overprinted by a later amphibolite metamorphism. This later metamorphism is strongest in shear zones within the Aurek gabbro. Typical amphibolite mineral assemblages include: hornblende + plagioclase + zoisite + calcite, and hornblende + scapolite + plagioclase + garnet. Where the shear zone amphibolitization is incomplete, mylonitic fabrics have developed with medium-grained (0.5-1.5 mm) garnet, pyroxene, and/or olivine porphyroclasts set in a fine-grained (0.05-0.1 mm) scapolite, plagioclase and/or hornblende neoblast matrix.

The Aurek Gabbro is encased by an amphibolite sheath 50-150 m thick. The gabbro is separated both above and below from the Vidja gneiss by this amphibolite. As noted above, both the degree of strain and amphibolite metamorphic assemblage increase toward the rim of the gabbro lens. The contact with the encasing Aurek Amphibolite is thus gradational on the scale of 10-50 m.

AUREK AMPHIBOLITE

The Aurek Amphibolite is a 50-100 m thick unit surrounding the Aurek Gabbro. It is named for outcrops on the east and west slopes of Stuor

Aurek. While the Aurek gabbro does not crop out north of the Singis Window, a thin horizon of the Aurek Amphibolite is present.

In hand sample, the unit is dark green to black with leucocratic plagioclase and scapolite horizons. Large (1-10 m) white gabbroic facoids occur throughout, the number increasing towards the Aurek Gabbro. In thin section, the amphioblite is well-foliated and commonly mylonitic. Mineral assemblages vary from hornblende + plagioclase + garnet + zoisite + magnetite ± biotite to actinolite + scapolite + calcite + quartz + garnet. As in the Aurek Gabbro, the Aurek Amphibolite has been locally mylonitized under greenschist facies conditions. Samples typically contain 0.5-1.0 mm hornblende and plagioclase porphyroclasts set in a fine-grained hornblende + plagioclase + calcite + zoisite + quartz matrix.

The Aurek Amphibolite is a reaction skarn (Brady, 1977) between the mafic Aurek Gabbro lens and quartzofeldspathic rocks of the surrounding Vidja Gneiss. "Black walls" of this type are a common feature associated with alpine-type eclogite pods encased in quartzo-feldspathic matrices (eg. Phillips and Hess, 1936; Sack, 1982).

VIDJA GNEISS

The Vidja Gneiss was named for a moderately west dipping (30-40°) sequence of quartzofeldspathic, muscovite and biotite gneiss that crops out northeast of Vidjajaure (Plate 1). The unit reaches its maximum structural thickness of about 1.5 km at the southeastern border of the study area. According to Kulling (1964) the Vidja Gneiss becomes even more areally extensive 10 km to the south, although its thickness cannot be determined from his map. While the main sequence of Vidja Gneiss crops out above the Aurek Gabbro in the study area, over 100 m of quartzofeldspathic gneiss is exposed on the east face of Stuor Aruek below the gabbro. The Vidja

Gneiss is also exposed along strike to the north of the Singis Window. Exposures of this unit to the east and northeast disappear below the Quaternary fill of the Tjaktjavagge glacial valley (Plate 1).

The Vidja Gneiss is lithologically heterogeneous, and was subdivided into three distinct units. The lowest unit is a somewhat massive weakly foliated light grey quartzo-feldspathic muscovite gneiss. Its basal contact with the Aurek Amphibolitie is very sharp, and can be followed north of the Singis Window. Mineralogically, the quartzofeldspathic gneiss consists of quartz + plagioclase + biotite + muscovite + garnet + kyanite ± calcite ± tourmaline. Plagioclase, muscovite and pink garnet occur as 1-5 mm porphyroclasts set in a fine-grained (0.1-0.5 mm) matrix of quartz, plagioclase, muscovite and biotite. Porphyroclasts of muscovite are typically folded and floating (Fig. 2-13), plagioclase commonly has deformation lamellae, whereas garnet is porphyroclastic, poikilitic and retrograded to biotite. Biotite has overgrown these earlier phases, and forms idioblastic aggregates with no preferred orientation.

Minor discontinuous lenses of foliated porphyroblastic muscovite gneiss occur throughout the quartzofeldspathic gneiss unit. These lenses become more abundant at structurally higher levels, such that a continuous unit 100-200 m thick of muscovite gneiss overlies the quartzofeldspathic gneiss. The contacts between the two lithologies are everywhere gradational. Characteristic muscovite gneiss is orange-brown and well foliated, with intrafolial muscovite porphyroblasts up to 2 cm in diameter. Mineralogically the muscovite gneiss is very similar to the quartzofeldspathic gneiss, but with a much greater abundance of muscovite and biotite.

North of the Singis Window, the muscovite gneiss forms the highest

Figure 2-13: Vidja Gneiss thin section. Field of view is 12mm. Note 1-5mm porphyroclasts of muscovite, feldspar and garnet. The matrix is characterized by secondary idioblastic biotite.

Figure 2-14: Biotite gneiss member of Vidja Gneiss. Note the sub-horizontal segregated gneissic foliation truncated by steep anastomosing shear zones. These shear zones have normal separation in the field. View is to northwest approximately 1 km northeast of Vidjajaure.

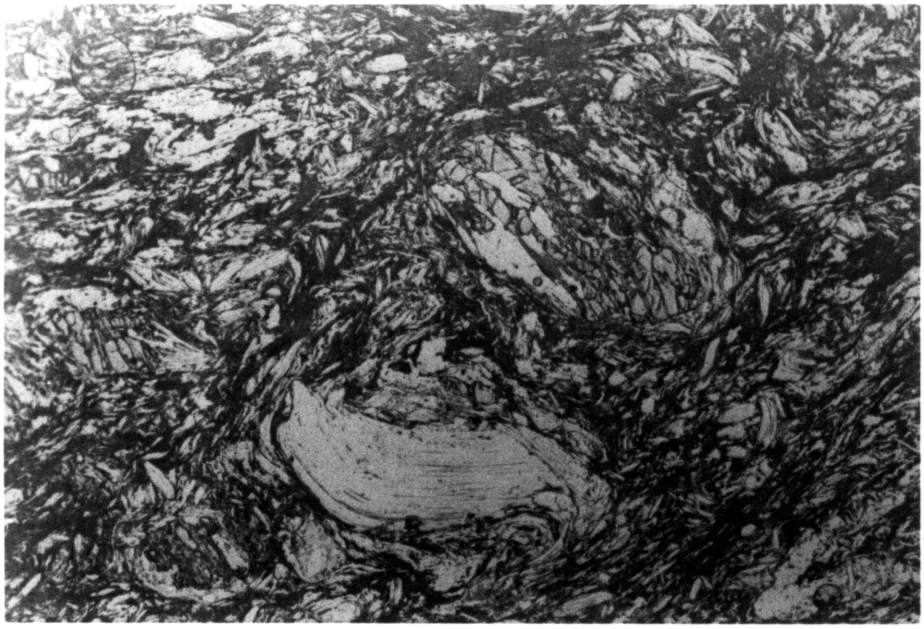

unit of the Vidja Gneiss, whereas south of the window it is gradationally overlain by the biotite gneiss unit.

The third unit in the Vidja Gneiss is a light to dark grey biotite gneiss with a strongly segregated gneissic foliation (Fig. 2-14). In thin section, this unit consists of leucocratic plagioclase bands, and thin melanocratic biotite + garnet + epidote ± hornblende lamellae. Similar to rocks in the quartzofeldspathic unit, garnet appears to be a retrogressed primary phase, overgrown in melanocratic shear zones by idioblastic biotite.

The upper contact of the Vidja Gneiss is formed by a sharp but complex shear zone called the Rusjka Fault (see Chapter 3) with Rusjka Calcareous Schist in the hanging wall.

VIDJA AMPHIBOLITE

A thin (10-50 m) discontinuous amphibolite crops out north and northeast of Vidjajaure between the Vidja biotite gneiss below, and Rusjka Calcareous Schist above (Plate 1). The unit is dark green to black in hand sample, moderately foliated and commonly strongly lineated (N60W-N90W). The Vidja Amphibolite is lithologically distinct from the Aurek Amphibolite below. It typically consists of hornblende + plagioclase + epidote + calcite ± garnet. The hornblende is blue-green, in contrast to olive-green hornblende in the Aurek Amphibolite. Whereas garnets in the Aurek Amphibolite are euhedral, and inclusion free, garnets in the Vidja Amphibolite are poikilitic, retrogressed and porphyroclastic.

The Vidja Amphibolite is correlated with the high-grade units of the Vidja and Aurek complexes below, rather than the relatively low-grade schists and psammites of the Salka Group above for the following reasons:

1) While garnet-hornblende amphibolite occurs in the Aurek Assemblage

no amphibolite is exposed within the schists and psammites above the Rusjka Fault.

2) The Rusjka Fault cuts out footwall units to the north, as evidenced by the disappearance of the Vidja biotite gneiss north of the Singis Window (Plate 1). Northeast of the study area, the Vidja Gneiss apparently has been cut out completely (Kulling, 1964). Similarly the most southerly exposure of the Vidja Amphibolite in the study area (500 m north of Vidjajaure) is also the thickest. The unit gradually thins to the northeast and does not crop out north of Rusjkajaure.

SALKA GROUP

INTRODUCTION

The Salka Group is a sequence of greenschist to lower amphibloite facies calcareous, graphitic, and psammitic schists. This Group is the lowest grade unit within the upper nappe complex of the study area; it is underlain by the kyanite-bearing Aurek Assemblage, and overlain by the amphibolite facies Litte Group. The Salka Group is subdivided into three distinctive units which are described below.

RUSJKA CALCAREOUS SCHIST

The Rusjka Calcareous Schist is named for exposures southeast of the mountain Rusjka in the southeastern part of the study area (Plate 1). Outcrops of this unit are also present northeast of the Singis Window, and in the hinge area of the Tsutsa anticline west of Matertjakka (Plate 1). In the eastern part of the study area, the Rusjka Calcareous Schist lies above the Vidja biotite gneiss and amphibolite, forming the hanging wall of the Ruskja Fault. In the western part of the area, the unit lies directly above shear zone rocks of the Storrit Complex.

The Rusjka Calcareous Schist consists of a heterogeneous assemblage of

chloritic psammite, marble, garnet-two-mica schist, garnet-hornblende -calcite schist, graphitic schist, and greenschist. Psammite forms the dominant matrix of this unit, with the other lithologies forming discontinuous lenses up to 200 m in length. The marble units are grey to light brown weakly foliated ankeritic zones with thin dark brown pelitic laminae. Greenschist is typically dark green and well-foliated with coarse-grained sub-idioblastic zoisite set in an epidote-actinolite -margarite-chlorite-quartz matrix. Garnet-muscovite-chlorite-biotite -albite-apatite schist has characteristic intrafolial quartz stringers. Euhedral garnets within this unit show evidence of syntectonic growth, followed by deformation at greenschist grade (see Chapter 3).

RUSJKA GRAPHITIC SCHIST

In sharp contact above the Rusjka Calcareous Schist is the Rusjka Graphitic Schist. Although thin (25-50 m), this unit is continuous within the study area. The graphitic schist weathers a dark rust, although fresh surfaces are black with white quartz stringers. In thin section, the unit consists of a well-foliated quartz-muscovite-graphite-albite schist.

The Rusjka Graphitic Schist is a characteristic marker unit in the eastern part of the study area. Reconnaissance mapping by Kulling (1964) has shown this unit to continue more than 10 km to the south. He also considers this unit to be the southerly continuation of the graphitic schist formation above the Nuolja marble in the western part of the Tornetrask area, 60 km to the north-northeast.

PATTA QUARTZITE

The green-grey Patta Quartzite was named by Kulling (1964) for exposures of this unit on Pattatjakka 5 km southwest of Vidjajaure. This unit forms the bulk of the two peaks, Rusjka and Salka which dominate the

the topography in the southeast part of the study area (Plate 1). On Rusjka and to the west, the Patta Quartzite dips gently west and has a structural thickness of about 2 km. Macroscopic and mesoscopic evidence (see Chapter 3) suggest this thickness is the result of tectonic repetition within the sequence.

The Patta Quartzite is predominantly a monotonous well foliated green-grey quartz-plagioclase-chlorite-muscovite-biotite-magnetite psammite. The green-grey color of this unit is because of abundant (up to 20%) pea-green idioblastic chlorite. The unit appears to coarsen upwards into a gritty quartzite in exposures north of Tjuolak. Here, deformed quartz and feldspar clasts are up to 2 mm in diameter. Coarsening continues upwards, such that on the east slope of Kaitumtjakka, a 1-3 m thick quartz pebble conglomerate layer is present (Fig. 2-15). The clasts are 1-4 cm in diameter, and supported by a pelitic matrix. Isoclinal folding has resulted in clasts being spherical at fold hinges and elongated up to 6:1 on fold limbs.

The basal contact of the Patta quartzite with the Rusjka Graphitic Schist is very sharp, but its upper contact with the overlying Njunjas and Rapetjakka schists is complex and will be discussed below.

East of Tjuolakjaure (Plate 1), a blue-grey quartzite crops out, and forms the western dip slope of Kuorkopare (Fig. 2-16). The flaser texture of this unit is due to elliptical quartz lenses 2-4 cm in length, separated by micaceous horizons 1-3 mm thick (Fig. 2-17). In thin section, the quartz lenses are aggregates of dislocation free, randomly oriented microcrystalline quartz. Fine-grained idioblasts of garnet and chlorite are present within the lenses. The micaceous layers are predominantly muscovite with subordinate chlorite. Along strike, about 5 km to the northwest, the distinctive blue-grey color and flaser texture of this zone

Figure 2-15: Patta Quartzite pebble conglomerate. Sub-spherical to strongly attenuated quartz pebbles in psammitic matrix. View to north on east slope of Kaitumtjakka, 2.5 km southwest of Tjuolakjaure. Note early foliation (bedding?) has been transposed by west-dipping SGd1 foliation.

Figure 2-16: Patta Quartzite lenticular zone. Located in stream valley approximately 1 km southeast of Tjuolakjaure.

Figure 2-17: Patta Quartzite lenticular zone. Close-up indicates flaser texture of this zone is due to elliptical quartz lenses 2-4 cm in length, separated by micaceous horizons 1-3 mm thick.

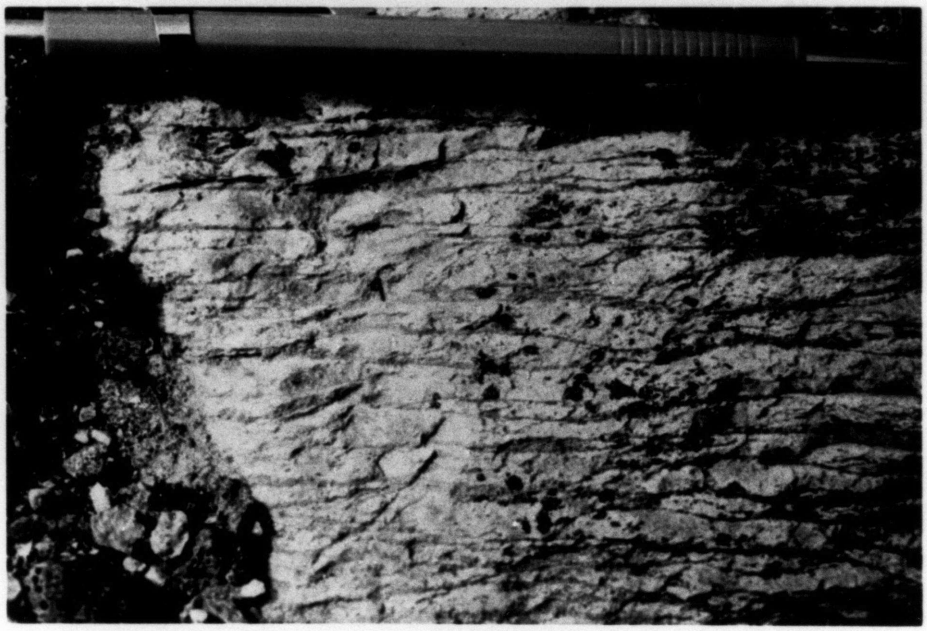

has disappeared, and has been replaced by gritty quartzite more characteristic of the upper Patta quartzite. Thin section study of the unit at this locality reveals it has a blastomylonitic fabric. Quartz grains up to 5 mm in diameter have high dislocation densities, and in some cases have been completely replaced by fine-grained strain free neoblasts. Quartz throughout this sample has a strong preferred orientation, with c-axes orthogonal to the foliation. Neither chlorite, garnet, nor biotite are present at this locality.

Several possibilities exist for the origin of the blue-grey quartzite:

1) Relict sedimentary structure. As noted above, on the outcrop scale this unit contains structures reminiscent of flaser bedding (Reinick and Wunderlich, 1968). Conglomerate as a protolith for this unit is precluded by the gradational nature of the quartzitic and micaceous segregations.

2) Metamorphic differentiation. Williams (1972) has described the segregation of quartz and layer silicates in metamorphic rocks. The layers apparently developed by the selective dissolution, removal and reprecipitation of quartz during the development of strain slip cleavage. This produced layers relatively rich in easily deformed mica alternating with mechanically resistant but easily dissolved quartz layers. The lack of fabric and random orientations of chlorite and small garnet idioblasts within the quartz lenses further suggests that strain was accommodated in the mica rich horizons.

The contact with the overlying Njunjas and Rapetjakka schists is gradational and pelitic layers increase in frequency and thickness at structurally higher levels. However, on the outcrop scale contacts between psammitic and pelitic horizons are very sharp (Fig. 2-18).

The observations presented above will be syntheiszed and amplified in

Figure 2-18: Tjuolak Thrust sliver zone. Alternating layers 0.1-1m thick of pelite and psammite characterize contact between Patta Quartzite and Litte Group. View to west approximately 1.5 km south-southest of Tjuolakjaure.

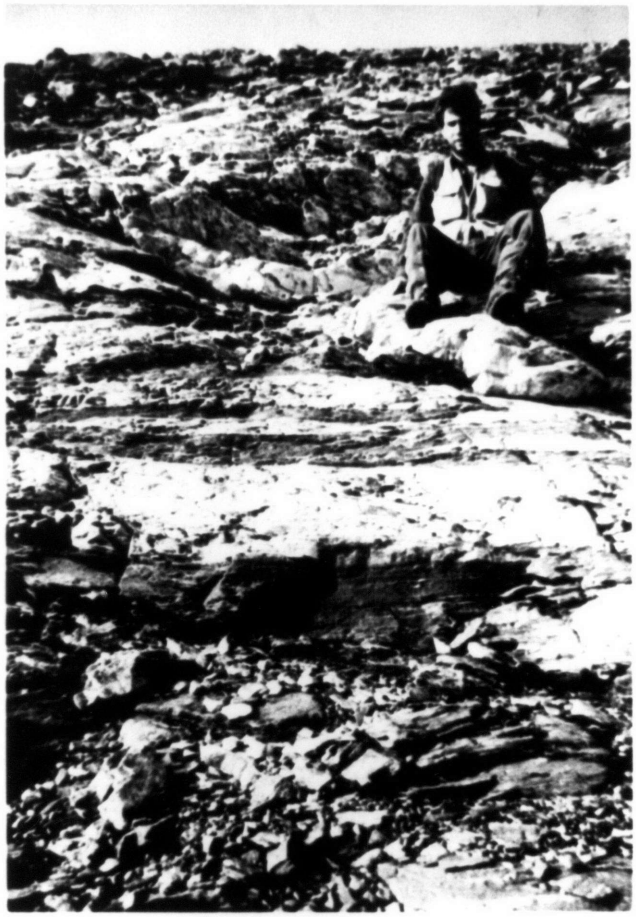

Chapter 3 to argue that the upper contact of the Patta Quartzite is a major shear zone separating genetically very different lithologies.

LITTE GROUP

INTRODUCTION

The Litte Group is a sequence of subhorizontal calcareous schists that crop out in the western half of the study area. In the Sitas-Singis area the group is subdivided into two formations: the Njunjas Schist and the Rapetjakka Hornblende Schist whose type localities are to the west of Sitasjaure (Plate 7; Crowley, 1985, Plate 1). In the area west of Sitasjaure, the Rapetjakka Schist is gradationally overlain by the Skjafjell Schist (Crowley,1985), which is therefore considered to be part of the Litte Group.

NJUNJAS SCHIST

The Njunjas Schist was named by Crowley (1985) for exposures on the Swedish Mountain Njunjas, southwest of Sitasjaure. In its type area, the Njungas Schist consists of a heterogeneous sequence of calcareous psammite and garnet two-mica schist. East of Sitasjaure, the Njunjas Schist was subdivided into structurally lower and upper members.

The lower Njunjas member consists of a dark grey quartz-albite-biotite -muscovite schist with abundant thin quartz stringers. In the study area, this unit crops out on Rassepakte west of Tutturjaure (Plate 1). Several discontinuous graphitic schist zones also crop out within the lower Njunjas.

The base of the lower Njunjas is marked by the roof thrust of the Storrit Complex. The upper contact of this member with the upper Njunjas schist is gradational and presumed stratigraphic.

The upper Njunjas member consists of quartz-plagioclase-garnet-biotite

-muscovite schist. Southwest of Tutturjaure, the basal contact of the upper Njunjas member with the lower Njunjas member is marked by the first appearance of garnet. East of Tutturjaure, the lower Njunjas member has been truncated by the Storrit Complex, placing garnetiferous upper Njunjas member directly on shear zone rocks. The upper Njunjas member is relatively subhorizontal and has a large areal distribution within the study area. Exposures of the member occur south of Tutturjaure on Skelta, southwest of Kaisejaure, and as far south as Ainavarto. In addition to graphitic zones, discontinuous marble and psammite lenses up to 10 m thick crop out throughout the upper Njunjas.

Mineralogically, the upper Njunjas is composed of garnet + biotite + muscovite + quartz + albite ± ilmenite ± chlorite ± calcite ± tourmaline ± apatite. Garnets typically form euhedra with varying degrees of chloritic retrogression.

RAPETJAKKA HORNBLENDE SCHIST

The Rapetjakka Hornblende Schist lies in gradational and presumed stratigraphic contact above the Njunjas Schist. It was named by Crowley (1985) for exposures on Rapetjakka southwest of Sitasjaure. In the study area, the Rapetjakka Hornblende Schist was subdivided into two distinctive lithologies; a lower garnetiferous unit, and an upper muscovite bearing unit.

The lower Rapetjakka Hornblende Schist member is a medium grey-weathering unit with discontinuous grey to brown marble and calc-schist lenses. The lower contact with the upper Njunjas member is gradational and marked by the first appearance of hornblende. In many places the hornblende occurs as large garben (Spry, 1983), but commonly they occur as small (1 cm) acicular prisms.

Mineralogically, the lower Rapetjakka Hornblende Schist member is more calcareous than the upper Njunjas member, with ankerite being a common phase. Typical mineralogy for this unit is: garnet + hornblende + quartz + biotite + muscovite + albite ± ankerite ± chlorite ± ilmenite ± apatite. Secondary cross foliation biotite is common and forms an intersection lineation trending approximately N70W. Idioblastic garnet and hornblende commonly contain planar helicitic quartz inclusion trails indicating post-tectonic growth of these phases (Fig. 2-19).

The base of the overlying muscovite-bearing upper Rapetjakka Hornblende Schist member is also gradational and presumed stratigraphic. The contact is marked by the disappearance of garnet, and a relatively abrupt increase in muscovite content, giving the unit a light grey reflective color.

The mineralogy of this member is muscovite + hornblende + biotite + epidote + ankerite + quartz + plagioclase ± ilmenite ± chlorite. Similar to the lower Rapetjakka Hornblende Schist, secondary cross-foliation biotite books and randomly oriented hornblende idioblasts appear to have grown after the final schistostity development.

The relatively subhorizontal Rapetjakka Hornblende Schist is the most areally extensive unit in the study area; exposures extend from the east shore of Sitasjaure in the west, to Tjuolak in the east (Plate 1). As noted above, south of Tutturjaure the Rapetjakka Hornblende Schist lies stratigraphically above the Njunjas Schist. However, to the east, from Kaisejaure south to Kaitumtjakka, Rapetjakka units are interleaved with psammite of the underlying Patta Quartzite (Plate 1).

Figure 2-19: Rapetjakka Hornblende Schist thin section. Field of view is 4 mm. Idioblastic garnet has statically overgrown LGd1 foliation.

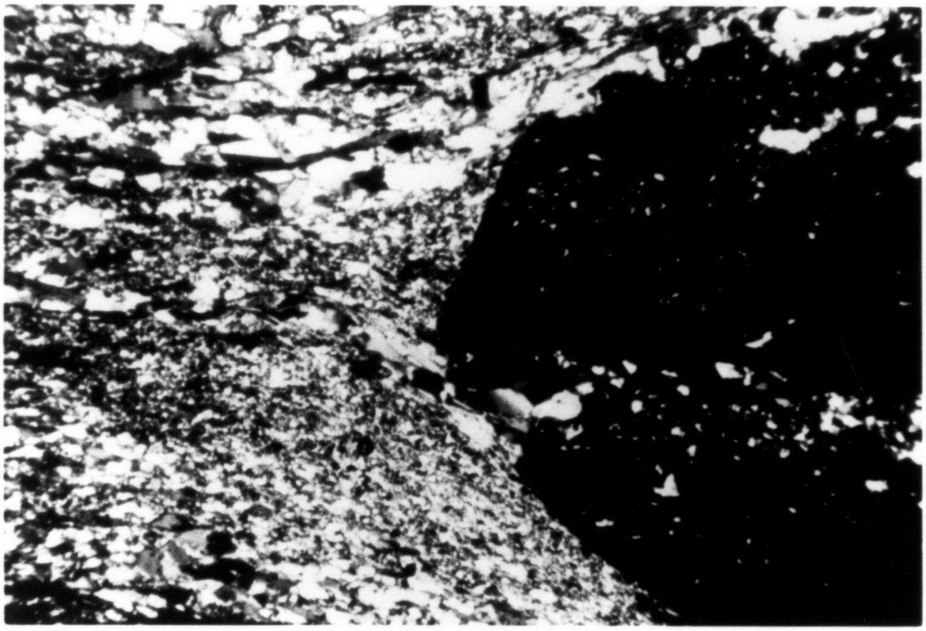

MAITAT COMPLEX

In sharp apparent tectonic contact (see Chapter 3) above the Rapetjakka Hornblende Schist is the Maitat Complex. The Maitat Complex is structurally the highest unit in the area forms a large (8 km diameter) klippe (Plate 1).

On Maitahamatjakka, the Maitat Complex is a chaotic calcareous schist containing discontinuous pods of marble and mafic rocks. Correlation of the Maitat Complex with the Filfjell Complex (Crowley, 1985) on Filfjell 40 km to the northwest is based on:

1) Similarity of distinctive matrix schist at both localities (see below).

2) Occurrence of mafic and calcareous pods at both localities. An important difference between the two localities is the absence of ultramafic pods on Maitahatjakka.

3) At both localities, the Filfjell Complex and the Maitat Complex lie in direct contact, structurally above the Rapetjakka schist.

Mafic pods in the study area range in size from a few meters to over 1 km in length. In outcrop, the pods are massive and weather a dark green. Thin sections show the pods contain up to 50% sub-idioblastic to granoblastic pea-green chlorite, and 30% lime-green idioblastic epidote. Calcite and ilmenite make up the remainder of the sample, with chloritized hornblende occasionally present.

Marble pods weather orange-brown, and typically contain quartz + calcite + plagioclase + muscovite + ilmenite.

The matrix of the Maitat Complex consists of a very distinct hornblende-garnet-chlorite-biotite-ilmenite-muscovite-plagioclase-quartz -epidote schist. The unit is typically pale green because of its high primary chlorite content. As in the underlying Rapetjakka Hornblende

Schist, hornblende forms late (post schistosity) random idioblasts.

The presence of discontinuous mafic and ultramafic pods within the Filfjell Complex led Crowley (1984) to consider this unit a tectonic melange developed in the accretionary prism of a subduction complex. While no ultramafic pods were found in exposures of the Maitat Complex in the study area, Crowley's interpretation appears plausible.

CHAPTER 3: STRUCTURE OF THE SITAS - SINGIS AREA

INTRODUCTION

Caledonian deformation within the Sitas-Singis area can be subdivided into eight temporally distinct events (D1 through D8). Different tectonostratigraphic elements within the study area experienced different combinations of these deformational events.

Within a given element, several deformational phases distinguished on the basis of structure may often be associated with a single event. In addition, a single continuous phase may have evolved during two or more deformational events. For this reason, the study area is subdivided into eight tectonostratigraphic elements. Structures and structural relationships within each element are described in terms of specific deformational phases. For example, the first Caledonian deformation phase to affect the Rombak-Sjangeli basement is termed RSd1, and occurred during the D4 deformational event. Also, some deformational phases (eg. RSd2 to RSd5) all occurred during a single deformational event.

Table 3-1 lists the eight deformational events that affected the area, and the main structures associated with them. These events may be subdivided into several groups:

1) D1 and D2 are associated with the high-grade metamorphism of units within the upper nappe complex.
2) D3 is a post-metamorphic imbrication of the different units within the upper nappe complex and early obduction of the complex onto the Baltic Shield basement.
3) D4 through D6 are associated with continued emplacement of the amalgamated upper nappe complex onto the Baltic Shield basement.
4) D7 is a post thrusting event that warps and backfolds the entire

TABLE 3-1. DEFORMATIONAL EVENTS IN THE SITAS-SINGIS AREA

D1: Deformation and associated upper amphibolite to eclogite facies metamorphism of Aurek Assemblage and Maitat Complex. Penetrative schistosity in Maitat Complex, completely transposed in Aurek Assemblage. Late Cambrian or Early Ordovician.

D2: Deformation and associated greenschist to amphibolite facies metamorphism of Salka and Litte Groups. Penetrative schistosity in Salka and Litte Groups. Metamorphic peak in Litte Group post-dates schistosity development. Late Ordovician to Early Silurian.

D3: Imbrication of upper nappe complex and early thrusting onto Baltica. Associated upper greenschist to lower amphibolite facies metamorphism. Southeast-vergent mylonite and syn-tectonic garnet along thrust faults. Penetrative schistosity in Aurek Assemblage. Silurian.

D4: Thrust faulting of upper nappe complex on Storrit Complex. Associated greenschist facies metamorphism of Storrit Complex and basement. Southeast-vergent mylonite within Storrit Complex and in upper nappe complex and basement near this shear zone. Silurian to Early Devonian(?).

D5: Thin-skinned detachment of Rombak-Sjangeli Window and thrusting on Matert Thrust. Southeast-vergent mylonite of Matert Shear Zone and folds and faults within Rombak-Sjangeli Window. Silurian(?) to Early Devonian (?).

D6: Thin-skinned detachment of Singis Window. Warping of units along northwest trending axes. Silurian(?) to Early Devonian.

D7: Backfolding. North trending, west-vergent backfolds deform entire sequence. Strongly developed in western part of study area. Devonian.

D8: West-vergent normal slip shear and extension within upper nappe complex. Northwest-vergent ductile shear zone with associated mesoscopic folds. Devonian to Carboniferous(?).

sequence.

5) D8 is a late extensional event recorded within the upper nappe complex in the eastern part of the study area.

Plate 6 is a table which relates deformational phases within each tectonostratigraphic element to the aforementioned eight events. Also listed are the approximate ages for the events based on regional considerations, and $^{40}Ar/^{39}Ar$ data (see chapters 5 and 6).

In this chapter, each tectonostratigraphic element and its associated deformational phases are described and discussed. This is followed by a discussion relating these phases to one another and the eight deformational events.

Fig. 3-1 is a domainal map of the Sitas-Singis area. The study area is subdivided into twenty structural domains. Equal area stereographic projections for many of the structural elements in each domain are included in Appendix A.

ROMBAK-SJANGELI BASEMENT

INTRODUCTION

As outlined in chapter 2, the Rombak-Sjangeli basement in the study area is composed of Proterozoic intrusive, metavolcanic and metasedimentary rocks of the Grunfjell Group overlain by Vendian to Middle Cambrian clastic sedimentary rocks of the Dividal Group. Precambrian structures and fabrics are present within the Grunfjell Group, and they have been overprinted by Siluro-Devonian structures that affected both the Grunfjell and the Dividal Groups.

Detailed mapping of the Rombak-Sjangeli basement in the study area indicate that six phases of Caledonian deformation affected rocks of this tectonostratigraphic element. Relative timing of the deformational phases

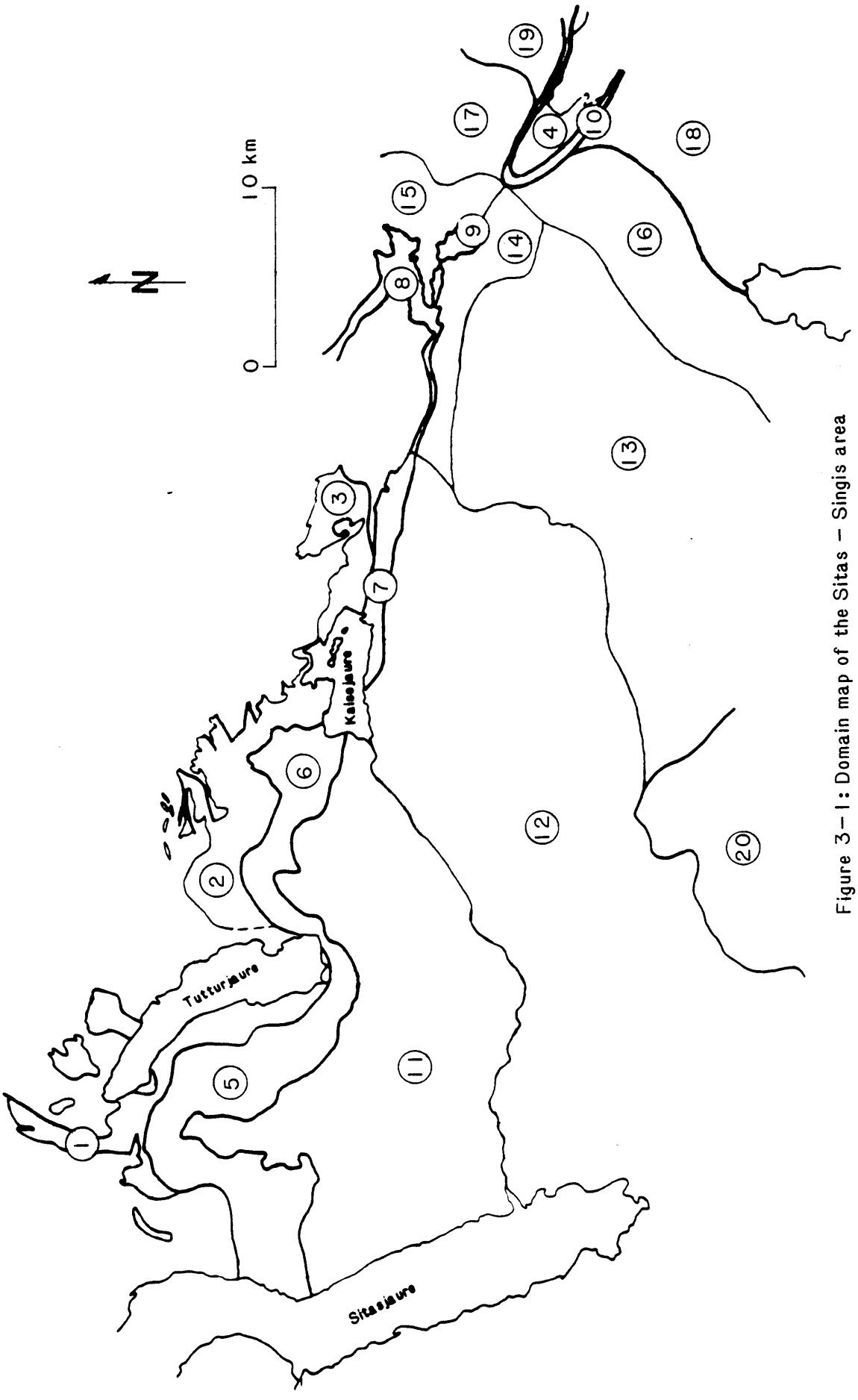

Figure 3–1: Domain map of the Sitas – Singis area

was determined from cross-cutting relations and interference patterns. All deformational phases are associated with S60E directed transport of the overriding upper nappe complex. Phases were distinguished on the basis of structural style (i.e. folds, faults and distributed shear strain). In most cases there is significant temporal overlap between the different deformational phases. This evidence combined with metamorphic and geochronological data (see chapters 3 and 4) suggest that all the Caledonian deformation within the Rombak-Sjangeli basement is associated with final emplacement of the upper nappe complex onto the Baltic Shield.

The Precambrian structures within the Grunfjell Group are reviewed, followed by a discussion of the Caledonian deformational phases (RSd1 through RSd6) that affected the Rombak-Sjangeli basement.

PRECAMBRIAN DEFORMATION

As noted in Chapter 2, the Grunfjell sedimentary rocks are the oldest unit within the Grunfjell Group, and typically contain a shallowly dipping foliation, which is absent in the younger Grunfjell Greenstone and Granite (Fig. 2-4). Crowley (1985, p. 82) noted a similar foliation within the Skaddaive mafic schists northeast of Sitasjaure.

Grunfjell Group units typically contain ductile shear zones striking N30E and dipping 50-60NW. Hodges (1982) and Crowley (1985) argued that these shear zones are Precambrian structures because they do not cut the sole thrust of the overriding Caledonian allochthon, but they are typically rotated into parallelism with the sole thrust. However, in the Kaisejaure area (Plate 4), basement involved shear zones with similar geometries also deform the Dividal Group sedimentary rocks implying that they are post-Middle Cambrian and therefore Caledonian. Also, the relatively consistent N30E strike of the shear zones in the basement is parallel to

other Caledonian structures developed within the Dividal Group and overlying shear zone. Thus, while it is possible that some shear zones are Precambrian, many if not all are certainly Caledonian.

CALEDONIAN DEFORMATION

RSd1-northeast trending, southeast vergent tight to isoclinal folds and basement involved thrusts

The earliest Caledonian deformation phase in the rocks of the Rombak-Sjangeli basement are northeast-trending, southeast-vergent tight to isoclinal folds with subhorizontal axes (Fig. 3-2). These folds developed irregularly within the Rombak-Sjangeli basement of the study area. The best examples are folds within Dividal Group sedimentary rocks northwest and northeast of Kaisejaure (Plates 1 and 4), and locally northwest of Tutturjaure and in the Tsutsajaure culmination (Plate 1).

Commonly associated with these RSd1 folds are southeast-vergent thrust faults that typically place Grunfjell granite or greenstone of the hanging wall on sedimentary rocks of the lower Tornetrask Formation of the footwall (Plate 4, Fig. 3-3). These thrust faults are developed as ductile shear zones with mylonitic fabrics penetrating up to 2 meters above and below the fault contact (Fig. 3-4).

In the footwall of RSd1 thrust faults, conglomerate of the lower sandstone member of the Tornetrask Formation are sensitive monitors of and record the associated finite strain. The lower sandstone member is commonly unstrained with sub-spherical clasts (Fig. 2-7). Within 10-20 meters of RSd1 thrust faults, a penetrative stretched pebble lineation is developed. The lineation has a well constrained mean trend of 0° to S60E (Fig. A-15). Within 2 meters of the fault, dynamic recrystallization of quartz clasts within the pebble conglomerate is well developed, with high

Figure 3-2: RSd1 southeast-vergent fold. View to north approximately 2.5 km north-northwest of Kaisejaure. N10E trending fold is cored by lower sandstone member of Tornetraxk Formation.

Figure 3-3: RSd1 southeast-vergent thrust fault. View to north approximately 1.5 km north of Kaisejaure. Thrust fault dips 10° north with Grunfjell Granite in the hanging wall, and red and green siltstone member of the Tornetrask Formation in the footwall.

Figure 3-4: RSd1 basement involved shear zone. Close-up view of shear zone associated with thrust fault of Fig. 3-3. Hammer head is on fault surface with mylonitic granite above and mylonitic quartzite below.

dislocation densities, subgrains, neoblasts, and deformation lamellae (Fig. 3-5). Coexisting feldspar clasts on the other hand are homogeneously flattened, with patchy undulatory extinction and multiple sets of discrete grain-scale faults (Fig. 3-6). Quartzite within the shear zones has been completely recrystallized (Fig. 3-7). Measurement of recrystallized grain size from several RSd1 shear zones yields a mean grain size of 36.5 microns (Table 3-2). Using the empirical flow stress vs. recrystallized grain size relationship of Ord and Christie (1984), flow stresses for RSd1 faults of approximately 75 MPa are implied.

Rocks of the Grunfjell Group are relatively undeformed more than 2 meters away from RSd1 thrust faults. Amplitude-wavelength ratios of RSd1 folds at the contact between Grunfjell Group lithologies and overlying Tornetrask Formation units are significantly less than at stratigraphically higher levels. Axial planar foliations within folds in the Tornetrask Formation die out rapidly in the crystalline basement. This suggests the crystalline basement behaved competently during RSd1 deformation, and that some RSd1 folds were formed as fault-propagation structures (Suppe, 1985).

RSd2-northwest trending tight to isoclinal folds

RSd2 folds are most clearly developed south of the northern end of Tutturjaure, and northwest of Kaisejaure (Plates 1 and 4). This deformation phase formed tight to isoclinal similar folds with subhorizontal axes, and axial surfaces striking approximately N60W and dipping 10-50° both SW and NE. Axial surface foliations are typically much more strongly developed in this phase than in RSd1 folds (Fig. 3-8).

At the northwest end of Tutturjaure, the axial surfaces of the RSd2 folds dip 20-30SW, and limb asymmetry suggests they have a northeast vergence (Fig. 3-8, Plate 1). Northwest of Kaisejaure, RSd2 folds are more

Figure 3-5: Pebble conglomerate 2 m from RSd1 fault, thin section. Field of view is 4 mm. Quartzite is almost completely recrystallized.

Figure 3-6: Pebble conglomerate 2 m from RSd1 fault, thin section. Field of view is 4 mm. Feldspar clast from same sample as Fig. 3-5. Note patchy extinction and multiple sets of grain scale faults.

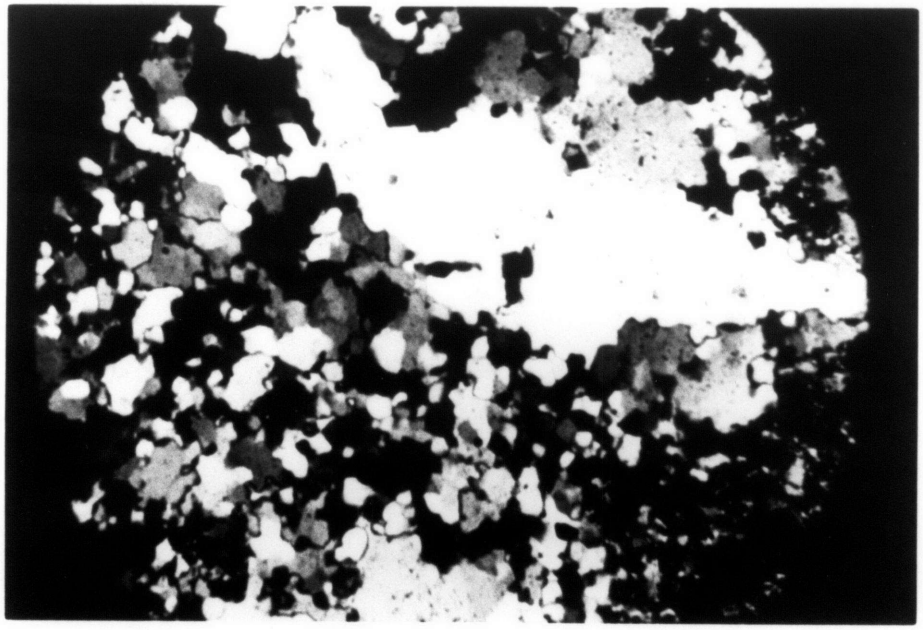

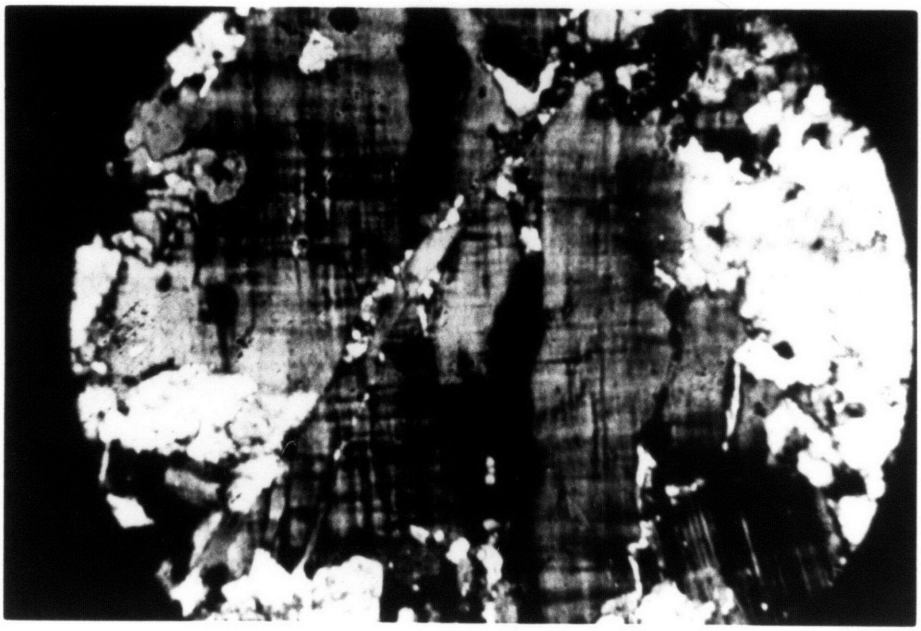

Figure 3-7: RSd1 quartzite mylonite thin section. Field of view is 4 mm. Quartzite within shear zone has been completely recrystallized.

Figure 3-8: RSd2 northwest trending tight to isoclinal folds. View to S60E approximately 500 m west of Tutturjaure. Note axial surfaces dip 20-30° SW and limb asymmetry suggests northeast vergence for deformed upper sandstone member of Tornetrask Formation.

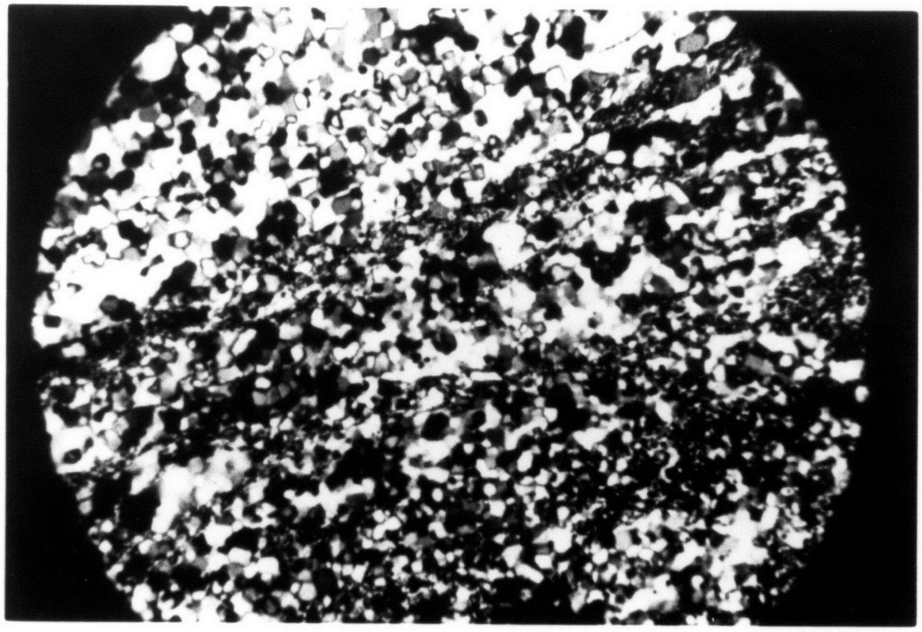

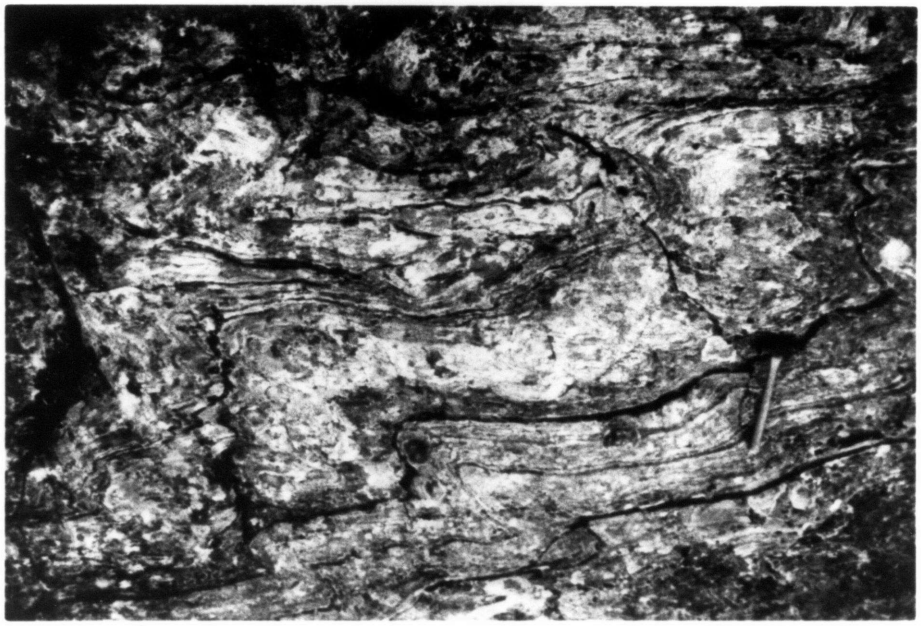

TABLE 3-2 QUARTZ PALEOPIEZOMETER DATA

$$\sigma = AD^{-n}$$

where: σ = deviatoric stress (MPa)

D = recrystallized grain size (μm)

A = 4090 (Ord and Christie, 1984)

n = 1.11 (Ord and Christie, 1984)

Sample	D	σ
84-6C	57.1 ± 12.8	45.9 +14.9/-9.2
84-6V	72.8 ± 21.3	35.1 +16.4/-8.7
84-12P	37.1 ± 5.5	74.1 +14.4/-10.6
84-28A	35.7 ± 7.9	77.3 +24.8/-15.4

Average +1 standard deviation/-1 standard deviation.

extensively developed and may be subdivided into two groups (Plate 4):

1) a southern group whose axial surfaces dip 10-20SW with limb asymmetries that indicate northeast vergence, and
2) a northern group whose axial surfaces dip 15-45NE with limb asymmetries that indicate southwest vergence.

These two groups are separated by an open anticlinal fold trending approximately N50W (Plate 4).

Arguments presented above and below indicate that transport direction of the upper nappe complex during final emplacement onto the Baltic Shield was S60E. RSd2 folds therefore developed with their fold axes trending approximately parallel to transport direction. The problem with folds whose axes are parallel to apparent transport direction is a long standing one in the Scandinavian Caledonides (e.g. Kvale, 1953; Hansen, 1971). A number of mechanisms have been proposed to explain these apparent anomalous fold orientations, and include:

1) Rotation of folds originally orthogonal to transport direction due to progressive strain (e.g. Bryant and Reed, 1969),
2) Initiation of folds with axes at low-angle to transport direction (Hansen, 1971), and
3) Tectonic shear strain parallel to orogenic strike (Olesen, 1971; Steltenpohl and Bartley, in press).

While mechanism 1 is relatively common in the study area (see below), it cannot explain the geometry of RSd2 folds. In addition to the vergence reversal noted above, weakly strained crystalline basement near the hinge areas of these folds argues against a rotational origin for these structures. RSd2 folds therefore appear to have nucleated and evolved in their present orientation.

The approximate orthogonality of RSd1 and RSd2 fold-axes has resulted in type 1 and 2 dome and basin interference patterns (Ramsay, 1967). Unfortunately, the symmetry and complexity of these interference patterns makes determination of relative timing difficult (Plate 4). For example, a Grunfjell cored type 1 dome in the east-central part of Plate 4 is formed by RSd1 and RSd2 folds with sub-vertical axial surfaces. As such, the symmetry of the pattern yields no information on relative timing. However, in the north-central portion of Plate 4 where the interference patterns are particularly striking, RSd1 axial surfaces are relatively gently dipping, yielding a type 2 interference pattern. The geometries here indicate RSd1 precedes RSd2.

RSd1 thrust faults have been folded locally during RSd2 (Plate 4), further supporting the interpretation that RSd1 precedes RSd2.

RSd3-northeast trending southeast vergent folds and rotational shear strain

Continued southeast directed shear strain resulted in the deformation of earlier RSd1 and RSd2 structures. Northwest trending RSd2 structures in the west-central part of Plate 4 have been refolded by a major northeast trending Grunfjell cored southeast vergent fold. Units of the Tornetrask Formation on the exposed eastern limb of this fold have been overturned to the southeast. While no thrusts are associated with this fold, extreme attenuation of lower Tornetrask Formation units suggests this structure, like many RSd1 folds, is an incipient fault-propagation fold.

East-northeast of Kaisejaure, an RSd1 fault-propagation fold, cored by Tornetrask Formation sedimentary rocks with Grunfjell sedimentary rocks in its upper limb has been rotated by progressive shear strain (Plate 1, and sec I-I' Plate 3). At the northwest end of this structure, southeast vergent RSd1 folds trend approximately N20E. To the southeast (at

structurally higher levels) these fold-axes have been rotated into parallelism with the direction of tectonic transport (S60E). Although this structure appears to be post RSd2, it is not necessarily coeval with RSd3 structures to the west.

RSd3 deformation is thus characterized by continued S60E directed shear strain which increases in magnitude upward towards the sole thrust of the Storrit Complex shear zone.

RSd4-north-northeast trending, west-dipping normal faults

Perhaps the most enigmatic Caledonian structures within the Rombak-Sjangeli basement are the six mapped west-dipping normal faults exposed northwest of Kaisejaure (Plates 1 and 4), and north-northwest of Tutturjaure (Plate 1). RSd4 normal faults strike N30-40E and dip 0-50W. Northwest of Kaisejaure, they place sedimentary rocks of the Tornetrask Formation in the hanging wall on Grunfjell basement rocks in the footwall. The faults can be traced north (structurally lower), where they juxtapose Grunfjell Group lithologies in both the hanging wall and footwall (Plate 1). These faults have only been noted where extensive exposure of Dividal Group sedimentary rocks crop out, because they are difficult to trace in massive crystalline basement rocks.

Whereas RSd1 thrust faults generally have a pronounced mylonitic fabric up to 4 m in width, RSd4 faults typically have a narrow 1-3 centimeter wide shear zone with no deformation evident in the rocks above or below the fault (Fig. 3-9). The brittle nature of these faults is further supported by the relatively common occurrence of epidotized slickensides which trend N20-60W.

RSd4 fault surfaces are sygmoidal in cross-section. Northwest of Kaisejaure, these faults have a maximum dip of 40-50°, but at structurally

Figure 3-9: RSd4 basement involved normal fault. View to west approximately 4 km north of Kaisejaure. Note narrow (1-3 cm) shear zone juxtaposing Grunfjell sedimentary rocks in hanging wall and footwall.

Figure 3-10: SWd2 northwest trending tight to isoclinal folds. View to southeast at northwest end of Singis Window. Note steep axial surfaces of folded upper sandstone member of Tornetrask Formation.

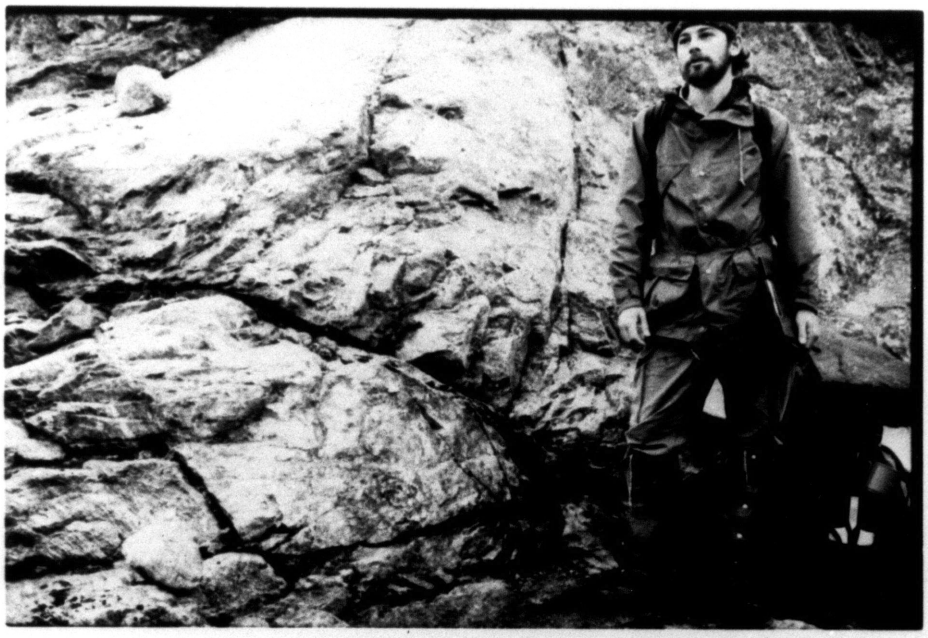

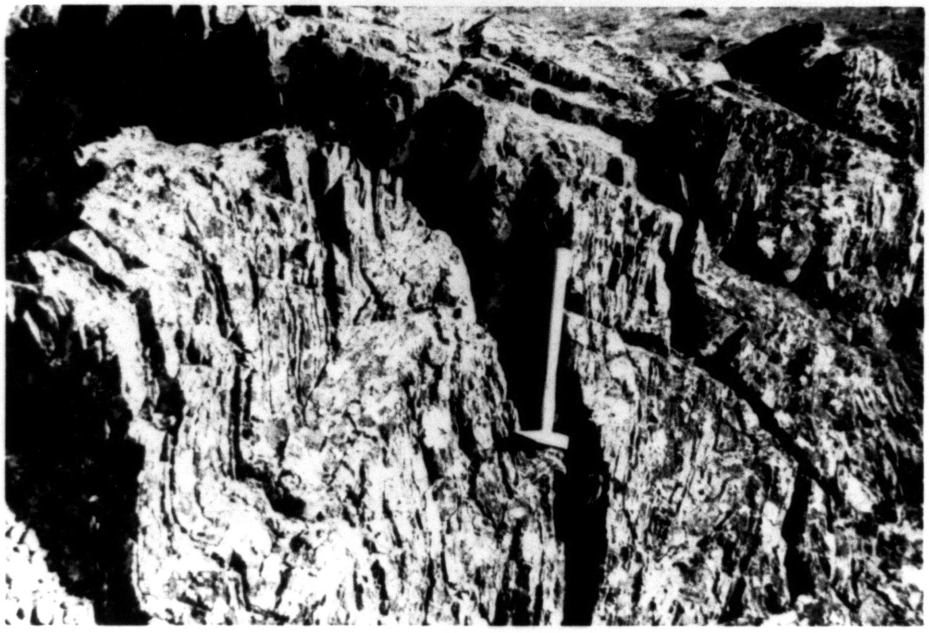

lower and higher levels, the dips decrease to between 0 and 30° (Plates 1 and 4). The shallowing with depth is due to either post-RSd4 rotation from increasing shear strain with depth, or syn-RSd4 listric behavior. The former seems unlikely in view of the unstrained nature of the Grunfjell basement. On the other hand, the shallowing upwards of these faults is probably due to post-RSd4 rotational shear strain within the incompetent siltstone of the upper Tornetrask Formaton.

Working in the Bjornfjell area at the northern margin of the Rombak-Sjangeli Window, Andresen and Cashman (1984) noted the occurrence of similar basement involved normal faults. The orientation, regular spacing and magnitude of offset of the faults is similar to those in the Kaisejaure area. Like the Kaisejaure faults, the Bjornfjell faults post-date basement involved thrusting (RSd1) and pre-date the final movement of the Storrit Complex above. In contrast to the Kaisejaure faults, the Bjornfjell faults have wide (2 meter) ductile shear zones (Cashman, pers. comm., 1985).

RSd5-continued S60E shear strain of Dividal Group

Continued southeast directed shear strain within the Dividal Group is evidenced by rotation of RSd4 normal faults into parallelism with the sole thrust of the overriding Storrit Complex.

RSd6-backfolding

A late backfolding phase affected the Rombak-Sjangeli basement of the study area. This phase is particularly pronounced north of Tutturjaure (Plate 1), where synclines cored by the Tornetrask Formation have shallow east-dipping western limbs (~N8E/16SE), and steep west-dipping eastern limbs (~N20E/65NW, Fig. A-1). This fold phase warps the sole thrust of the Storrit Complex, and therefore appears to postdate final movement of the shear zone.

SINGIS BASEMENT

INTRODUCTION

The Singis Window is a small (10 km x 2 km), N60W trending basement cored dome southeast of the Rombak-Sjangeli basement cored culmination west of Tsutsajaure (Plates 1 and 7). The western half of the window is exposed at the easternmost part of the study area (Plate 1).

Crystalline basement rocks comparable to the Grunfjell Granite, and rhyolitic hypabyssal rocks locally intruded by greenstone dikes are exposed in the core of the window. Exposures of the Tornetrask Formation occur around the perimeter. Two phases of Caledonian deformation are evident in the western half of the window (SWd1 and SWd2). Although morphologically similar to RSd1 and RSd2 respectively, arguments presented below suggest that structures within the Singis Window postdate similar structures within the Rombak-Sjangeli Window.

SWd1-northeast trending southeast vergent tight to isoclinal folds

SWd1 structures exposed in the western half of the Singis Window are morphologically very similar to RSd1 folds. While no basement involved thrust faults crop out in the western half of the Window, mapping by Burchfiel and Page (in progress) has found RSd1 type faults in the eastern half.

SWd2-northwest trending tight to isoclinal folds

SWd2 folds control the outcrop pattern of the sedimentary rocks of the Tornetrask Formation in the northwest part of the window. SWd2 folds typically have steeper axial surfaces than RSd2 folds (Fig. 3-10), and plunge 10-20 to N60W. The axial surfaces 'fan', such that at the southwestern margin of the window they dip 40-50SW, are sub-vertical in the core of the window, and dip 40-50NE at the northeastern margin of the

window. Limb asymmetries of these folds are consistent with a vergence reversal from northeast at the southern margin to southwest at the northern margin of the window. These vergence relationships are similar to those present in the RSd2 folds northwest of Kaisejaure, and argues for a common genesis.

SHEAR ZONE ROCKS

Shear zone rocks of the Middle Allochthon (Kulling, 1964) separate Grunfjell and Dividal Group rocks from the overlying upper nappe complex (see also chapter 2). The shear zone is quite variable in style and thickness, both within the study area and in the northern Caledonides as a whole.

Arguments presented below suggest that deformation within the Storrit Complex of the Rombak-Sjangeli Window preceded final movement along the Matert Shear Zone exposed in the Singis Window. The geometric and temporal relationships of these two shear zones have important implications on the nature of basement involvement during final emplacement of the upper nappe complex.

STORRIT COMPLEX

Introduction

The Storrit Complex has experienced a long continuous deformation history associated with southeast-directed transport of the upper nappe complex. Early formed fabrics have often been completely overprinted by later ones. As such, this early history is discussed in terms of a single deformation phase SCd1. As the shear zone propagated to lower structural levels (Matert Shear Zone), later deformational phases SCd2 to SCd4 overprinted SCd1. The final deformational phase within the Storrit Complex

is recorded by SCd5 backfolding of the entire complex.

SCd1-southeast directed thrusting of upper nappe complex

As discussed in chapter 2, the Storrit Complex is a highly strained assemblage of granitic, psammitic and phyllonitic lithologies. Detailed mapping within the complex has shown these lithologies to be similar to those present in the basement rocks (Hodges, 1982; Crowley, 1985; this work). There is no evidence of any rocks belonging to upper nappe complex units to be present within the shear zone.

Work by Crowley (1985) west of Sitasjaure has shown granitic slivers within the shear zone dip gently west (~5-10°) with respect to the relatively flat lying roof and sole thrusts. This observation led Crowley (1985) to suggest that the Storrit Complex is a highly strained 'duplex' (Boyer and Elliott, 1982). As the shear zone duplex contains only basement lithologies, it must have formed by the forward progression of footwall flats and ramps. Thus, barring continued strain within the shear zone, the youngest zone of deformation is the sole thrust (Boyer and Elliott, 1982).

Evidence for S60E directed shear strain within the basement during final emplacement of the upper nappe complex has been discussed above. There is abundant evidence of a similar sense of strain within the Storrit Complex. In fact, a pervasive ~N60W trending lineation is one of the most striking features within the Storrit Complex (Fig. A-12). As discussed in chapter 2; within psammitic and phyllonitic units this lineation is predominantly defined by the intersection of mylonitic C-surface and N60W trending mesoscopic isoclinal folds (Fig. 3-11). While in some cases, it can be demonstrated that these are true 'sheath folds', the random vergence and shallow axial surfaces (Fig. A-14) of the bulk of these folds suggests a rotational origin.

Figure 3-11: Isoclinal folds within Storrit Complex. View to N60W approximately 2 km east of Tutturjaure. Isoclinally folded matrix schist with shallow axial surface.

Figure 3-12: Roof thrust of Storrit Complex. View S30W approximately 2 km west-northwest of Kaisejaure. Hammerhead is on fault surface with chloritized upper Njunjas Schist in hanging wall and Storrit Complex matrix schist in footwall.

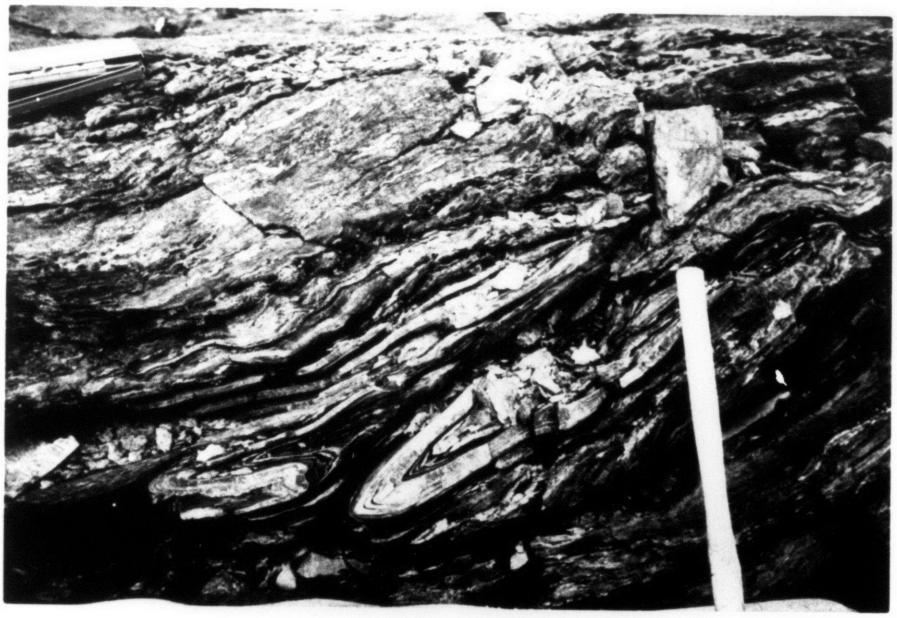

Within the granitic mylonite slivers, the N60W trending lineation is typically a stretching or mineral growth lineation. Although grain size is typically very reduced, remnant porphyroclasts often have asymmetric pressure shadows indicating S60E directed transport. S-C fabrics (Lister and Snoke, 1984), poorly developed within the Storrit Complex of the study area, are often well developed in rocks of the Matert Shear Zone (see below).

The bulk composition of lithologies within the Storrit Complex of the the study area makes precise estimation of thermal conditions difficult. The absence of garnet, and the presence of biotite and epidote implies lower greenschist facies for pelitic assemblages. Plastic behavior of feldspar, and static annealing of quartz dislocations and subgrains suggests temperatures in excess of 350°C. Northwest and north of Sitasjaure, pelitic units within the Storrit Complex are garnetiferous (Hodges, 1982; Crowley, 1985). Crowley (1985) obtained mean p-T conditions of 510°C and 710 MPa for these units (see chapter 4).

SCd1-conclusions

Along the southern margin of the Rombak-Sjangeli Window, the Storrit Complex thins from over 1 km to the north of Sitasjaure to approximately 50 meters in the Tsutsajaure Culmination. The apparent duplex nature, and foreland directed taper of the complex are reminiscent of orogen scale foreland fold and thrust belts (e.g. Dahlstrom, 1970).

The Storrit Complex thins rapidly from 500 m west of Tutturjaure, to 200 m east of the lake (Section C-C', Plate 2). This thinning is associated with a rapid structural thickening in Dividal Group sedimentary rocks exposed below the shear zone. Intersection lineations within the Storrit Complex (F2) rotate from S57E west of Tutturjaure (Fig. A-12), to

S72E east of the lake (Fig. A-13). These relationships are compatible with ramping of the sole thrust of the Storrit Complex along an oblique frontal footwall ramp.

The refraction of F2 lineations and the presence of footwall ramps also supports the assertion that significant shear strain was accommodated at the sole of the Complex, with relatively minor internal deformation. Mylonitic fabrics within the complex therefore predate final movement along the sole thrust. Crowley (1985, p.138) states that garnet growth within the western Storrit Complex preceded development of the mylonitic foliation. Therefore, p-T values calculated for the Storrit Complex (710 MPa, 510°C) probably represent much hotter conditions than those that existed during final thrusting.

SCd2-northeast trending, southeast vergent tight to isoclinal folds

Although the roof and sole thrusts of the Storrit Complex are locally difficult to locate within 10 meters, they are generally sharp and relatively planar (Fig. 3-12). However, at the eastern end of the Tsutsajaure culmination, rocks of the shear zone are infolded with Rombak-Sjangeli basement below, and rocks of the upper nappe complex above (Fig. 3-13). These folds have a mean orientation of 4° to N30E, with moderate scatter probably due to post-nucleation rotational strain (Fig. A-35). Vergence deduced from limb asymmetries and locally developed axial surface foliation is consistently to the southeast (Fig. 3-14).

This fold phase postdates SCd1, and is associated with movement of the basement rocks of the Rombak-Sjangeli Window and all the tectonic units above it on the Matert Shear Zone.

SCd3-northwest trending macroscopic warping

SCd3 folding is responsible for the doming event which led to the

Figure 3-13: Folded sole thrust of Storrit Complex. View to north approximately 200 m south of Tsutsajaure. Mylonitic Grunfjell granite (left) is isoclinally infolded with Storrit Complex matrix schist (right).

Figure 3-14: Folded Storrit Complex matrix schist. View north at northeastern end of Tsutsajaure. Eastern limb of Salka Anticline is sub-vertical.

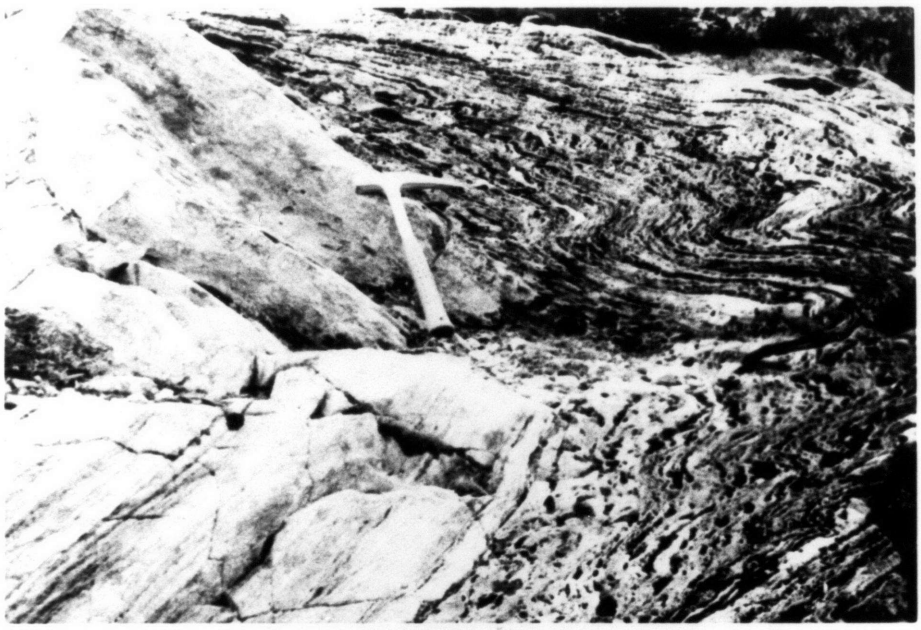

gentle southwest dip of the southern margin of the Rombak-Sjangeli Window (Fig. A-11). The mean trend of SCd3 warps is 0° to N68W. These folds are subparallel to RSd2 folds in the Rombak-Sjangeli basement, and appear to be coeval.

SCd4-northwest trending open to isoclinal folds

SCd4 folding is responsible for development of the Tsutsajaure Culmination (Plate 1, Section J-J', Plate 3). The northern limb of the culmination strikes N55W, sub-parallel to mesoscopic isoclinal folds within the granite. The SCd3 fold axis of the culmination is on strike with and parallel to the SWd2 northwest trending axis of the Singis Window and is presumably coeval.

SCd5-backfolding

A late backfolding phase along north-northeast trending axes affected the Storrit Complex. The large north-trending synform on Rassepakte to the west of Tutturjaure (Plate 1) has a shallow south plunge with gently dipping limbs (8-10°). Although SCd5 backfolding is only manifested by gentle warping of the shear zone in the study area, basement rocks north of Tutturjaure have been strongly affected (RSd6).

Klippen of Storrit Complex rocks northwest of the study area, along the north coast of Sitasjaure, also have a pronounced backfolded limb asymmetry (Crowley, 1985). The western limbs of these structures dip moderately east (15-25°), while the eastern limbs dip more steeply west (30-50°).

MATERT SHEAR ZONE

Introduction

Where exposed in the western half of the Singis Window, the Matert Shear Zone is 20-40 meters thick (Plate 1 and 2, Fig. 2-17). The Matert

Shear Zone presents similar problems as the Storrit Complex in deciphering its structural history. Thrusting is treated as a single phase, MTd1, that was overprinted by warping along northwest trending axes, MTd2.

MTd1-southeast directed thrusting

Like the Storrit Complex, the Matert Shear Zone is a heterogeneous shear zone of highly strained basement lithologies. The sole thrust forms a sharp topographic bench (Fig. 2-17).

Metamorphic grade within the shear zone is significantly lower than in the Storrit Complex, 3 km to the northwest. Garnet-bearing units immediately above the roof thrust have been completely chloritized.

S-C fabrics, while rare in the Storrit Complex are extensively developed within the Matert Shear Zone (Fig. 3-15). These fabrics give a consistent sense of S60E directed shear strain.

Multiple phases of deformation are evidenced by mesoscopic S60E vergent folds (Fig. 3-16). These structures fold an earlier phyllonitic foliation.

MTd2-northwest trending macroscopic warping

An MTd2 northwest trending open upright fold is responsible for the elongate domal structure of the Singis Window. The axis of the window trends approximately N55W, compared to the mean N68W trend of SCd3 in the Storrit Complex (see above).

UPPER NAPPE COMPLEX

The upper nappe complex of the study area is subdivided into four distinct tectonostratigraphic elements: the Aurek Assemblage, Salka Group, Litte Group, and Maita Complex (see chapter 2). These assemblages are broadly similar to upper nappe complex units elsewhere in the Scandinavian

Figure 3-15: Matert Shear Zone. View to north at northern margin of Singis Window. Field of view is 15 cm. S-C fabric indicating dextral shear strain is well-developed in granitic mylonite of Matert Shear Zone.

Figure 3-16: Southeast vergent fold within Matert Shear Zone. View to S30W at southern margin of Singis Window. While these folds do not deform the roof or sole thrust of the shear zone, they do deform an earlier phyllonitic foliation.

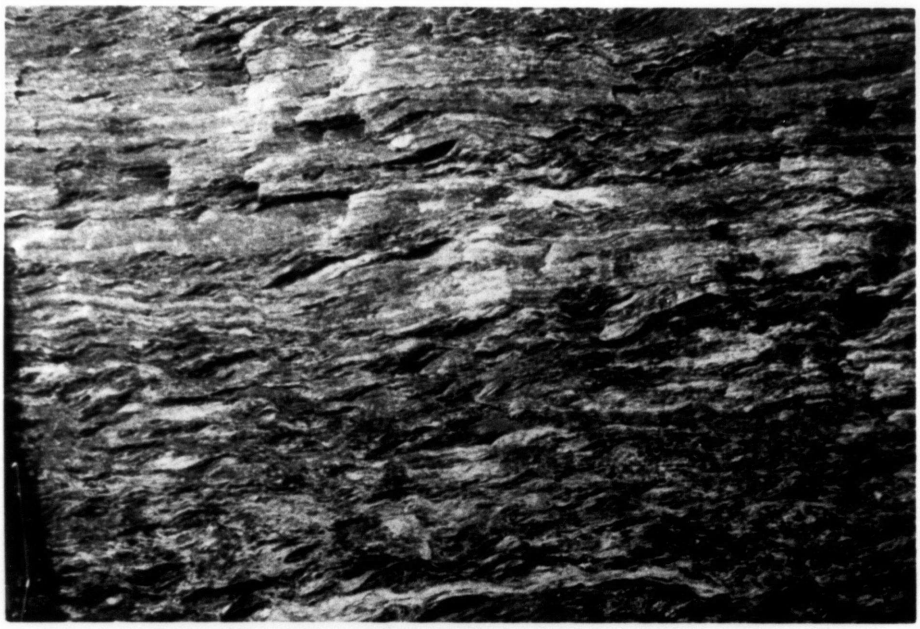

Caledonides in that they thin to the west; pinching out between shear zone rocks below, and higher units above (Plates 1 and 2).

The deformations discussed previously, affecting the basement and shear zone rocks, were the youngest deformations that affected the upper nappe complex and are superposed on several older deformational events recorded in the rocks of the nappe complex. Prior to their final emplacement on the Baltic Shield, rocks of the upper nappe units experienced a complex metamorphic and structural history.

Both early and late phases of deformation affecting each tectonostratigraphic element will be discussed below, beginning at the structurally lowest level. Many of the early deformational phases that affected the upper nappe complex are associated with high-grade metamorphism. Therefore, these phases are often temporally distinguished on the basis of textural relations and mineral parageneses rather than structural cross-cutting relations.

AUREK ASSEMBLAGE

Introduction

The Aurek Assemblage, crops out at the southeast margin of the study area, and consists of a sequence of kyanite bearing paragneiss containing discontinuous meta-gabbro lenses (see chapter 2). ^{40}Ar-^{39}Ar data presented in chapter 5 indicate the Aurek Assemblage experienced deformation (AAd1) and an associated high-grade metamorphism in Late Cambrian or Early Ordovician time. AAd1 was overprinted in Early Silurian time by deformation associated with a biotite grade metamorphism that imparted the regional foliation to rocks in the study area. The entire Aurek Assemblage was then thrust onto the Baltic Shield during a younger deformational phase (AAd3), and warped along later northwest trending folds (AAd4). Late

normal-slip shear is recorded along the upper contact of the Aurek Assemblage with the overlying Salka Group (AAd5).

AAd1-high-grade metamorphism and deformation

Very little information can be obtained on the nature of the early AAd1 deformation. The fabrics associated with this phase have been almost completely transposed by AAd2.

Within the Vidja Gneiss, AAd1 metamorphic minerals such as garnet, kyanite and muscovite are present mainly as highly dismembered porphyroclasts. Muscovite books typically form randomly oriented floating folds (Fig. 2-13).

The Aurek Gabbro, which is much more competent than the surrounding gneissic units, has retained its igneous fabrics. The gabbro locally contains gneissic fabrics which are generally randomly oriented and strongly discordant to later AAd2 shear zones.

The Aurek Amphibolite reaction skarn or "black wall" (see chapter 2) separates the Aurek Gabbro from surrounding Vidja Gneiss. Textural evidence presented in chapter 4 indicates the Aurek Amphibolite developed late during AAd1, when the eclogitized gabbro was hydrously intercalated with the Vidja Gneiss (cf. Andreasson et al., 1985).

AAd2-deformation and associated greenschist-grade metamorphism

AAd2 deformation and associated biotite grade metamorphism is responsible for the prominent schistosity developed in the Vidja Gneiss (Fig. A-16, A-17). The schistosity developed during AAd2 was folded by late northwest trending folds formed during the AAd4 deformational phase and resulted in a girdle pattern for the schistosity with mean orientation of N16E/28NW (Fig. A-18).

The fabric developed during AAd2 is a penetrative biotite grade

mylonitization (Fig. 3-17). Trouw (1973), working in the Seve nappe east of the Borgefjell Window (Fig. 1-1), noted a similar post-metamorphic deformation. No S-C fabrics, asymmetric folds, or other kinematic indicators are associated with AAd2 deformation within the Vidja Gneiss. However, rotated garnets at the base of the overlying Salka Group (see below) which apparently developed during this phase indicate southeast-directed shear strain.

AAd3-southeast directed thrusting on shear zone rocks

The mylonitic AAd2 fabric within the Aurek Assemblage has been rotated into parallelism near the underlying Matert Shear Zone (Plate 1). Although the roof thrust of the Matert Shear Zone is quite sharp, mylonitic fabrics and chloritic retrogression extend up to 5 meters into the hanging wall (Fig. 2-11). These AAd3 fabrics overprint and transpose the biotite grade AAd2 foliation.

AAd4-northwest trending macroscopic warping

The same deformational phase which folded the Matert Shear Zone along a N55W trending axis (MTd2) is responsible for a similar fold within the Aurek Assemblage (Plate 1). In addition to the Singis Window itself, AAd4 macroscopic warps are particularly well-developed east of Vidjajaure on the west slope of Stuor Aurek. The mean trend of these structures is approximately N60W (Fig. A-19).

AAd5-west-northwest directed normal faulting

The upper contact of the Aurek Assemblage with the overlying Salka Group is a complex shear zone, named the Rusjka Fault. Textural evidence in the hanging wall (see below) indicates early east-vergent thrusting (AAd2) was followed by west-vergent normal-slip shear along the fault.

Limited evidence of late west-vergent shear exists in the upper 50

Figure 3-17: Mylonitized Vidja Gneiss thin section. Field of view is 12 mm. Porphyroclasts of garnet and feldspar in biotite neoblast matrix.

Figure 3-18: SGd4 southeast-vergent folding of Salka Group. View N30E approximately 700 m south of Tsutsajaure. Southeast-vergent folds associated with development of Matert Shear Zone transpose SGd1 foliation of Rusjka Calcareous Schist.

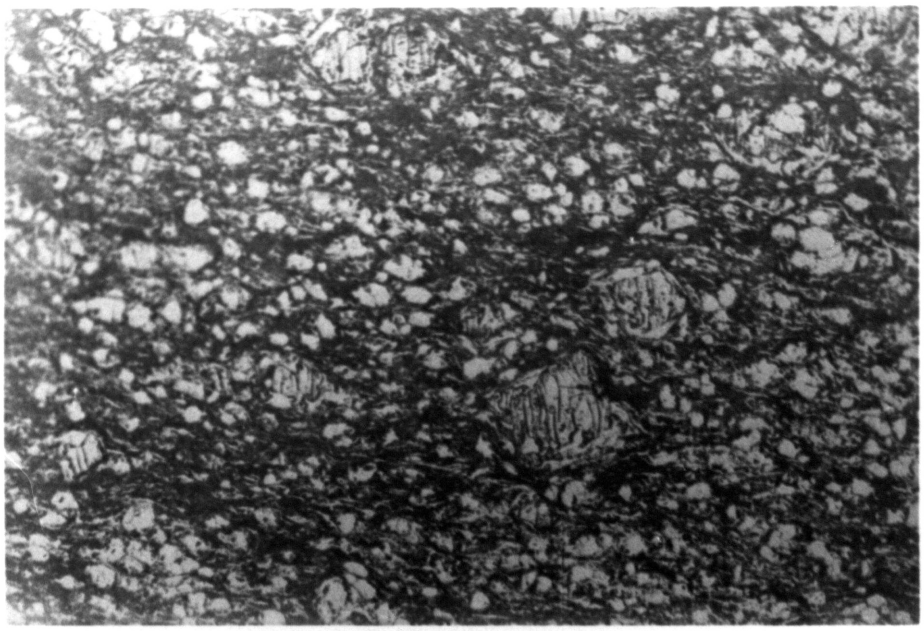

meters of the Aurek Assemblage. Gneissic units have been cut by anastomosing, west-dipping faults with apparent normal separation (Fig. 2-4).

SALKA GROUP

Introduction

The Salka Group is a thick sequence of greenschist grade psammites and calcareous schists (see chapter 2). Tentative correlation of this package with the Bjorkvattnet Nappe of Stephens (1982), implies an Ashgill to middle Llandovery depositional age (see Chapter 6). All the deformation and metamorphism of the Salka Group must therefore be post-middle Llandovery (≈433 Ma, Harland et al., 1982).

Despite being the youngest and lowest grade unit within the upper nappe complex of the study area, the Salka Group has a complex history. Deformation within the Group was subdivided into six phases, SGd1 to SGd6.

SGd1-lower greenschist facies metamorphism

Pelitic assemblages within the Patta Quartzite indicate the primary schistosity development, SGd1 was associated with chlorite grade metamorphism. Lack of microstructural deformation fabrics associated with this phase implies either static metamorphism or post tectonic annealing.

SGd2-imbrication of upper nappe complex

The Rusjka Fault at the base, and Tjuolak Thrust at the top of the Salka Group are both SGd2 thrusts. The nature of these contacts was discussed in chapter 2, and will be amplified here.

The stratigraphically lowest unit within the Salka Group is the Rusjka Calcareous Schist; a gritty psammite with discontinuous horizons of marble and calcareous schist (see chapter 2). The Rusjka Calcareous Schist is separated from Vidja Gneiss below by the Rusjka Fault. Up to 50 meters

structurally above the fault are garnet-bearing calcareous zones that contain important information on the strain history. While rotational axes were not determined, these garnets have sygmoidal inclusion trails indicating syn-growth southeast directed thrusting (Fig. 3-21; cf. similar studies by Rosenfeld (1970) from the Appalachian Orogen. In the footwall, there is apparently no decrease in strain away from the Rusjka Fault. In fact, AAd2 biotite grade mylonitization which appears coeval with SGd2, penetratively deforms the entire Vidja Gneiss of the study area.

The upper contact of the Salka Group with the Litte Group, the Tjuolak Thrust, places garnet-hornblende calc-schists in the hanging wall, on chlorite psammites in the footwall. The thrust is not as sharp as the Rusjka Fault, and appears to be a sliver zone up to several hundred meters thick (Plates 1 and 2). This 'schuppen zone' is particularly well-developed on Kaitumtjakka, southwest of Tjuolakjaure (Plate 1), where a section of intercalated slivers of Salka Group psammite and Litte Group schist is approximately 1500 meters thick. Individual slivers within this zone range from one to tens of meters thick. Blastomylonitic fabrics contain both highly strained quartz grains, and dislocation free subgrains with a pronounced crystallographic anisotropy. While no kinematic indicators (e.g. S-C fabrics) were found associated with the Tjuolak Thrust, transport direction is inferred to be S60E.

The monotony of the Patta Quartzite precludes complete documentation stratigraphic repetition within the sequence. However, the great structural thickness of this unit (~1500 meters, section C-C' Plate 2), and occurrence of SGd1 parallel shear zones throughout, suggests significant SGd2 internal imbrication.

SGd3-southeast directed thrusting on shear zone rocks

As in the Aurek Assemblage, the early SGd1 foliation within the Salka Group has been transposed by SGd3 mylonitic fabrics within 5 meters of the Storrit Complex. However, drag folds, associated with movement on the Storrit Complex, have developed within the Salka Group up to 2 km south of the shear zone (southeast of Kaisejaure, Plate 1). These SGd3 folds are variable in style and range from open warps to tight isoclinal folds. Axial surface foliations are well developed within the tight folds, and range from horizontal to vertical in orientation. Although generally sub-parallel to transport direction (S60E), fold axis orientations are also variable. These folds do not deform the roof thrust of the Storrit Complex.

SGd3 folds are more extensively developed within the Litte Group (LGd4, see below). The range in orientation of these folds from orthogonal to parallel with transport direction suggests they may have developed as drag folds, and were subsequently rotated during progressive shear strain. SGd3 folds have developed up to 300 meters above the roof thrust of the Storrit Complex. Thus, where the structural depth of the Storrit Complex is unclear, the presence or absence of these folds provides an estimate as to the possible depth of the Storrit Complex (e.g. Plate 2).

SGd4-southeast vergent folding with development of Matert Shear Zone

SGd4 southeast vergent folds transpose earlier fabrics between the Singis and Rombak-Sjangeli Windows at the northeastern margin of the study area (Plates 1 and 2). This phase is responsible for the apparent northeast trending synformal structure separating the two windows. The SGd4 deformational phase is the same phase as SCd2 (discussed above) that infolds the Storrit Complex with upper nappe complex rocks above and

Rombak-Sjangeli basement below.

On the northwestern slope of Matertjakka (Plate 1), SGd4 folds clearly transpose the SGd1 foliation (Fig. 3-18). Southwest of the Singis Valley on the northeast slope of Rusjka (Plate 1), the Rusjka Graphitic Schist is isoclinally infolded with Patta Quartzite above, and Rusjka Calcareous Schist below (Plates 1 and 2). These folds can be followed north, to the south slope of Salka. A strong macroscopic axial surface cleavage also developed during this phase. Commonly, this cleavage overprints earlier structures on a map scale (Fig. 3-19).

The mesoscopic SGd4 folds are parasitic to the major N30E-trending, east-vergent "Salka Anticline" which plunges gently north under Salka, and south under Rusjka (Plate 1). The Salka Anticline is cored by Rombak -Sjangeli basement, such that isoclinally folded Storrit Complex mylonites crop out in the vertical eastern limb at the northwestern end of the Singis Valley (Plates 1 and 2). Thus, all the structural elements west of the Singis Window have been deformed by the Salka Anticline: the Rombak-Sjangeli basement, the Storrit Complex and the upper nappe complex.

SGd5-internal imbrication of the Salka Group

Continued southeast directed internal imbrication of the Salka Group is evidenced by late thrusts on Rusjka, Salka and east of Matertjakka (Plate 1). Temporal evidence for this phase of post-SGd4 thrusting is clearest at the eastern end of the Tsutsajaure Culmination. Here, a gently west-dipping fault exposed on both sides of the Culmination cuts SGd3 structures parasitic to the Salka Anticline. The fault is very sharp, has no shear zone associated with it, and locally truncates the SGd1 foliation in the hanging wall (Fig. 3-20). This fault appears to be a thrust on the basis of east-vergent mesoscopic folds within Patta Quartzite of the

Figure 3-19: Patta Quartzite on Matertjakka. View north at Matertjakka. Flat-lying SGd1 foliation is weakly transposed by west-dipping SGd4 cleavage.

Figure 3-20: Late east-vergent thrust fault in Salka Group. View south approximately 1.5 km south of Tsutsajaure. Gently west-dipping fault with narrow shear zone places Patta Quartzite in hanging wall on Rusjka Calcareous Schist in footwall.

hanging wall. A series of at four SGd5 thrusts were also mapped on the eastern slope of Matertjakka. These faults branch laterally and duplicate the Rusjka Graphitic Schist - Patta Quartzite contact. All these SGd5 faults root into the roof thrust of the Matert Shear Zone.

Apparently associated with this phase of SGd5 thrusting is a major backfold, the axis of which trends N45E along the southeast slope of Rusjka, and changes trend northeast of Matertjakka to NS. As this fold does not deform the underlying Matert Shear Zone the simplest interpretation is that it is a fault-bend fold (Suppe, 1983) developed on the trailing limb of an antiformal stack during the SGd5 thrusting.

SGd6-normal shear at Rusjka Fault

Mesoscopic and microscopic fabrics indicate a phase of late west-directed normal-slip shear along the Rusjka Fault. These fabrics overprint earlier AAd2 and SGd2 textures associated with southeast-directed thrusting.

Garnets within calcareous schist horizons immediately above the Rusjka Fault are excellent strain markers. Sygmoidal inclusion trails indicate a phase of early southeast directed syn-crystallization thrusting (SGd2). This fabric is overprinted by post-crystallization west-northwest directed normal shear. The most pronounced normal faulting fabrics are asymmetric quartz pressure shadows (sinistral shear, Fig. 3-21). Further evidence of post-crystallization sinistral rotation is revealed by back-scattered SEM imagery (Fig. 3-22) that reveals a normal-slip rotation of early formed pressure shadows. Asymmetric microscopic folds within the late pressure shadows also indicate normal-slip shear. A pronounced lineation interpreted as the mean slip direction, is caused by the late quartz pressure shadows has a mean N70W trend.

Figure 3-21: Garnet-bearing Rusjka Calcareous Schist thin section. Field of view 12 mm. View N10E, 2.5 km S40E of Rusjka approximately 50 m above Rusjka Fault. Garnet inclusion trails indicate dextral shear strain during growth. Late quartz pressure shadows indicate sinistral shear strain following garnet growth.

Figure 3-22: SEM image of Rusjka Calcareous Schist garnet. Field of view 2.5 mm. Same sample and view as Fig. 3-21. Note sygmoidal quartz inclusion trails indicating dextral rotation during growth. Also note early quartz pressure shadows to left and right of garnet that have been rotated sinistrally.

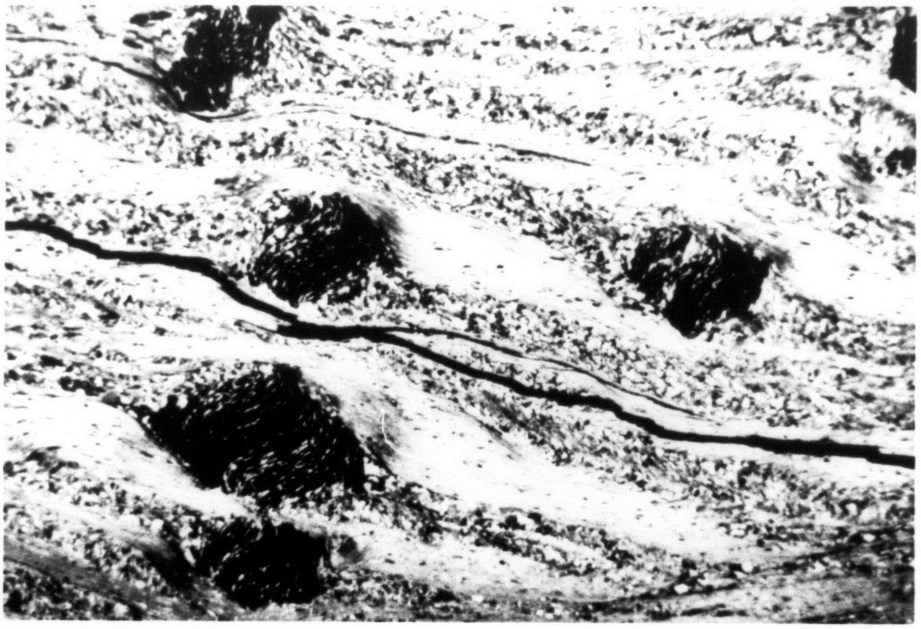

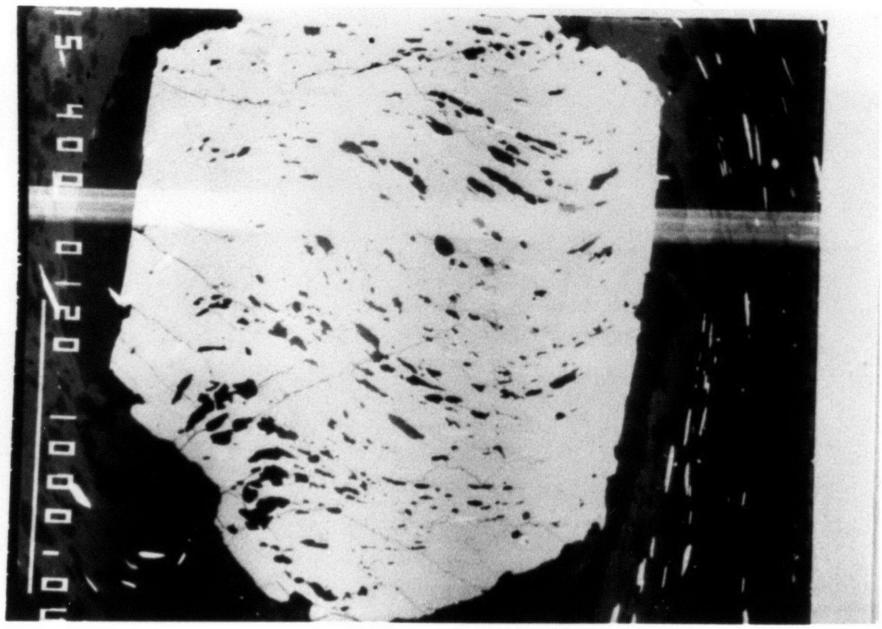

Late SGd6 west-vergent mesoscopic folds overprint earlier fabrics up to 100 meters structurally above the Rusjka Fault (Fig. 3-23, Plate 1). While the mean trend of these folds is 36° to N37W (Fig. A-28), they define a girdle striking N16E/45NW. This great circle is sub-parallel to the SGd1 foliation in the hanging wall of the fault (Fig. A-23). The coplanarity, noncylindrical nature, and systematic vergence of these folds satisfy the definition of "discon folds" (Hansen, 1971). While the resultant separation arc of these folds is quite large (N70W to S22W), the bisectrix of the fold axis girdle is 45° to N74W, sub-parallel to the pressure shadow lineation. These folds therefore appear to be drag folds associated with normal-slip shear on the Rusjka Fault.

Like SGd5 thrusts, the SGd6 normal fault roots into the roof thrust of the Matert Shear Zone. Extensional fabrics are common within the Rusjka Calcareous and Graphitic Schists immediately above the Matert Shear Zone. Conjugate tension gashes and low-angle mesoscopic normal faults are the youngest fabrics and indicate SGd6 normal faulting post-dated the final thrusting (SGd5) on the Matert Shear Zone.

LITTE GROUP

Introduction

The Litte Group is the most areally extensive unit in the study area (Plate 1). It consists of a relatively horizontal sequence of garnet + muscovite + biotite ± hornblende ± ankerite schist (see chapter 2). Crowley (1985) suggested a Caradocian age for deposition of the Litte Group, based on correlations to the south (see chapter 6). This implies that the deformation and amphibolite grade metamorphism of the Litte Group is post-Caradoc (<448 Ma, Harland et al., 1982).

Like other upper nappe complex units, the Litte Group reveals several

Figure 3-23: West-vergent folds within Salka Group. View north-northwest approximately 2.5 km southeast of Rusjka. Rusjka Calcareous Schist folded by west-vergent SGd6 fold.

Figure 3-24: Chevron folds within Litte Group. View N40E approximately 5 km southwest of Luli Litte, 10 m below Maitat Thrust. Note northeast trending chevron folds which imply northwest-southeast compression.

phases of deformation and associated metamorphism. In the study area, deformational structures were subdivided into four phases LGd1-LGd4.

LGd1-deformation and associated amphibolite facies metamorphism

The primary horizontal schistosity of the Litte Group is associated with an early LGd1 deformation (Figs. A-29, A-30). Late LGd1 garnet, hornblende and biotite have statically overgrown the early LGd1 schistosity (Fig. 2-19) and form randomly oriented porphyroblasts with sub-planar helicitic inclusion trails. These relationships suggest that peak thermal conditions within the Litte Group post-dated development of the LGd1 regional mica-foliation. This observation contrasts with that of Crowley (1985), who argued that peak thermal conditions within the Langvatn Assemblage west of the Sitas-Singis area were coeval with development of the regional mica-foliation.

LGd2-imbrication of upper nappe complex

Within the upper nappe complex, the Litte Group is bounded at the base by the Tjuolak Thrust, and at the top by the Maitat Thrust (e.g. see F-F', Plate 2). The Tjuolak Thrust is the schuppen zone at the base of the Litte Group discussed previously (SGd2) that places the Litte Group onto the underlying Salka Group.

The Maitat Thrust forms the upper contact of the Litte Group with the Maitat Complex. There appears to be a single relatively horizontal sharp fault surface marking the thrust (Plate 1). While no intensification of strain or mylonitic fabric was noted, late chevron folds are common within a few meters of the contact (Fig. 3-24). These folds have steep axial surfaces and subhorizontal fold-axes trending N35-45E, which indicate approximately N50W-S50E compression during late movement on the thrust (Ramsay, 1967). LGd2 or later movement on the Maitat Thrust is further

supported by the discordance of the MCd1 (see below) schistosity with the subhorizontal fault (c.f. F-F' Plate 2 and Fig. A-34).

LGd3-southeast-directed thrusting on shear zone rocks

LGd3 deformation within the Litte Group is broadly similar to the SGd3 deformation affecting Salka Group lithologies (see above). In contrast to fabrics in the Salka Group, deformational microfabrics associated with LGd3 southeast-directed thrusting are penetrative in rocks up to 100 meters above the Storrit Complex. Within 5 to 10 meters of the shear zone, there is a clear transposition of LGd1 foliation into parallelism with the thrust. Further above the Storrit Complex, late LGd1 porphyroblasts have also been rotated into sub-parallelism with the foliation due to LGd3 shear strain.

Mesoscopic drag folds, similar to those in the Salka Group are ubiquitous within the Litte Group up to about 300 meters structurally above the shear zone. These folds are extremely variable in style and orientation.

On Rassepakte, west of Tutturjaure, a map scale LGd3 fold has a sub-vertical axial surface foliation, and trends roughly north-south (Plate 1). Another north-trending LGd3 fold crops out on the northwest shore of Luli Litte. South of Kaisejaure, immediately above the Storrit Complex, LGd3 folds appear to have been rotated, such that they trend approximately east-west (Fig. A-32).

LGd4-backfolding

A late phase of backfolding warped the entire Litte Group and its lower contact with the Storrit Complex along north-trending axes.

MAITAT COMPLEX

Introduction

The Maitat Complex is the structurally highest tectonostraphic element within the study area (Plate 1). It is the only upper nappe complex unit not affected by late movement within the underlying shear zone because it was never close enough to have been affected. The unit consists of a heterogeneous calc-schist containing discontinuous mafic slivers. As discussed in chapter 2, the Maitat Complex is probably related to the Filfjell and Rauvatn complex melange units west of the study area (Crowley, 1985).

^{40}Ar-^{39}Ar data (see chapter 5) indicate the Rauvatn Complex (and presumably the Maitat Complex), like the Aurek Assemblage experienced its high-grade metamorphism and deformation in Late Cambrian or Early Ordovician time. This early deformation is recorded in the first two phases MCd1 and MCd2, followed by later thrusting along the Maitat Thrust during MCd3 deformation.

MCd1-internal imbrication and regional foliation development

Internal imbrication of mafic pods with the maitrix schist occurred prior to MCd2 peak thermal conditions. This imbrication was possibly associated with development of the primary schistosity which presently strikes N15W/8SW (Fig. A-34).

MCd2-amphibolite facies metamorphism

Amphibolite facies, calcareous mineral assemblages have statically overgrown earlier MCd1 fabrics.

MCd3-imbrication of upper nappe complex

Presumed southeast-directed movement of the Maitat Complex on the Maitat Thrust was discussed above in the section on LGd2 deformation.

CONCLUSIONS

INTRODUCTION

The deformational phases discussed above can often be correlated between different tectonostratigraphic elements within the study area. These phases serve as structural tie points which allow other non-uniquely related phases in different units also to be correlated with one another. Sets of temporally distinct phases are then grouped into distinct deformational events. Using these relationships, the deformational phases discussed above were grouped into eight events (see Plate 6). In what follows, the timing and structural style of each deformational event are discussed. In addition, the arguments for including a set of phases within a given event are presented.

DEFORMATIONAL EVENTS

D1-deformation and associated high-grade metamorphism

^{40}Ar-^{39}Ar data presented in chapter 5 suggest that both the Aurek Assemblage and Maitat Complex experienced a high-grade metamorphism and deformation during Late Cambrian or Early Ordovician time. Event D1 is thus the Late Cambrian or Early Ordovician high-grade deformation and metamorphism of the Aurek Assemblage and Maitat Complex. Deformation phases AAd1, MCd1 and MCd2 are included in D1.

D2-deformation and associated high-grade metamorphism

As mentioned above, correlations with units to the south (eg. Wilson, 1970; Stephens, 1977) suggest Upper Ordovician to earliest Silurian depositional ages for the Salka and Litte Groups. In addition, ^{40}Ar-^{39}Ar data yield an Early Siluran age for the high-grade metamorphism of the Litte Group. Because the early deformation of the Salka and Litte Groups (SGd1 and LGd1 respectively) is apparently younger than D1, these phases

are included in the D2 deformational event. The distinction between D1 and D2 is based solely on timing relations as there is little structural or textural evidence for distinguishing these events.

D3-imbrication of upper nappe complex and early thrusting onto Baltica

Post D1 and D2 imbrication of the entire upper nappe complex occurred during D3. Deformational phases AAd2, SGd2, LGd2 and MCd3 are all associated with D3 stacking. It is important to note, that D1 to D3 in this study are equivalent to the D1 and D2 of Crowley (1985).

Early garnet grade deformation of the Storrit Complex at the southwestern margin of the Rombak-Sjangeli Window may be associated with late-D2 high-grade metamorphism of the upper nappe complex (see chapter 4). This suggests obduction of the upper nappe complex onto the Baltic Shield basement may have begun by late-D2 or early-D3 time.

D4-thrusting of upper nappe complex on Storrit Complex

The earliest deformational phases recorded in the Rombak-Sjangeli basement (RSd1), Storrit Complex (SCd1), Singis Window (early SWd1) and Matert Shear Zone (early MTd1) are associated with greenschist grade thrust faulting of the upper nappe complex onto the Baltic Shield. This D4 event is also associated with AAd3, SGd3, and LGd3 deformation at the base of the upper nappe complex. Movement along the Storrit Complex eventually became locked as Rombak-Sjangeli basement, Storrit Complex and Salka Group lithologies became infolded in southeast vergent folds late during the RSd1, SCd2 and SGd4 phases respectively.

The D4 deformational event thus includes fabrics associated with early emplacement of the amalgamated upper nappe complex onto the Baltic Shield, through to the end of major translation along the Storrit Complex. This event correlates with D5 of Hodges (1985) and Crowley (1985).

D5-thrusting on Matert Shear Zone

Infolding of RSd1, SCd2 and SGd4 structures of the Rombak-Sjangeli basement and cover during late D4 represents the initial propagation of the Matert Shear Zone below the Rombak-Sjangeli Window. These structures are seen more clearly in sections A-A' and B-B' of Plate 2. In section A-A', the Rombak-Sjangeli Window is shown as a 1 kilometer thick sliver detached along the underlying Matert Shear Zone. During D5, the now amalgamated Rombak-Sjangeli Window and upper nappe complex are translated S60E along the Matert Shear Zone (late MTd1).

Northwest-trending RSd2 folds in the Rombak-Sjangeli basement, and the SCd3 south-dipping southern border of the Window also appear to have evolved during this event. These folds are interpreted to be related to the development of a lateral ramp anticline associated with termination of the Rombak-Sjangeli basement sliver a few kilometers south of the margin of the window.

Arguments for the nature and kinematic consequences of this D5 "thin-skinned" detachment of the Rombak-Sjangeli basement are presented and amplified in chapter 6.

A variety of other structures continued to develop within the hanging wall during D5. AAd3 mylonitic deformation at the base of the Aurek Assemblage continued until the end of D5. SGd5 thrust faults and fault bend folds developed as a consequence of continued shortening within the upper nappe complex. Although RSd3 through RSd5 structures within the Rombak-Sjangeli basement probably developed during D5, all or some of the phases may be D6.

D6-thrusting below the Singis Window

The most prominent structure developed during D6 is the N55W trending

Tsutsajaure Culmination (SCd4), and coaxial Singis Window (MTd2). Northwest-trending SWd2 folds within the Singis Window also developed during this event. These structures are later and not coaxial with otherwise similar northwest-trending folds in the Rombak-Sjangeli Window (RSd2 and SCd3).

D6 structures, like D5 northwest-trending folds, are associated with detachment on a lower thrust, and development of lateral ramp anticlines. The D6 thrust associated with this detachment may be the sole thrust of shear zone rocks exposed in the foreland, 20 kilometers southeast of the study area (Plate 7).

These D6 structures will also be further discussed in chapter 6, within the broader context of "thin-skinned" basement detachment.

D7-backfolding and warping along north-south axes

Warping of the entire package along roughly north-south trending fold-axes (RSd6, SCd5 and LGd4) followed the cessation of major translation along D4 through D6 thrust faults. This event is correlated with D6 of Crowley (1985) and Hodges (1985).

D8-west-vergent normal-slip shear along Rusjka Fault

Evidence for west-vergent normal faulting along the Rusjka Fault was discussed above (AAd5 and SGd6). Although the exact timing of D8 faulting is unclear, it appears to post-date D5 thrusting along the Matert Shear Zone. It is not unreasonable to assume that D8 extensional structures post-date the last compressional structure (D7). Arguments presented in chapter 5 suggest that this event may be related to the post-tectonic gravitational collapse of the orogen.

CHAPTER 4: METAMORPHISM OF THE SITAS - SINGIS AREA

INTRODUCTION

The degree of metamorphism within rocks of the Sitas-Singis area is quite variable, ranging from lower greenschist facies within the Rusjka Group to eclogite facies in the Aurek Assemblage. Structural relationships, ^{40}Ar-^{39}Ar thermochronology, and metamorphic mineral assemblages indicate the area experienced several episodes of metamorphism.

In this section, the metamorphic petrology of the major tectonostratigraphic elements in the Sitas-Singas area is discussed. Comparisons where applicable are made with correlative units to the west of the study area.

ANALYTICAL TECHNIQUES

More than 200 thin sections of samples from the Sitas-Singis area were examined to evaluate the conditions and timing of metamorphism. In order to expand the metamorphic studies already completed to the west (Hodges and Royden, 1984; Crowley, 1985), seven polished thin sections were prepared from upper nappe complex samples in the Sitas-Singis area (Fig. 4-1). Minerals from these samples were analyzed with the automated 3-spectrometer JEOL 733 "Superprobe" at M.I.T.. Synthetic and natural silicate standards were used and the Bence and Albee (1968) corrections were made by an on-line data reduction system. Representative mineral analyses of these samples are listed in Appendix B.

Temperature as a function of pressure for garnet-bearing metapelites was calculated using the FeMg exchange thermometer calibrated by Ferry and Spear (1978):

$$\underset{\text{pyrope}}{Mg_3Al_2Si_3O_{12}} + \underset{\text{annite}}{KFe_3AlSi_3O_{10}(OH)_2} = \underset{\text{almandine}}{Fe_3Al_2Si_3O_{12}} + \underset{\text{phlogopite}}{KMg_3AlSi_3O_{10}(OH)_2} \quad (1)$$

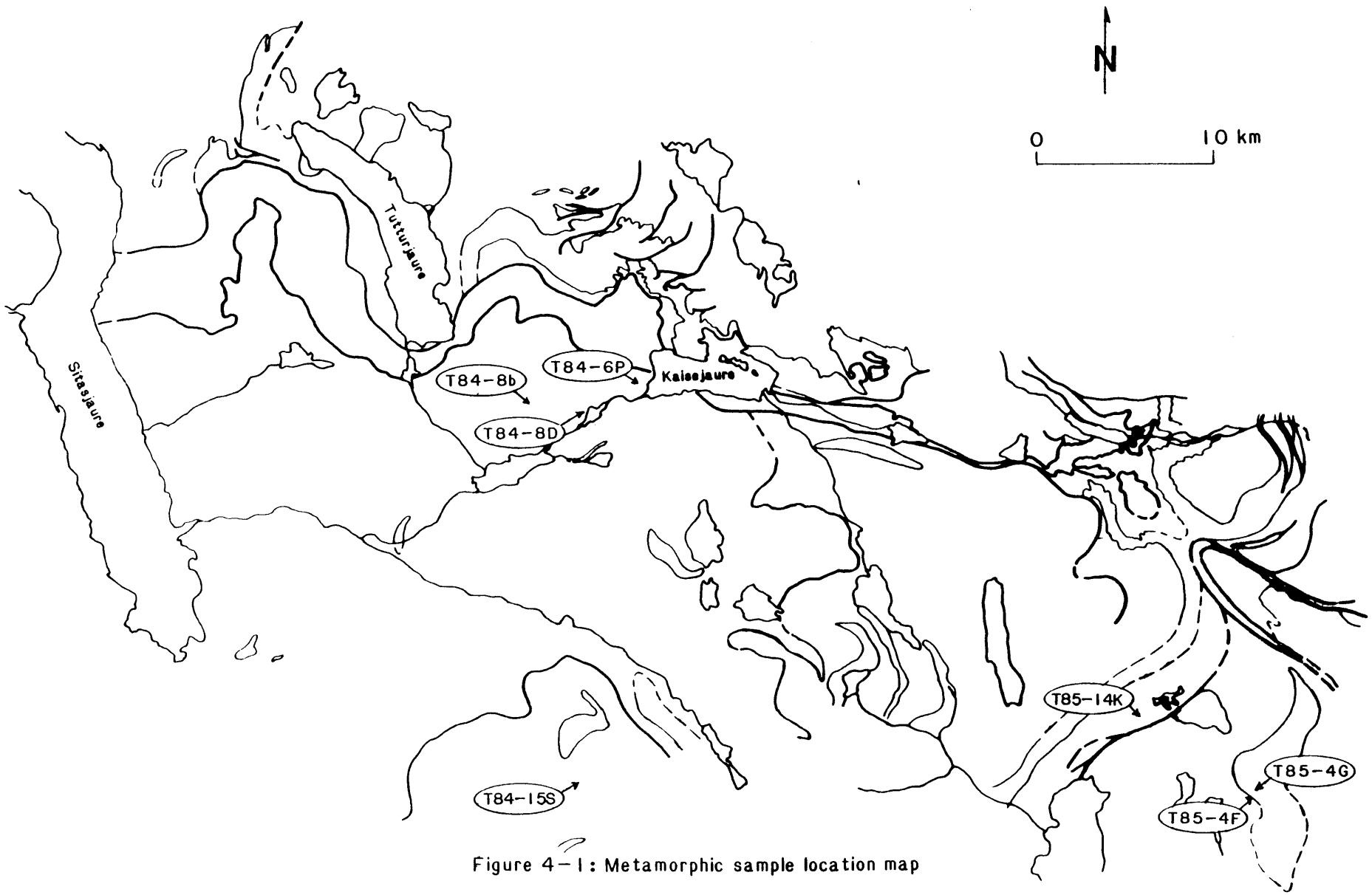

Figure 4-1: Metamorphic sample location map

Using the linear regression method of York (1969), Hodges and McKenna (submitted) re-regressed the experimental data of Ferry and Spear (1978) to obtain more accurate values for the enthalpy (ΔH) and entropy (ΔS) of the reaction. A unique solution for temperature and pressure was evaluated by solving reaction (1) simultaneously with the aluminum silicate free net transfer reaction:

$$\underset{\text{almandine}}{Fe_3Al_2Si_3O_{12}} + \underset{\text{grossular}}{Ca_3Al_2Si_3O_{12}} + \underset{\text{muscovite}}{KAl_3Si_3O_{10}(OH)_2} = \underset{\text{anorthite}}{3CaAl_2Si_2O_8} + \underset{\text{annite}}{KFe_3AlSi_3O_{10}(OH)_2} \quad (2)$$

Hodges and Crowley (1985) empirically calibrated this reaction against the garnet-biotite and garnet-plagioclase-aluminosilicate-quartz thermobarometers. The thermodynamic relations and values used for ΔH and ΔS in reactions (1) and (2) are listed in Appendix C. The solution models of Hodges and Crowley (1985) were used for both reactions. Assuming 3% analyical error, 2σ error ellipses were estimated for each sample using a Monte Carlo error propagation technique (Hodges and McKenna, submitted).

The value obtained for pressure and temperature through simultaneous solution of reactions (1) and (2) is valid only if certain criteria are satisfied. The most important of these is the assumption that the two reactions effectively "closed" at the same time. The rate of reaction (2) will depend on a variety of parameters including mass transfer rates and the availability of reactants. On the other hand, the rate of reaction (1) is principally dependent on $FeMg_{-1}$ interdiffusion in garnet. It is therefore possible that reactions (1) and (2) will close at different temperatures and pressures. In fact, consideration of the rate controlling parameters of reactions (1) and (2) suggests that (2) will likely close at a higher temperature than (1). The effect of this

discordance in closure temperature is illustrated in Figure 4-2. In the hypothetical uplift and cooling path, reaction (2) closes at T_2, while reaction (1) closes at the lower temperature T_1. Simultaneous solution of (1) and (2) however, yields p_3 and T_3, offset from the path. Extreme caution must therefore be applied when interpreting pressure-temperature data calculated in this manner.

ROMBAK-SJANGELI BASEMENT

Along the southwestern margin of the Rombak-Sjangeli Window, the basement is predominantly unfoliated to strongly foliated Grunfjell granite gneiss (Hodges, 1982; Crowley, 1985). To the east, the crystalline basement is far more heterogeneous with abundant pendants of amphibolite and metasedimentary rocks. In the Sitas-Singis area, the crystalline basement is overlain by autochthonous sedimentary rocks of the Dividal Group (see chapter 2).

None of the lithologies within the crystalline basement or overlying Dividal Group are garnet bearing. The absence of garnet makes quantitative estimates of peak pressure and temperature conditions difficult. However, application of the two-feldspar geothermometer of Whitney and Stormer (1977) to granite mylonite samples, Crowley (1985) estimated the peak temperature experienced by the basement as 400-450°C.

In the Sitas-Singis area, Grunfjell Greenstone has been recrystallized under epidote-amphibolite facies conditions (Chapter 2). Quartzitic siltstone of the red and green siltstone member of the overlying Tornetrask Formation contains dark brown metamorphic biotite. These phase relations suggest that Crowleys temperature estimate of approximately 400-450°C is probably valid for the basement of the southern margin of the Rombak -Sjangeli Window.

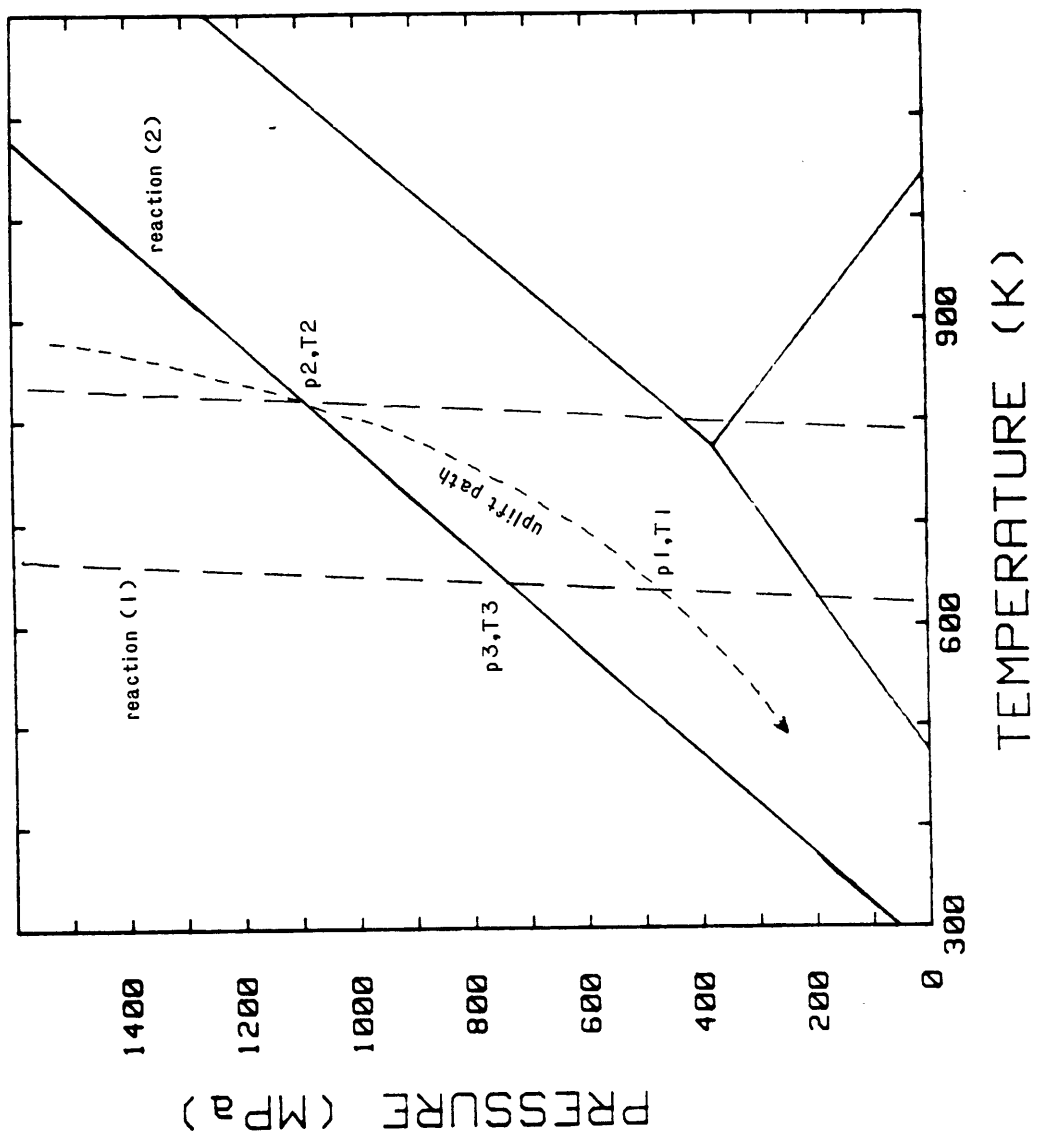

Figure 4-6: Effect of discordant closure temperature on calculated p-T data

STORRIT COMPLEX

Exposed along the southern margin of the Rombak-Sjangeli Window, the Storrit Complex is a shear zone which separates basement rocks within the window from upper nappe complex rocks above (Plate 7). The shear zone is a complex, heterogeneous assemblage of highly strained slivers of basement rock. In the Sitas-Singis area pelitic assemblages within the complex indicate metamorphism under biotite to chlorite grade conditions (chapters 2 and 3). However, west of Sitasjaure where the bulk composition of pelitic assemblages within the complex appear to be the same, garnets become abundant (Hodges, 1982; Crowley, 1985). Crowley (1985) analyzed six of these garnet bearing samples from the western shore of Sitasjaure. Assuming equilibrium phase relations, pressures and temperatures for the samples have been recalculated (Table 4-1) using reactions (1) and (2) above. These data (Figure 4-3) yield a mean value of 510°C and 710 MPa. Crowley (1985) interpreted these p-T values to represent the peak metamorphic conditions experienced by the Storrit Complex in this area. As noted earlier, the rocks of the Storrit Complex appear to have been derived from the Baltic Shield basement. Because the peak temperature of the immediately subjacent Baltic Shield basement of the Rombak-Sjangeli Window is estimated at 400-450°C (see above), significant S60E directed transport of the Storrit Complex must have occurred at temperatures and pressures below 510°C and 710 MPa. Furthermore, 510°C and 710 MPa is a minimum estimate of the peak p-T conditions of the basement terrain from which the Storrit Complex was derived.

Locally, Storrit Complex garnets have sygmoidal inclusion trails indicating syntectonic growth (Crowley, 1985, p. 138). The garnets have been variably overprinted by mylonitic fabrics indicating continued

TABLE 4-1: STORRIT COMPLEX PRESSURE-TEMPERATURE DATA

Sample	Source	Pressure (MPa)	Temperature (°C)
RP-4	1	678.6	519.5
RP-17	1	716.3	510.0
RP-20	1	781.0	536.0
RP-22	1	699.2	499.2
RP-24	1	764.8	491.8
FF-3	1	618.1	501.4

TABLE 4-2: LITTE GROUP PRESSURE-TEMPERATURE DATA

Sample	Source	Pressure (MPa)	Temperature (°C)
84-6P	2	886.0	534.6
84-8D	2	1094.7	617.4
84-8B	2	843.1	552.6
FF-2	1	936.8	601.9
FF-11	1	906.2	585.4
FF-12	1	1067.0	643.6
RP-25	1	1048.8	646.0
RP-31	1	959.9	592.6

1 - Crowley, 1985

2 - Tilke, this study

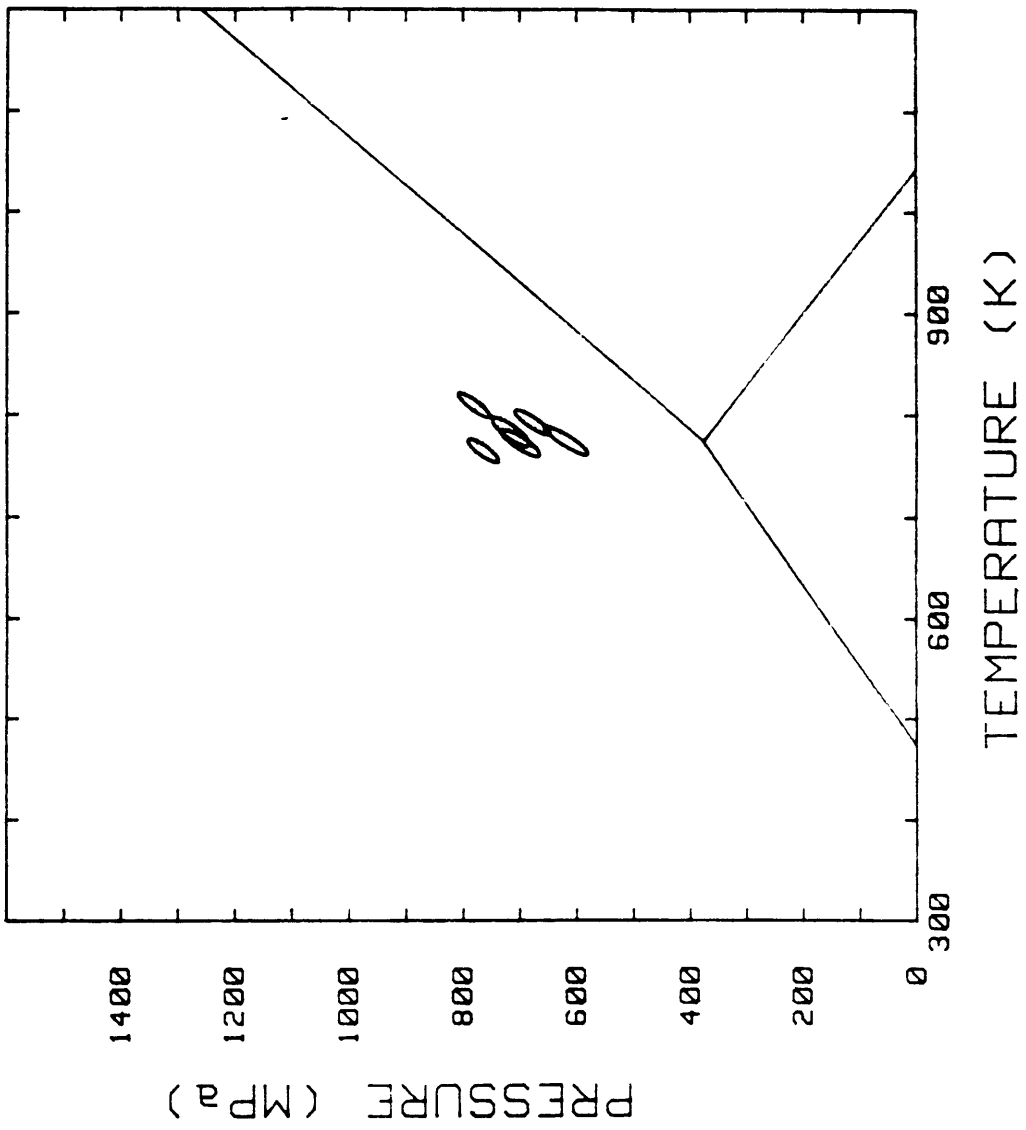

Figure 4-3: Storrit Complex p-T data

development and deformation of the shear zone as it cooled to chlorite grade conditions. The absence of garnet within the shear zone to the east may be due to two factors: 1) complete retrogression of garnet-bearing lithologies to chlorite or biotite grade during progressive shear strain, 2) continued accretion of material at sub-garnet grade conditions.

AUREK ASSEMBLAGE

INTRODUCTION

The Aurek Assemblage, exposed at the southeast margin of the study area is the structurally lowest unit within the upper nappe complex west of Singis (Plates 1, 2 and 7). In the Sitas-Singis area this unit has been subdivided into three lithologies: Aurek Gabbro, Aurek Amphibolite and Vidja Gneiss. The petrographic and structural relations of the Aurek Assemblage have been discussed in chapters 2 and 3 respectively. In this section the metamorphic petrology of each unit within the Assemblage is discussed in terms of phase relations and mineral compositions.

AUREK GABBRO

The Aurek Gabbro ranges from gabbro to olivine-gabbro in modal mineralogy. Much of this unit has retained its igneous mineralogy and granoblastic fabric, although it has been variably overprinted by anhydrous upper amphibolite to eclogite facies metamorphism. This eclogite facies metamorphism was in turn overprinted by a hydrous amphibolite facies metamorphism. Sample T85-4G1 contains phase and textural relations representative of these successive reactions (Fig. 4-4).

Sample T85-4G1 is from a silica undersaturated portion of the Aurek Gabbro with modal igneous olivine. The olivine has multiple corona structures: an internal corona of orthopyroxene, surrounded by a corona of

Figure 4-4: SEM image of Aurek Gabbro corona structure. Field of view 2.5 mm. Multiple corona structure in eclogitic olivine gabbro. Igneous olivine core with internal enstatite corona and external garnet corona. Surrounding matrix is plagioclase.

Figure 4-5: SEM image of Aurek Gabbro corona structure. Field of view 700 μ. Close up of garnet corona of same sample as Fig. 4-3. Note growth of secondary enstatite and kyanite needles at external margin of garnet corona.

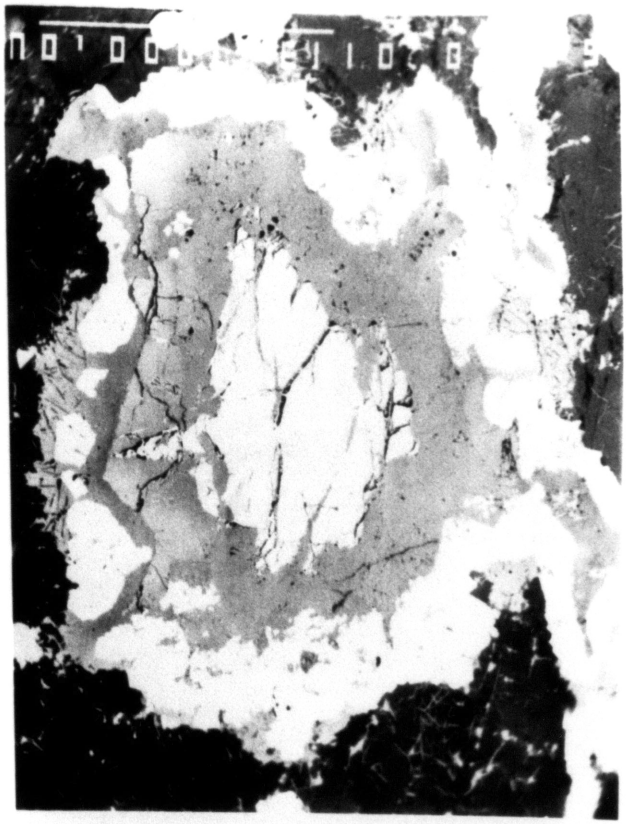

garnet, which in turn is surrounded by a discontinuous external corona of orthopyroxene (Fig. 4-4). The presence of ferro magnesian oxides within the olivine and internal orthopyroxene suggests the reaction for the initial breakdown of olivine is:

$$\underset{\text{olivine}}{2(Fe,Mg)_2SiO_4} \rightarrow \underset{\text{oxide}}{2(Fe,Mg)O} + \underset{\text{orthopyroxene}}{(Fe,Mg)_2Si_2O_6} \quad (3)$$

However, Green and Ringwood (1967) noted that the assemblage orthopyroxene + plagioclase is unstable above approximately 800-1000 MPa at 700°C. This instability results in the contemporaneous reaction producing the garnet corona:

$$\underset{\text{plagioclase}}{CaAl_2Si_2O_8} + \underset{\text{orthopyroxene}}{2(Fe,Mg)_2Si_2O_6} + \underset{\text{spinel}}{(Fe,Mg)Al_2O_4} \rightarrow \underset{\text{garnet}}{2Ca_{0.5}(Fe,Mg)_{2.5}Al_2Si_3O_{12}} \quad (4)$$

Evidence for this reaction is supported by Figure 4-6 which is a mineral zonation profile across part of the corona structure. The profile begins at the olivine-internal orthopyroxene boundary, crosses the surrounding garnet, and ends at the garnet-external orthopyroxene interface. At the contact with internal orthopyroxene, garnet has a composition similar to that predicted by reaction (4) above. Application of the garnet -orthopyroxene Fe-Mg exchange thermometer (Harley, 1984) to this interface yields a temperature of 700-730°C for the eclogite fácies metamorphism at 1000-1500 MPa. The K_D line for this thermometer is plotted in Figure 4-7.

As may be seen in the T85-4G1 garnet profile (Fig. 4-6), the outer portion of the garnet is associated with a 0.2 mole fraction increase in the grossular component, and a corresponding decrease in the pyrope component. Associated with this compositional change in the garnet is the growth of enstatite on the external margin of the garnet (Fig. 4-5). Acicular kyanite needles have also grown in both the outer portion of the garnet and within the external enstatite. These relations can be explained

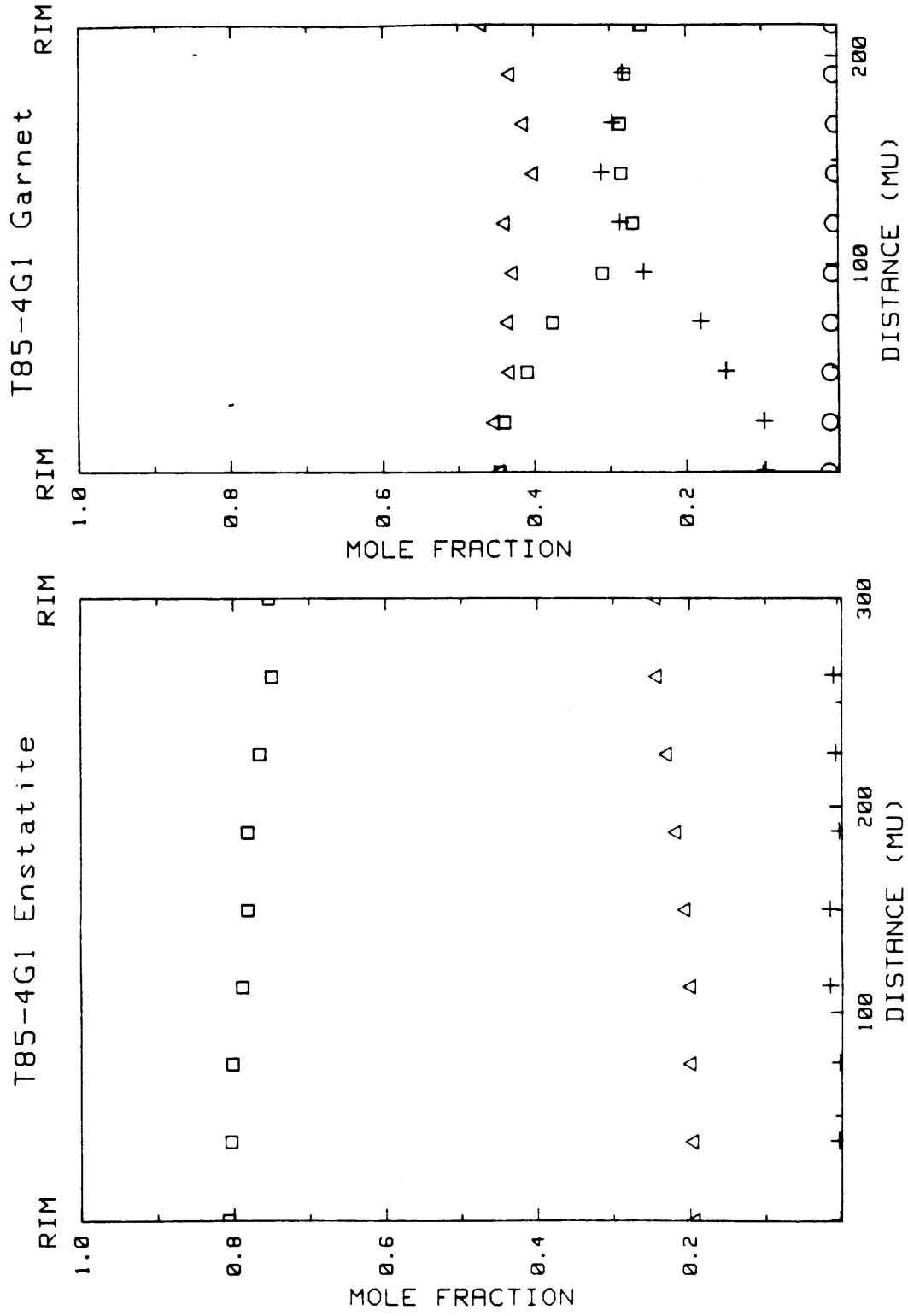

Figure 4-6: T85-4G1 enstatite and garnet zonation profiles
Symbols: triangles - Fe, squares - Mg, crosses - Ca, circles - Mn

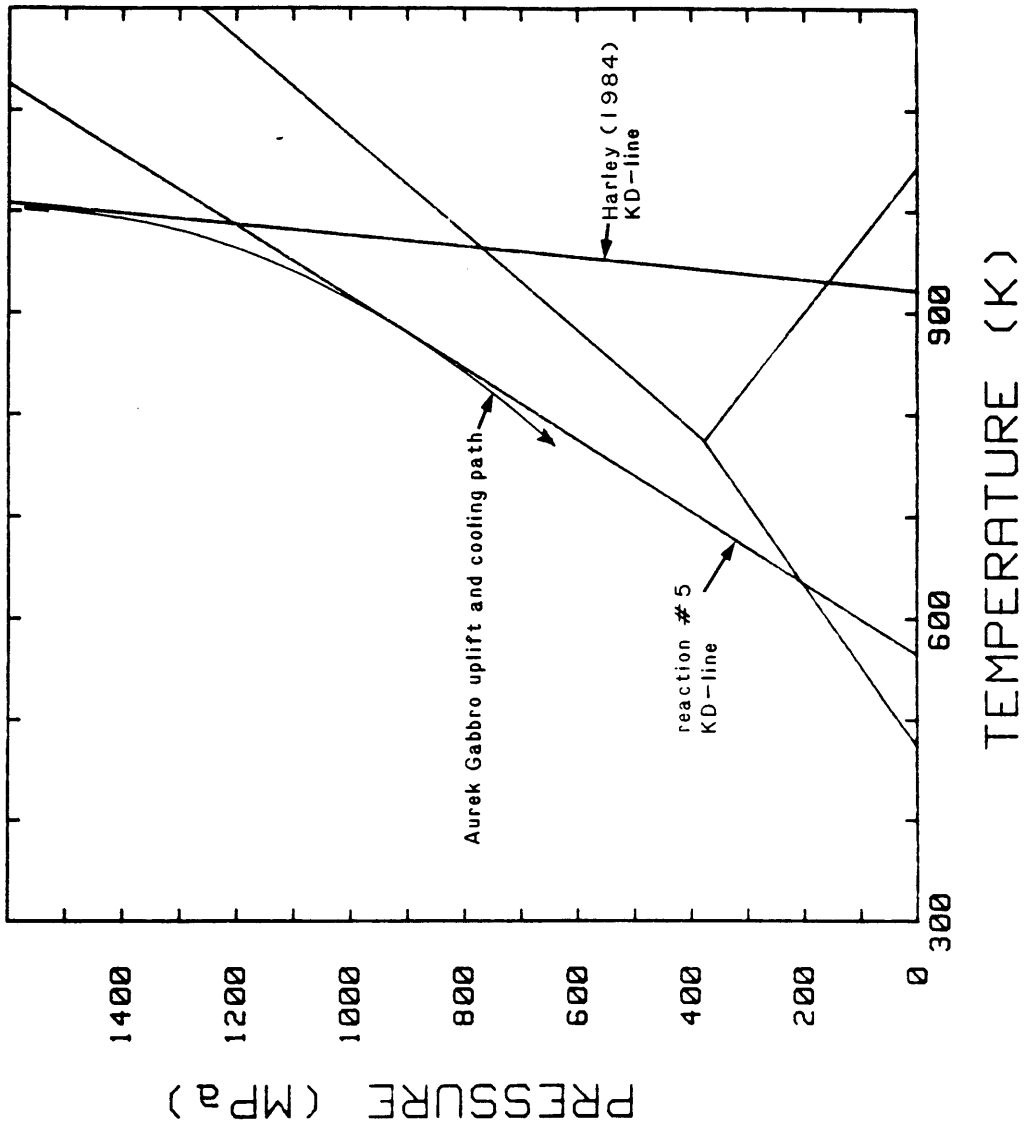

Figure 4-7: Aurek Gabbro sample T85-4G1 p-T path

by the reaction:

$$2CaAl_2Si_2O_8 + 2/3Mg_3Al_2Si_3O_{12} \rightarrow 2/3Ca_3Al_2Si_3O_{12} + 2Al_2SiO_5 + Mg2Si_2O_6 \quad (5)$$
anorthite pyrope grossular kyanite enstatite

Although this reaction has not been calibrated, a barometer was derived using the solution models of Newton and Perkins (1982), (see Appendix D). Using mineral compositions near the garnet-external enstatite interface, reaction (5) yields the K_D line in Figure 4-7. As noted above, the assemblage orthopyroxene + plagioclase is unstable at high pressures. Therefore, the production of enstatite in reaction (5) implies the Aurek Gabbro had decompressed below approximately 800-1000 MPa.

All the reactions discussed so far have been anhydrous. However, following or near closure of reaction (5), hydrous amphibolite facies retrogression ensued. In T85-4G1, this retrogression may be associated with the growth of zoisite within the plagioclase matrix, and the alteration of garnet and external orthopyroxene to hornblende (Fig. 4-5).

While there are large errors (>50°C) associated with the calculated K_D lines, the hypothetical uplift and cooling history of the Aurek Gabbro inferred from the relations discussed above is illustrated in Figure 4-7. The K_D line of the Harley (1984) geothermometer is interpreted to represent the peak temperature experienced by the Aurek Gabbro, and for reasons discussed earlier this must be on the high-pressure side of reaction (5). The Aurek Gabbro must therefore have experienced pressures greater than approximately 1200 MPa. The flat pyrope and grossular profiles for the outer portion of the T85-4G1 garnet suggests the Aurek Gabbro remained on the calculated K_D line of reaction (5) before cooling below the closure temperature of the reaction.

Eclogite facies metamorphism of basic rocks is narrowly defined by the complete consumption of plagioclase and presence of the diagnostic

assemblage omphacite-pyropic almandine-rutile (Green and Ringwood, 1966; Turner, 1981). Although T85-4G1 is not a true eclogite, plagioclase has been completely consumed in other localities within the Aurek Gabbro. This suggests that variations in the degree of eclogite facies metamorphism are due to a complex interplay of variations in bulk composition, kinetic factors and the presence or absence of fluids.

Andreasson et al. (1985) described similar eclogite facies rocks from the Seve Nappe in the Grapesvare area approximately 180 km south of the study area. These workers estimated temperatures of eclogite facies metamorphism for these units of 550-750°C. Roermund (1985) has also described eclogites from the lower part of the Seve Nappe where temperatures of 600°C were obtained for the eclogite crystallization.

AUREK AMPHIBOLITE

The Aurek Amphibolite is a reaction skarn or "black wall" separating the Aurek Gabbro from surrounding Vidja Gneiss (see chapter 2 for description). The garnet-hornblende Fe-Mg exchange thermometer of Graham and Powell (1985) yields a rim temperature of 616°C for sample T85-4F (Fig. 4-8). If the Aurek Gabbro was still on the K_D line defined by reaction (5), this temperature implies a pressure of approximately 925 MPa during the retrogression.

Later greenschist facies deformation in the Aurek Amphibolite and Gabbro is evidenced by blastomylonitic fabrics within the Amphibolite and locally in amphibolitic shear zones of the Gabbro (see Chapter 2).

VIDJA GNEISS

No microprobe analyses of samples from the Vidja Gneiss are reported, because early high-grade phases have been variably retrogressed by a

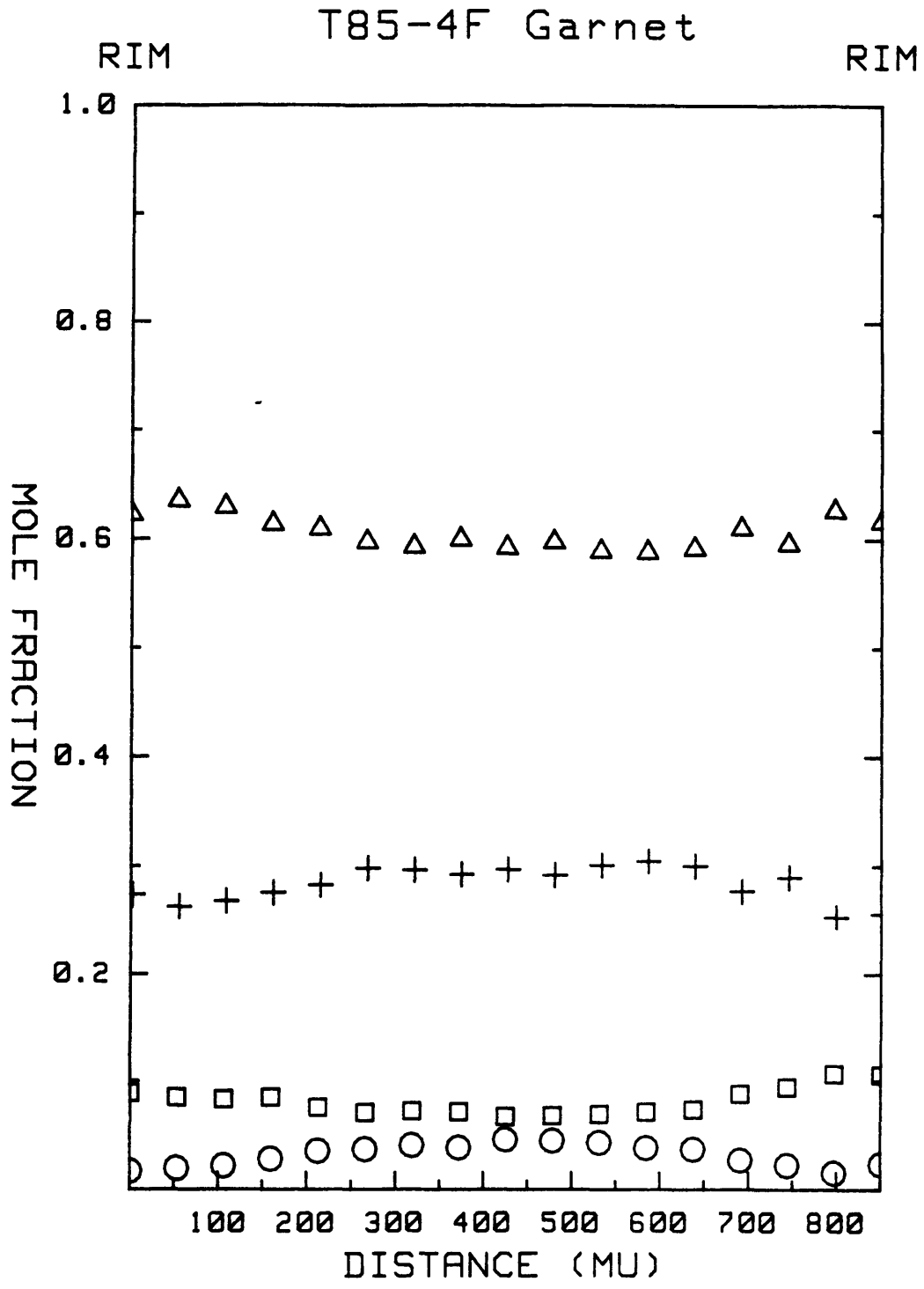

Figure 4-8: T85-4F garnet zonation profile (symbols as in Fig. 4-6)

biotite facies mylonitic deformation (see Chapter 2). However, the absence of K-feldspar, the presence of kyanite and muscovite, and the absence of symplectite in the primary metamorphic assemblage of the Vidja Gneiss constrains the peak metamorphic conditions to the shaded area of Figure 4-9. These relations suggest that the Vidja Gneiss did not attain the high pressure conditions of the Aurek Gabbro (cf. Fig. 4-7). Further, the approximate 925 MPa, 616°C hydrous retrogression of the Aurek Amphibolite discussed above is probably associated with the amphibolite facies intercalation of the Aurek Gabbro and Vidja Gneiss.

The biotite grade mylonitization of the Vidja Gneiss is responsible for the locally pronounced schistosity. As discussed in chapter 3, this deformation and metamorphism appears to be associated with thrust faulting on the Ruskja Fault during imbrication of the entire upper nappe complex.

SALKA GROUP

The Salka Group is a thick (1.5-2 km) sequence of predominantly chlorite grade calc-schists, graphitic schists and psammitic schists overlying the Aurek Assemblage in the eastern part of the study area. The Group was subdivided into three members: Rusjka Calcareous Schist, Rusjka Graphitic Schist, and Patta Quartzite (see chapter 2 for a detailed discussion of these units).

While the bulk of the Salka Group is characterized by the lower to middle greenschist facies assemblage quartz + muscovite + albite + chlorite + biotite + magnetite, garnet occurs near the lower and upper boundaries.

As discussed in chapter 3, up to 50 meters above the Rusjka Fault syntectonic garnets have grown within pelitic lenses of the Rusjka Calcareous Schist. Sygmoidal inclusion trails within the garnets indicate southeast directed shear strain associated with thrusting of the Salka

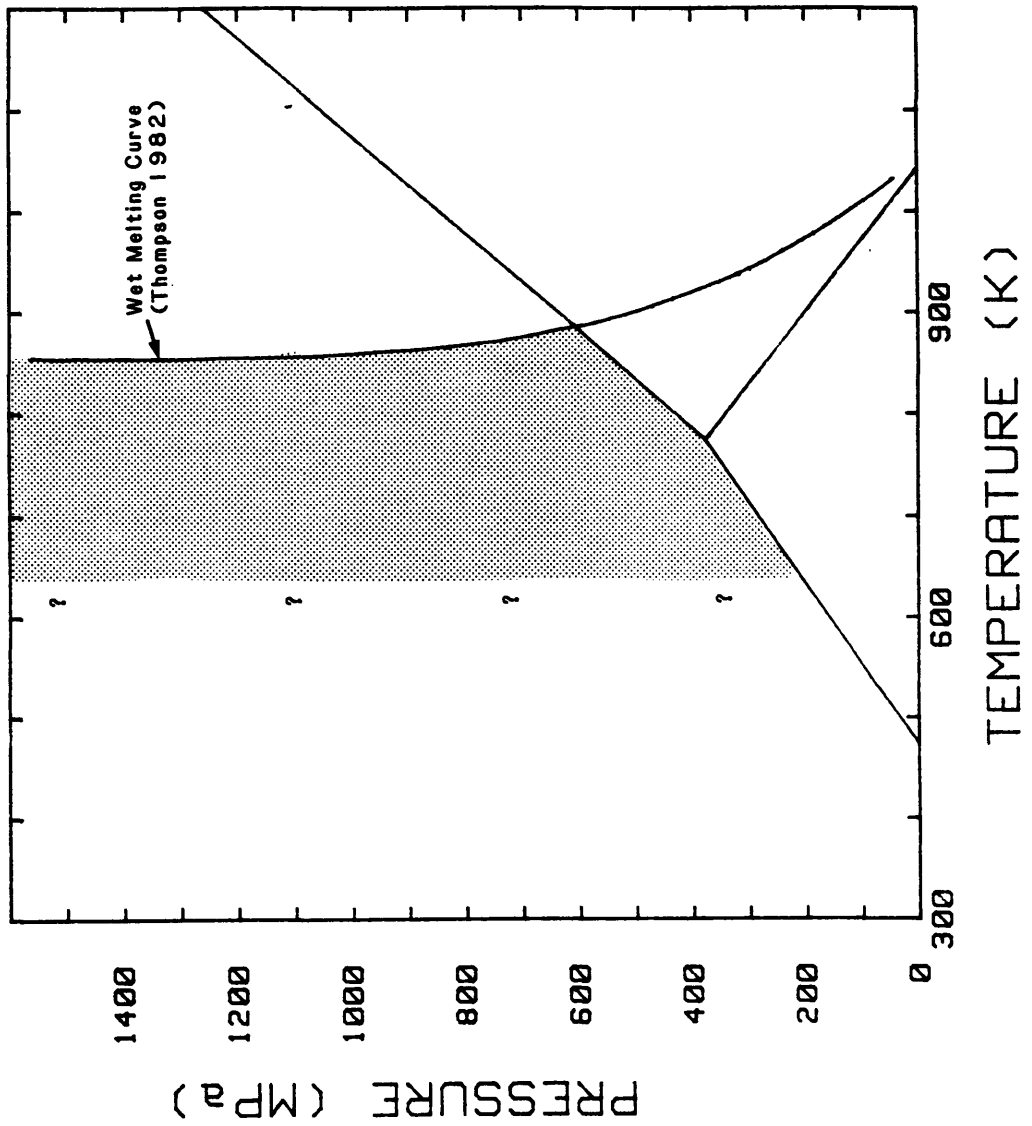

Figure 4-9: Vidja Gneiss peak metamorphic conditions

Group onto the Aurek Assemblage (Fig. 3-21). The presence of albitic plagioclase, and absence of a more anorthitic phase, prevents a quantitative pressure estimate using the garnet-plagioclase-muscovite -biotite geobarometer of Hodges and Crowley (1985). However, the garnet-biotite Fe-Mg exchange thermometer (reaction (1) above) yields a rim temperature of 530°C between 400-600 MPa for sample T85-14K. This temperature is interesting in that within similar lithologies over 50 m above the Rusjka Fault, the Salka Group is characterized by the much lower temperature chlorite to biotite grade assemblages. Similarly, the mylonitic deformation of the Vidja Gneiss associated with thrust faulting on the Rusjka Fault is associated with crystallization of biotite. This association of apparent low temperature mineral assemblages above and below the Rusjka Fault, with relatively high temperature assemblages within the shear zone may be a consequence of shear heating along the fault.

Towards the top of the Patta Quartzite, as the sliver zone of the Tjuolak Thrust is approached, fine-grained garnet idioblasts appear and become locally abundant (see chapters 2 and 3). There is no petrographic evidence for a change in bulk composition, which suggests the appearance of garnet is associated with an increase in metamorphic grade rather than a change in bulk composition. The thermal pulse responsible for this increase in grade may be associated with emplacement of the amphibolite grade Litte Group along the Tjuolak Thrust.

LITTE GROUP

INTRODUCTION

The Litte Group is the most areally extensive horizontal unit in the study area (Plates 1 and 7). It consists of a relatively flat-lying sequence of garnet + muscovite + biotite + quartz ± chlorite ± hornblende ±

ankerite schist. East of Sitasjaure, the Litte Group is subdivided into two formations: the Njunjas Schist, and Rapetjakka Schist (see chapter 2). The Litte Group continues to the west of Sitasjaure, where garnet two-mica schists of the Skjafjell Schist stratigraphically overlie the Rapetjakka Schist (Crowley, 1985). Although structural complexities make direct correlation with the Efjord area difficult, the Skjafjell Schist also crops out northeast of Efjord (Plate 1 of Hodges, 1985; Plate 7).

In the Sitas-Singis area, mineral growth post-dates the primary schistosity development. Garnet, hornblende and cross-foliation biotite typically form idioblasts with planar helicitic quartz inclusion trails (Fig. 2-19). The degree of visible retrogression is highly variable; locally, near the roof thrust of the Storrit Complex ferromagnesian phases have been completely chloritized.

In this section the p-T estimates for three relatively unaltered samples from west of Kaisejaure (Plate 1) are presented. These results are compared with p-T estimates obtained by Crowley (1985) for Litte Group and Storrit Complex units from southwest of Sitasjaure.

KAISEJAURE AREA SAMPLES

Two samples from the Upper Njunjas Schist were analyzed. Sample T84-6P (Fig. 4-10) contains variably retrograded euhedral garnets, with biotite, muscovite, epidote, peristeritic albite and oligoclase, minor chlorite, and quartz. Sample T84-8D, although having the same modal mineralogy as T84-6P is more calcic and has a complex garnet zonation profile (Fig. 4-11). The compositional jumps seen in the profile seem to be associated with discontinuous reactions, rather than multiple metamorphic events. For example, the decrease in grossular component at

200 and 800μ (Fig. 4-11) is associated with the disappearance of quartz inclusions (Fig. 4-12). These changes could be due to the appearance of a calcium silicate phase in the matrix, e.g. epidote or plagioclase. Rim temperatures and pressures from these samples were calculated using reactions (1) and (2) and are listed in Table 4-2.

Sample T85-8b was collected from the Lower Rapetjakka Schist and contains the typical assemblage of this unit: garnet + hornblende + biotite + muscovite + epidote + oligoclase + chlorite + quartz. The calculated temperature and pressure for this sample using reactions (1) and (2) is 553°C and 843 MPa respectively (Table 4-2). This temperature is approximately 60°C higher than that obtained using the garnet-hornblende thermometer of Graham and Powell (1984); the discrepancy is probably well within the error limits of the two reactions.

METAMORPHISM OF THE LITTE GROUP IN THE EFJORD-SINGIS AREA

In addition to the three Litte Group samples from the Kaisejaure area, pressures and temperatures for five Litte Group samples from west of Sitasjaure (Crowley, 1985) are listed in Table 4-2. Sample RP-36 of Crowley (1985) is not included, as the reported plagioclase analysis is albite, for which the plagioclase solution model of Hodges and Crowley (1985) is not applicable.

These pressure-temperature data are plotted in Figure 4-13 along with the recalculated Storrit Complex (see earlier) data. It is clear from this plot that Litte Group p-T estimates overlap, despite being from localities up to 35 km apart. The "trend" in p-T space defined by the Litte Group data is subparallel to the K_D line of reaction (2). Therefore, this array may not be an uplift and cooling path, but rather as discussed earlier a

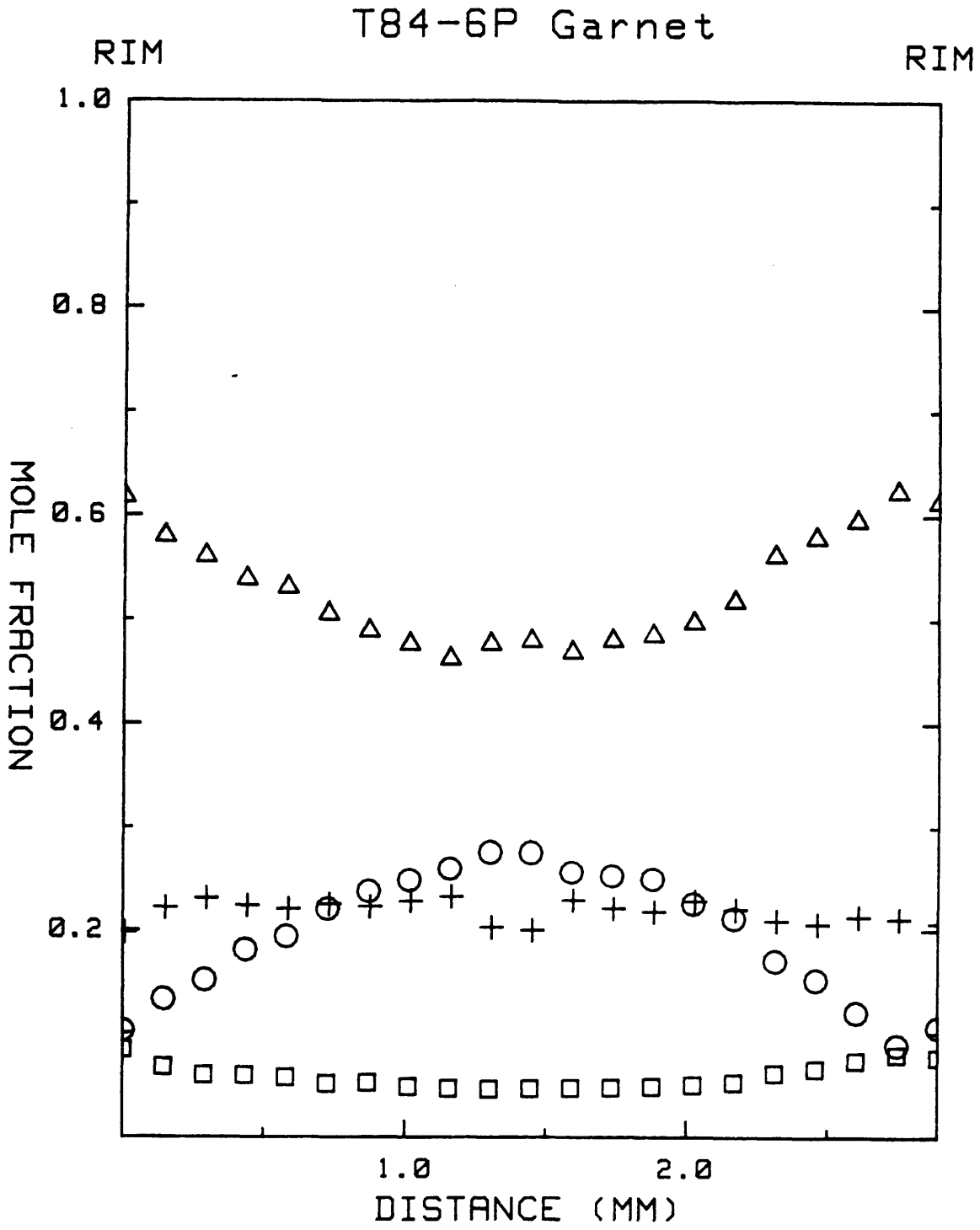

Figure 4-10: 84-6P garnet zonation profile (symbols as in Fig. 4-6)

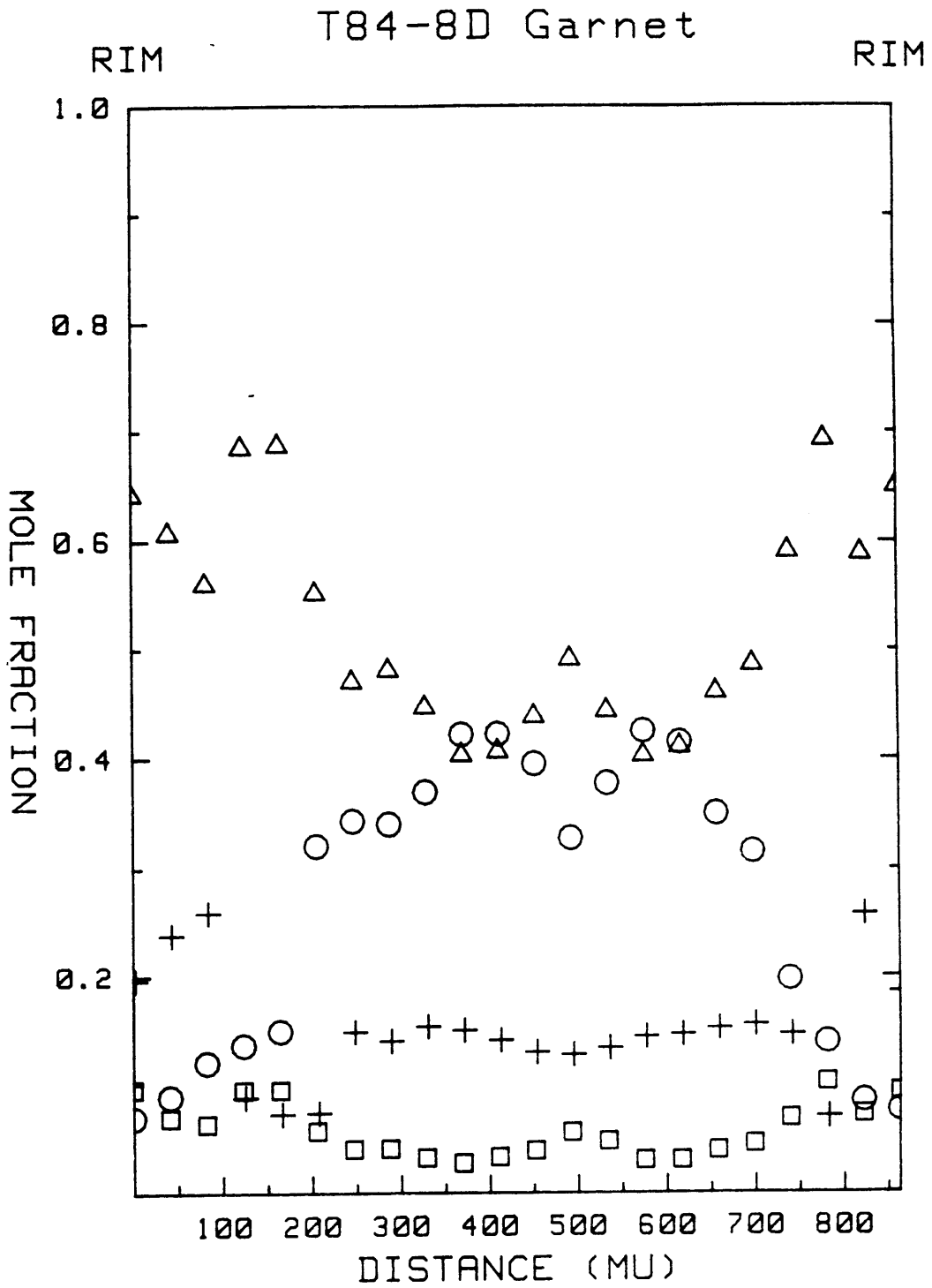

Figure 4-11: T84-8D garnet zonation profile (symbols as in Fig. 4-6)

Figure 4-12: SEM image of upper Njunjas Schist garnet. Field of view 1000 μ. Note euhedral garnet outline and multiple corona structures. Inclusion rich core surrounded by inclusion free rim. Note dark external 200 μ rim associated with increase in grossular component.

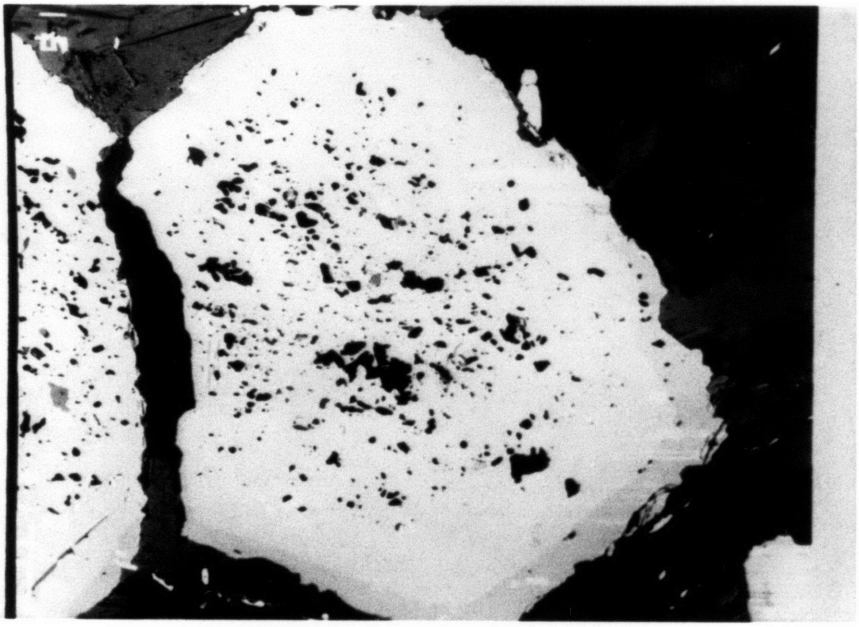

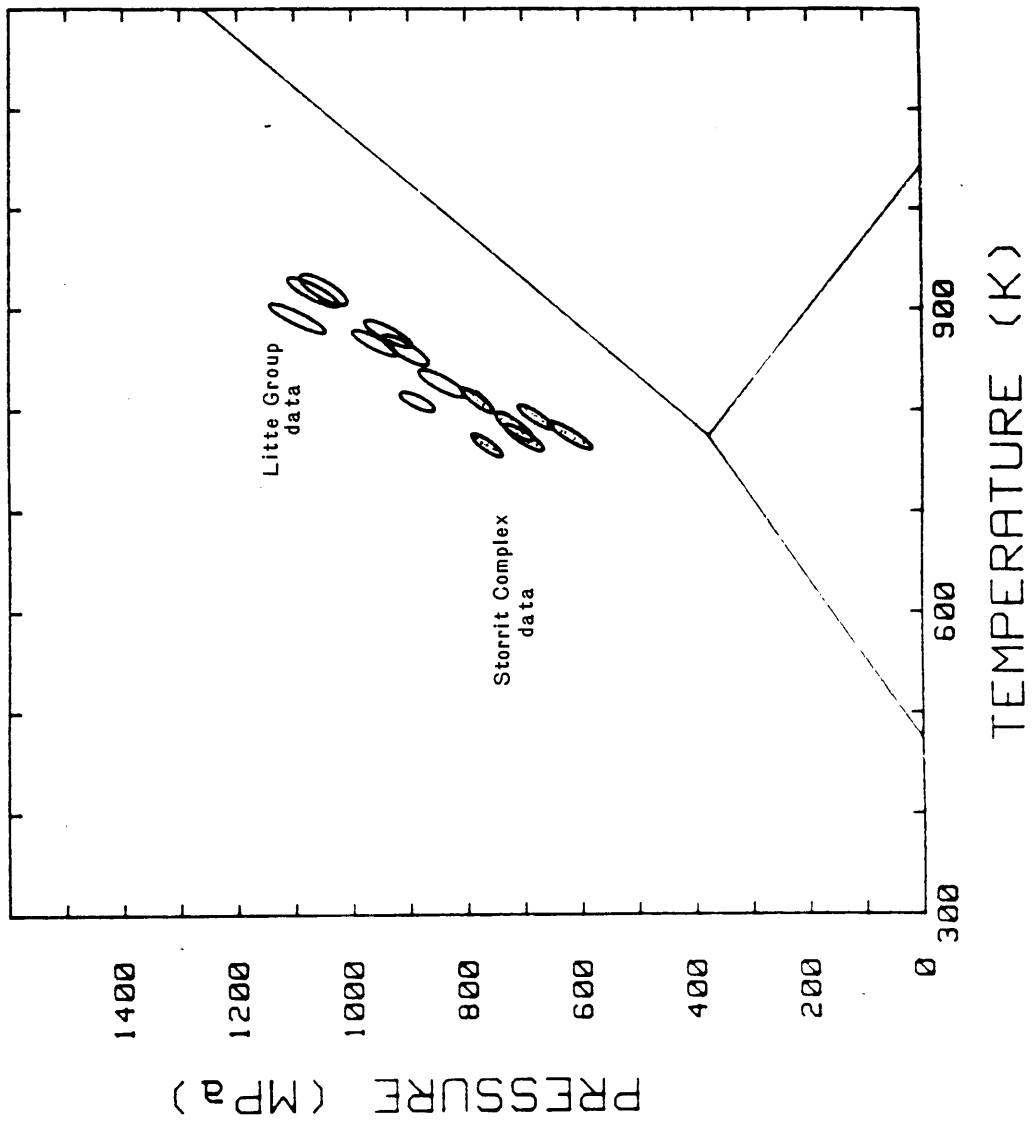

Figure 4-13: Litte Group and Storrit Complex p-T data

consequence of the difference in closure temperature of reactions (1) and (2). The Litte Group may have cooled below the closure temperature of (2), with different samples closing to reaction (1) at progressively lower temperatures. If this is the case, the points at the high p-T end of the array would most closely approximate the intersection of the reaction (2) K_D line with the true p-T path of the Litte Group at approximately 1070 MPa and 635^{o}C.

Regardless of whether the Litte Group p-T array is an uplift and cooling path or a consequence of different closure temperatures for (1) and (2), the entire array records pressures at least 130 MPa higher than the mean pressure recorded by the Storrit Complex data. However, at present the entire Litte Group overlies the Storrit Complex; this implies more than 3.5 km post metamorphic vertical movement of the Litte Group relative to the Storrit Complex.

MAITAT COMPLEX

The Maitat Complex is exposed as a large klippen near the southern boundary of the study area (Plates 1 and 7). As discussed in chapter 2, the high primary chlorite content of the unit gives it a distinctive pale green color. The distinctive matrix lithology, presence of discontinuous mafic pods, and structural position above the Rapetjakka Schist makes correlation with the Filfjell Complex (Crowley, 1985) compelling. Crowley (1985) noted the similarity between the Filfjell Complex and more areally extensive Rauvatn Complex (Plate 7).

Textural and petrological evidence suggests the Maitat Complex may have been affected by two metamorphic events. Two generations of garnet are present within Maitat Complex samples (Fig. 4-15). The earlier generation deflects the MCd1 foliation (Chapter 3), contains abundant

quartz and feldspar inclusions, and is strongly retrogressed. Second generation garnets are idioblastic, overgrow the foliation, and contain relatively few inclusions. Therefore the first episode was prior to or synchronous with development of the MCd1 schistosity, while the second episode clearly postdates MCd1. The retrograde nature of the first generation garnets compared to the pristine second generation suggests the second metamorphic event was a lower grade than the first.

Second generation garnet from the Maitat Complex yields a prograde zonation profile (Fig. 4-16). Since albite was the only plagioclase phase present, pressures could not be estimated using reaction (2). However, garnet-biotite geothermometry yields temperatures of about 520°C at 400-800 MPa.

Figure 4-14: Multiple garnet growth in Maitat Complex thin section. Field of view 12 mm. Note two generations of garnet. Early garnet has asymmetric pressure shadows, is strongly retrogressed and contains abundant inclusions. Second generation garnet is idioblastic, has overgrown foliation and contains relatively few inclusions.

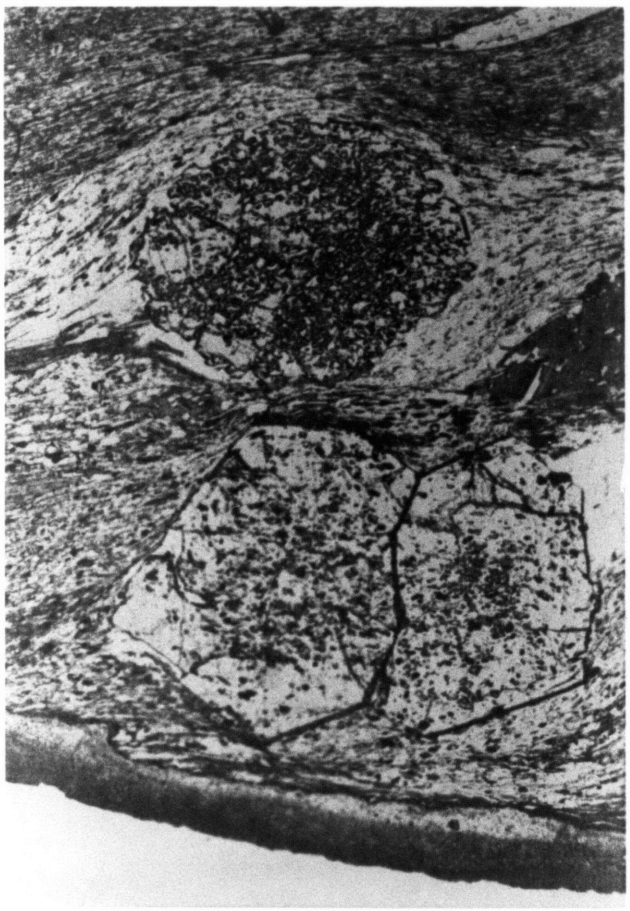

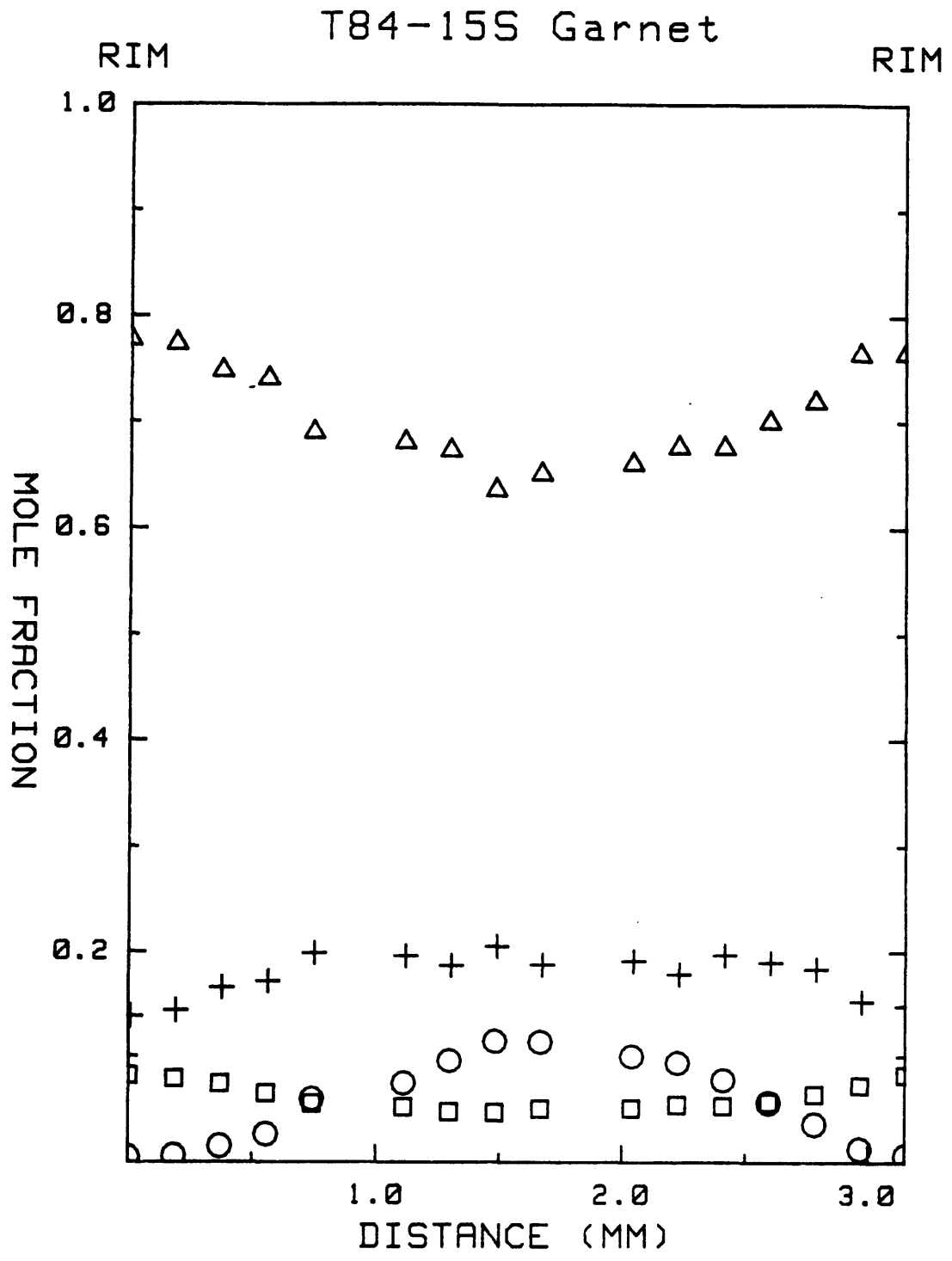

Figure 4-15: T84-15S garnet zonation profile (symbols as in Fig. 4-6)

CHAPTER 5: ^{40}Ar-^{39}Ar GEOCHRONOLOGY OF THE EFJORD - SINGIS AREA

INTRODUCTION

The timing of early and middle Paleozoic metamorphism, deformation and cooling in the Scandinavian Caledonides is a controversial subject. The presence of Upper Ordovician to Lower Silurian fossils and Early Silurian to Early Devonian K-Ar and Rb-Sr mineral dates has led most workers to consider the main phase of Caledonian deformation and metamorphism in this area to be an Early Silurian to Early Devonian event (e.g. Gee, 1975). However, evidence of a Late Cambrian to Early Silurian high-grade metamorphic and deformational events affecting the miogeocline of Baltica has been documented in north Norway (Sturt et al., 1975, 1978) and in the Bergen area (Henriksen, 1981). This event is termed the Finnmarkian Orogeny and recent results suggest a broadly coeval event may have affected several units within the upper nappe complex of central and northern Scandinavia (e.g. Claesson, 1980a, 1980b; Dallmeyer et al., 1985; Dallmeyer and Gee, 1986). While evidence for this Late Cambrian to Early Ordovician event is compelling, many questions concerning it still exist. Is the Finnmarkian Orogeny in the central and northern Caledonides a reality, or is it an artifact of the isotopic data? If this event is real, which tectonostratigraphic elements has it affected? Further, is it a distinct orogenic episode, or is it part of a continuous deformational phase extending from Late Cambrian to Early Devonian time as suggested by Dallmeyer et al. (1985)?

In the area of the Lofoten-Kebnekaise transect, detailed mapping at a scale of 1:25,000 indicates the existence of multiple metamorphic and deformational events (Hakkinen, 1977; Bartley, 1981; Hodges, 1982, 1985; Crowley, 1985; Tilke, this work). While these studies have yielded much

information on the nature and magnitude of these events, many of the timing relationships are unclear. Are the thrust faults which separate upper nappe complex rocks from the underlying crystalline basement a single fault, or are they multiple faults which imbricate the basement? Further, if these faults imbricate the basement, what are their geometric and temporal relationships to one another, and how do they relate to faults within the upper nappe complex?

Hodges (1982) and Hodges and Royden (1984) have documented a high-grade uplift and cooling path for the Sjurvatnet and Skjafjell Schists in the Efjord area. Royden and Hodges (1984) attempted to model this path. What is the true cooling history of the area, and can the relatively straightforward thermal modelling of Royden and Hodges (1984) be applied to the northern Scandinavian Caledonides?

It was with these questions in mind that a systematic sampling of amphibolites and pelites for ^{40}Ar-^{39}Ar dating was made between the Efjord and Singis areas (plate 7). These samples are all from the contiguous study areas of Hodges (1982), Crowley (1985), and Tilke (this work), which together form a 90 km transect across the orogen. As excess ^{40}Ar contamination is a major problem in the Caledonides (see below), the ^{40}Ar-^{39}Ar incremental step-heating technique was applied to these samples. During the analyses, it became apparent that extraneous ^{40}Ar in these samples was typically of non-atmospheric composition. However, the isotope correlation technique of Roddick et al. (1980) allows, under the appropriate conditions, the extraneous ^{40}Ar composition to be calculated, and the true age of the sample determined. This technique was modified and successfully applied to nine hornblende release spectra. However, high and relatively constant $^{40}Ar/^{36}Ar$ values in micas (see Appendix E1) prevented

use of the technique on these minerals.

In this chapter, analytical techniques are reviewed, followed by a discussion of previous geochronological work done in the Lofoten-Sitasjaure area. The basic theory of the isotope correlation technique is reviewed, along with modifications to overcome the problems of heterogeneous excess argon. The actual ^{40}Ar-^{39}Ar results from this study are then presented, followed by an interpretation of the data. Finally, the thermal evolution of the Efjord-Kebnekaise area implied by these data is discussed.

All the heating schedules, release spectra, and hornblende correlation diagrams for the data of this study are included in appendices E1, E2 and E3 respectively. The release spectrum of sample T84-19G, for example, is therefore Figure E2 T84-19G.

ANALYTICAL TECHNIQUES

Standard thin sections were prepared from over fifty potential ^{40}Ar-^{39}Ar samples collected in the Efjord-Singis area. Samples were rejected from consideration on the following bases: fine grain-size, chloritic or sericitic alteration, disequilibrium textures, and abundant inclusions. Twenty samples from 1-2 kg blocks were then crushed and sieved to a 0.45-0.25 mm size fraction. 15 hornblende, 3 muscovite and 6 biotite separates were obtained using standard magnetic and heavy liquid techniques. Samples were handpicked to remove composite grains with biotite, muscovite and oxides, until over 99 percent pure. 400 mg hornblende and 100 mg mica fractions of these samples were wrapped in Al foil and stored in evacuated glass vials. Biotite monitor SB51 was also loaded between each hornblende pellet, and every second mica pellet. This monitor from the Songo granodiorite in western Maine has a K-Ar age of 246.7 +/- 2 Ma using the decay constants and isotopic abundances

recommended by Steiger and Jager (1977). The vials were irradiated for 48 hours at 1 MW in the H-5 position of the Ford reactor at the University of Michigan. Isotope analyses were performed in the geochronology lab at the University of Maine, Orono (supervised by Dan Lux) on a Nuclide 6-60 SGA 1.25 automated mass spectrometer. Ar extraction was performed with a radiofrequency induction furnace, the temperatures of which were determined by an optical photometer to an accuracy of +/-50°C. The rare gas was purified from the samples with a CuO-Cu getter used in conjunction with a zeolite dessicant, and a SAES Zr-Al getter. 12-18 increments were run on each hornblende, and 6 on each mica separate. This procedure allows one gas fraction to be purified every 70 minutes, although "piggybacking" of these steps allows an analysis every 35 minutes. Correction factors to account for interfering isotopes were measured on CaF_2 and K_2SO_4 salts, and are: $(^{39}Ar/^{37}Ar)_{Ca} = 7.53 \times 10^{-4}$, $(^{36}Ar/^{37}Ar)_{Ca} = 2.75 \times 10^{-4}$ and $(^{40}Ar/^{39}Ar)_{K} = 3.91 \times 10^{-2}$. K/Ca ratios were calculated for each increment from the $^{39}Ar/^{37}Ar$ ratios. Knowledge of the ^{40}Ar line blank concentration becomes crucial for the correlation diagram technique (see below and Roddick et al., 1980). Values obtained for the blank correction were obtained by repeat measurements following "bakeouts" of the argon clean up line. Repeat measurements yielded values ranging from 1.2×10^{-13} to 6×10^{-13} moles per increment. Many of the samples were saturated with excess argon, yielding uninterpretable release spectra which are neither presented nor discussed in this chapter.

PREVIOUS GEOCHRONOLOGY

In an attempt to understand the tectonothermal evolution of the transect area, several workers have pursued isotopic studies, meeting with varying degrees of success (Bartley, 1981; Hodges, 1982; Crowley, 1985; see

Table 5-1). In this section, the results of these studies from East Hinnoy, the Efjord area and the Sitasjaure area are presented and discussed.

Bartley (1981) obtained Rb-Sr whole rock ages from the crystalline basement of the Lofoten block and whole rock-biotite ages from both the Lofoten block and the upper nappe complex on East Hinnoy (see Figure 1-3). A Rb-Sr whole rock errorchron (Brooks et al., 1972) of 1726 +/-31 Ma was obtained from the Middagstind Quartz Syenite, a pre-Caledonian intrusive body. This age is similar to ten Rb-Sr whole rock ages reported by Griffin et al. (1978) from west of Hinnoy, and is interpreted to be related to the same phase of "Svecofennian" mangerite intrusions. Four Rb-Sr biotite -whole rock ages were obtained from the Middagstind Quartz Syenite and the allochthonous Ruggevik Tonalite Gneiss (Table 5-1). While the younger age of sample 27F is not understood, the other three samples yield a weighted mean average age of 360.3 Ma. This result is interpreted to reflect the time of cooling of East Hinnoy below the closure temperature of Sr diffusion in biotite (331°C at a cooling rate of 9°C/Ma, see below).

Hodges (1982) obtained 4 K-Ar biotite ages, and 3 K-Ar hornblende ages from basement and upper nappe complex units in the Efjord area (Table 5-1). The heterogeneity of these ages and the results of the present study indicate that the samples are plagued with excess argon. The most that can be interpreted from these data is that the Efjord area cooled from 500°C to 300°C during Caledonian time.

Crowley (1985) obtained a three point Sm-Nd isochron age of 887 +/-90 Ma from a gabbro sheet within the Marko Complex west of Sitasjaure (Plate 7). Crowley (1985) interpreted this result to represent the age of crystallization of the gabbro sheet. This result is interesting in that it

TABLE 5-1: PREVIOUS GEOCHRONOLOGIC DATA FROM THE LOFOTEN-KEBNEKAISE TRANSECT

Sample	Source	Lithology	System	Age
-	1	Middagstind Qtz Syenite	Rb-Sr w.r.	1726±31
26R	1	Middagstind Qtz Syenite	Rb-Sr biot-w.r.	361±3
27F	1	Middagstind Qtz Syenite	Rb-Sr biot-w.r.	347±4
HQ-5	1	Ruggevik Tonalite Gneiss	Rb-Sr biot-w.r.	358±4
780C	1	Ruggevik Tonalite Gneiss	Rb-Sr biot-w.r.	362±5
791G	2	Tysfjord granite	K-Ar biot	376±32
79-5C	2	Sjurvatn schist	K-Ar biot	377±32
79-12E	2	Sjurvatn schist	K-Ar biot	369±32
79-3H	2	dike in Tysfjord Granite	K-Ar biot	393±26
79-3H	2	dike in Tysfjord Grantie	K-Ar hbl	463±38
79-7D	2	Raudvatn Amphibolite	K-Ar hbl	436±36
79-14D	2	dike in Sjurvatn Schist	K-Ar hbl	448±40
-	3	Marko Complex gabbro	Sm-Nd w.r.	877±90

1 - Bartley, 1981

2 - Hodges, 1982

3 - Crowley, 1986

statistically overlaps with the 735 +/- 260 Ma Rb-Sr whole rock isochron obtained by Claesson (1977) for the Ottfjallet dike swarm of the Sarv Nappe in the central Scandinavian Caledonides. Gee (1975) considers the Ottfjallet tholeiitic dike swarm to reflect extension associated with initial rifting and subsequent formation of the Iapetus Ocean.

^{40}Ar-^{39}Ar CORRELATION DIAGRAM THEORY

INTRODUCTION

Correct application of the K-Ar dating method, like all geochronological techniques, is based on several assumptions (Dalrymple and Lanphere, 1969; Faure, 1977). Three of the most commonly violated of these assumptions are:

a) the system has remained closed with respect to ^{40}Ar loss following metamorphic recrystallization.

b) no "excess argon" has entered the system subsequent to metamorphic recrystallization.

c) a mineral system lost all its radiogenic ^{40}Ar during metamorphism.

Here, the term "excess argon" is used for all ^{40}Ar within the system other than that produced by in situ decay of ^{40}K following closure of the system to ^{40}Ar loss.

The northern and central Scandinavian Caledonides are one of the type localities for excess argon (e.g. Wilson, 1972). As such, application of K-Ar dating to Caledonian problems in northern Scandinavia requires careful assessment of non-radiogenic ^{40}Ar within the sample.

In this section, application of the isotope correlation plot (Roddick et al., 1980) to determine the composition of excess argon in the ^{40}Ar-^{39}Ar dating technique is discussed. Knowledge of the composition of this excess argon permits a more accurate age estimate to be made.

EXCESS ARGON

Conventionally, extraneous (non-radiogenic) argon is assumed to have an atmospheric composition, i.e. $^{40}Ar/^{36}Ar = 295.5$ (e.g. Dalrymple et al., 1981). The radiogenic $^{40}Ar/^{39}Ar$ ratio is then calculated assuming all ^{36}Ar is atmospherically derived:

$$(^{40}Ar/^{39}Ar)_{rad} = (^{40}Ar/^{39}Ar)_{meas} - 295.5 * (^{36}Ar/^{39}Ar)_{meas} \quad (1)$$

where:

$(^{40}Ar/^{39}Ar)_{rad}$ = radiogenic $^{40}Ar/^{39}Ar$

$(^{40}Ar/^{39}Ar)_{meas}$ = measured $^{40}Ar/^{39}Ar$

$(^{36}Ar/^{39}Ar)_{meas}$ = measured $^{36}Ar/^{39}Ar$

Often, however, extraneous argon can have an $^{40}Ar/^{36}Ar$ ratio significantly higher than 295.5. Excess ^{40}Ar not associated with atmospherically derived ^{36}Ar has the effect of increasing the $(^{40}Ar/^{36}Ar)_{extr}$ value, viz:

$$(^{40}Ar/^{36}Ar)_{extr} = (^{40}Ar_{excess} + {}^{40}Ar_{atmos})/{}^{36}Ar_{atmos} > 295.5 \quad (2)$$

where:

$(^{40}Ar/^{36}Ar)_{extr}$ = extraneous $^{40}Ar/^{36}Ar$

$^{40}Ar_{atmos}$ = atmospherically derived ^{40}Ar

$^{36}Ar_{atmos}$ = atmospherically derived ^{36}Ar

A likely source for this excess ^{40}Ar is through degassing of the underlying 1.7 Ga Baltic Shield basement during Caledonian metamorphism. This degassed ^{40}Ar may have been transported in solution to rocks within the overlying upper nappe complex.

While excess ^{40}Ar is of ubiquitous occurrence in the samples studied, it is particularly concentrated in amphibolites from the Aurek Assemblage (see below). Lux (1985) noted a similar phenomenon in samples from the Western Gneiss Terrain of southwestern Norway. It was found that excess

argon contamination was much greater within eclogite pods than in the surrounding gneissic units. Along these lines Foland (1983) argued that excess ^{40}Ar within "dry" polymetamorphic rocks may remain trapped along grain boundaries following metamorphism rather than being removed in solution. Subsequent reheating may result in incorporation of this ^{40}Ar by minerals as a consequence of metamorphic crystallization, recrystallization or by diffusion. Thus, the complex excess ^{40}Ar patterns of the Aurek Assemblage samples may be a consequence of at least two different reservoirs for the gas.

ISOTOPE CORRELATION PLOTS

In order to determine the extraneous argon composition, data obtained using the ^{40}Ar-^{39}Ar incremental heating technique can be plotted in three ways: $(^{39}Ar/^{36}Ar)$ v. $(^{40}Ar/^{36}Ar)$, $(^{36}Ar/^{39}Ar)$ v. $(^{40}Ar/^{39}Ar)$, or $(^{36}Ar/^{40}Ar)$ v. $(^{39}Ar/^{40}Ar)$. Each increment will contain varying amounts of extraneous and radiogenic argon. If the extraneous argon is of constant $(^{40}Ar/^{36}Ar)$, then the various increments will fall along a straight line with pure $(^{40}Ar/^{39}Ar)_{rad}$ as one end-member and pure $(^{40}Ar/^{36}Ar)_{extr}$ as the other. Depending on which way the data is plotted, this "mixing line" will have one of the following three forms:

$$(^{40}Ar/^{36}Ar)_{meas} = (^{40}Ar/^{39}Ar)_{rad}*(^{39}Ar/^{36}Ar)_{meas} + (^{40}Ar/^{36}Ar)_{extr} \quad (2)$$

$$(^{40}Ar/^{39}Ar)_{meas} = (^{40}Ar/^{36}Ar)_{extr}*(^{36}Ar/^{39}Ar)_{meas} + (^{40}Ar/^{39}Ar)_{rad} \quad (3)$$

$$(^{39}Ar/^{40}Ar)_{meas} = -(^{39}Ar/^{40}Ar)_{rad}*(^{40}Ar/^{36}Ar)_{extr}*(^{36}Ar/^{40}Ar)_{meas} + (^{39}Ar/^{40}Ar)_{rad} \quad (4)$$

Figure (5-1) illustrates each of these relationships.

Of the three isotopes considered in these plots, ^{40}Ar is by far the most abundant. Therefore, errors in the calculated ratios will be

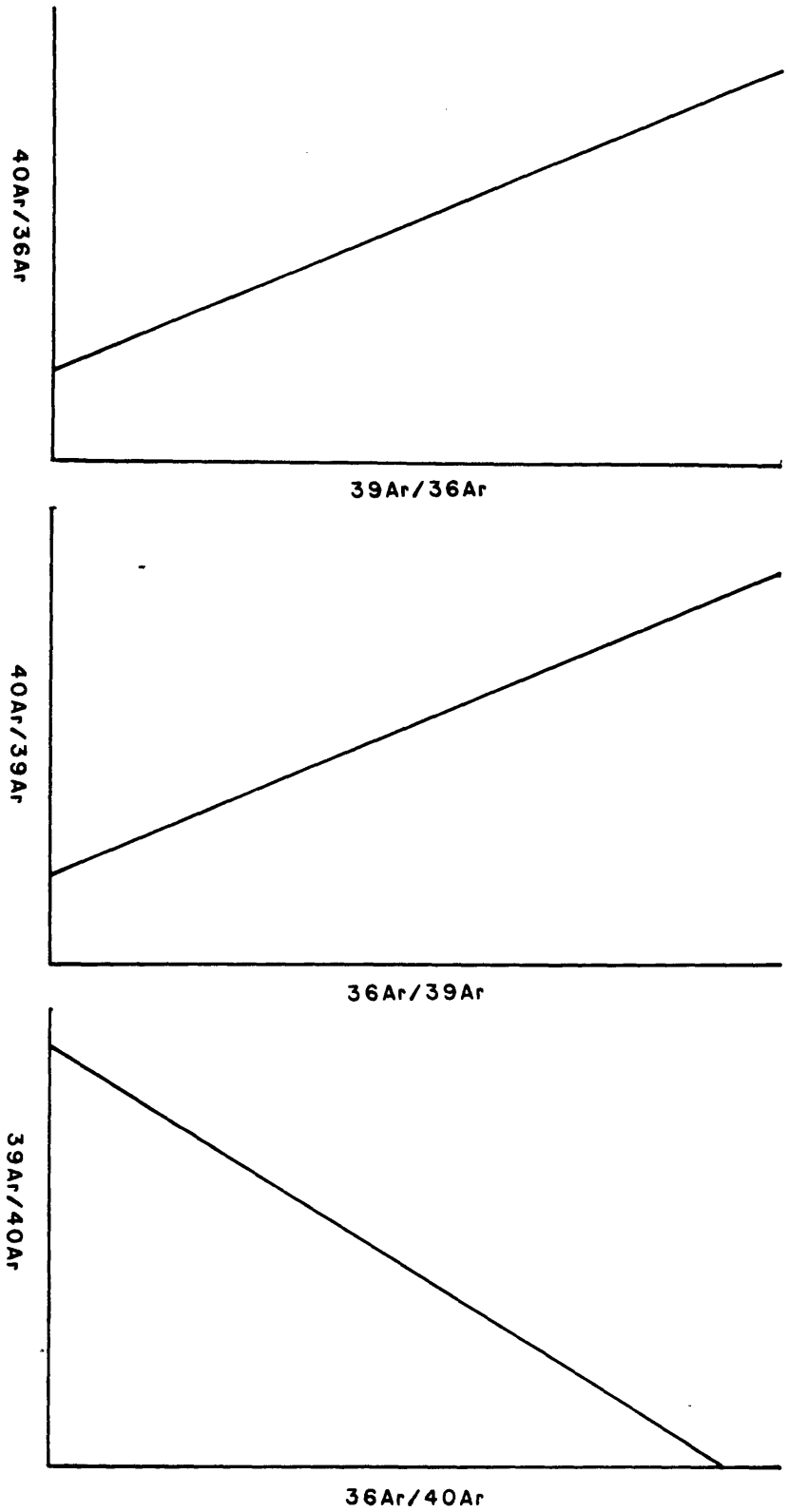

Figure 5-1: Ar-Ar correlation diagrams - see text for discussion

dominated by errors in the measurement of ^{36}Ar and ^{39}Ar. The result is a high correlation between abscissa and ordinate errors in equations (2) and (3). In equation (4), however, ^{40}Ar is the isotope common to both abscissa and ordinate, resulting in a relatively low error correlation. Since regression of data with uncorrelated errors is simpler and more precise (Brooks et al., 1972), equation (4) is used to obtain $(^{40}Ar/^{39}Ar)_{rad}$ and $(^{40}Ar/^{36}Ar)_{excess}$.

LINE BLANK CORRECTION

The slope of the line defined by equation (4) is given by:

$$-(^{39}Ar/^{40}Ar)_{rad}*(^{40}Ar/^{36}Ar)_{extr} \quad (5)$$

which, if the correction for line blank contributions by ^{36}Ar and ^{40}Ar has not been made must be rewritten:

$$-(^{39}Ar/^{40}Ar)_{rad}*((^{40}Ar_{extr} + {}^{40}Ar_{blank})/(^{36}Ar_{extr} + {}^{36}Ar_{blank})) \quad (6)$$

Repeat measurements in this study and by other workers (eg. Roddick, 1978) indicate that within experimental error $(^{40}Ar/^{36}Ar)_{blank} = 295.5$. If the ratio $(^{40}Ar/^{36}Ar)_{extr}$ also has an atmospheric value (ie. 295.5) then an unknown blank will have no effect on the magnitude of the slope defined by equation (5). However, in samples containing excess ^{40}Ar the ratio $(^{40}Ar/^{36}Ar)_{extr}$ will be greater than 295.5. In this case, the presence of a blank will have the effect of decreasing the magnitude of the slope defined by equation (6) viz:

$$\underset{\text{true value}}{(^{40}Ar/^{36}Ar)_{extr}} > \underset{\text{measured value}}{((^{40}Ar_{extr} + {}^{40}Ar_{blank})/(^{36}Ar_{extr} + {}^{36}Ar_{blank}))} > 295.5$$

This problem is overcome by measuring the ^{36}Ar and ^{40}Ar line blank contributions between runs, and subtracting these values from the measured quantities obtained during the run.

ANALYTICAL ERROR

The 2σ errors in apparent age reported in Appendix E1 were calculated by propagation of uncertainties in the various input parameters. Isotope peak heights and errors were calculated by least squares linear regression of eight cycles to the time at which the mass spectrometer was equilibrated with the inlet section. While analytical error is a function of the increment gas size, average values during this study were (2σ): 4% for $^{36}Ar/^{39}Ar$, 1% for $^{37}Ar/^{39}Ar$, and 1% for $^{40}Ar/^{39}Ar$.

GEOLOGICAL ERROR

As mentioned earlier, if the excess $^{40}Ar/^{36}Ar$ is of constant composition throughout the sample, all the points on the correlation plot should fall along a straight line (e.g. Figure E3 T84-19G). However, low temperature increments commonly fall off a line defined by high temperature ones (e.g. Figure E3 T85-2A). Two major factors appear to cause this apparent heterogeneity within the excess $^{40}Ar/^{36}Ar$ compositions:

a) Samples may have experienced more than one excess argon event, or one with changing $^{40}Ar/^{36}Ar$ composition. Following closure of the system to Ar diffusion, excess argon of an homogeneous composition is trapped within the system. Subsequent diffusion of excess argon of different composition into weakly bound sites will lead to an heterogeneous distribution of $^{40}Ar/^{36}Ar$ throughout the sample.

b) Contaminant phases with different closure temperatures and consequently different excess $^{40}Ar/^{36}Ar$. For example, biotite inclusions may have trapped $^{40}Ar/^{36}Ar$ of different composition than host hornblende.

Correct regression of a hornblende release spectrum therefore requires the filtering out of increments containing heterogeneous excess $^{40}Ar/^{36}Ar$ components. Appendix E2 contains release spectra of all the hornblende

samples used in this study. These spectra allow increments to be removed from the regression on the following bases:

a) Increments with apparent ages significantly greater than adjacent ones were removed, as their $(^{40}Ar/^{36}Ar)_{excess}$ is possibly different in composition.

b) K/Ca ratios are typically consistent at intermediate to high release temperatures and indicate an homogeneous phase (i.e. hornblende) is being degassed. Increments deviating from this plateau represent another phase also degassing. As this second phase may have a different closure temperature, and possibly different $(^{40}Ar/^{36}Ar)_{excess}$ these increments are also removed.

While this filtering system proved reliable for most of the samples, those particularly rich in heterogeneous extraneous ^{40}Ar required more careful scrutiny of the correlation diagram. The data for each sample and the interpreted ages are discussed in the results section.

REGRESSION OF THE CORRELATION PLOT

In order to determine the error associated with a calculated age and extraneous $^{40}Ar/^{39}Ar$ composition, two-error regression techniques were applied to the correlation plots (York, 1969). To assess whether all the points fall within the estimated 2σ error limits of the best fit regression line, the mean square of weighted deviates (MSWD) was calculated for each regression. This value may be obtained from S in the York (1969) regression by the relation:

$$MSWD = S/(n-2)$$

where n is the number of data points. As pointed out by Roddick (1978); in reviewing the various regression techniques, Brooks et al. (1972)

erroneously introduced a square root in the conversion from S to MSWD, ie:

$$MSWD = \sqrt{S/(n-2)}$$

Brooks et al. (1972) recommended that a MSWD less than 1 is free from geological effects and is an isochron. A MSWD greater than 2.5 indicates excess scatter (errorchron), while values between 1 and 2.5 are inconclusive. Brooks et al. (1972) also noted that these "cutoff" values will only be valid if 1) the regression analysis is based on a very large number of data points and 2) the assigned experimental errors have been calculated from a very large number of replicates. The analytical errors discussed earlier are those related to a single analysis of a single gas fraction. It is highly likely that replicate analyses of a sample would indicate that a significantly greater error is associated with a measurement than that revealed by a single analysis. For example, Roddick et al. (1980) report that duplicate analyses of sample gas fractions indicate a precision of 0.2% (2σ) in measured $^{40}Ar/^{39}Ar$. However, replicate analyses of different samples indicate that ^{40}Ar is determined to only 1.5% (2σ) in a single analysis. In the absence of replicate analyses of a sample, how does one estimate the true experimental error associated with a single analysis? Hart (pers. comm. 1986) recommends that a sample be selected for which the isochroneity is assumed. The analytical errors are then increased until the MSWD decreases to 1. This approach was applied to sample T84-19G for which the release spectrum (Figure E2 T84-19G) indicates the sample was affected by a single extraneous argon component of approximately atmospheric composition. The K/Ca spectrum for this sample indicates the seven high temperature increments representing 55 percent of the evolved gas tapped hornblende of constant composition. Regression of these seven increments by the York (1969) method yielded an

isochron (MSWD = 0.95) when the measured analytical errors were multiplied by a factor of 2.5. The thirteen high temperature increments of sample T85-2D also yielded an isochron (MSWD = 0.80) after multiplying the measured errors by a factor of 2.5. This factor was therefore applied to the measured analytical errors of all the samples in the study, and is interpreted to represent the true precision of an individual analysis.

^{40}Ar-^{39}Ar RESULTS

INTRODUCTION

^{40}Ar-^{39}Ar sample localities, along with their corresponding intercept ages are shown in Plate 7. Geochronological samples were obtained from most of the major tectonostratigraphic elements within the Efjord -Kebnekaise portion of the transect. In this section, the samples and their corresponding release spectra are discussed, beginning at the structurally lowest level.

The heating schedules for these samples are included in Appendix E1, and the corresponing release spectra in Appendix E2. Reported errors in the apparent age for individual increments are 2σ measured analytical. The corresponding isotope correlation diagrams for these analyses are included in Appendix E3. The error boxes in these plots are the corrected (x 2.5) 2σ analytical errors. The solid line is the best fit York (1969) line for the regressed increments, while the dashed lines are the 2σ limits of this line.

The reported 2σ error in the calculated ages were corrected for excess scatter by multiplying the calculated errors by the MSWD for the regression if that value was greater than 1 (York, 1969).

ROMBAK-SJANGELI BASEMENT

Sample H81-11A, collected by K.V. Hodges, is a coarse-grained hornblende-plagioclase amphibolite. The sample is from a foliated mafic body within Rombak Gneiss, approximately 50 m below the sole thrust of the Storrit Complex. Foliation within the amphibolite is subparallel to the Storrit Complex foliation, and is interpreted to be related.

The K/Ca release spectrum of this sample (Figure E2 H81-11A) has a relatively good plateau for increments 5-14 (1010-FUSE). Regression of the correlation plot yielded an isochron age (MSWD = 0.31) of 411.0 +/- 10.8 Ma (Table 5-2). Although ten increments were included in this regression, it is essentially a two-point isochron: eight of the increments cluster at approximately ($^{36}Ar/^{40}Ar$) = 0.001 and ($^{39}Ar/^{40}Ar$) = 0.012, while the 1040°C increment constrains the regression at ($^{36}Ar/^{40}Ar$) = 0.00045 and ($^{39}Ar/^{40}Ar$) = 0.016 (Figure E3 H81-11A).

FORSA THRUST

The Forsa Thrust of Hodges (1982) is an east-dipping thrust fault cropping out on the Norwegian west coast. It places high-grade rocks of the upper nappe complex on Tysfjord granite gneiss. Associated with the thrust is a schuppenzone consisting of discontinuous slivers of garnetiferous pelite and hornblende amphibolite. Hornblende from the amphibolite (T85-2D), and muscovite (T85-2EM) and biotite (T85-2EB) from the pelite all yield precise ^{40}Ar-^{39}Ar ages.

Sample T85-2D is a weakly foliated granoblastic hornblende-plagioclase -garnet amphibolite. In thin section, porphyroblasts are unstrained with equant grain boundaries, indicating no post-recrystallization strain. While a statistically valid plateau is not developed in the release spectrum of this sample (Figure E2 T85-2D), the last seven increments

TABLE 5-2: EFJORD-SUNUIS ^{40}Ar-^{39}Ar DATA

Sample	Phase	#	K/Ca	Age_1*	Age_2*	MSWD	Excess*
T85-2EB	biot	4	-	357.5±3.6	358.0±2.8		-
T85-2EM	musc	4	-	368.8±4.0	369.7±3.3		-
T85-4E	musc	1	-	450.2±4.1	-		-
T85-13B	musc	1	-	448.4±5.1	-		-
H81-11A	hbl	10	0.049	417.7±13.9	411.0±10.8	0.31	336.5±56.0
T84-19G	hbl	7	0.072	434.5±3.9	431.6±3.8	0.95	300.2±10.7
T85-2A	hbl	12	0.024	454.6±4.2	424.7±23.7	5.36	448.6±224.0
T85-2B	hbl	4	0.022	428.3±4.0	421.3±45.3	3.27	288.7±387.0
T84-2D	hbl	13	0.039	397.8±4.4	386.7±4.4	0.80	379.0±35.5
T85-3B1	hbl	6	0.045	416.2±3.8	390.0±11.3	1.19	580.9±238.7
T85-3B2	hbl	5	0.012	516.6±6.2	500.4±42.5	0.30	293.1±217.2
T85-28A	hbl	14	0.026	502.2±5.8	496.3±10.2	1.66	394.5±103.3
T85-28C	hbl	11	0.058	419.4±3.9	411.2±4.4	0.29	385.0±43.4

where: Phase - biot = biotite, musc = muscovite, hbl = hornblende

- number of increments included in plateau or intercept age calculation

K/Ca - mean K/Ca ratio for increments included in intercept age calculation

Age_1 - minimum age from heating schedule of increments included in plateau or intercept age calculation (Ma)

Age_2 - plateau or intercept age (Ma)

MSWD - mean square of weighted deviates

Excess - $(^{40}Ar/^{36}Ar)_{excess}$ from intercept

* Errors are 2σ analytical

(1065-FUSE) which contain 80% of the gas, have a relatively constant K/Ca ratio (mean = 0.0389). Regression of these seven increments yielded an intercept age of 386.7 +/- 4.4 Ma (Figure E3 T85-2D) with MSWD = 0.80.

Sample T85-2E is a well foliated biotite-muscovite-quartz-plagioclase -garnet schist. Although the garnet is strongly retrograde, it is in equilibrium contact with biotite. Muscovite (T85-2EM) and biotite (T85-2EB) from this sample yielded precise plateau ages of 369.7 +/- 3.3 Ma and 358.0 +/- 2.8 Ma respectively.

Biotite ages are difficult to interpret in areas of excess argon. Numerous workers have reported well-defined biotite plateaus of anomalously old age (e.g. Pankhurst et al., 1973; Roddick et al., 1980; Foland, 1983; Dallmeyer et al., 1985). These plateaus are apparently due to heterogeneities in the $^{40}Ar/^{39}Ar$ distribution being obscured during the extraction process. Roddick et al. (1980) showed that this homogenization is <u>not</u> due to recoil during irradiation. However, Giletti (1974) has shown that Ar loss from biotite during heating in a vacuum is not a volume diffusion process, but appears to be caused by destruction of the crystal.

AUREK ASSEMBLAGE

Release spectra of several hornblende separates from the Aurek Gabbro and Aurek Amphibolite were obtained. Unfortunately, these samples are saturated with heterogeneous excess argon and their spectra are consequently uninterpretable. Sample T85-4F is typical of the saddle-shaped release spectra obtained from Aurek Assemblage hornblendes (Figure E2 T85-4F).

Muscovite separates from the Vidja Gneiss (T85-4E and T84-13B), yield more interpretable release spectra. Although collected over 3 km apart, the age spectra of these samples are essentially identical. Neither sample

forms a plateau, however the base of the saddle constrains the maximum age of the samples to be 450.2 +/- 4.1 Ma and 448.4 +/- 5.1 Ma respectively. Page (unpub. data) obtained a muscovite release spectrum from the Vidja Gneiss with a relatively wide range in $^{36}Ar/^{40}Ar$ composition (~ 0-0.0004). Regression of this analysis yielded an intercept age of 442.0 +/- 5.9 Ma (MSWD = 0.02).

The saddle-shaped release spectra of the Vidja Gneiss muscovite separates indicate $^{40}Ar/^{39}Ar$ retains its heterogeneous distribution during the extraction process. Thus, unlike biotite, muscovite may release Ar by volume diffusion rather than through destruction of the crystal.

LITTE GROUP

Sample T84-19G is a coarse grained garnet-hornblende-muscovite-biotite -ankerite-quartz garbenschist. The K/Ca release spectrum of the hornblende separate (Figure E2 T84-19G) indicates that K-rich biotite inclusions have degassed with the hornblende at lower temperatures. However, the final seven increments (1050-FUSE) have relatively constant K/Ca ratios (mean = 0.0717) indicating homogeneous hornblende is degassing. Regression of these seven increments yields an intercept age of 431.6 +/- 3.8 Ma (Figure E3 T84-19G) with a MSWD = 0.95.

BAUGEFJELL AMPHIBOLITE

The Baugefjell Amphibolite is a thin (10-50 m thick) but laterally continuous dark to light green weathering fine-grained amphibolite cropping out west and northwest of Sitasjaure (Crowley, 1985). In the area of the lake Baugvatnet, this unit separates melange rocks of the Rauvatn Complex from calcareous pelites to the north and south.

In thin section, sample T85-28C is a fine-grained hornblende-epidote-

plagioclase-quartz-sphene amphibolite. The K/Ca release spectrum of this sample (Figure E2 T85-28C), indicates homogeneous hornblende is degassed during increments 7 to 15 (mean K/Ca = 0.0581), with a slightly lower value for increments 5 and 6. Regression of these eleven increments yielded an isochron age (MSWD = 0.17) of 411.2 +/- 5.1 Ma (Figure E3 T85-2C).

RAUVATN COMPLEX

The Rauvatn Complex, first recognized by Hodges (1982), is an areally extensive unit cropping out northwest and north of Sitasjaure (Plate 7). The unit is a chaotic sequence of lenses of marble, amphibolite, and ultramafic rocks in a matrix of psammitic garnet two-mica schist (Crowley, 1982). Three hornblende separates from amphibolite lenses within the unit yield interpretable release spectra: T85-3B1, T85-3B2, and T85-28A.

Sample T85-28A is a granoblastic hornblende-garnet-plagioclase-quartz -sphene amphibolite, collected 2 km southwest of the Baugefjell Amphibolite sample (T85-28C, Plate 7). The release spectrum of the hornblende separate is unusual in having a "double saddle" (Figure E2 T85-28A). This spectrum, with two age minima at 31 and 54 percent ^{39}Ar released is similar to the three cycle hornblende release spectrum of Harrison and Fitzgerald (1986). These workers attribute their multiple cycles to hornblende exsolution in cummingtonite. The first 4 percent ^{39}Ar released in sample T85-28A has a relatively high K/Ca ratio; this may be due to degassing of biotite inclusions. The next increment (1000°C) has a low K/Ca of 0.019. The K/Ca then rises steadily until 1040°C, such that the last 65 percent ^{39}Ar released has a relatively constant K/Ca of approximately 0.026. Although this sample has not been analyzed with an electron microprobe, exsolution of low-K actinolitic hornblende within a hornblende matrix could be responsible for the double saddle, with actinolitic hornblende degassing at

a lower temperature. Alternatively, since the peak in the release spectrum at ~50 percent ^{39}Ar released coincides with a relatively flat portion of the K/Ca spectrum, the double-saddle may have no relation to variations in the K/Ca ratio but could be due to exsolved hornblende with different Fe/Mg ratios. The range in K/Ca from increments 4 to 17 is not large (0.019-0.027) and a regression through these points yielded a good fit (MSWD = 1.66) with an intercept age of 496.3 +/- 10.3 Ma (Figure E3 T85-28A).

Samples T85-3B1 and T85-3B2 were collected from an amphibolite pod cropping out on the southwest shore of lake Hjertevatnet in the Efjord area (see Plate 7 and Hodges, 1985, Plate 1). These samples are both weakly lineated amphibole-epidote-plagioclase-quartz amphibolites. Petrographic examination and comparison of K/Ca ratios suggests the amphibole in T85-3B1 is hornblende (mean K/Ca=0.0451), while that in T85-3B2 is actinolitic hornblende (mean K/Ca=0.0122). These samples were collected 10 meters away from each other.

T85-3B2 has a significant amount of excess argon, resulting in a saddle-shaped age spectrum (Figure E2 T85-3B2). The last 96 percent ^{39}Ar released has a constant K/Ca of approximately 0.0122. The correlation diagram of sample T85-3B2 (Figure E3 T85-3B2) indicates that more than one component is responsible for the high excess argon concentration in this sample. Regression of increments 10-14 (1085-1135^{o}C) yielded the best fit line shown in Figure E3 T85-3B2. These data indicate the extraneous $^{40}Ar/^{36}Ar$ component affecting these increments was of approximately atmospheric composition (Table 5-2). Increments 1-9 all fall below this mixing line suggesting that a second component much richer in ^{40}Ar was absorbed into the weakly held sites. Figure 5-2 illustrates the

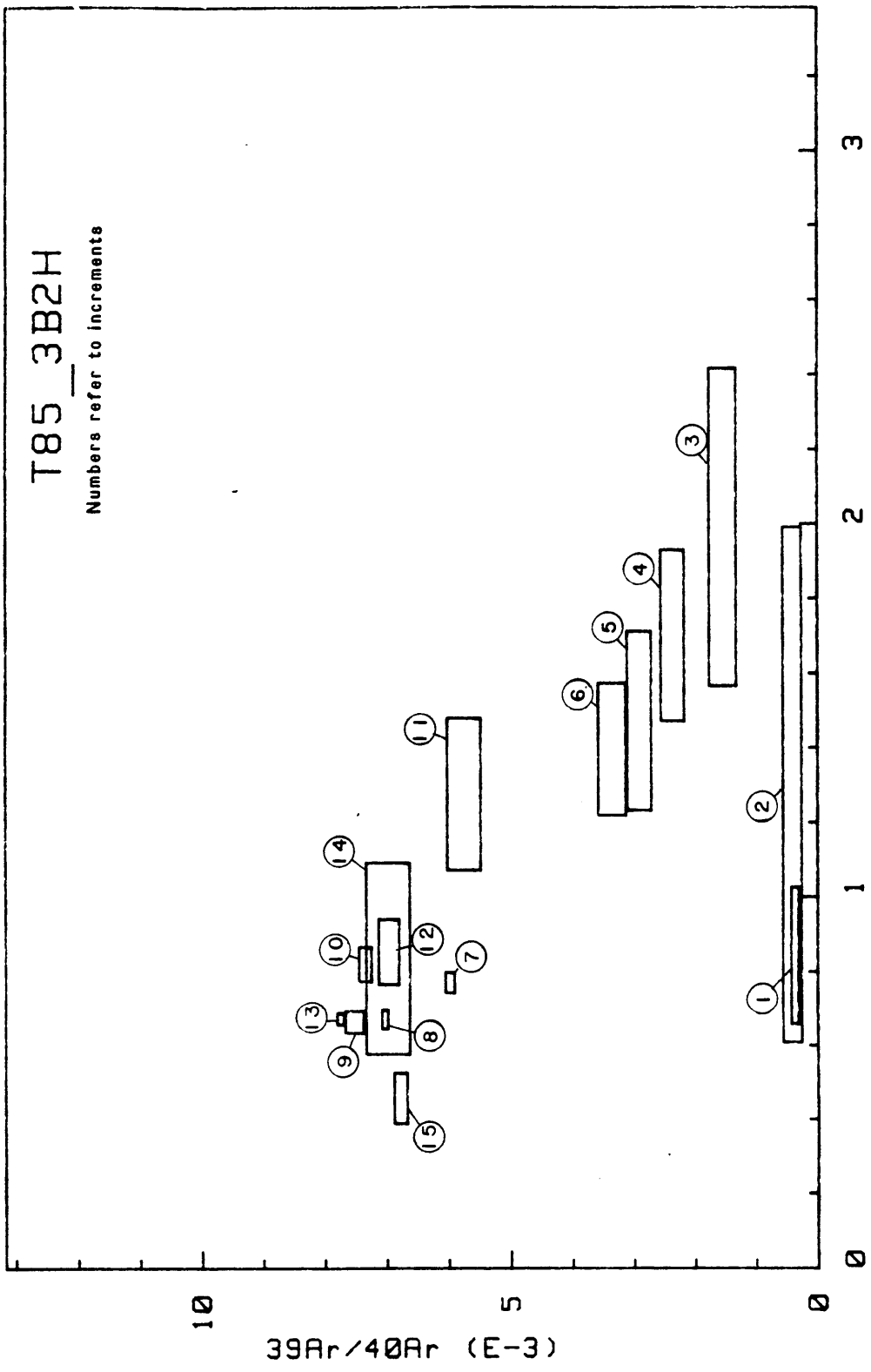

Figure 5-2: T85-3B2 isotope correlation diagram

progressive evolution of these increments on the correlation plot. The simplest interpretation is one in which pure $^{40}Ar_{excess}$ mixes with the $^{40}Ar_{rad}$ and $^{40}Ar_{atmos}$ components. In the initial low temperature increments $^{40}Ar_{excess}$ has a high concentration relative to $^{40}Ar_{atmos}$ but then decreases. At higher temperatures (increments 4-7) as the $^{40}Ar_{rad}$ component increases, the relative proportion of $^{40}Ar_{excess}$ and $^{40}Ar_{atmos}$ remains constant. From increments 8 to 10 the $^{40}Ar_{excess}$ component drops to zero, such that increments 10 to 14 form the isochron (MSWD = 0.30) plotted in Figure E3 T85-3B2 (intercept age 500.4 +/- 42.5 Ma). It is therefore possible that as sample T85-3B2 cooled below the closure temperature of Ar diffusion it trapped extraneous Ar of atmospheric composition. Later in the samples history, a high partial pressure of ^{40}Ar led to diffusion of ^{40}Ar into weakly held sites.

The release spectrum of T85-3B1 differs markedly from T85-3B2 (Figure E2 T85-3B1). Increments 6-11 have a relatively constant K/Ca ratio of 0.0451 and yielded 70 percent of the ^{39}Ar. The final five increments (12-16) have a somewhat lower K/Ca ratio of 0.0393. Regression of increments 6-11 yielded a very good fit (MSDWD = 1.19) with an itercept age of 390.0 +/- 11.3 Ma. As in sample T85-3B2, the first five increments of this sample indicate a second high $^{40}Ar_{excess}$ component (Figure E3 T85-3B1).

SALANGEN GROUP

The Salangen Group is the structurally highest unit within the Efjord-Kebnekaise area (Plate 7). It is composed dominantly of calcitic and dolomitic marbles (Hodges, 1982; Steltenpohl, 1985). No fossils have been found in the Salangen Group, but correlation with the fossil-bearing Balsfjord Group, located about 100 km to the northeast, suggests an Upper

Ordovician-Lower Silurian depositional age (Binns and Matthews, 1981; Steltenpohl et al., 1985). In the transect area, the base of the Salangen Group is marked by the Elvenes Conglomerate, which most workers consider to have been deposited directly on the underlying Sjurvatnet Schist (Hodges, 1982; Steltenpohl et al., 1985; Tull et al., 1985). Locally, the matrix of this conglomerate is amphibolitic; and it was from one of these localities that samples T85-2A and T85-2B were collected. Although hornblende separates from the samples yield concordant ages for the unit (weighted mean = 423.9 Ma), they are both errorchrons. In thin section, both samples are light-green actinolitic granoblastic hornblende-plagioclase-quartz -biotite amphibolites.

Sample T85-2A has a strongly discordant age release spectrum (Figure E2 T85-2A). However, the twelve highest temperature fractions, representing 91 percent of ^{39}Ar released (Figure E3 T85-2A), have a relatively constant K/Ca of approximately 0.024. Regression of these twelve increments yielded an errorchron age (MSWD = 5.36) of 424.7 +/- 23.7 Ma.

The age spectrum of the T85-2B hornblende separate again has a pronounced saddle shape (Figure E2 T85-2B). Increments 4-10 have a relatively constant K/Ca of 0.022. To avoid regression problems associated with heterogeneous $(^{40}Ar/^{36}Ar)_{excess}$, only the four youngest increments yielding 67 percent of the gas were included in the regression. This filtering yielded an errorchron age (MSWD = 3.27) of 421.3 +/- 45.3 Ma.

CONCLUSIONS

Table 5-2 summarizes the hornblende intercept ages, and mica plateau ages discussed above. Also listed are the number of increments included in the regression or plateau calculation, the mean K/Ca ratio, and minimum age

and associated MSWD of these increments. The last column in table 5-2 lists the interpolated $(^{40}Ar/^{36}Ar)_{excess}$ compositions calculated from the York (1969) regression of the hornblende correlation plots. These calculated compositions typically have high 2σ errors which may mask any systematic variations.

INTERPRETATION OF ^{40}Ar-^{39}Ar RESULTS

INTRODUCTION

The calculated age of a mineral or rock reflects the time at which the system became closed to diffusive gain or loss of the isotopes in question. This age does not necessarily correspond to the crystallization age of the sample. Hart (1964), for example, showed that variations in K-Ar and Rb-Sr ages within a metamorphic contact aureole were due to cooling of the various minerals below their respective "closure temperatures".

Solid diffusion processes are thermally activated and follow a simple Arrhenius relation:

$$D = D_0 \exp(-E/RT)$$

where D is the volume diffusion coefficient at absolute temperature T, D_0 is the diffusion coefficient at infinite temperature, E is the activation energy for volume diffusion, and R is the universal gas constant. Dodson (1973) derived an approximate solution expressing the closure temperature, T_c of a cooling system as a function of its cooling rate dT/dt:

$$T_c = (E/R)/\ln((ART_c^2D_0)/(Ea^2dT/dt))$$

where A is a geometric constant, and a is the characteristic diffusion dimension of the system. Table 5-3 lists values of these parameters for Ar diffusion in hornblende (Harrison, 1981), muscovite (Harrison et al., 1985), and biotite (Norwood, 1974; Harrison et al., 1985). Harrison et al. (1985) noted that the activation energy of Ar diffusion in biotite is a

TABLE 5-3: DIFFUSION PARAMETERS

Parameter	Ar-Biot[1,2]	Ar-Musc[3]	Ar-Hbl[4]	Sr-Biot[5]
$D_o(cm^2/s)$	0.077	6.03×10^{-7}	0.024	0.0154
E (Kcal/mol)	48±1	40	64.1	48
A	27	27	55	27
a(mm)	0.015	0.015	0.008	0.015

1 - Harrison et al., 1985

2 - Norwood, 1974

3 - Robbins, 1972

4 - Harrison, 1981

5 - Harrison and McDougall, 1980

strong function of annite composition. The experiment of Harrison et al. (1985) was performed on a biotite of $annite_{56}$ composition yielding an activation energy of 47.0 $kcalmol^{-1}$. Norwood (1974) performed a similar hydrothermal experiment on $annite_{37}$ yielding an activation energy of 49.0 $kcalmol^{-1}$. Metamorphic biotites from the Efjord-Singis area range in composition from approximately $annite_{40}$ to $annite_{50}$. Therefore, in this study a mean value of 48.0 $kcalmol^{-1}$ has been selected, and biotite closure temperatures are reported with an error to reflect the compositional variation.

Based on discordant K-Ar hornblende and biotite ages, Hodges (1982) argued that the cooling rate for the Efjord area was approximately 3°C/Ma. Using the data from table 5-3, this cooling rate would imply closure temperatures of 480°C, 388°C, and 306 +/- 11°C for hornblende, muscovite and biotite respectively. However, arguments presented below and in previous chapters suggest that the Efjord-Kebnekaise area experienced a complex structural history that took place at temperatures between about 300°C and 500°C. It is therefore unlikely that the area cooled uniformly between these temperatures. Because the cooling rate is not known a priori, a value of 2-10°C/Ma is assumed, which translates to closure temperatures for hornblende, muscovite and biotite of 475-500°C, 380-415°C and 300-320°C respectively.

The ^{40}Ar-^{39}Ar age data listed in table 5-2 may be subdivided into five groups:

1) 500-440 Ma Finnmarkian retrograde metamorphism.
2) 430-420 Ma Scandian retrograde metamorphism and early thrusting onto the Baltic Shield.
3) 415-410 Ma imbrication of upper nappe complex and thrusting onto

the Baltic Shield.

4) 390-385 Ma final thrusting of upper nappe complex onto the Baltic Shield.

5) 385-355 Ma post-thrusting uplift and cooling.

With the concept of closure temperature in mind, these groups are discussed below, integrating the age data with the structural and metamorphic data presented earlier.

500-440 MA FINNMARKIAN RETROGRADE METAMORPHISM

Samples T85-3B2 and T85-28A have a mean age of 496.5 Ma (Table 5-2). This age suggests the Rauvatn Complex experienced its high-grade metamorphism during Late Cambrian or Early Ordovician time and cooled through the closure temperature of hornblende at 496.5 Ma. While no hornblende ages were obtained from the Aurek Assemblage, muscovite separates T85-4E and T85-13B yield a maximum age of approximately 449.5 Ma. As noted earlier, Page (unpub. data) has obtained a muscovite age of 442.0 Ma from the Aurek Assemblage. Therefore, the eclogite facies metamorphism experienced by the Aurek Gabbro must have occurred some time prior to 442.0 Ma. One hundred eighty kilometers south of the study area, the Seve nappe, which is correlated with the Aurek Assemblage (see chapter 6) has also yielded 491 Ma hornblende and 440 Ma muscovite ages (Dallmeyer and Gee, 1986). It therefore appears that both the Aurek Assemblage and the Rauvatn Complex underwent their high-grade metamorphism and deformation (D1) during Late Cambrian or Early Ordovician time.

430-420 MA SCANDIAN RETROGRADE METAMORPHISM AND EARLY THRUSTING ONTO BALTIC SHIELD

The medium-to high-grade metamorphism which affected Upper Ordovician

to Lower Silurian units throughout the upper nappe complex is termed the Scandian Orogeny (Gee, 1975). This event is recorded by the hornblende cooling age of 431.6 Ma from the Litte Group (sample T84-19G). Post Scandian cooling may also be recorded by the errorchrons from samples T85-2A and T85-2B (424.6 Ma and 421.3 Ma respectively). In any event, if the stratigraphic correlations discussed earlier are valid, the metamorphism of the Salangen Group must be post Lower Silurian (younger than approximately 428 Ma, Harland et al., 1982).

As discussed in chapter 4, the Scandian p-T array recorded by trhe Litte Group and Storrit Complex yield minimum garnet-biotite temperatures of 535°C and 500°C respectively (see Table 4-2). Even for rapid cooling rates (e.g. 10°C/Ma), the closure temperature for Ar diffusion in hornblende is only 500°C. Therefore, the p-T array recorded by the Litte Group, and the early metamorphism of the Storrit Complex must be older than approximately 430 Ma.

415-410 MA IMBRICATION OF UPPER NAPPE COMPLEX AND CONTINUED THRUSTING ONTO BALTIC SHIELD

As noted above, west and northwest of Sitasjaure, the Baugefjell Amphibolite serparates the Rauvatn Complex above from the Skjafjell Schist below (see Plate 7 or Crowley, 1985, Plate 1). Crowley (1985) considered the gradational contact between the Skjafjell Schist and structurally lower

younger than either. This age is interpreted to represent sub 475-500°C recrystallization. If the temperature of the Baugefjell Amphibolite had exceeded 475-500°C, sample T85-28A would have been reset to this younger age. Nor can the unit be an overturned depositional contact, as garnet-biotite geothermometry within the Skjafjell Schist indicates temperatures in excess of 600°C. The Baugefjell Amphibolite must therefore represent a shear zone which juxtaposed the Rauvatn Complex and Skjafjell Schist-Litte Group at temperatures below 475-500°C.

Sample H81-11A from a foliated amphibolite body within the Rombak -Sjangeli basement (see above and Plate 7) yields a hornblende age of 411.0 Ma. As the immediately superjacent Storrit Complex and Litte Group appear to have cooled below 475-500°C by approximately 431 Ma, this age must also be a recrystallization age rather than a cooling age. The shallowly dipping mylonitic foliation within the southwestern Rombak-Sjangeli basement and associated hornblende recrystallization may therefore be related to sub 475-500°C thrusting.

These data are supported by petrologic evidence (chapter 4) in suggesting that early development of the Storrit Complex and thrusting onto the Baltic Shield (before 431 Ma), preceded D3 imbrication of the upper nappe complex.

390-385 MA FINAL THRUSTING OF UPPER NAPPE COMPLEX ONTO BALTIC SHIELD

Sample T85-2D from the Forsa Complex yields a hornblende age of 386.7 +/-4.4 Ma (Table 5-2; Plate 7). This age is statistically coincident with the 390.1 +/- 11.3 Ma hornblende age of sample T85-3B1 located approximately 500 m above the Forsa Complex within the Rauvatn Complex. The weighted mean age of 387.1 Ma is interpreted to be the time of sub 475-500°C recrystallization associated with final movement on the Forsa

Thrust.

Several lines of evidence, similar to those presented for the Baugefjell Amphibolite and Rombak-Sjangeli basement samples, support the assertion that these numbers represent sub 475-500°C recrystallization ages:

1) Sample T85-3B2, located 10 m from T85-3B1 yields an isochron age of 500.4 +/- 42.5 Ma. As discussed in the results section, this older amphibole is more actinolitic (K/Ca=0.012) than the younger amphibole (K/Ca=0.045). This difference in K/Ca ratios between T85-3B1 and T85-3B2 may be due to heterogeneous fluid flow associated with movement along the underlying Forsa Thrust leading to localized retrogressive recrystallization in the hanging wall.

2) Petrologic and thermochronologic evidence (see above and chapter 4) indicates that the Narvik Group in the hanging wall of the Forsa Thrust was at 475-500°C by 420-410 Ma.

The absence of mylonitic or cataclastic fabrics within sample T85-2D indicates the absence of any post-recrystallization shear strain. Therefore, the 386.7 Ma age of sample T85-2D appears to be the time of final movement within the shear zone. The same argument does not apply to sample H81-11A within the Rombak-Sjangeli basement, since it is from ~50 m below the sole thrust of the Storrit Complex. However, these timing relations do indicate that some phase of sub 475-500°C thrusting along the base of the Storrit Complex took place approximately 25 Ma before final movement on the Forsa Thrust. These data have important implications on the nature of basement involvement during final emplacement of the upper nappe complex (see chapter 6).

385-355 MA POST-THRUSTING UPLIFT AND COOLING

Following final movement on the Forsa Thrust at 387.1 Ma, mica ag rom within the Forsa Complex record the ~300-400°C cooling history of the area. Separates from sample T85-2E yield plateau ages of 369.7 +/- 3.3 Ma and 358.0 +/- 2.8 Ma for muscovite and biotite respectively. Whether the biotite age is a true plateau or an excess argon spectrum is not immediately clear, but several lines of evidence suggest it is an accurate age:

a) the coexisting muscovite has essentially no excess argon, implying the sample as a whole may have very little excess argon.

b) the biotite age is significantly younger than the 369-393 Ma K-Ar biotite ages obtained by Hodges (1982) for neighboring samples in the Efjord area.

c) Bartley (1981) obtained Rb-Sr biotite ages on East Hinnoy with a mean value of 360.3 Ma. Harrison and McDougall (1985) argue that the closure temperature for ^{87}Sr in biotite is 20-30°C greater than that for Ar.

If the muscovite and biotite cooling ages are accurate, the diffusion parameters in table 5-3 yield closure temperatures of 410°C and 320 +/- 12°C for muscovite and biotite respectively, with a cooling rate of 7.8 +/- 1.0°C/Ma for this portion of the path. Interestingly, if one considers the diffusion coefficient of ^{87}Sr in biotite to be $0.7 \log_{10}$ units lower than that for Ar (Harrison and McDougall, 1985), this cooling rate implies an Rb-Sr biotite age of 360.7 Ma (cf. (c) above).

THERMAL EVOLUTION OF THE EFJORD-KEBNEKAISE AREA

FINNMARKIAN UPLIFT AND COOLING HISTORY

^{40}Ar-^{39}Ar muscovite ages from the Aurek Assemblage are approximately 442 Ma, the Aurek Assemblage experienced its high-grade metamorphism prior to this time. As discussed earlier, the Seve nappe of the Nassafjell area, 180 km to the south, is correlated with the Aurek Assemblage (see chapter 6) and has yielded 491 Ma hornblende and 440 Ma muscovite ^{40}Ar-^{39}Ar ages. The Aurek Assemblage may therefore have experienced its eclogite facies metamorphism in Late Cambrian or Early Ordovician time. The Nassafjell data imply a Finnmarkian cooling rate of 1.8°C/Ma from 470°C to 375°C. If the Aurek Assemblage experienced a similar cooling rate, then it would have been at 375°C at 442 Ma. For a geothermal gradient of 20-40°C/km these data imply the Aurek Assemblage was between 10 to 20 km depth when deposition of the Salangen Group to the west was beginning. The biotite grade mylonitic deformation of the Aurek Assemblage discussed in chapter 3 is inferred to be related to the 415-410 Ma imbrication of the upper nappe complex. Therefore, the sub 350-375°C cooling history of the Aurek Assemblage must be entirely a Scandian event.

SCANDIAN UPLIFT AND COOLING HISTORY

All the units within the Efjord-Kebnekaise area have experienced the thermal effects of Scandian metamorphism. Unfortunately, the uplift and cooling paths determined from garnet phase relations (see chapter 4) represent conditions above the closure temperature of Ar diffusion in hornblende. Therefore, cooling rates determined from ^{40}Ar-^{39}Ar thermochronology cannot be directly translated to uplift rates using dp/dT data obtained from these paths. However, the ^{40}Ar-^{39}Ar data does provide a

window on the thermal history not quantitatively revealed by metamorphic petrology.

As discussed above, a significant amount of deformation took place within the Efjord-Kebnekaise area at temperatures between ~500-400°C (the closure temperatures of hornblende and muscovite respectively). Therefore, one must be cautious in making generalizations about the cooling history of the entire area. For example, units on opposite sides of the Baugefjell Amphibolite probably experienced somewhat different thermal histories prior to final movement on the fault.

The youngest hornblende age in the Efjord area interpreted to be a cooling age is 424.0 Ma in the Elvenes conglomerate. All younger hornblende ages from this area appear to be recrystallization ages associated with thrust faulting. The next youngest cooling age is the post-tectonic 369.7 Ma muscovite age from the Forsa Complex. These two ages imply a linear cooling rate of 1.6°C/Ma from 470°C to 376°C. However, as noted previously, the biotite separate T85-2E also from the Forsa Complex yields a cooling age of 358.0 Ma; implying a cooling rate of 7.8 +/- 1.0°C/Ma from 410°C to 320 +/- 12°C. The markedly different cooling rates are responsible for the difference in the calculated closure temperatures of muscovite (376°C and 410°C). If one assumes a mean muscovite closure temperature of 394°C, a cooling rate of 4°C/Ma at this temperature is implied. Figure 5-2 illustrates the hypothesized 430 Ma to 350 Ma cooling history of the upper nappe complex in the area of the Elvenes Conglomerate samples. From ~420 Ma to ~387.1 Ma the mean cooling rate was very slow. When thermal inversions and tectonic thickening of the upper nappe complex ceased (386.7 Ma for the Forsa Thrust), the cooling rate rapidly increased to ~10°C/Ma by 358.0 Ma. This cooling rate may be

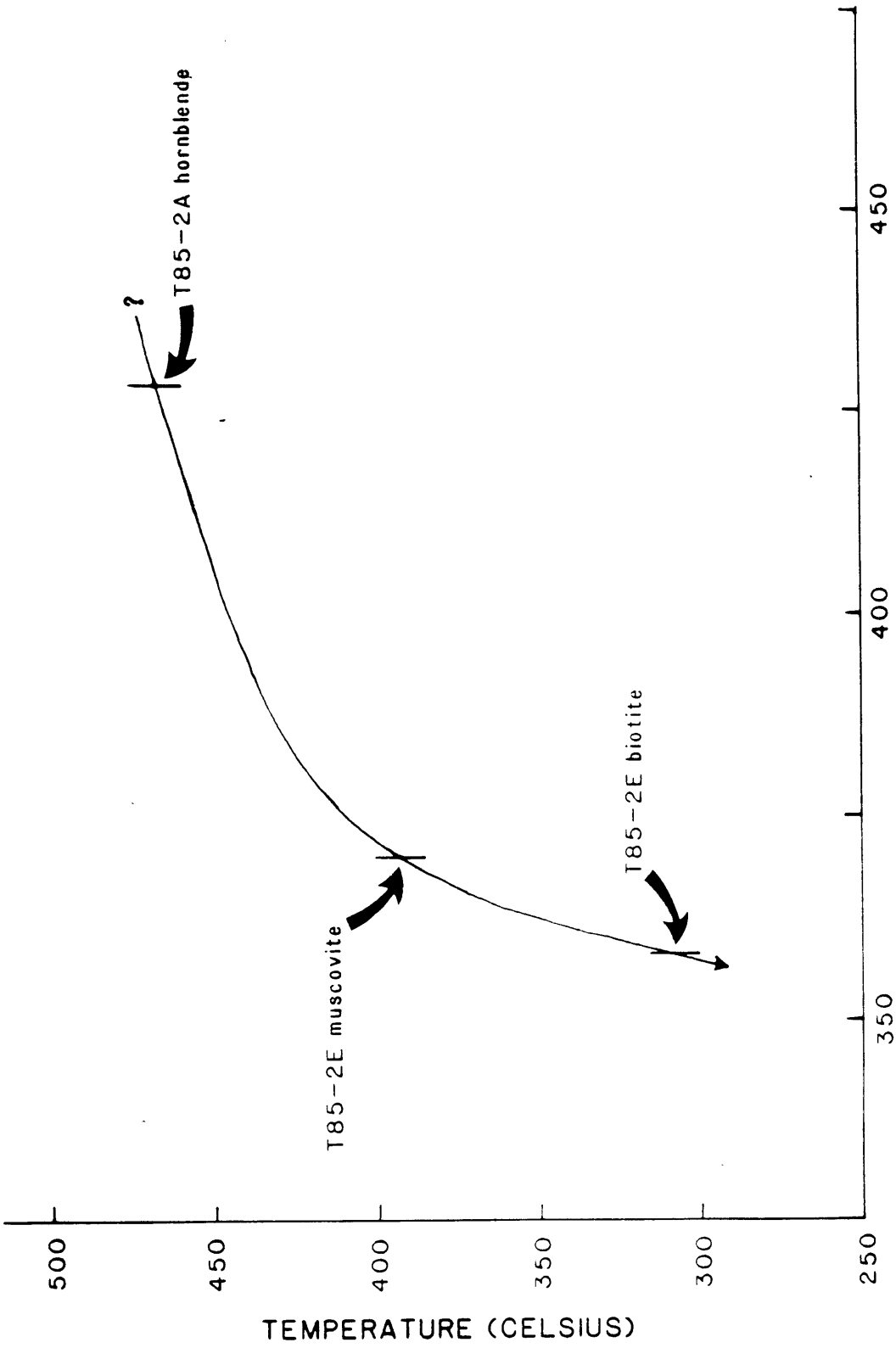

Figure 5-3: Cooling history of the Efjord area inferred from Ar-Ar data

too rapid to be due solely to erosion, and may have been augmented by tectonic thinning of the nappe stack. D8 normal faulting along the Rusjka Fault in the Singis area may be an effect of a gravitational collapse of the orogen.

CHAPTER 6: CONCLUSIONS

INTRODUCTION

The northern Scandinavian Caledonides is an ideal area to study the mid crustal effects of collisional orogenesis. Integration of the results of this study with previous work in the area has allowed the questions outlined in chapter 1 to be addressed. In this chapter, the tectonostratigraphy of the Efjord-Kebnekaise area is compared with sequences elsewhere in the orogen. The metamorphic evolution of the area is then reviewed, followed by a discussion of the nature of basement involvement during emplacement of the upper nappe complex.

REGIONAL NAPPE CORRELATION

Regional correlations within the upper nappe complex are complicated by the paucity of fossils, high metamorphic grade, structural complexity, and lack of lateral continuity of units. Further, while the Efjord-Singis area has been studied in detail, much of the northern Scandinavian Caledonides has only been mapped in reconnaisance (eg. Kulling 1964, 1982). In this part of the orogen correlations must therefore be based on lithologic similarities, stratigraphic sequences, metamorphic petrology and structural relationships.

In the Sitas-Singis area, the upper nappe complex is subdivided into four tectonostratigraphic elements: the Aurek Assemblage, Salka Group, Litte Group and Maitat Complex (see chapter 2). In this section, correlation of these elements with sequences to the south is discussed, and compared with the structurally higher nappes of the Efjord-Sitas area further west.

The Aurek Assemblage of the study area consists of a sequence of quartzo-feldspathic paragneiss containing discontinuous mafic lenses. To

the east and structurally below the Aurek Assemblage is a thick areally extensive sequence of amphibolite, gneiss, and mafic schist of the "Kebnekaise amphibolite" (see Plate 7, and Kulling, 1964). The Kebnekaise amphibolite also crops out south of the Akkajaure Window, forming the Sarek Mountains (Kulling, 1982). The Aurek Assemblage however, appears to pinch-out in the Sarek area beneath low-grade schist and psammite equivalent to the Salka Group. South of the Sarek Mountains, a thick sequence of quartzo-feldspathic schist reappears above the "Sarek amphibolite" and below Salka Group equivalents. This unit, the Juron quartzite of Kulling (1982), like the Aurek Assemblage commonly contains discontinuous lenses of amphibolite and metagabbro. It is from some of these lenses in the Grapesvare area that Andreasson et al. (1985) have described eclogite-bearing rocks that yield p-T conditions similar to the Aurek Gabbro. The Aurek Assemblage of the Efjord-Kebnekaise area is therefore considered equivalent to the Juron quartzite of the Nassafjell area.

Scandinavian workers consider the high-grade amphibolite and gneiss such as the Sarek amphibolite and Juron quartzite within the central part of the orogen to be part of the Seve Nappe Complex (Trouw, 1973; Zwart, 1974; Williams and Zwart, 1977; Gee and Zachrisson, 1979). Some units within the Seve Nappe Complex contain tholeiitic dikes similar to the Ottfjallet dike swarm of the Sarv Nappe (Gee, pers. comm.). The clastic sequences of the Sarv Nappe are interpreted to be part of the upper Proterozoic miogeoclinal wedge that developed marginal to Baltica (Kumpulainen, 1982). Both U-Pb zircon and Rb-Sr whole-rock dating from some gneissic portions of the Seve Nappe Complex yield ages of 1600-1700 Ma (Reymer, 1979; Claesson, 1982). The Seve Nappe Complex therefore appears

to represent an element of marginal Baltica that was metamorphosed under upper amphibolite to eclogite facies conditions before being obducted and translated eastward onto the Baltic Shield.

Psammite, graphitic schist and calcareous schist similar to that of the Salka Group crops out to the south of Akkajaure structurally above the Sarek amphibolite and Juron quartzite (Kulling, 1982). These units continue south of the Nassafjell Window where Stephens (1982) has mapped low-grade psammitic schist in the Bjorkvattnet area lithologically similar to the Salka Group. This sequence was named the Bjorkvattnet Nappe by Stephens (1982), and is subdivided into several formations. The Slatdal and Vojtja Formations of the Bjorkvattnet Nappe consist of fossil-bearing calcareous schist and quartzite, which yield an Ashgill depositional age. The overlying Broken Formation consists of graptolite-bearing graphitic schist. The fossils indicate a middle (to late?) Llandovery depositional age. Locally associated with this unit are basic volcanic lenses (Stephens et al., 1985). The lithologic descriptions of the Slatdal-Vojtja and Broken Formations are similar to the Rusjka Calcareous and Rusjka Graphitic Schists respectively. While it may be unrealistic to imagine stratigraphic continuity for 300 km, it seems likely the Salka Group is broadly correlative with the Bjorkvattnet Nappe. Further, it may therefore be reasonable to assume a latest Ordovician - earliest Silurian depositional age for the Salka Group.

The Koli Nappes, containing metamorphosed sedimentary, volcanic and intrusive rocks of early Paleozoic age have been subdivided commonly into three laterally continuous tectonostratigraphic elements - Lower, Middle and Upper Koli (Stephens, 1980). The Bjorkvattnet Nappe is the type section of the Lower Koli (Stephens, 1982). The Salka Group is therefore

considered part of the Lower Koli.

Crowley (1985, p. 196) correlated the Reppi Schist and Rapetjakka Hornblende Schist with the Furulund Group of Nicholson and Rutland (1969). The low-grade portion of the Furulund Group in the Sulitjelma area has yielded Upper Ordovician to Lower Silurian fossils (Wilson, 1970). If the Reppi Schist, Skjafjell Schist and Litte Group are part of a relatively coherent stratigraphic sequence as suggested by Crowley (1985), then the Litte Group may also have an Upper Ordovician to Lower Silurian depositional age.

In the north-central Scandinavian Caledonides, the Lower Koli is tectonically overlain by calcareous phyllites of the Middle Koli (eg. Stephens, 1977, 1980; Haggbom, 1978). The Litte Group may therefore be part of the Middle Koli.

As discussed in chapter 2, the Maitat Complex is correlated with the Filfjell and Rauvatn Complexes of Crowley (1985). Northwest of Sitasjaure (Plate 7), the Filfjell and Rauvatn Complexes appear to be tectonically intercalated with calcareous units of the Skjafjell Schist. Arguments presented in chapter 4 suggest the Baugefjell Amphibolite, which crops out west of Sitasjaure and encases the Rauvatn Complex, is associated with a late-metamorphic shear zone within the upper nappe complex. These relationships suggest that while contacts between the Litte Group, Skjafjell Schist and Reppi Schist appear gradational and have been interpreted as depositional (Crowley, 1985), there may be numerous intraformational thrust faults juxtaposing lithologically indistinguishable units.

Plate 7 is a tectonic map of the Efjord-Kebnekaise area. At the structurally highest levels within the upper nappe complex of the transect

area, regional correlations are problematic due to the high metamorphic grade, structural complexity and lithologic heterogeneity of the units. As noted above, the Rauvatn, Filfjell and Maitat Complexes are considered to be lenses tectonically intercalated with other upper nappe complex units along late-metamorphic thrust faults. This interpretation allows the Marko Complex (Crowley, 1985) south of Efjorden to be correlated with the Sjurvatnet Schist (Hodges, 1985) to the north of Efjorden (Plate 7).

North of Efjorden (Plate 7) the Sjurvatnet Schist is unconformably overlain by the Salangen Group (Hodges, 1985; Steltenpohl, 1985; Tull et al., 1985). Although no fossils have been found in the high-grade units of the Efjord area, correlation with the low-grade fossil-bearing Balsfjord Group, located in the Lyngen area about 100 km to the northeast, suggests a Llandoverian depositional age (Binns and Matthews, 1981; Steltenpohl et al., 1985).

Interestingly, in the Lyngen area, the Ullsfjord nappe complex (Binns, 1978) which underlies the Balsfjord Group contains the Lyngen Gabbro that was obducted during the Finnmarkian Orogeny (Minsas and Sturt, 1981). Furthermore, the base of the Ullsfjord nappe complex has been metamorphosed to a higher metamorphic grade than the overlying Balsfjord Group. These relationships suggest the base of the Balsfjord Group is marked by a post-Finnmarkian - pre-Scandian unconformity (Sturt, pers. comm.).

If the Elvenes Conglomerate at the base of the Salangen Group in the Efjord area is also the "Finnmarkian unconformity", then the underlying Sjurvatnet Schist must have experienced both an early Finnmarkian and a later Scandian metamorphism.

METAMORPHIC EVOLUTION OF THE EFJORD-KEBNEKAISE AREA

Arguments presented above and in chapters 3, 4 and 5, indicate that rocks of the Efjord-Kebnekaise area have experienced two high-grade metamorphic events: the Late Cambrian or Early Ordovician "Finnmarkian", and Early Silurian "Scandian". These two events were then overprinted by a Late Silurian to Early Devonian upper greenschist facies metamorphism associated with tectonic intercalation of the entire upper nappe complex and early obduction onto the Baltic Shield. The Baltic Shield within the study area was then metamorphosed to greenschist facies during final emplacement of the upper nappe complex. In this section the stratigraphic, structural, thermochronologic and petrologic data presented earlier are incorporated in a model of the metamorphic evolution of the transect area.

^{40}Ar-^{39}Ar data presented and discussed in chapter 5 strongly suggests the upper amphibolite to eclogite facies metamorphism of the Aurek Assemblage and Rauvatn Complex was a Late Cambrian or Early Ordovician event. There is also much evidence of Finnmarkian age deformation and metamorphism elsewhere in the transect area.

Tectonostratigraphic and structural relations indicate the Filfjell and Maitat Complexes are correlative with the Finnmarkian Rauvatn Complex (see chapter 5), implying these units may also have been metamorphosed during Finnmarkian time. Furthermore, textures within rocks from the Maitat Complex indicate the unit was affected by two high-grade metamorphic events (Fig. 4-13). The earlier metamorphism (Finnmarkian?) appears to be syn-kinematic with development of the MCd1 schistosity, while the later event (Scandian?) clearly postdates schistosity development.

As discussed earlier, the Sjurvatnet Schist in the Ejford area may also have experienced both a Finnmarkian and a Scandian high-grade

metamorphism. Structural and textural relations in the Efjord area led Hodges (1985) to suggest the high-grade metamorphism occurred during emplacement of the upper nappe complex onto the Baltic Shield. Hodges and Royden (1984), Hodges (1985) and Hubbard (unpub. data) presented pressure-temperature data for samples from the Efjord area. Data from the Sjurvatnet Schist are plotted in Figure 6-1. Hodges and Royden (1984) argued that the apparent trend in p-T space recorded by these data is a post-deformational retrograde path associated with uplift and cooling of the Efjord area. In the Efjord area the Skjafjell and Reppi Schists crop out structurally below the Sjurvatnet Schist (Plate 7; Hodges, 1985, Plate 1). If the depositional age of the Skjafjell and Reppi Schists appears to be Late Ordovician to Early Silurian, these units cannot have experienced a Finnmarkian age metamorphism. Figure 6-2 is a plot of pressure-temperature data from the Skjafjell Schist in the Efjord area. The trend recorded by these data is conincident with that of the Sjurvatnet Schist data (Fig. 6-1). The metamorphism recorded by the Sjurvatnet Schist must therefore be a Scandian event.

Comparison of Litte Group pressure-temperature data from the Sitasjaure area (Fig. 4-12) with the Efjord area Skjafjell Schist data (Fig. 6-2) indicates the two arrays may be distinct. Although the Litte Group data are from samples up to 25 km apart (see chapter 4), the p-T array is well-defined (Fig. 4-12). It therefore seems unlikely that the difference between the Efjord and Sitasjaure trends is due to the relative positions of the two sample sets. However, as can be seen in Plate 7, the Sjurvatnet Schist samples are interpreted to be from a thrust sheet structurally above the Rauvatn Complex, while the Litte Group samples are from a thrust sheet below the Rauvatn Complex. Prior to the post-

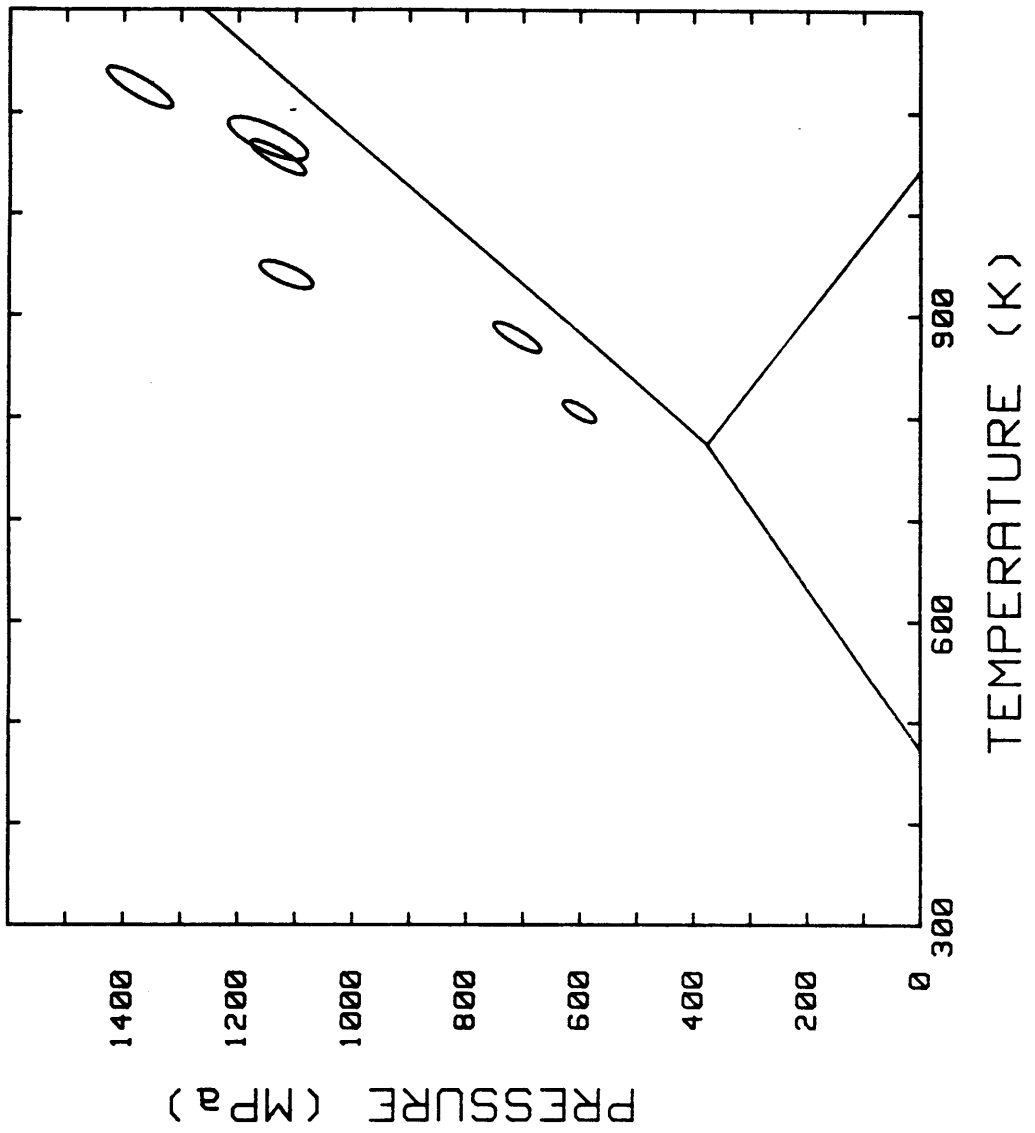

Figure 6-1: Sjurvatnet Schist p-T data

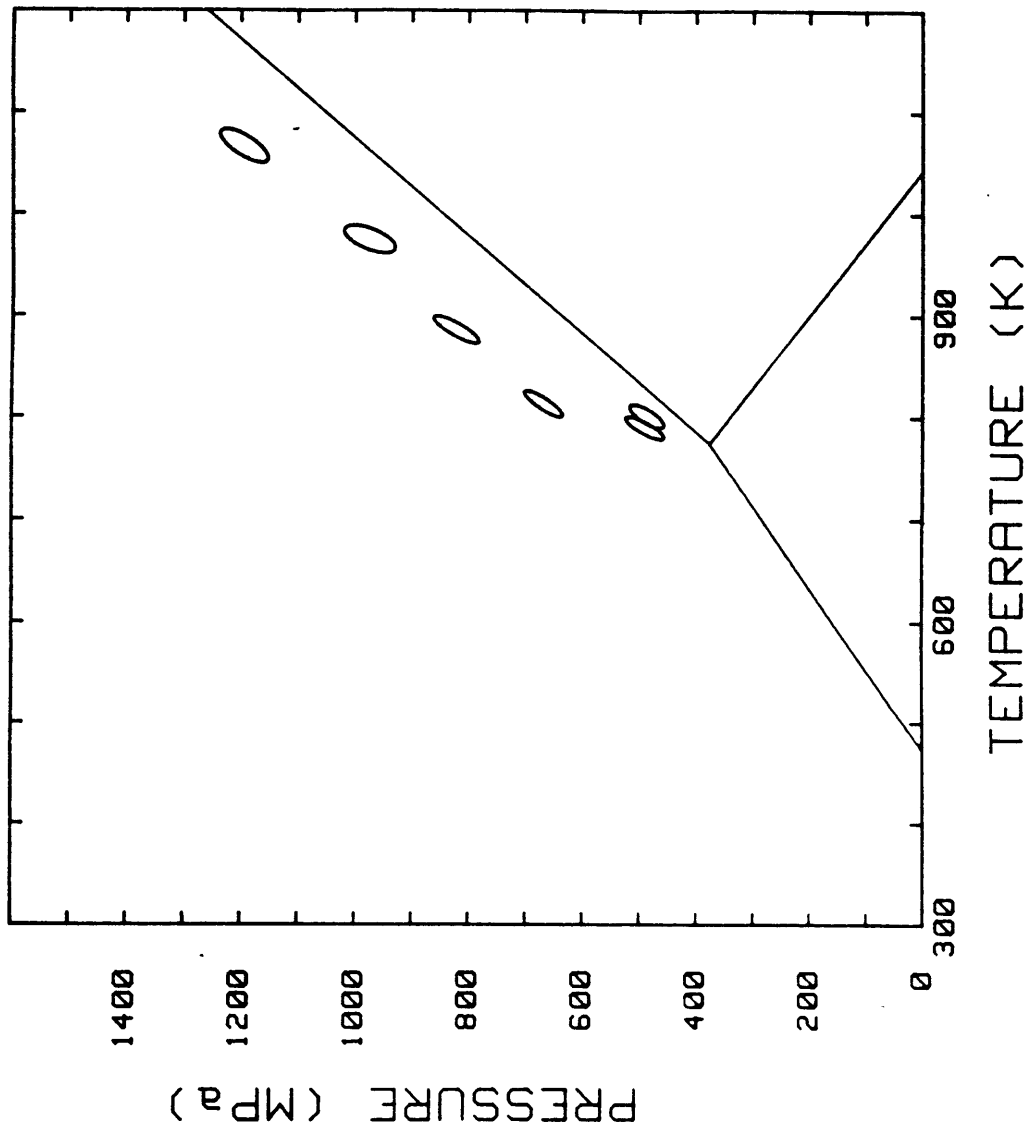

Figure 6-2: Skjafjell Schist p-T data

metamorphic imbrication of the upper nappe complex, the Sjurvatnet Schist and Litte Group must have been farther apart than at present, and conceivably experienced significantly different Scandian metamorphic histories.

The imbrication of the upper nappe complex occurred at greenschist to lower amphibolite facies conditions, leading to inverted metamorphic sequences and growth of both prograde and retrograde mineral assemblages associated with the thrust faults. For example, the Baugefjell Amphibolite that crops out to the west of Sitasjaure appears to be a shear zone separating the Rauvatn Complex from surrounding Skjafjell Schist units (chapter 5; Plate 7). ^{40}Ar-^{39}Ar data and mineral parageneses of the Baugefjell Amphibolite indicate the unit was recrystallized at epidote -amphibolite facies conditions. Syntectonic garnet growth near the base of the Salka Group is associated with thrust faulting along the Rusjka Fault during this event. Furthermore, the appearance of garnet towards the top of the Salka Group is related to emplacement of the Litte Group on the Tjuolak Thrust during this event. AAd2 biotite grade mylonitic deformation of the Aurek Assemblage is also related to this deformational event.

BASEMENT DEFORMATION DURING COLLISIONAL OROGENESIS

The nature of basement involvement during collisional orogenesis is an issue of much controversy, both in northern Scandinavia and orogenic belts in general. Bjorklund (1985) working in the Akkajaure Window south of the study area (Plate 7) has shown the allochthonous units to be dominated by Precambrian crystalline rocks. This Akkajaure Nappe Complex appears to be composed of at least six granitoid thrust sheets each with a thin cover of sedimentary rocks. Bjorklund (1985) concluded that the Complex was derived

from west of the Lofoten islands. This interpretation implies that during final emplacement of the upper nappe complex the bulk of the Baltic Shield basement remained relatively undeformed while the upper few hundered meters were detached. Based on work in the Efjord and Hinnoy areas, Hodges et al. (1982) presented an alternative model for the nature of basement involvement. This model argued that the early stages of collision involved en bloc subduction of the continental margin to depths of at least 30 km. As convergence continued, the Baltic Shield basement became involved in a series of imbricate thrusts similar to those in foreland fold and thrust terrains. In this scenario, the Forsa Thrust (Hodges, 1985) is younger than the Storrit Complex and is in fact cut by it (see Hodges, 1985, Plate 2). Correspondingly, in this 'basement shortening' model the Akkajaure Nappe Complex must be rooted east of the Lofoten islands rather than to the west.

Structural relationships at the northeastern margin of the study area indicate the Rombak-Sjangeli Window is detached along the Matert Thrust (see chapter 3 and Plate 2). Between the Rombak-Sjangeli and Singis Windows, the Storrit Complex and underlying Grunfjell basement are folded by the S60E vergent Salka Anticline. Here, where the Matert Thrust shear zone dips under the Rombak-Sjangeli Window it crops out approximately 200 m below flat-lying Storrit Complex rocks west of the Anticline (Plate 2, sec. B-B'). Structural cross sections in the area of the Singis Window and Tsutsajaure Culmination indicate the northwest trending MCd2 fold-axis which deforms the Matert Thrust plunges 8^{o} to N60W. The Matert Thrust must therefore dip 8^{o} under the Salka Anticline (Plate 2, secs. A-A', B-B'). Structural relationships of the Tornetrask Formation at the western end of the Singis Window indicate the Matert Thrust, like the Storrit Complex is

roughly parallel to the basement-cover interface. The 8° northwesterly dip of the fault surface is therefore due to later folding rather than footwall ramping.

Two hundred meters southwest of Tsutsajaure, rocks of the lower sandstone member of the Tornetrask Formation crop out below the sole thrust of the Storrit Complex (Plate 1). To the west of Tsutsajaure the sole thrust of the Storrit Complex remains at a relatively constant elevation. This implies that the underlying Matert Thrust must also be relatively horizontal, as any footwall ramps of the Matert Thrust would deform the overlying Grunfjell basement and Storrit Complex (eg. Woodward et al., 1985). The folding of the Matert Thrust from an 8° dip to N60W east of the Salka Anticline to a 0° dip west of the Anticline constrains the depth to the Matert Thrust below the Rombak-Sjangeli Window to be approximately 1 km (Plate 2, sec. B-B').

The most extensive exposures of Dividal Group sedimentary rocks within the Rombak-Sjangeli Window occur in the Kaisejaure area. However, small exposures of autochthonous sediment occur locally around the entire perimeter of the window (Kulling, 1964; Gustavson, 1978). These relationships and the common association of sedimentary rock with granitic slivers in the overlying Storrit Complex indicate the absence of any major footwall ramps of the Storrit Complex sole thrust. Correspondingly, the absence of any major monoclines with northeast trending axes which deform the entire Storrit Complex and Rombak-Sjangeli basement precludes any footwall ramping of the Matert Thrust. Woodward et al. (1985) noted that thrust faults with ramp-flat geometries can be restored by matching hangingwall ramps with corresponding footwall ramps. The Salka Anticline is the hangingwall ramp anticline of the Matert Thrust. The corrresponding

footwall ramp must lie west of the Rombak-Sjangeli Window, implying a minimum S60E transport distance on the Matert Thrust of 60 km. North of Sitasjaure, along the western margin of the window (Plate 7), the Storrit Complex dips 8-10^{o} to the northwest (Hodges, 1982; Crowley, 1985). Local outcrops of the autochthonous Tornetrask Formation below the sole thrust of the Storrit Complex (Hodges, 1985) indicate this structure is not due to footwall ramping of the Storrit Complex. Indeed, this structure may be related to footwall ramping of the Matert Thrust.

Figure 6-3 is of two schematic N60W to S60E cross-sections thruough the Efjord-Singis area illustrating the hypothesized structural relationships of the basement. The only difference between the two cross sections is the relationship between the Storrit Complex and the Forsa Thrust. Fig. 6-3a is based on the model of Hodges et al. (1982) in which the Storrit Complex cuts the Forsa Thrust and continues beneath the Western Gneiss Terrain. In Fig. 6-3b, the Storrit Complex and Matert Thrust merge into the Forsa Thrust. Hodges et al. (1982) and Hodges (1985) argued on textural grounds that the Forsa Thrust is older than the Storrit Complex and is cut by it. In the Efjord area no mylonitic fabrics are associated with the Forsa Thrust and the high-grade metamorphic foliation of the hanging wall is parallel to the fault surface. Hodges (1985) interpreted the high-grade metamorphism and thrust faulting to be coeval. However, Hodges (1985) also reports an 'intensification' of the foliation towards the Forsa Thrust. This intensification could in fact be a secondary Sitasjaure area to the east, the metamorphic foliation is clearly transposed by the mylonitic foliation of the Storrit Complex, indicating that latest movement on the Storrit Complex postdated peak metamorphic conditions in the hanging wall. The possibility of the Forsa Thrust being

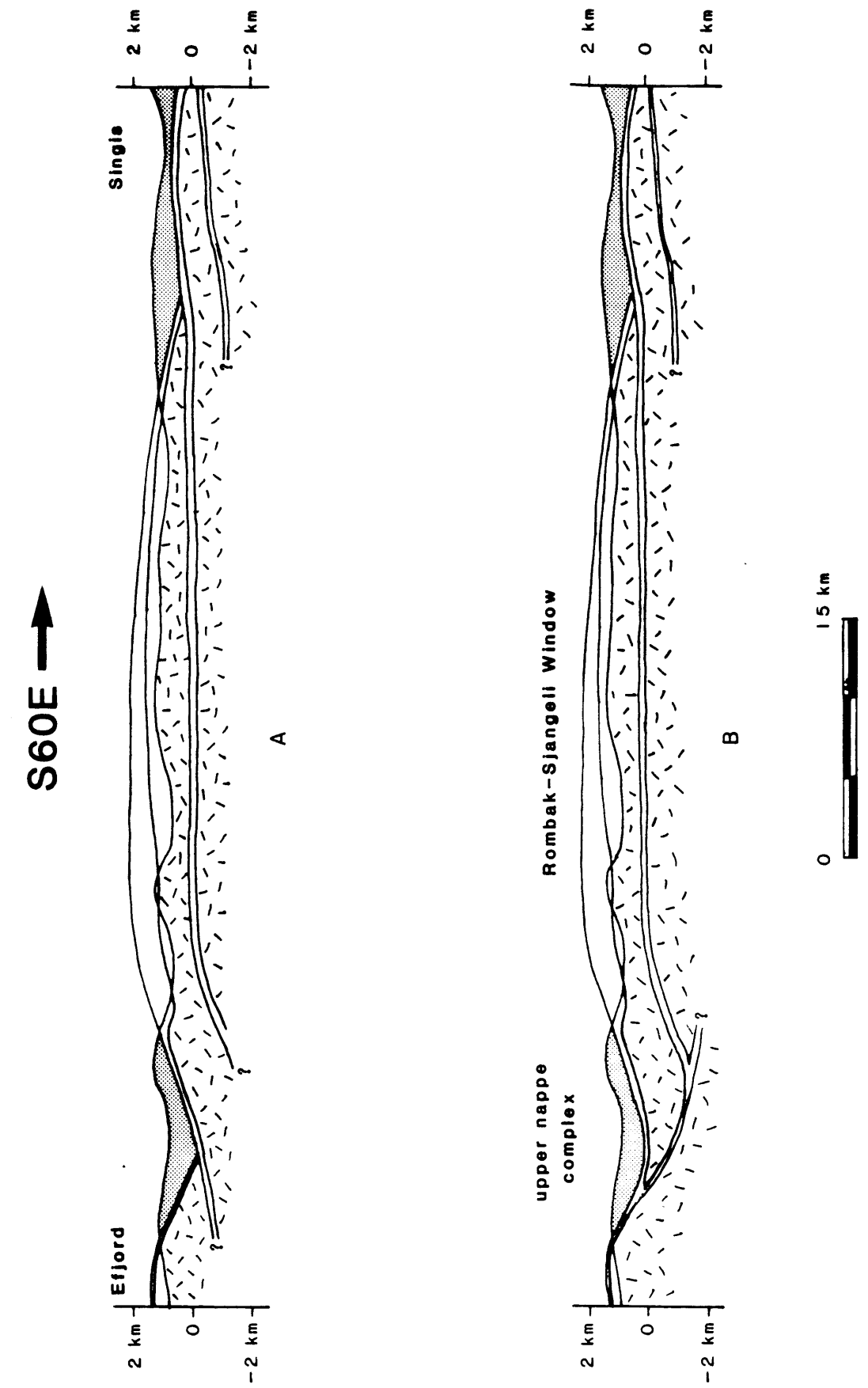

Figure 6-3: Structure cross-section of the Efjord-Singis area

the same age as or even younger than the Storrit Complex cannot be ruled out.

As discussed in chapter 5, a foliated amphibolite body from the Rombak-Sjangeli basement immediately below the Storrit Complex yielded a ^{40}Ar-^{39}Ar hornblende recrystallization age of 416.2 Ma. Hornblende from the Forsa Thrust on the other hand yielded an age of 388.5 Ma. Final movement on the Forsa Thrust leading to hornblende recrystallization within the shear zone therefore appears to have occurred approximately 28 Ma after mylonitic deformation of the Rombak-Sjangeli basement. These data are difficult to reconcile with the geometry of Fig. 6-3a. However, the ambiguous textural data and ^{40}Ar-^{39}Ar data are not inconsistent with the interpretation of Fig. 6-3b. This geometry is similar to that proposed by Bjorklund (1985) for the Akkajaure Nappe Complex in which the upper few hundred meters of the basement became detached while the bulk remained relatively undeformed.

If the Rombak-Sjangeli Window is a detached sliver of basement approximately 1 km thick, an obvious question concerns the degree of lateral continuity of the sliver. The inferred transport direction during final emplacement of the upper nappe complex is approximately S60E (see chapter 3). Interestingly, the southern (and northern) margin of the Rombak-Sjangeli Window strikes about S60E (Plate 7). Furthermore a major S60E trending synform separates the Rombak-Sjangeli Window in the north from the Akkajaure Window to the south (Plate 7). Steltenpohl (1985) argued that the northwest trending folds in the Scandinavian Caledonides are related to a 90^{o} rotation in the direction of compression from N60W-S60E to approximately N30E-S30W. A much simpler interpretation of these northwest trending macroscopic warps is that they are related to

lateral ramps within the detached basement slivers. Thus, the synform separating the Rombak-Sjangeli and Akkajaure Windows appears to be a depression within the upper nappe complex formed by the southerly pinch-out of the Rombak-Sjangeli basement sliver and the northerly pinch-out of part of the Akkajaure Nappe Complex.

Steltenpohl (1985) argued that northwest trending 'cross folds' in the northern Scandinavian Caledonides are north-vergent. However, in the Kaisejaure area the main northwest-trending RSd2 open anticline has parasitic southwest-vergent folds on the northeast limb, and parasitic northeast-vergent folds on the southwest limb (see chapter 3, and Plates 4 and 5). This reversal in the vergence direction can best be explained by northeast-southwest flexural slip during development of the southern lateral ramp anticline of the Rombak-Sjangeli Window (Fig. 6-4). Similarly, as discussed in chapter 3, the northwest-trending Tsutsajaure Culmination (SCd4) and coaxial Singis Window (MTd2) fold formed during D6 detachment of the Singis Window basement and subsequent lateral ramping of this sliver.

Thelander et al. (1980) have shown the Nassafjell Window 180 km south of the study area to be allochthonous. These workers found a window within the window consisting of crystalline basement and a parautochthonous siltstone cover sequence. Thus, the Nassafjell Window also appears to be a thin detached sheet of Baltic Shield basement.

There has been much debate concerning the origin of Scandinavian gneiss domes such as the Rombak-Sjangeli and Nassafjell Windows. Ramberg (1966) compared the development of these gneiss domes to diapriric structures produced experimentally using centrifuge techniques. Steltenpohl (1985) on the other hand argued that the gneiss domes formed as

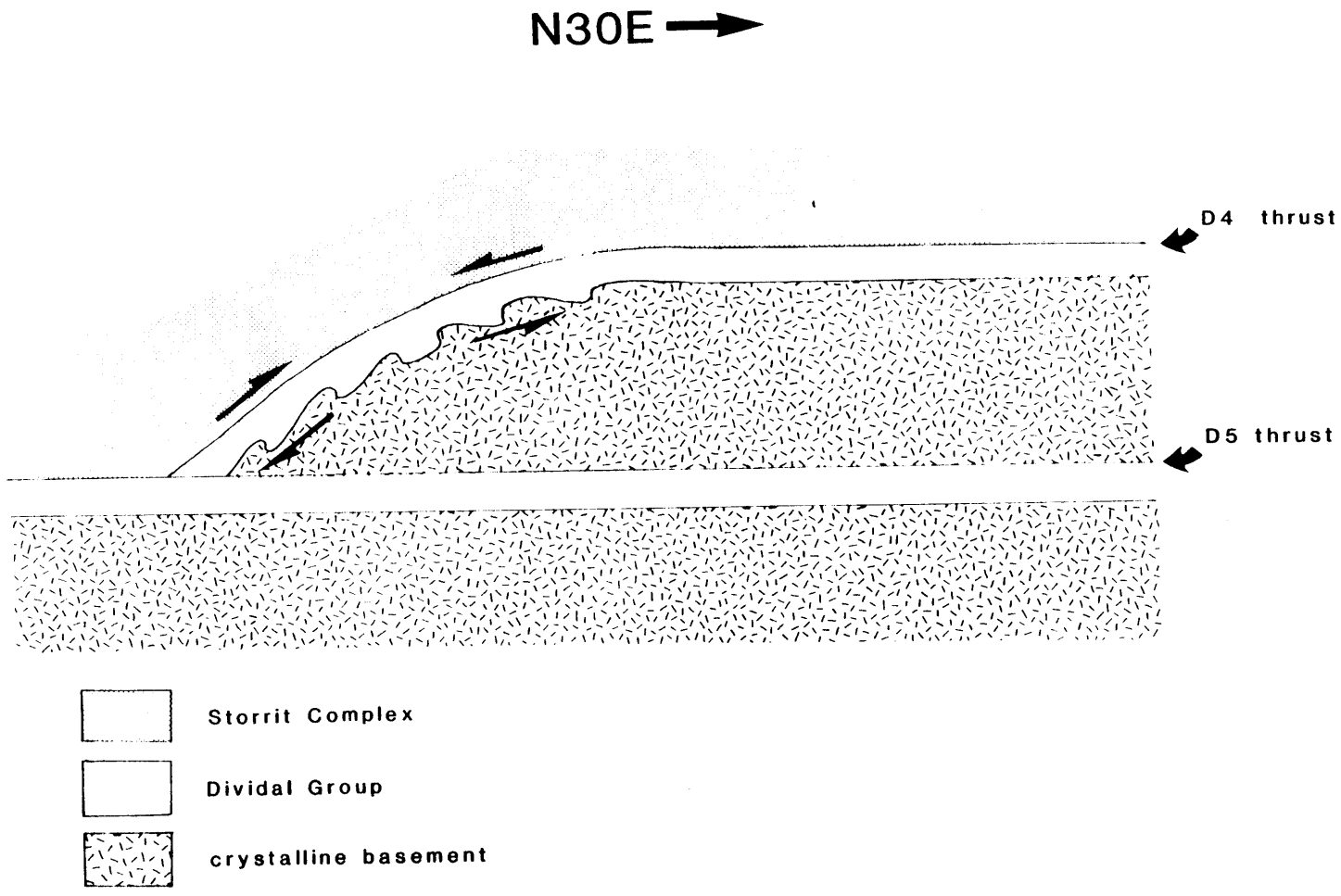

Figure 6-4: Flexural slip folding during lateral ramp development

a Ramsay type 1 fold interference pattern during two orthogonal compressive strain events. However, structural relationships within the Rombak-Sjangeli, Akkajaure and Nassafjell Windows indicates that some Scandinavian gneiss domes formed as a consequence of tectonic stacking during emplacement of thin laterally discontinuous slivers of crystalline basement.

REFERENCES

Adamek, P.M., 1975, Geology and mineralogy of the Kopparasen urannitesulphide mineralization, Norrbotten County, Sweden, Sver. Geol. Unders. C. 712.

Ahlberg, P., 1979, Early Cambrian tribolites from Mount Luopakte, northern Sweden, Sver. Geol. Unders. C. 765, 12 pp.

Ahlberg, P., 1980, Early Cambrian tribolites from northern Scandinavia, Norges Geol. Unders. 60, 153-159.

Ahlberg, P., and Bergstrom, J., 1978, Lower Cambrian ptychopariid trilobites from Scandinavia, Sver. Geol. Unders. Ca 49, 41 pp.

Anderson, G.M., 1976, Error propagation by the Monte Carlo method in geochemical calculations, Geochim. Cos. Acta, 40, 1533-1538.

Andersson, A., Dahlmann, B., Gee, D.G., and Snoll, S., 1985, The Scandinavian Alum Shales, Sver. Geol. Unders. Ca 56, 50 pp.

Andreasson, P.G., Gee, D.G., and Sukotjo, S., 1985, Seve eclogites in the Norrbotten Caledonides, Sweden, in D.G. Gee and B.A. Sturt (eds.), The Caledonide Orogen - Scandinavia and Related Areas, John Wiley and Sons.

Andresen, A., and Cashman, P.H., 1984, Extensional faulting during nappe emplacement, Scandinavian Caledonides, Geol. Soc. Amer. Abs. with Progs., 16, 431.

Bartley, J.M., 1980, Structural geology, metamorphism and Rb/Sr geochronology of East Hinnoy, north Norway, Ph.D. thesis, Mass. Inst. Tech., Cambridge, MA, 263 pp.

Bartley, J.M., 1981, Lithostratigraphy of the Storvann Group, East Hinnoy, north Norway, and its regional implications, Norges Geol. Unders., 370, 11-24.

Bartley, J.M., 1982, Limited basement involvement in Caledonian deformation, Hinnoy, north Norway, and tectonic implications, Tectonophysics, 83, 185-203.

Bell, T.H., and Etheridge, M.A., 1973, Microstructure of mylonites and their descriptive terminology, Lithos. 6, 337-48.

Bence, A.E., and Albee, A.L., 1968, Empirical correction factors for the electron microanalysis of silicates and oxides, J. Geol., 76, 382-403.

Berthe, D., Choukroune, P., and Jegouzo, P., 1979, Orthogneiss, mylonite and non-coaxial deformation of granites: The example of the South Amorican Shear Zone, J. Struc. Geol., 1, 31-42.

Binns, R.E., 1978, Caledonian nappe correlation and orogenic history in Scaninavia north of lat. 67°N., Bull. Geol. Soc. Am., 89, 1475-1490.

Binns, R.E., and Matthews, D., 1981, Stratigraphy and structure of the Balsfjord Supergroup, Troms, north Norway, Norges Geol. Unders., 365, 39-54.

Birkeland, T., 1976, Skjomen, bergrunnsgeologisk kort N10-M, 1:100,000, Norges Geol. Unders.

Bjorklund, L., 1985, The Akkajaure Nappe Complex, Northern Scandinavian Caledonides, in D.G. Gee and B.A. Sturt (eds.), The Caledonide Orogen - Scandinavia and Related Areas, John Wiley and Sons.

Boyer, S.E., and Elliott, D., 1982, Thrust Systems, Amer. Assoc. Petrol. Geol. Bull., 66, 1196-1230.

Brooks, C., Hart, S.R., and Wendt, I., 1972, Realistic use of two-error regression treatments as applied to Rubidium-Strontium data, Rev. Geophys. and Space Phys., 10, 551-577.

Bryant, B.D., and Reed, J.C., Jr., 1969, Significance of lineation and minor folds near major thrust faults in the southern Appalachian and the British and Norwegian Caledonides, Geol. Mag., 106, 412-429.

Burchfiel, B.C., and Davis, G.A., 1975, Nature and controls of Cordilleran orogenesis, western United States: extensions of an earlier synthesis, Amer. Jour. Sci., 275A, 363-396.

Claesson, S., 1977, The age of the Ottfjallet dolerites of the Sarv Nappe, Swedish Caledonides, Geol. Foren. Stockh. Forh., 98, 370-374.

Claesson, S., 1980a, Pre-silurian orogenc deformation in the north-central Scandinavian Caledonides, Geol. Foren. Stock. Forh., 101, 353-356.

Claesson, S., 1980b, A Rb-Sr isotope study of granitoids and related mylonites in the Tannas Augen Gneiss Nappe, southern Swedish Caledonides, Geol. Foren. Stockholm Forh., 102, 403-420.

Crowley, P.D., 1985, The structural evolution of the Sitas area, northern Norway and Sweden, Ph.D. thesis, Mass. Inst. Tech., Cambridge, MA, 253 pp.

Dahlstrom, C.D.A., 1969, Balanced cross sections, Can. Jour. Earth Sci., 6, 743-757.

Dallmeyer, R.D., and Gee, D.G., 1986, $^{40}Ar/^{39}Ar$ mineral dates from retrogressed eclogites within the Baltoscandian miogeocline: implications for a polyphase Caledonian orogenic evolution, Bull. Geol. Soc. Amer., 97, 26-34.

Dallmeyer, R.D., Gee, D.G., and Beckholmen, 1985, $^{40}Ar/^{39}Ar$ mineral age record of early Caledonian tectonothermal activity in the Baltoscandian miogeocline, central Scandinavia, Amer. Jour. Sci., 285, 532-568.

Dalrymple, G.B., and Lanphere, M.A., 1974, ^{40}Ar-^{39}Ar age spectra of some undisturbed terrestrial samples, Geochim. Cosmochim. Acta, 38, 715-738.

Dalrymple, G.B., Alexander, E.C., Lanphere, M.A., and Kraker, G.P., 1981, Irradiation of samples for $^{40}Ar/^{39}Ar$ dating using the geological survey TRIGA reactor, USGS prof. paper, 1176, 55 pp.

Dodson, M.H., 1973, Closure temperature in cooling geochronological and petrological systems, Contr. Mineral. and Petrol., 40, 259-274.

Dyrelius, D., Gee, D.G., Gorbatschev, R., Ramberg, H., and Zachrisson, E., 1980, A profile through the central Scandinvian Caledonides, Tectonophysics, 69, 247-284.

Emmett, T.F., 1982, Structure and petrology of the Bergen-Jotun kindred rocks from the Gjendebu region, Jotunheimen, central southern Norway, Norges Geol. Unders., 373, 1-32.

Faure, G., 1977, Principles of Isotope Geology, Wiley, New York, N.Y., 464 pp.

Ferry, J.M. and Spear, F.S., 1978, Experimental calibration of the partitioning of Fe and Mg between biotite and garnet. Contr. Mineral. Petrol., 66, 113-117.

Fitch, T.J., 1970, Earthquake mechanisms in the Himalayan, Burmese and Andaman regions and continental tectonics in central Asia, Jour. Geophys. Res., 75, 2699-2709.

Foland, K.A., 1983, $^{40}Ar/^{39}Ar$ incremental heating plateaus for biotites with excess argon, Isotope Geoscience, 1, 3-21.

Foyn, S., 1967, Dividal-gruppen ("Hyolithus-sonen") i Finnmark og dens forhold til de eokambrisk-kambriske formasjoner (with English summary), Norges Geol. Unders., 249, 1-84.

Furnes, H., Thon, A., Nordas, J. and Garmann, L.B., 1982, Geochemistry of Caledonian metabasites from some Norwegian ophiolite fragments, Contrib. Mineral. Petrol., 79, 295-307.

Gee, D.G., 1975, A tectonic model for the central part of the Scandinavian Caledonides, Amer. Jour. Sci., 275A, 468-515.

Gee, D.G., Kumpulainen, R., Thelander, T., 1978, The Tasjon Decollement, central Swedish Caledonides, Sveriges Geol. Unders., C742, 35 pp.

Gee, D.G. and Wilson, M.R., 1974, The age of orogenic deformation in the Swedish Caldonides, Amer. Jour. Sci., 274, 1-9.

Gee, D.G., and Zachrisson, E., 1979, The Caledonides in Sweden, Sveriges Geol. Unders., C769, 48 pp.

Gilette, B.J., 1974, Studies in diffusion I:Ar in phlogopite mica, in Geochemical Transport and Kinetics, eds. A.W. Hofmann et al., Carnegie Publ. 634, 107-115.

Graham, C.M. and Powell, R., 1984, A garnet-hornblende geothermometer: calibration, testing, and application to the Pelona Schist, Southern California, Jour. Metam. Geol., 2, 13-31.

Green, D.H., and Ringwood, A.E., 1967, An experimental investigation of the gabbro to eclogite transformation and its petrological applications, Geochim. Cosmo. Acta, 31, 767-833.

Griffin, W.L., Taylor, P.N., Hakkinen, J.W., Heier, K.S., Iden, I.K., Krogh, E.J., Malm, O., Olsen, K.L., Ormaasen, D.E., and Tveten, E., 1978, Archean and Proterozoic crustal evolution in Lofoten-Vesteraalen, North Norway, Jour. Geol. Soc. Lond., 135, 629-647.

Gunner, J.D., 1981, A reconnaissance Rb-Sr study of Precambrian rocks from the Sjangeli-Rombak window and the pattern of initial $^{87}Sr/^{86}Sr$ ratios from northern Scandinavia, Norsk Geol. Tidsskr., 61, 281-290.

Gustavson, M., 1966, The Caledonian mountain chain of the southern Troms and Ofoten area, Part 1: Basement rocks and Caledonian metasediments, Norges Geol. Unders., 239, 162 pp.

Gustavson, M., 1974, Berggrunnskort Narvik, 1:250,000, Norges Geol. Unders.

Gustavson, M., 1978, Caledonides of north-central Norway., in IGCP Project 27, Caledonian-Appalachian Orogen of the North Atlantic Region Geol. Surv. Canada Paper, 78-13, 25-30.

Hakkinen, J.W., 1977, Structural geology and metamorphic history of western Hinnoy and adjacent parts of eastern Hinnoy, north Norway, Ph.D. thesis, Rice University, Houston, Texas, 161 pp.

Hansen, E., 1971, Strain Facies, Springer-Verlag, 207 pp.

Harley, S.L., 1984, An experimental study of the partitioning of Fe and Mg between garnet and orthopyroxene, Contrib. Mineral. Petrol., 56, 359-373.

Harrison, T.M., 1981, Diffusion of ^{40}Ar in hornblende, Contrib. Mineral. Petrol. 78, 324-331.

Harrison, T.M., and Fitzgerald, J.D., 1986, Exsolution in hornblende and its consequences for $^{40}Ar/^{39}Ar$ age spectra and closure temperature, Geoch. Cosmo. Acta, 50, 247-253.

Harrison, T.M., Duncan, I., McDougall, 1985, Diffusion of ^{40}Ar in biotite: Temperature, pressure and compositional effects, Geoch. Cosmo. Acta, 49, 2461-2468.

Hart, S.R., 1964, The petrology and isotopic-mineral age relations of a contact zone in the Front Ranges, Colorado, Jour. Geol. 72, 493-525.

Heier, K.S., and Compston, W., 1969, Interpretation of Rb-Sr age patterns in high-grade metamorphic rocks, north Norway, Norsk Geol. Tiddskr., 49, 257-283.

Henriksen, H., 1981, A major unconformity within the Lower Paleozoic sequence of the Major Bergen Arc, Osteroy, western Norway, Norges Geol. Unders., 367, 65-75.

Henriksen, H. and Higgins, A.K., 1976, East Greenland Caledonian fold belt, in Escler, A. and Watt, W.S. (eds.), Geology of Greenland, Gron. Geol. Unders., Copenhagen, 186-242.

Hodges, K.V., 1982, Tectonic evolution of the Aefjord-Sitas area, Norway-Sweden, Ph.D. thesis, Mass. Inst. Tech., Cambridge, MA, 191 pp.

Hodges, K.V., Bartley, J.M., and Burchfiel, B.C., 1982, Structural evolution of an A-type subduction zone, Lofolen-Rombak area, northern Scandinavian Caledonides, Tectonics, 1, 441-462.

Hodges, K.V., and Crowley, P.D., 1985, Error estimation and empirical geothermobarometry for pelitic systems, Amer. Mineral., 70, 702-709.

Hodges, K.V., and Royden, L., 1984, Geologic thermobarometry of retrograded metamorphic rocks: an indication of the uplift trajectory of a portion of the northern Scandinavian Caledonides, Jour. Geophys. Res., 89, 7077-7090.

Holdaway, M.J., 1971, Stability of andalusite and the aluminosilicate phase diagram, Amer. Jour. Sci., 271, 97-131.

Kulling, O., 1964, Oversikt over norra norrbotten-fjallens Kaledonberggrund, Sveriges Geol. Unders., Ba 19, 166 pp.

Kulling, O., 1972, The Swedish Caledonides - in T. Strand and O. Kulling: The Scandinavian Caledonides, Wiley-Interscience, London, 147-285.

Kulling, O., 1982, Oversikt over sodra Norbottensfjallene kaledonberggrund, Sveriges Geol. Unders., Ba26, 295 pp.

Kumpulainen, R. 1982, The upper Proterozoic Risback Group, central Swedish Caledonides, Uppsala Univ. Dept. Min. Pet., res. rep. 28, 60 pp.

Kvale, A., 1953, Linear structures and their relation to movement in the Caledonides of Scandinavia and Scotland, Quart. Jour. Geol. Soc. Lond., 109, 51-73.

Le Fort, P., 1975, Himalayas: the collided range, present knowledge of the continental arc, Amer. Jour. Sci., 275A, 1-44.

Lister, G.S., and Snoke, 1984, S-C mylonites, Jour. Struc. Geol., 6, 617-638.

Lux, D.R., 1985, K/Ar ages from the Basal Gneiss Region, Stadlandet area, Western Norway, Norsk Geol. Tiddskr., 65, 277-286.

Minsaas, O. and Sturt, B.A., 1981, The Ordovician clastic sequence immediately overlying the Lyngen gabbro complex and its environmental significance, Terra Cognita, 1, 59.

Moberg, J.C., 1908, Bidrag till kannedomen om de kambriska lagren vid Tornetrask, Sveriges Geol. Unders., C212, 30 pp.

Newton, R.C., and Haselton, H.T., 1981, Thermodynamics of the garnet-plagioclase-Al_2SiO_5-quartz geobarometer, in R.C. Newton et al. (eds.), Thermodynamics of Minerals and Melts, Springer-Verlag, 131-147.

Newton, R.C., and Perkins, D., 1982, Thermodynamic calibration of geobarometers based on the assemblages garnet-plagioclase-orthopyroxene (clinopyroxene)-quartz, Amer. Mineral., 67, 203-222.

Norwood, C.B., 1974, Radiogenic argon diffusion in the biotite micas, m.s. thesis, Brown University, Rhode Island, 58 pp.

Oftedahl, D., 1980, Geology of Norway, Norges Geol. Unders., 356, 3-114.

Ord, A., and Christie, J.M., 1984, Flow stresses from microstructures in mylonitic quartzites of the Moine Thrust zone, Assynt area, Scotland, Jour. Struc. Geol., 6, 639-654.

Pankhurst, R.J., Moorbath, S., Rex, D.G., Turner, G., 1973, Mineral age patterns in ca. 3700 m.y. old rocks from West Greenland, Earth Planet. Sci. Lett., 20, 157-170.

Pettersen, K., 1878, Det nordlige Sveriges og Norges Geologi, Archiv for Mathematik og Naturvidenskab, 1-38.

Phillips, A.H., and Hess, H.H., 1936, Metamorphic differentiation at contacts between serpentinite and siliceous country rocks, Am. Min., 21, 333-362.

Price, R.A. and Mountjoy, E.W., 1970, Geologic structure of the Canadian Rocky Mountains between Bow and Athabaska rivers - a progress report, in Structure of the southern Canadian Corillera, J.O. Wheeler (ed.), Geol. Assoc. Canada, Special Paper 6, 7-26.

Ramberg, H., 1966, The Scandinavian Caledonides as studied by centrifuged dynamic models: Bulletin of the Geological Institute of the University of Uppsala, 43, 1-45.

Ramsay, J.G., 1967, Folding and Fracturing of Rocks, McGraw-Hill, 568 pp.

Ramsay, J.G., 1981, Tectonics of the Helvetic nappes, in K.R. McClay and N.J. Price (eds.), Thrust and nappe tectonics, Spec. Pub. Geol. Soc. Lond., 9, 293-309.

Reinick, H., and Wunderlich, F., 1968, Classification and origin of Flaser and Lenticular Bedding, Sedimentology, 11, 99-104.

Reymer, A.P.S., 1979, Investigations into the metamorphic nappes of the central Scandinavian Caledonides on the basis of Rb-Sr and K-Ar age determinations, Ph.D. thesis, Univ. of Leiden, 123 pp.

Robbins, G.A., 1972, Radiogenic Ar diffusion in muscovite under hydrothermal conditions, m.s. thesis, Brown University, Providence, Rhode Island.

Roberts, D., 1981, Some features of tectonic deformation of Old Red Sandstone sediments on Hitra, west central Norway, Norges Geol. Unders., 370, 45-48.

Roberts, D. and Wolff, F.C., 1981, Tectonostratigraphic developemnt of the Trondheim region Caledonides, central Norway, Jour. Struc. Geol., 3, 487-494.

Roddick, J.C., Cliff, R.A., Rex, D.C. 1980, The evolution of excess argon in Alpine biotites - a ^{40}Ar-^{39}Ar analysis, Earth Planet. Sci. Lett., 48, 185-208.

Roecker, S.W., 1982, Velocity structure of the Pamir-Hindu Kush region: Possible evidence of subducted crust, Jour. Geophys. Res., 87, 945-960.

Rosenfeld, J.L., 1970, Rotated garnets in metamorphic rocks, Geol. Soc. Amer. Spec. Paper, 129, 105 pp.

Royden, L., and Hodges, K.V., 1984, A technique for analyzing the thermal and uplift histories of eroding orogenic belts: a Scandinavian example, Jour. Geophys. Res., 89, 7091-7106.

Sack, R.O., 1982, Reaction skarns between quartz-bearing and olivine-bearing rocks, Amer. Jour. Sci., 282, 970-1011.

Sibson, R.H., 1977, Fault rocks and fault mechanisms, J. Geol. Soc. London, 133, 191-213.

Spry, A., 1983, Metamorphic Textures, Pergamon Press, 352 pp.

Steiger, R.H., and Jager, E., 1977, Subcommission on geochronology: conventions on the use of decay constants in geo- and cosmochronology, Earth Planet. Sci. Lett., 36, 359-362.

Steltenpohl, M.G., 1985, The structural and metmorphic history of Skanland, north Norway, and its significance for tectonics in Scandinavia, Ph.D. thesis, University of North Carolina, Chapel Hill, NC.

Steltenpohl, M.G., Andresen, A., and Tull, J.F., 1985, Evidence for lithostratigraphic correlation between the Salangen Group (Ofoten) and Balsfjord (Troms) and its regional implications (abs.), Geolognytt, 20, 47.

Stephens, M.B., 1977, Stratigraphy and relationship between folding, metamorphism and thrusting in the Tarna-Bjorkvattnet area, northern Swedish Caledonides, Sver. Geol. Unders., 726, 146 pp.

Stephens, M.B., 1980, Occurrence, nature and tectonic signivicance of volcanic and high-level intrusive rocks within the Swedish Caledonides, in Wones, D.R. (ed.), The Caledonides in the USA, Virginia Polytechnic Inst. and State Univ., Dept. Geol. Sci. Mem., 2, 289-298.

Stephens, M.B., 1982, Field relationships, petrochemistry and petrogenesis of the Stekenjokk volcanites, central Swedish Caledonides, Sver. Geol. Unders., C786, 111 pp.

Stephens, M.B., Gustavson, M., Ramberg, I.B., and Zachrisson, E., 1985, The Caledonides of central-north Scandinavia - a tectonostratigraphic overview in D.G. Gee and B.A. Sturt, (eds.), The Caledonide Orogen - Scandinavia and Related Areas, John Wiley and Sons.

Sturt, B.A., Pringle, I.R., and Ramsay, D.M., 1978, The Finnmarkian phase of the Caledonian orogeny, Geol. Soc. Lond. Jour., 135, 597-610.

Sturt, B.A., Pringle, I.R., and Roberts, D., 1975, Caledonian nappe sequence of Finnmark, northern Norway, and the timing of orogenic deformation and metamorphism, Geol. Soc. Amer. Bull., 86, 710-718.

Suppe, J., 1983, Geometry and kinematics of fault-bend folding, Amer. Jour. Sci., 283, 684-721.

Suppe, J., 1985, Principles of Structural Geology, Prentice-Hall, 537 pp.

Sveonnius, F., 1892, Om berggrunden i Norrbottenslan, Sveriges Geol. Unders., C126, 43 pp.

Thelander, T., 1982, The Tornetrask Formation of the Dividal Group, Northern Swedish Caledonides, Sveriges Geol. Unders., C789, 41 pp.

Thelander, T., Bakker, E., Nicholson, R., 1980, Basement-cover relationships in the Nassafjallet Window, central Swedish Caledonides, Geol. Foren. Stock. Forh., 102, 569-580.

Thompson, A.B., 1982, Dehydration melting of pelitic rocks and the generation of H_2O undersaturated granitic liquids, Amer. Jour. Sci., 282, 1567-1595.

Tornebohm, A.E., 1888, Om Fjallproblemat, Geol. For. Foren., 10, 328-336.

Trouw, R.A.J., 1973, Structural geology of the Marsfjallen area, Caledonides of Vasterbotten, Sweden, Sver. Geol. Under., 689, 115 pp.

Tull, J.F., Bartley, J.M., Hodges, K.V., Andresen, A., Steltenpohl, M.G., White, J.M., 1985, The Caledonides in the Ofoten region (68°-69°), north Norway: key aspects of tectonic evolution, in D.G. Gee, and B.A. Sturt, (eds.), The Caledonide Orogen - Scandinavia and Related Areas, John Wiley and Sons.

Turner, F.J., 1981, Metamorphic petrology, McGraw Hill, 524 pp.

Vogt, T., 1950, Narvik berggrunsgeologisk kort, 1:100,000, Norges Geol. Unders.

Vogt, T., 1967, Fjellkjedestudier i den ostlige del av Troms, Norges Geol. Unders.

Whitney, J.A. and Stormer, J.C., 1977, The distribution of $NaAlSi_3O_8$ between coexisting microcline and plagioclase and its effect on geothermomic calculations, Amer. Mineral., 62, 687-691.

Williams, P.F., 1972, Development of metamorphic layering and cleavage in low-grade metamorphic rocks in Bermagni, Australia, Amer. Jour. of Sci., 272, 1-47.

Williams, P.F. and Zwart, H.J., 1977, A model for the development of the Seve-Koli Caledonian Nappe Complex, in Saxena, S.K. and Bhattacharji (ed.), Energetics of Geological Processes, Springer, Berlin, 169-187.

Wilson, M.R., 1972, Excess radiogenic argon in metamorphic amphiboles and biotite from the Sulitjelma region, central Norwegian Caledonides, Earth Planet. Sci. Lett., 14, 403-412.

Woodward, N.B., Boyer, S.E., Suppe, J., 1985, An outline of balanced cross-sections, Univ. Tennessee, Studies in Geology 11, 2nd ed., 171 pp.

Yardley, B.W.D., 1977, An empirical study of diffusion in garnet, Amer. Mineral., 62, 793-800.

York, D., 1966, Least-squares fitting of a straight line, Can. Jour. Phys., 44, 1079-1086.

York, D., 1969, Least squares fitting of straight line with correlated errors, Earth and Plan. Sci. Let., 5, 320-324.

Zwart, H.J., 1974, Structure and metamorphism in the Seve-Koli nappe complex (Scandinavian Caledonides) and its implication concerning the formation of metamorphic nappes, in Geolgie des demaines crystallins: Liege, Centre Geologie Belgique, p. 129-144.

APPENDIX A

STRUCTURAL DATA FROM THE SITAS-SINGIS AREA

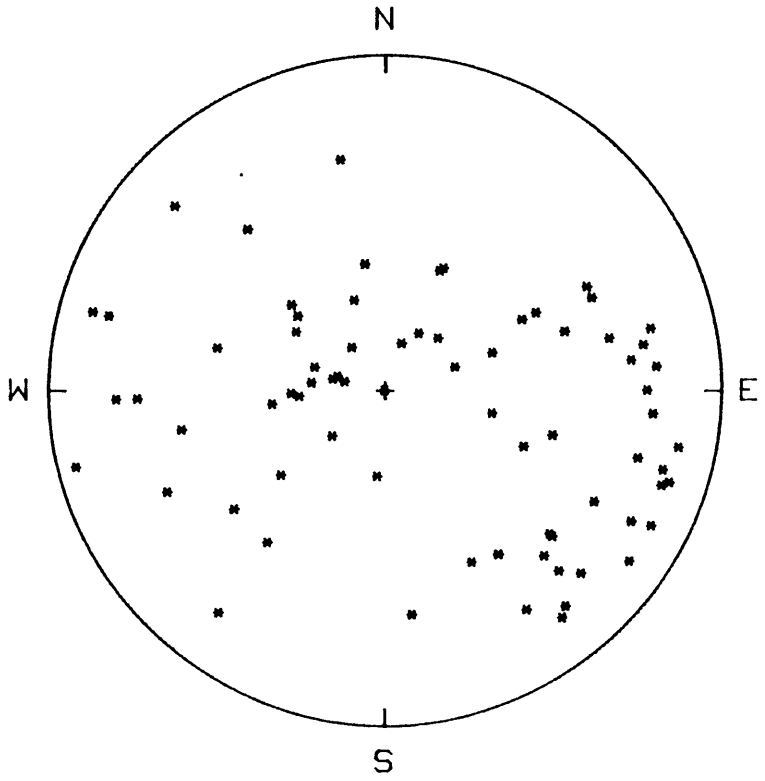

DOMAIN #1: RS bedding POLES
PROJECTION = EQUAL AREA
NUMBER OF POINTS = 75

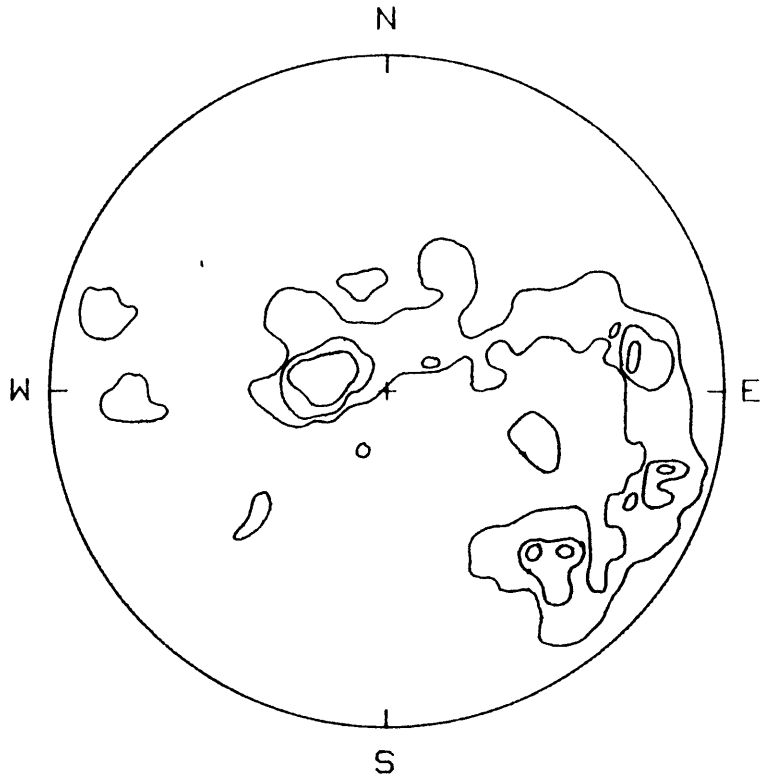

DOMAIN #1: RS bedding CONTOURS
PROJECTION = EQUAL AREA
SCANNING CIRCLE = 1.000%
CONTOURS: 3% 5% 7%

Figure A-1

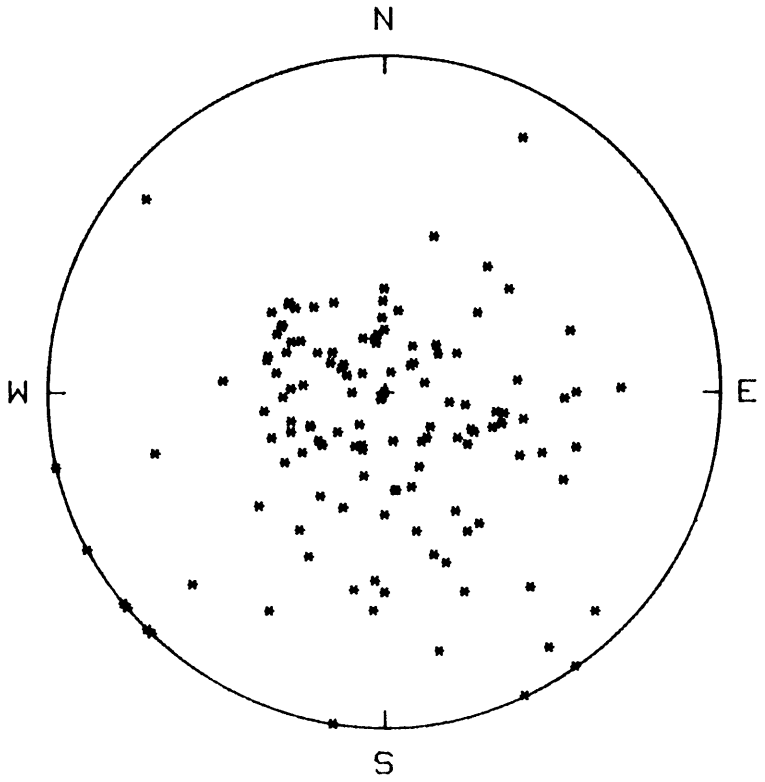

DOMAIN #2: RS bedding POLES
PROJECTION = EQUAL AREA
NUMBER OF POINTS = 141

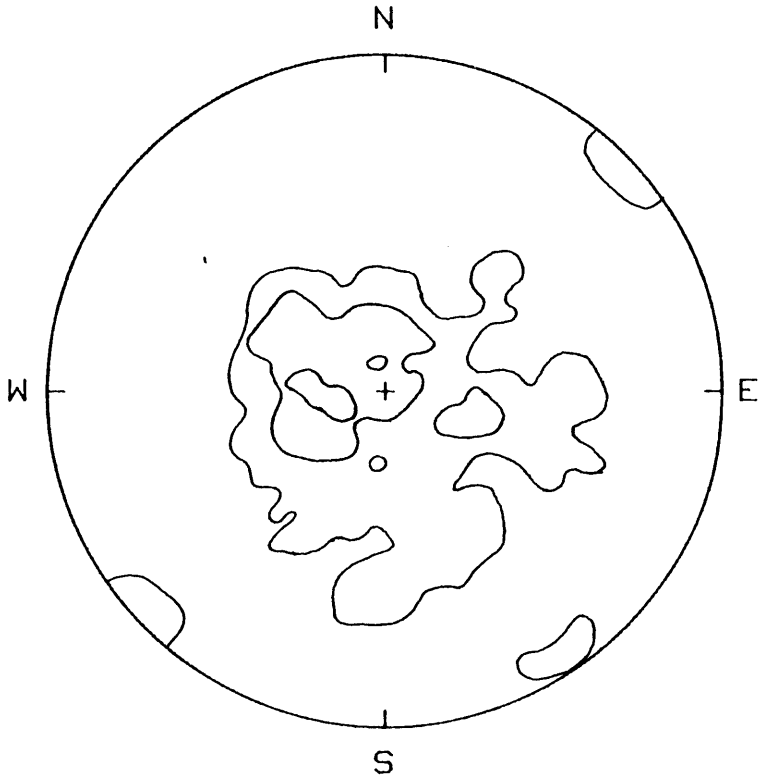

DOMAIN #2: RS bedding CONTOURS
PROJECTION = EQUAL AREA
SCANNING CIRCLE = 1.000%
CONTOURS: 1% 5% 10%

Figure A-2

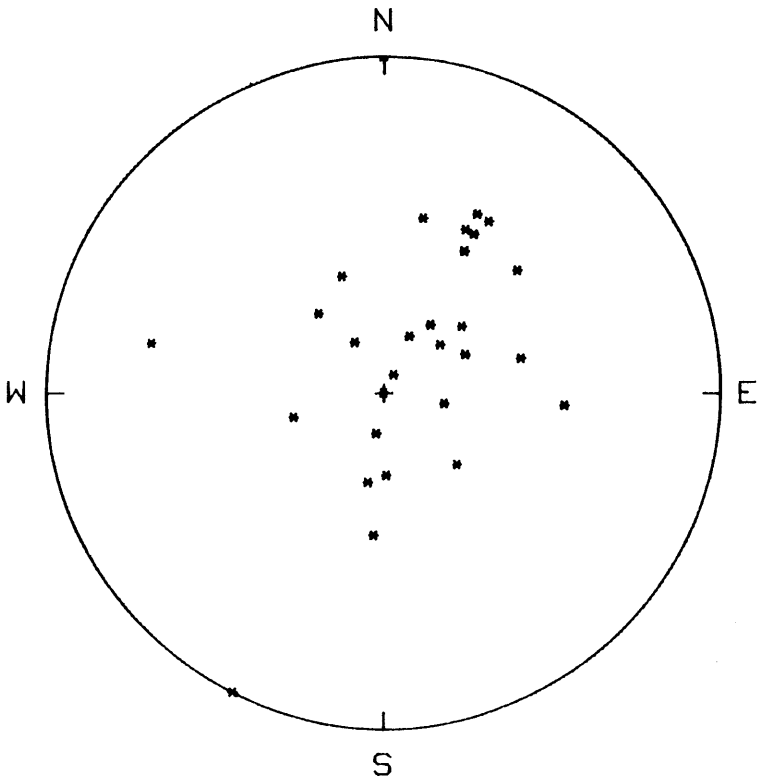

DOMAIN #3: RS bedding POLES
PROJECTION = EQUAL AREA
NUMBER OF POINTS = 31

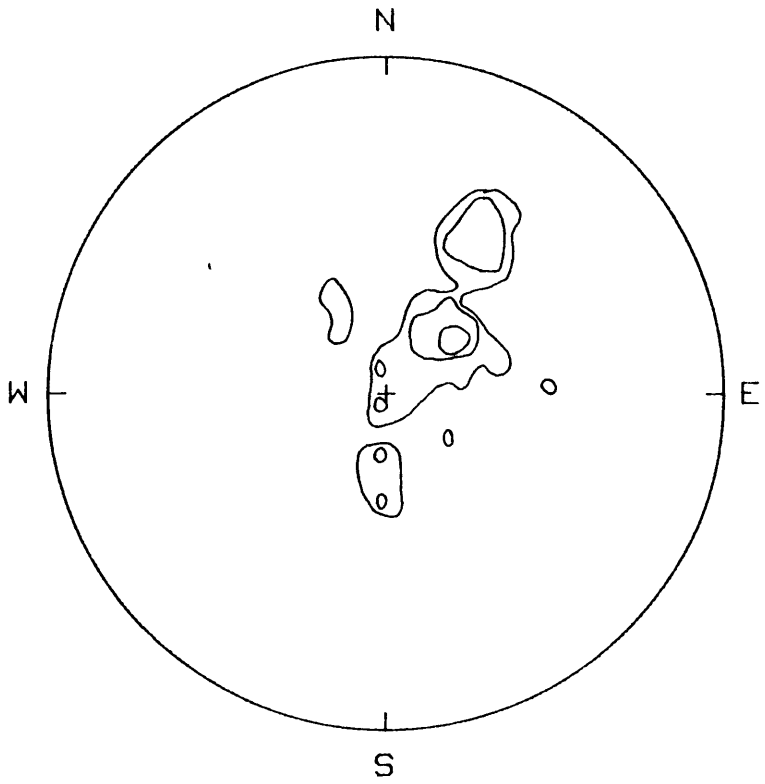

DOMAIN #3: RS bedding CONTOURS
PROJECTION = EQUAL AREA
SCANNING CIRCLE = 1.000%
CONTOURS: 5% 10% 15%

Figure A-3

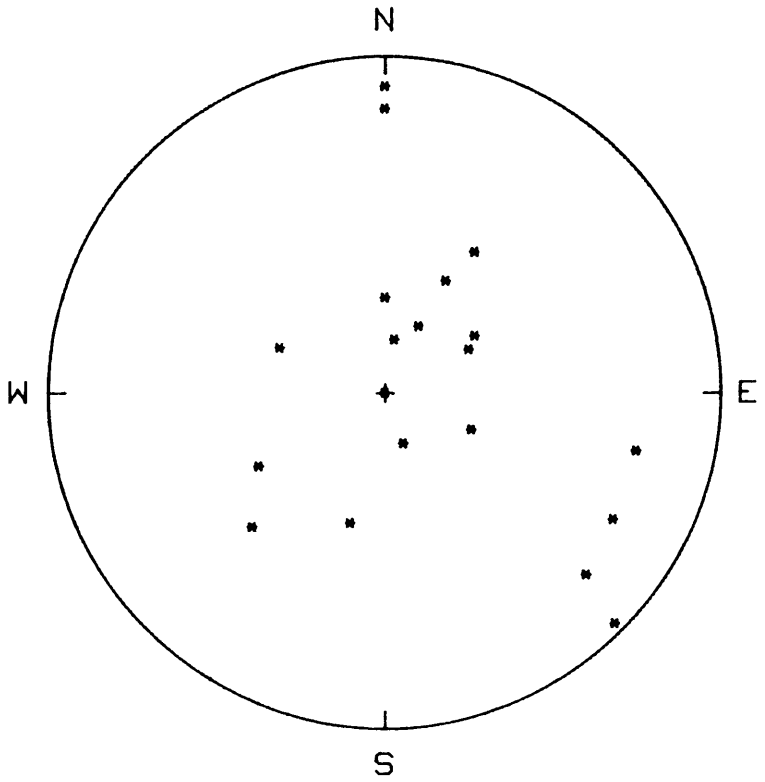

DOMAIN #1: RSd5 POLES
PROJECTION = EQUAL AREA
NUMBER OF POINTS = 20

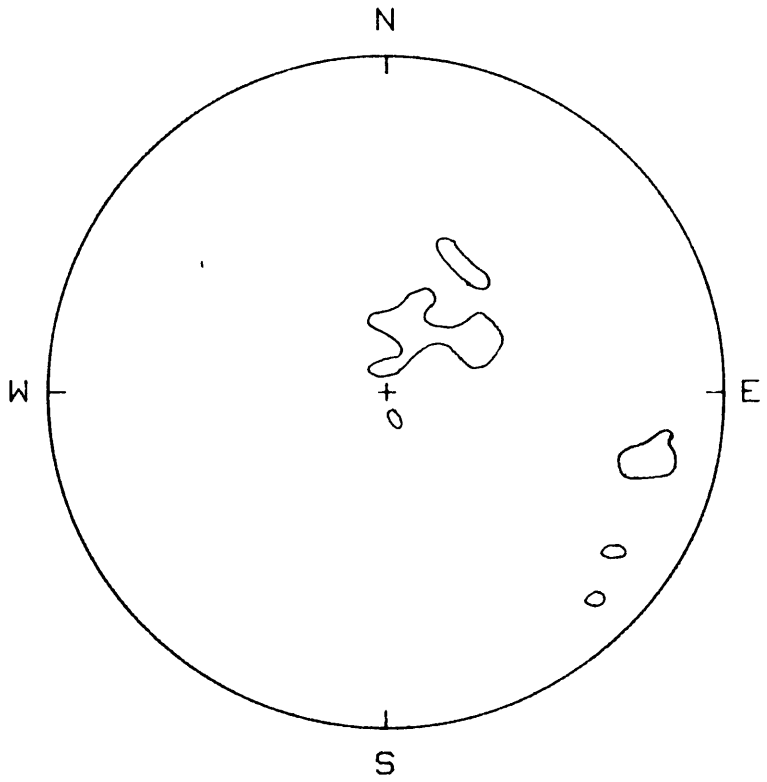

DOMAIN #1: RSd5 CONTOURS
PROJECTION = EQUAL AREA
SCANNING CIRCLE = 1.000%
CONTOURS: 10%

Figure A-4

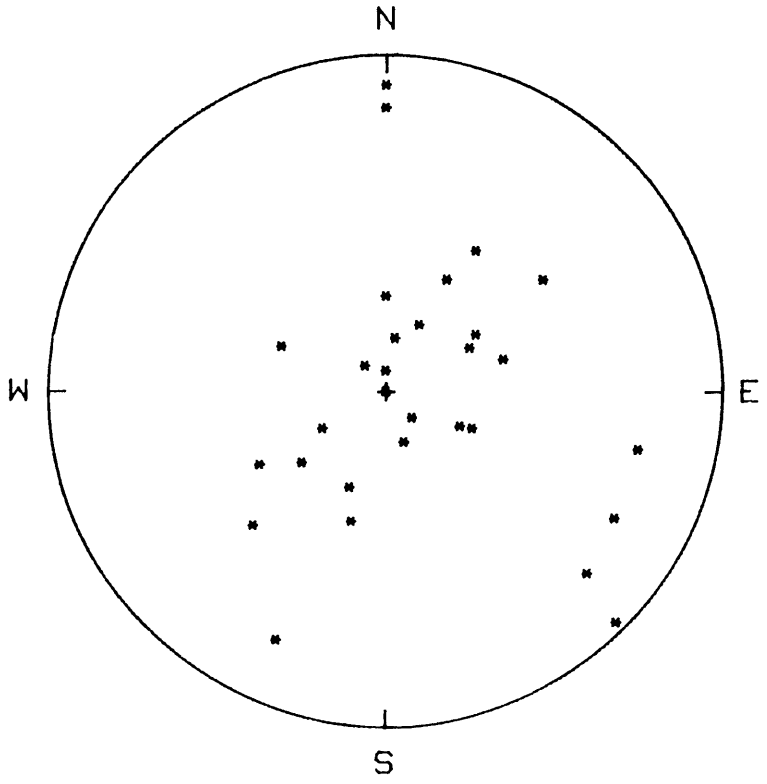

RSd5 POLES
PROJECTION = EQUAL AREA
NUMBER OF POINTS = 32

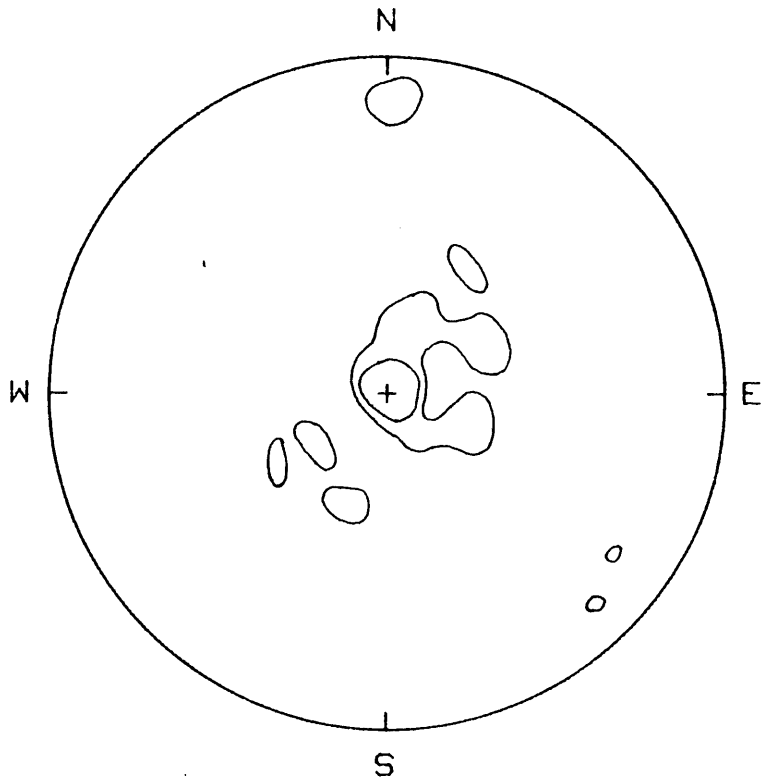

RSd5 CONTOURS
PROJECTION = EQUAL AREA
SCANNING CIRCLE = 1.000%
CONTOURS: 5% 10%

Figure A-5

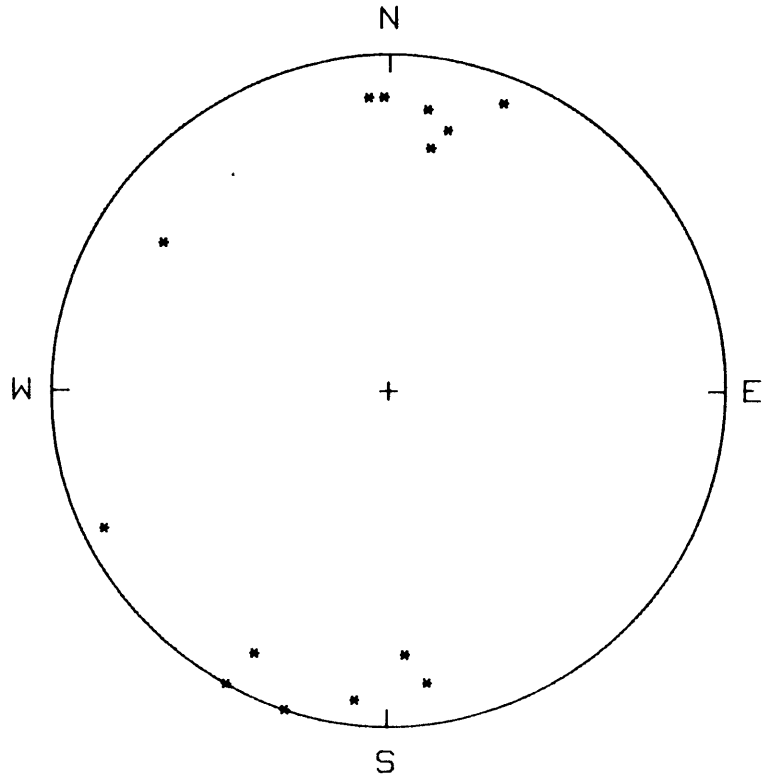

DOMAIN #1: RSd6 FOLDS
PROJECTION = EQUAL AREA
NUMBER OF POINTS = 14

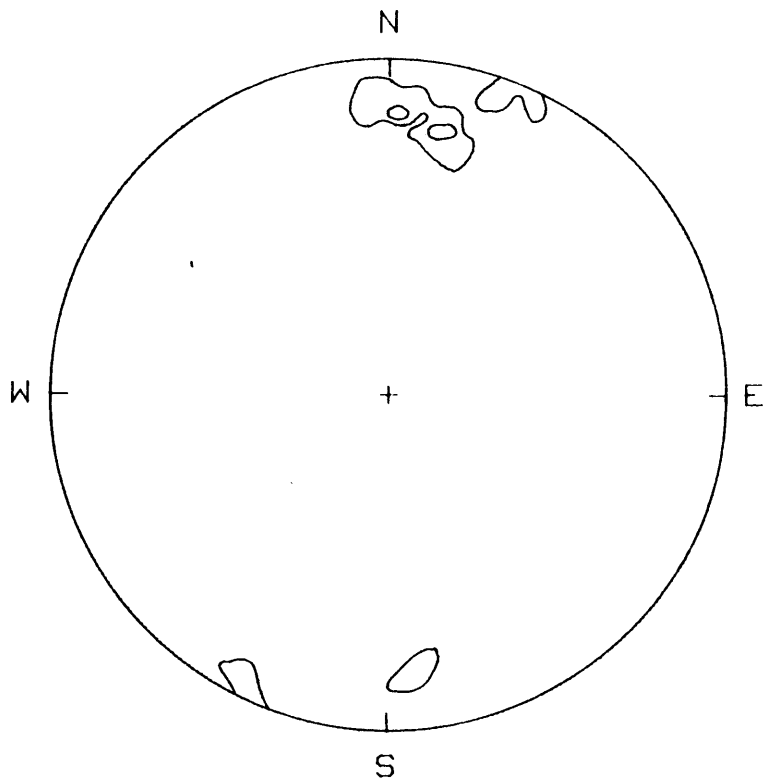

DOMAIN #1: RSd6 CONTOURS
PROJECTION = EQUAL AREA
SCANNING CIRCLE = 1.000%
CONTOURS: 10% 20%

Figure A-6

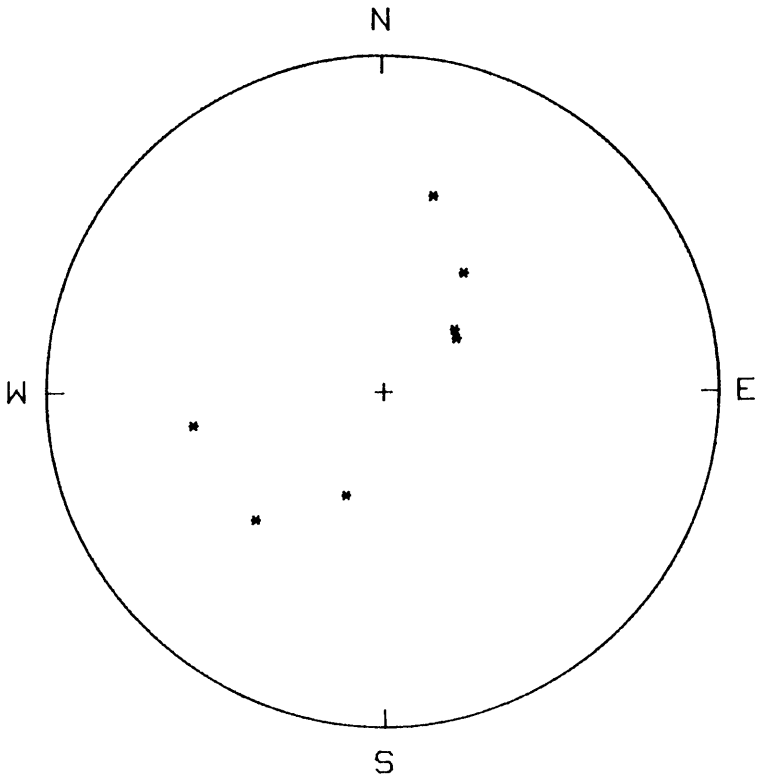

DOMAIN #4: SW bedding POLES
PROJECTION = EQUAL AREA
NUMBER OF POINTS = 7

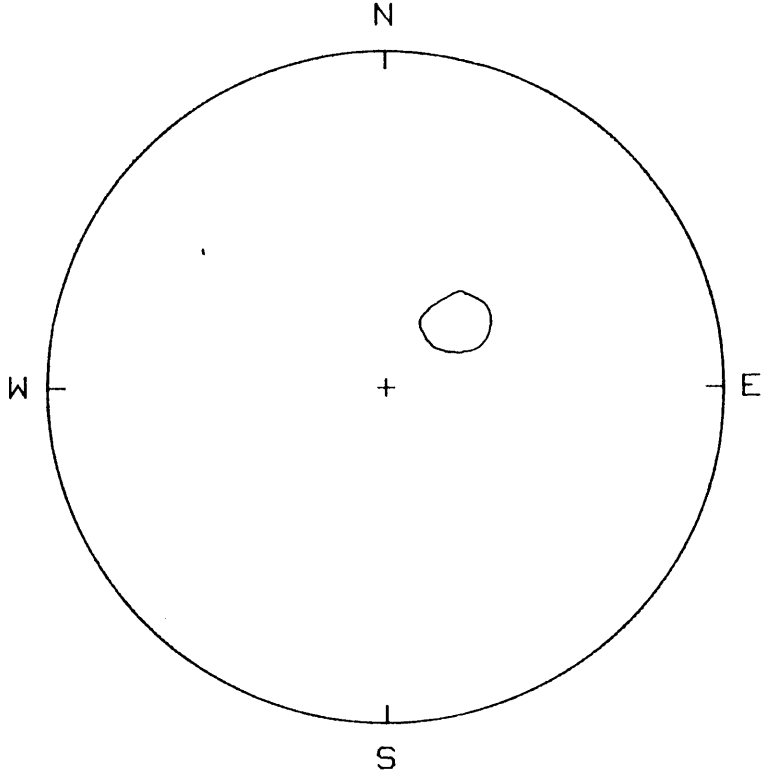

DOMAIN #4: SW bedding CONTOURS
PROJECTION = EQUAL AREA
SCANNING CIRCLE = 1.000%
CONTOURS: 20%

Figure A-7

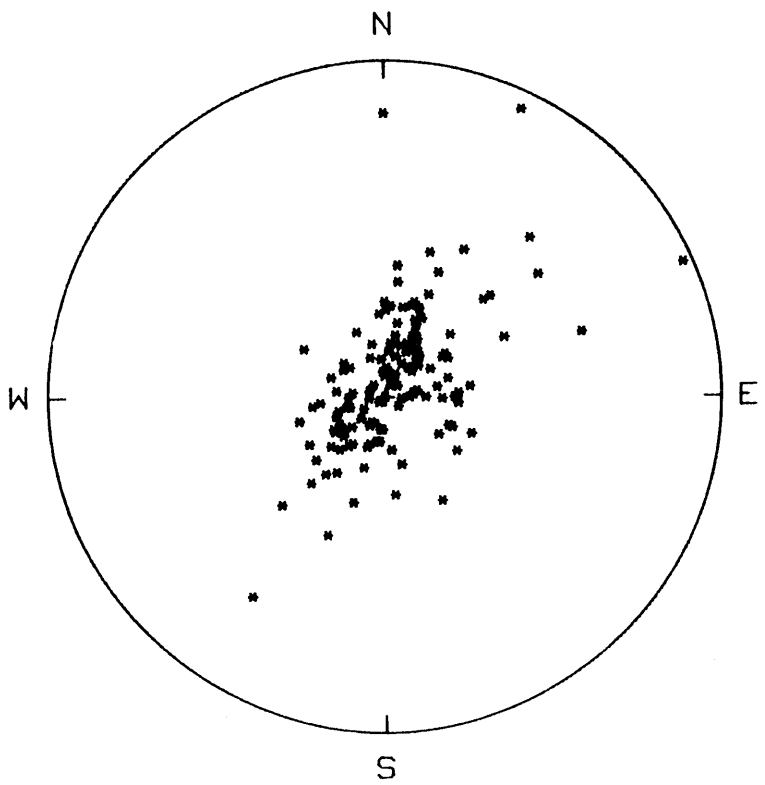

DOMAIN #5: SCd1 POLES
PROJECTION = EQUAL AREA
NUMBER OF POINTS = 146

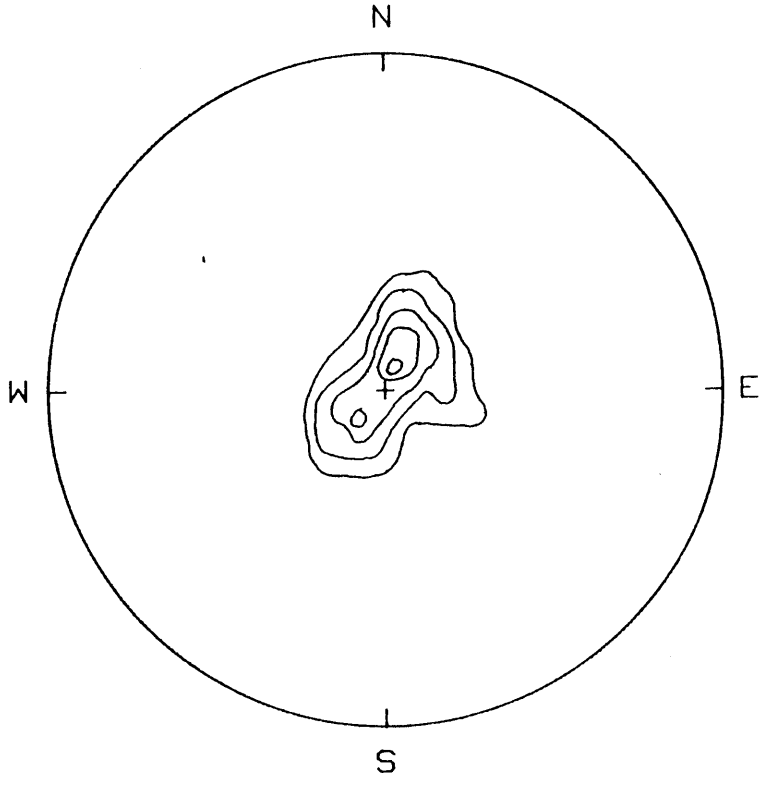

DOMAIN #5: SCd1 CONTOURS
PROJECTION = EQUAL AREA
SCANNING CIRCLE = 1.000%
CONTOURS: 5% 10% 15% 20%

Figure A-8

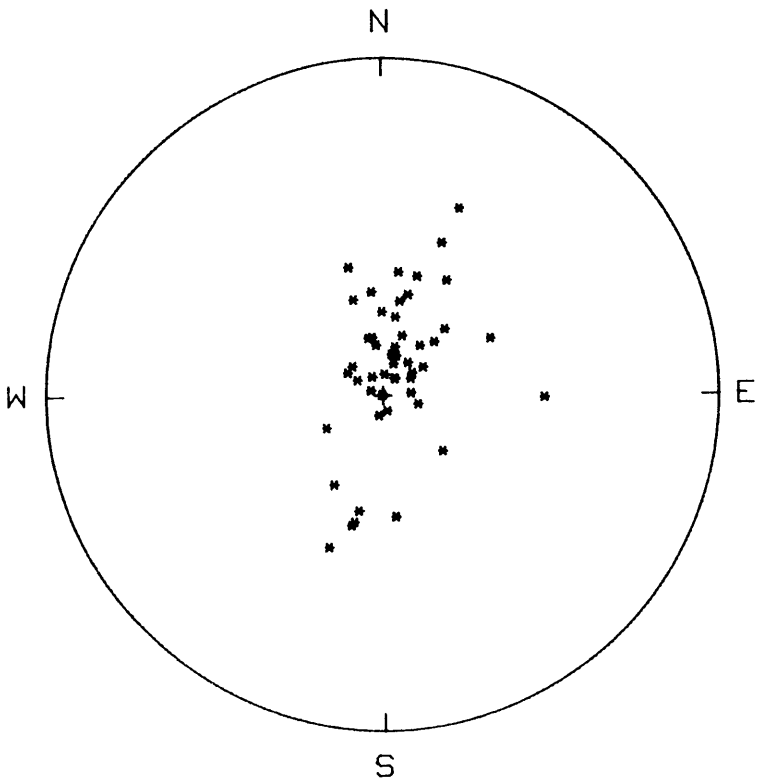

DOMAIN #6: SCd1 POLES
PROJECTION = EQUAL AREA
NUMBER OF POINTS = 56

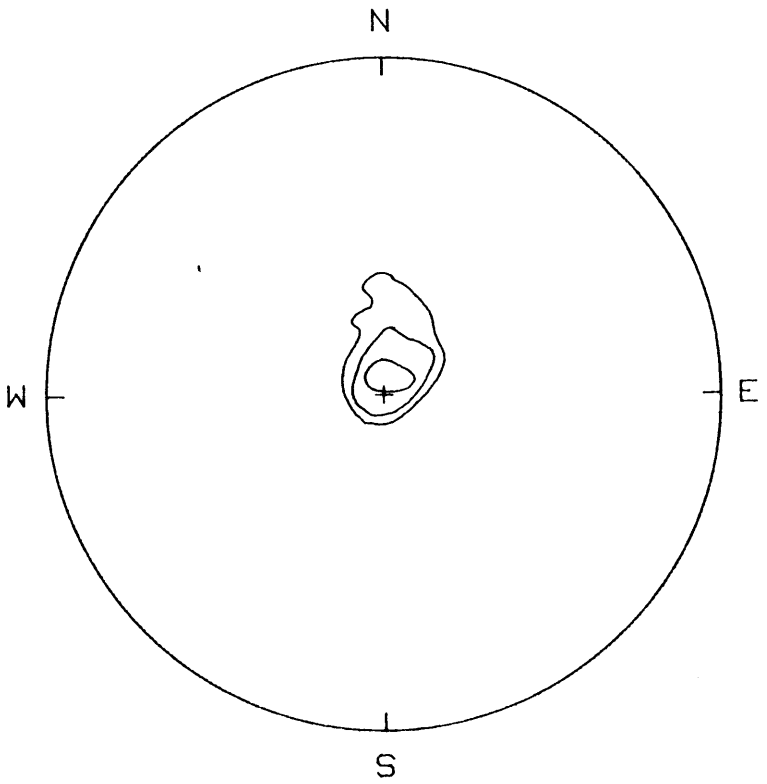

DOMAIN #6: SCd1 CONTOURS
PROJECTION = EQUAL AREA
SCANNING CIRCLE = 1.000%
CONTOURS: 10% 20% 30%

Figure A-9

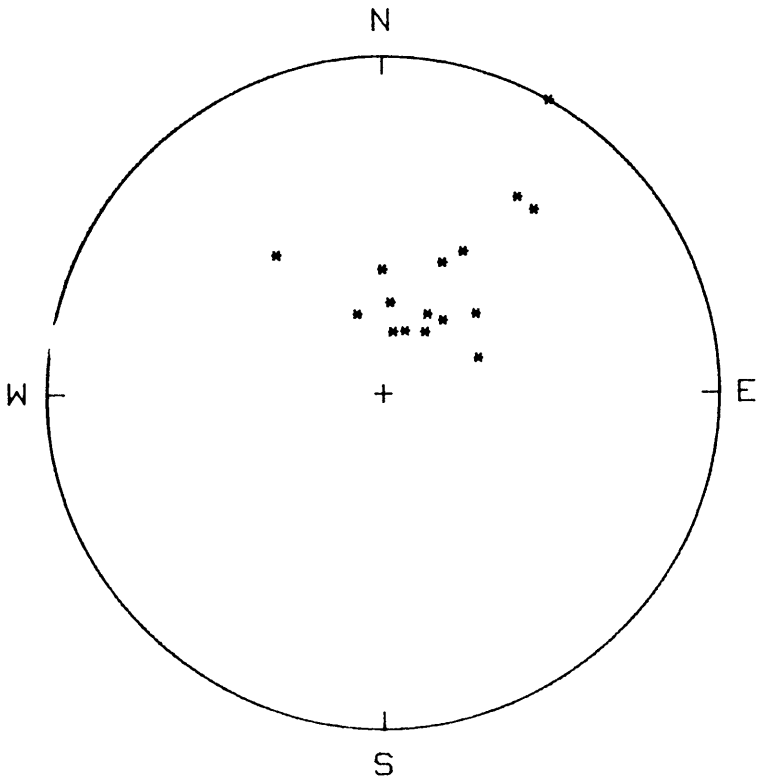

DOMAIN #7: SCd1 POLES
PROJECTION = EQUAL AREA
NUMBER OF POINTS = 16

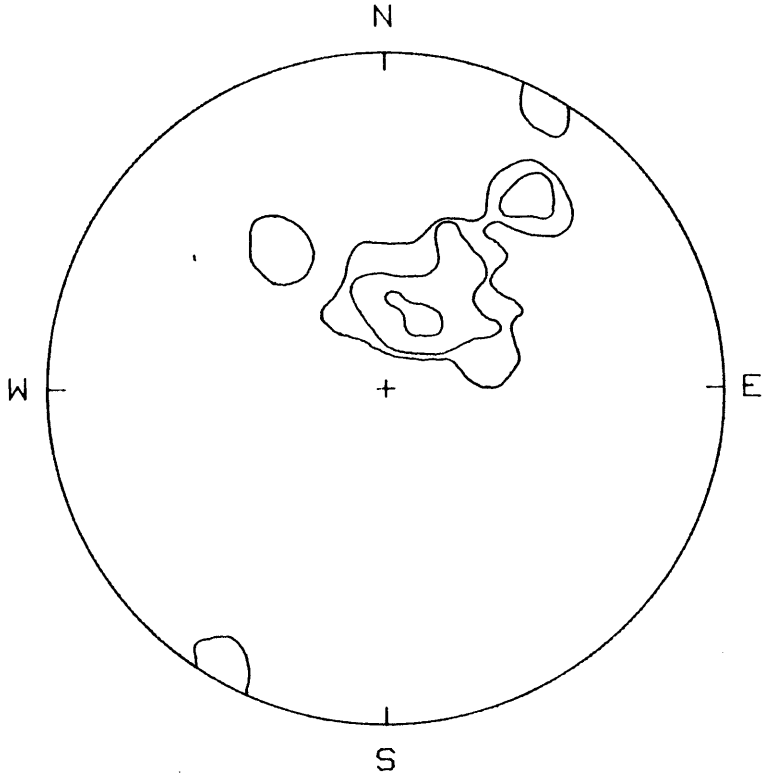

DOMAIN #7: SCd1 CONTOURS
PROJECTION = EQUAL AREA
SCANNING CIRCLE = 1.000%
CONTOURS: 5% 10% 20%

Figure A-10

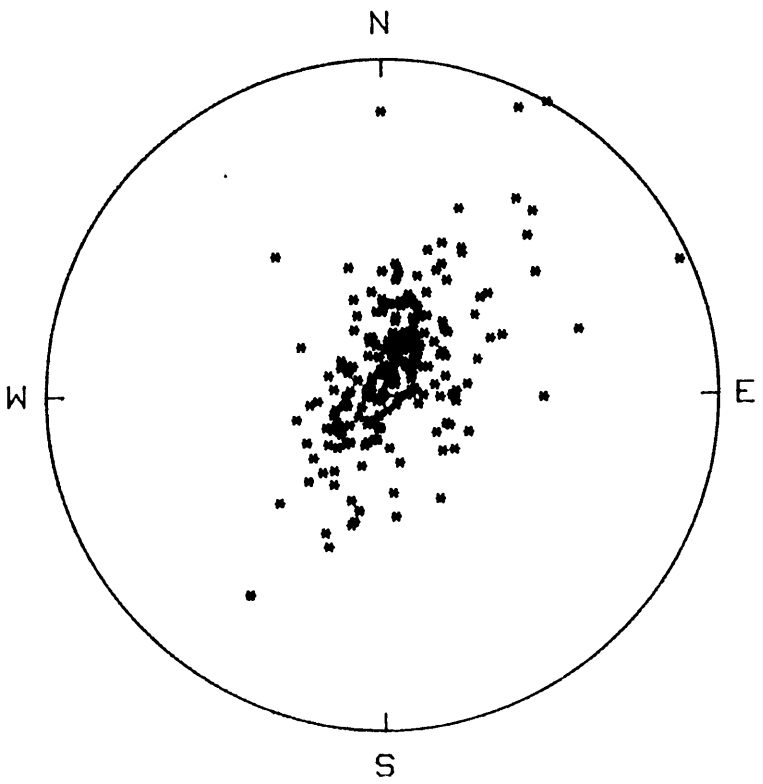

SCd1 POLES
PROJECTION = EQUAL AREA
NUMBER OF POINTS = 218

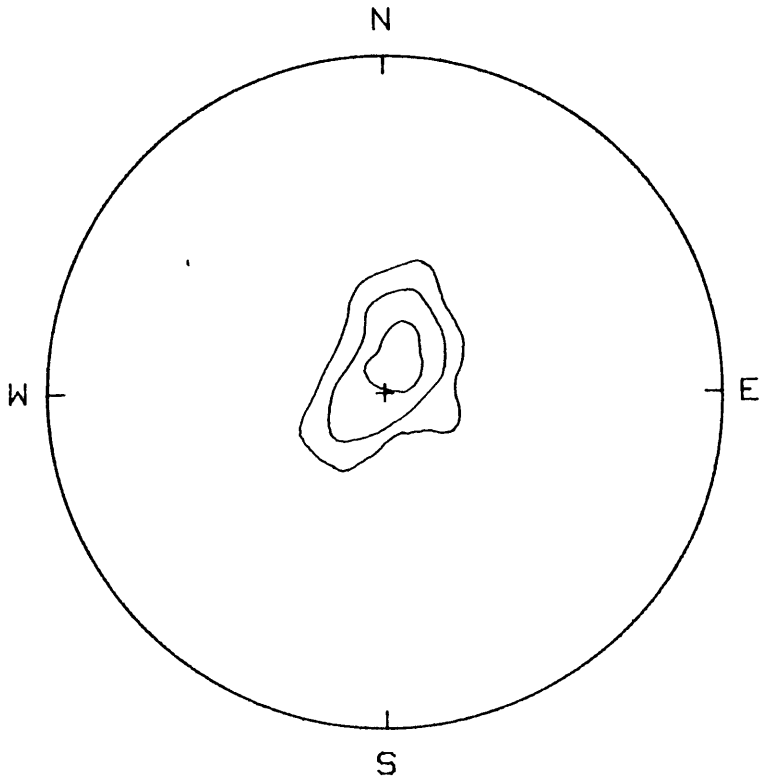

SCd1 CONTOURS
PROJECTION = EQUAL AREA
SCANNING CIRCLE = 1.000%
CONTOURS: 5% 10% 20%

Figure A-11

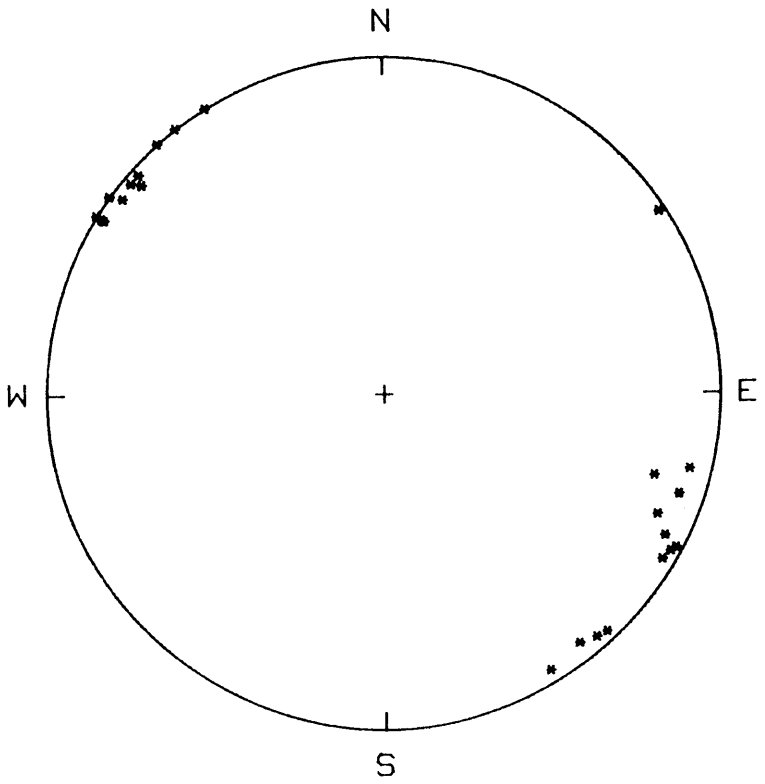

DOMAIN #5: SCd1 FOLDS
PROJECTION = EQUAL AREA
NUMBER OF POINTS = 26

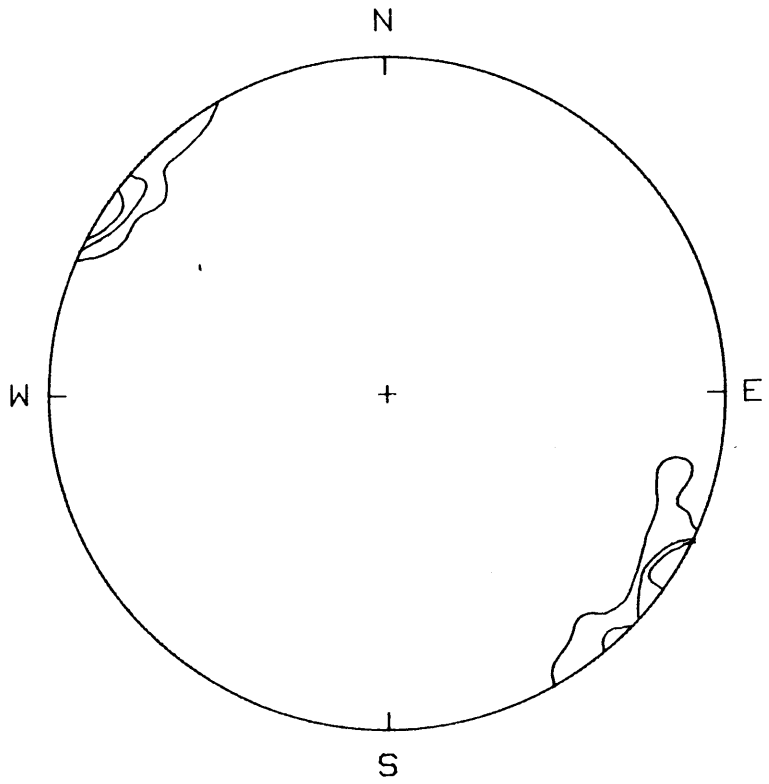

DOMAIN #5: SCd1 CONTOURS
PROJECTION = EQUAL AREA
SCANNING CIRCLE = 1.000%
CONTOURS: 10% 20% 30%

Figure A-12

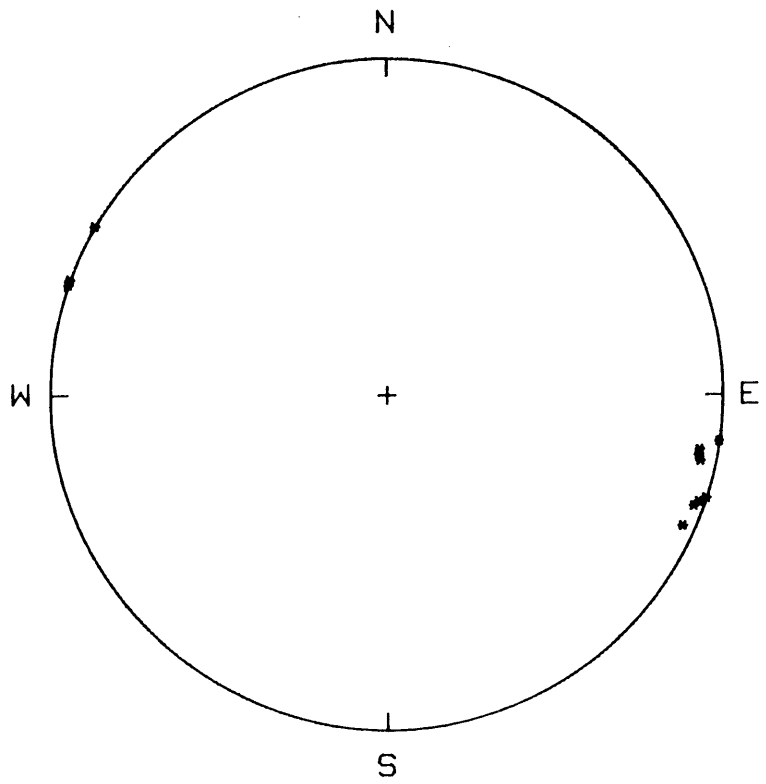

DOMAIN #6: SCd1 FOLDS
PROJECTION = EQUAL AREA
NUMBER OF POINTS = 12

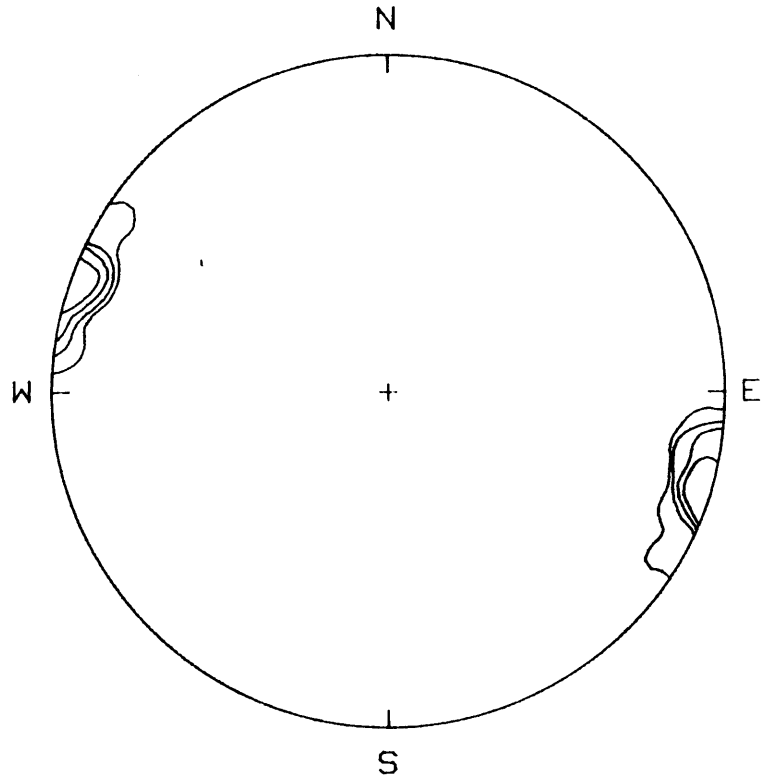

DOMAIN #6: SCd1 CONTOURS
PROJECTION = EQUAL AREA
SCANNING CIRCLE = 1.000%
CONTOURS: 10% 20% 30% 50%

Figure A-13

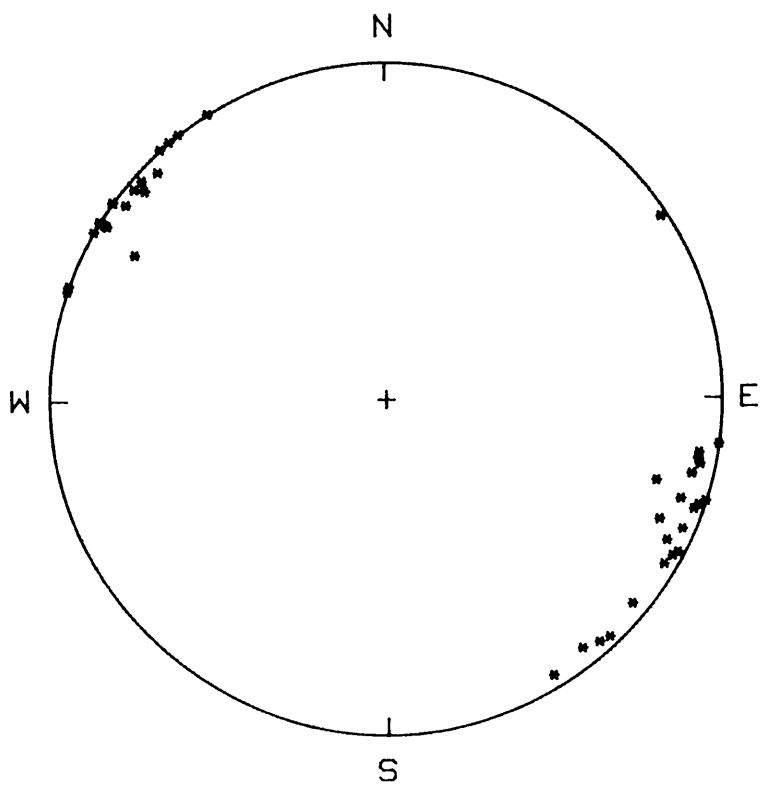

SCd1 FOLDS
PROJECTION = EQUAL AREA
NUMBER OF POINTS = 44

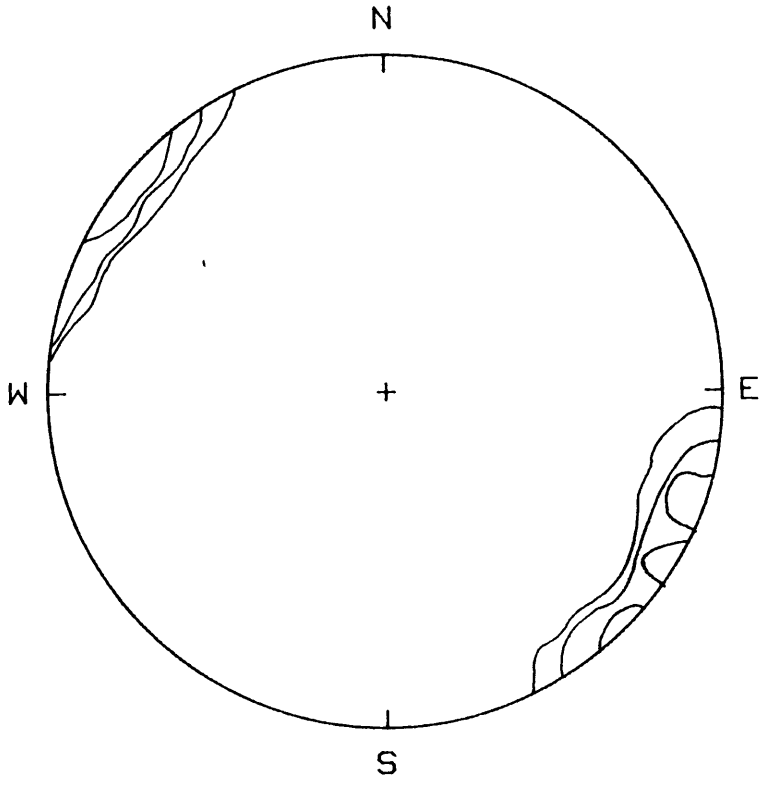

SCd1 FOLD CONTOURS
PROJECTION = EQUAL AREA
SCANNING CIRCLE = 1.000%
CONTOURS: 5% 10% 20%

Figure A-14

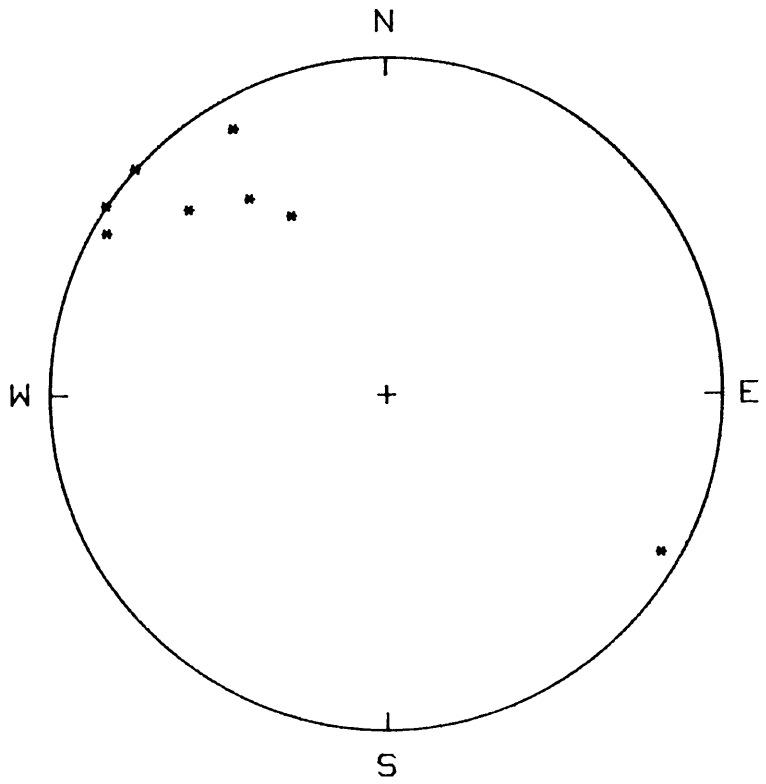

SCd1 PEBBLE LINEATIONS
PROJECTION = EQUAL AREA
NUMBER OF POINTS = 8

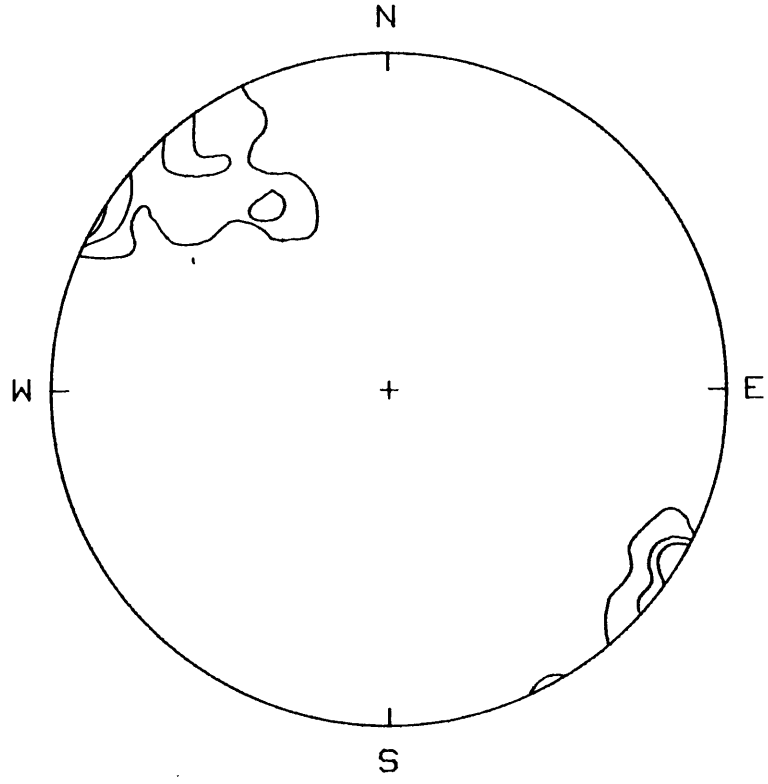

SCd1 PEBBLE LINEATION CONTOURS
PROJECTION = EQUAL AREA
SCANNING CIRCLE = 1.000%
CONTOURS: 10% 20% 30%

Figure A-15

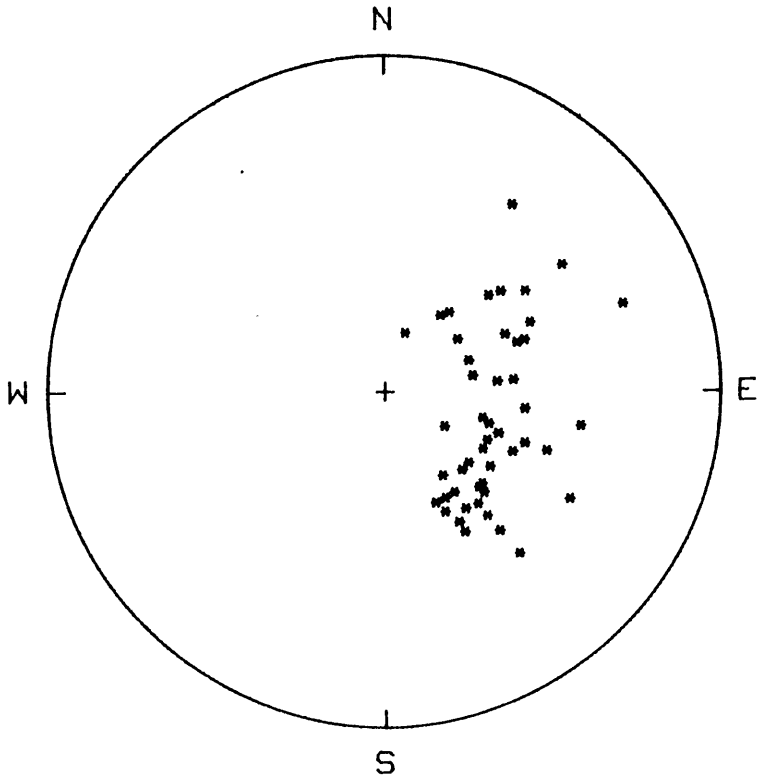

DOMAIN 18: AAd2 POLES
PROJECTION = EQUAL AREA
NUMBER OF POINTS = 50

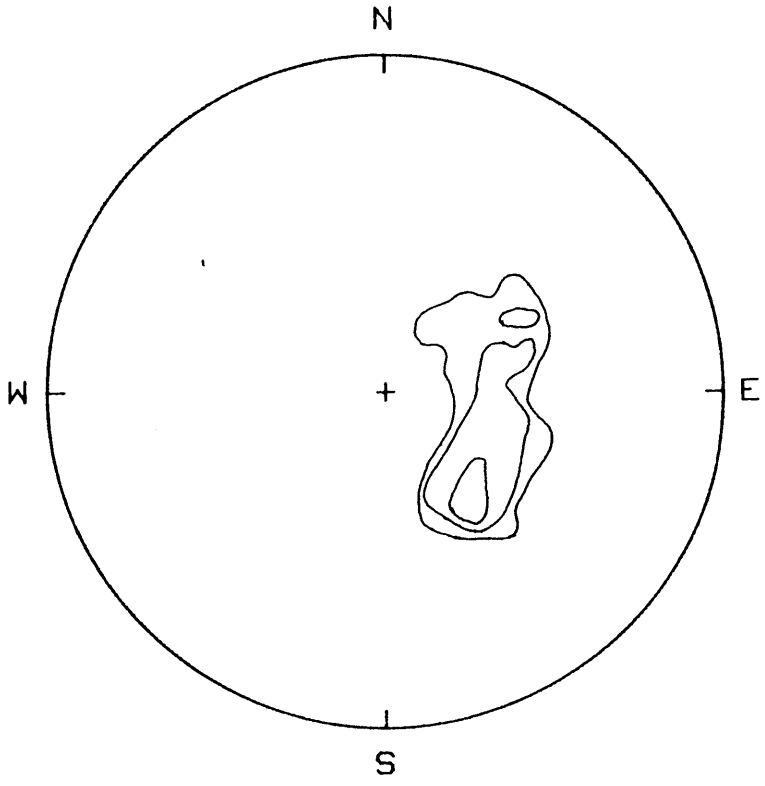

DOMAIN 18: AAd2 CONTOURS
PROJECTION = EQUAL AREA
SCANNING CIRCLE = 1.000%
CONTOURS: 5% 10% 20%

Figure A-16

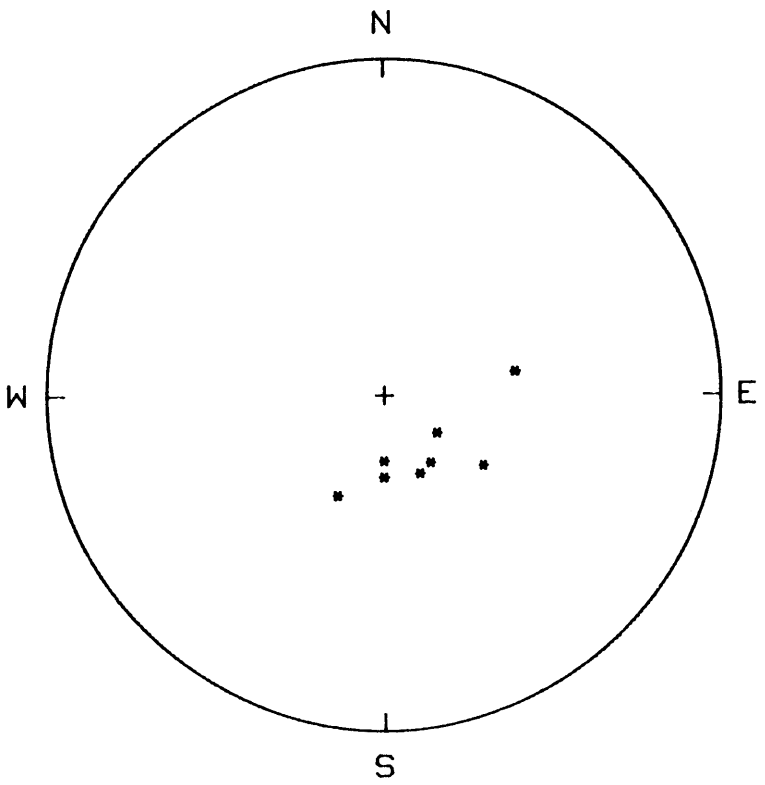

DOMAIN 19: AAd2 POLES
PROJECTION = EQUAL AREA
NUMBER OF POINTS = 8

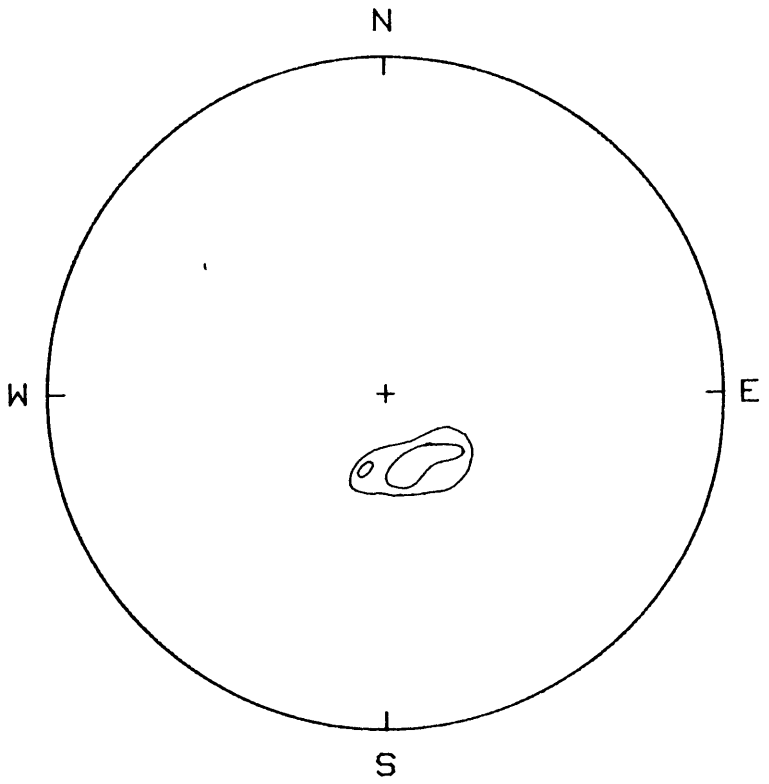

DOMAIN 19: AAd2 CONTOURS
PROJECTION = EQUAL AREA
SCANNING CIRCLE = 1.000%
CONTOURS: 20% 30%

Figure A-17

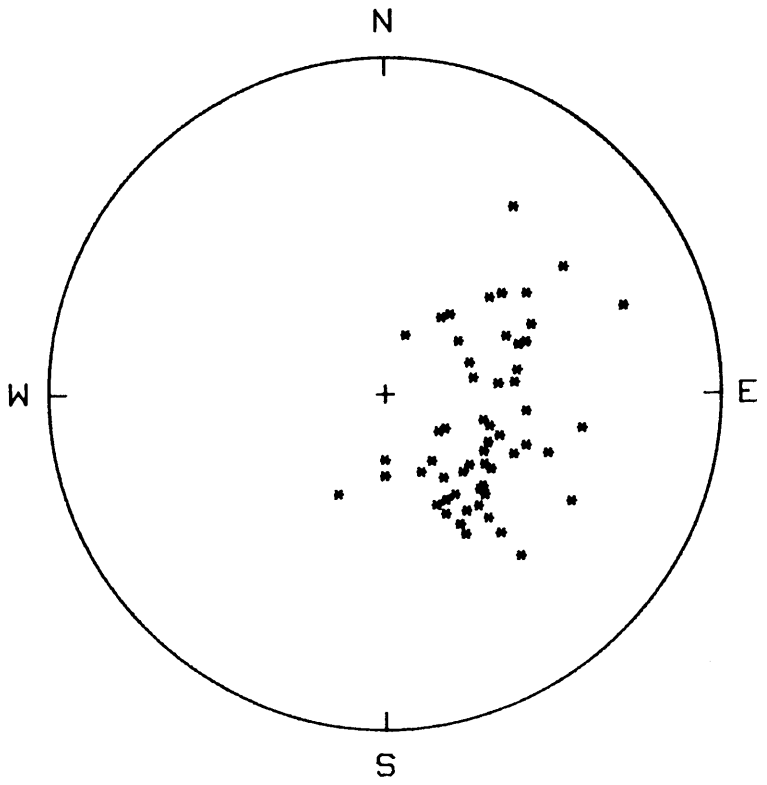

AAd2 POLES
PROJECTION = EQUAL AREA
NUMBER OF POINTS = 58

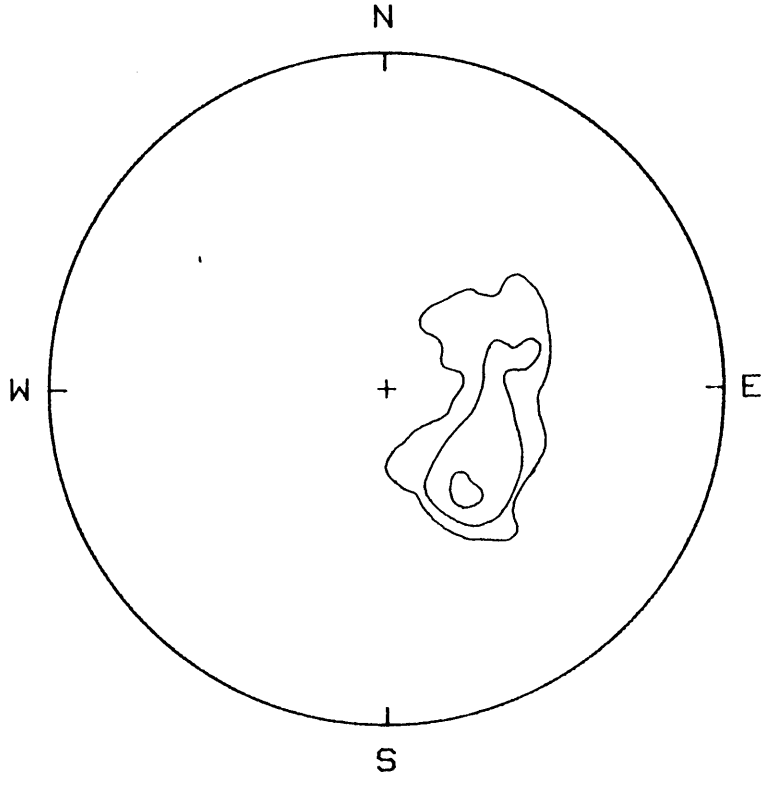

AAd2 CONTOURS
PROJECTION = EQUAL AREA
SCANNING CIRCLE = 1.000%
CONTOURS: 5% 10% 20%

Figure A-18

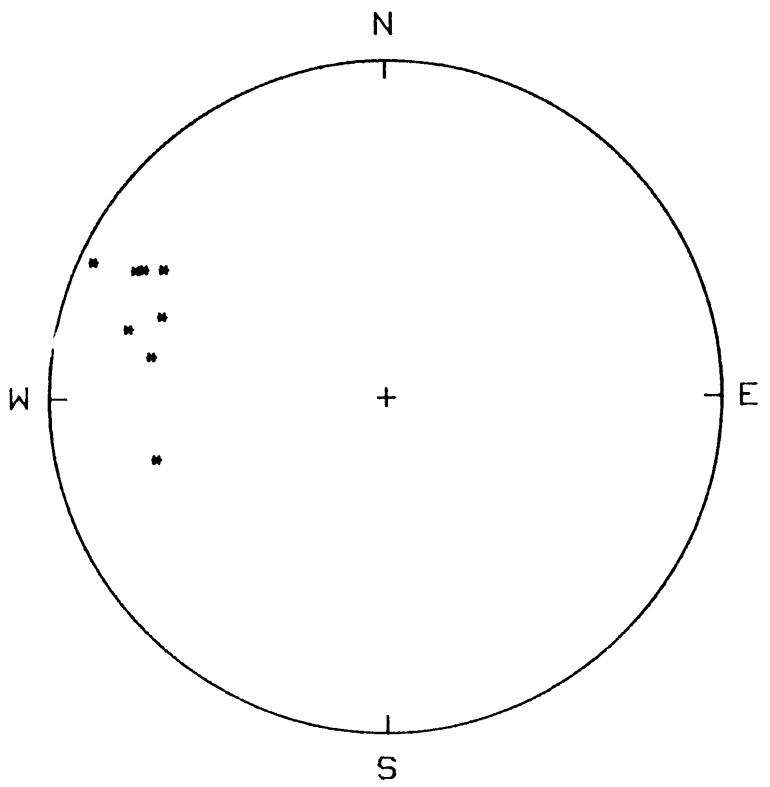

DOMAIN #18: AAd4 FOLDS
PROJECTION = EQUAL AREA
NUMBER OF POINTS = 8

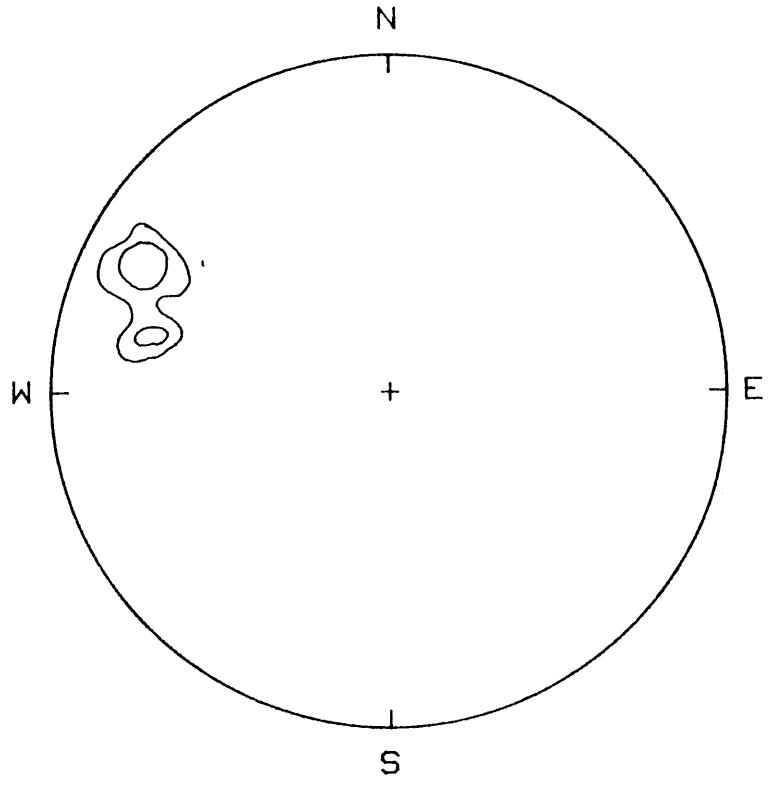

DOMAIN #18: AAd4 CONTOURS
PROJECTION = EQUAL AREA
SCANNING CIRCLE = 1.000%
CONTOURS: 20% 30%

Figure A-19

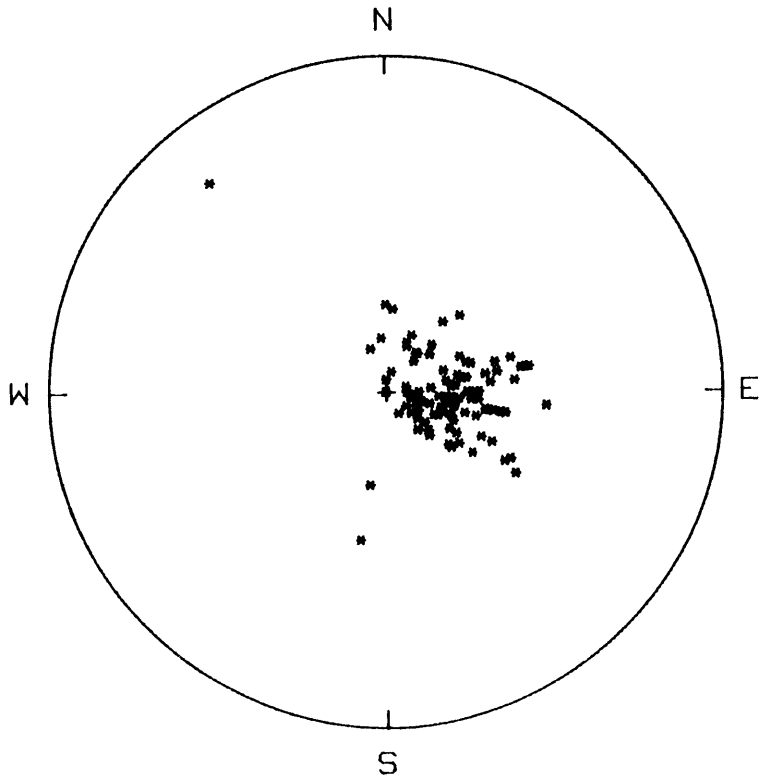

DOMAIN #13: SGd1 POLES
PROJECTION = EQUAL AREA
NUMBER OF POINTS = 100

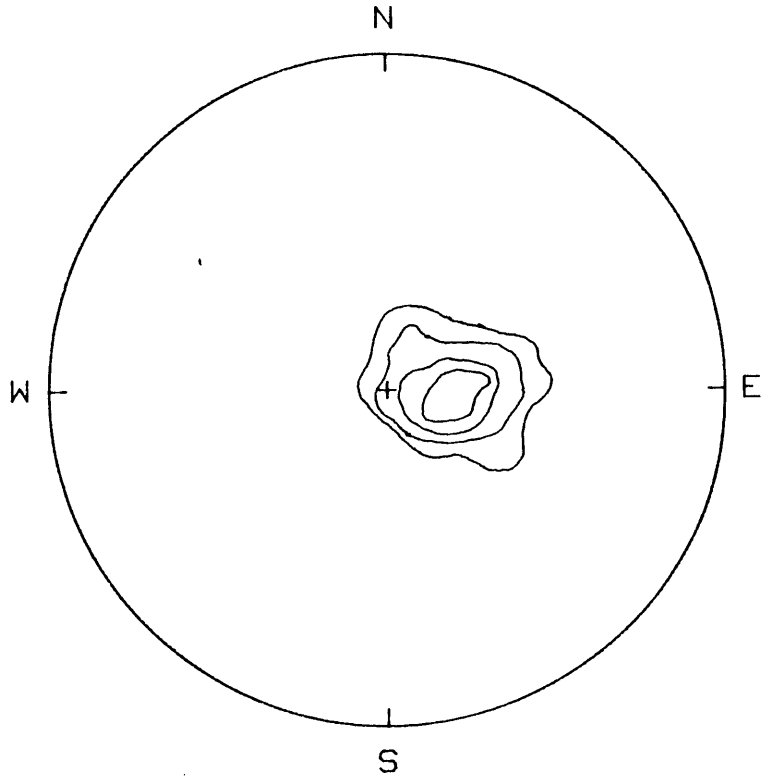

DOMAIN #13: SGd1 CONTOURS
PROJECTION = EQUAL AREA
SCANNING CIRCLE = 1.000%
CONTOURS: 5% 10% 20% 30%

Figure A-20

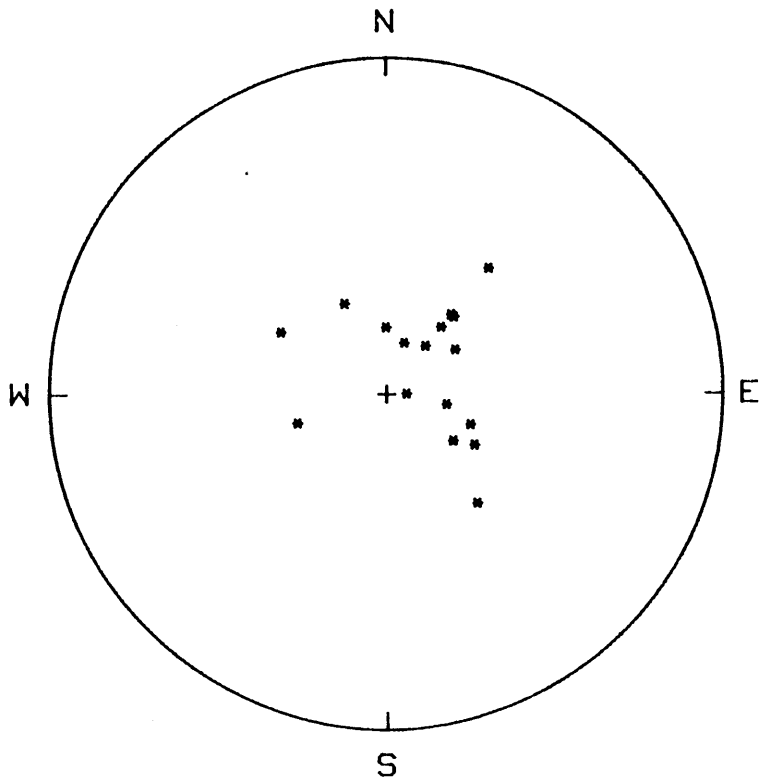

DOMAIN #14: SGd1 POLES
PROJECTION = EQUAL AREA
NUMBER OF POINTS = 17

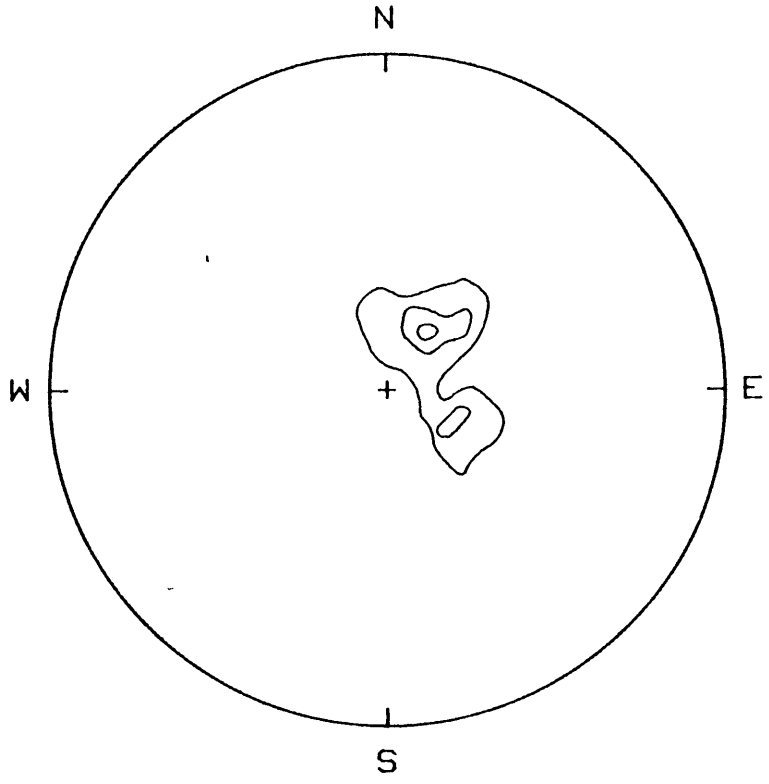

DOMAIN #14: SGd1 CONTOURS
PROJECTION = EQUAL AREA
SCANNING CIRCLE = 1.000%
CONTOURS: 10% 20% 30%

Figure A-21

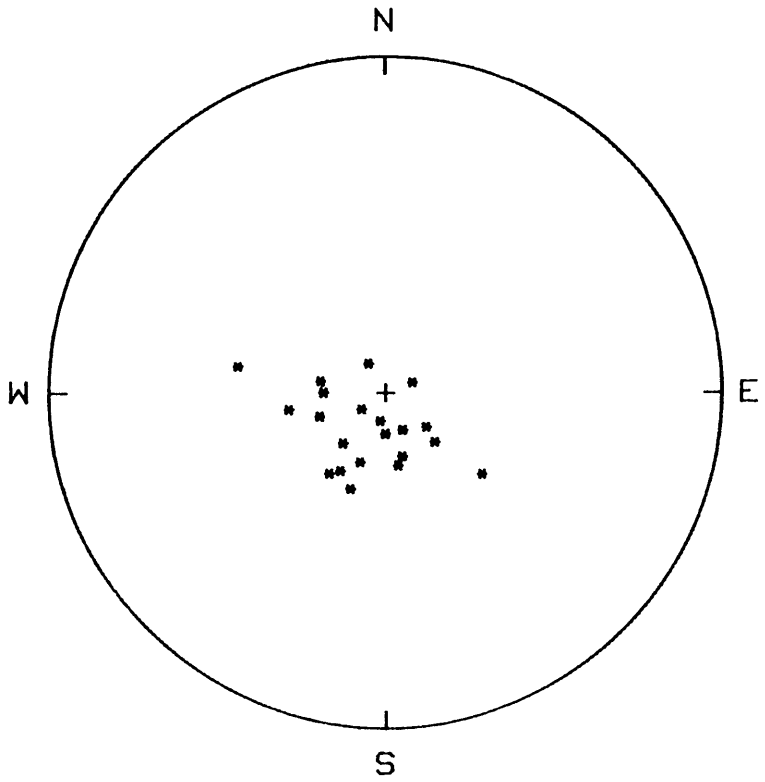

DOMAIN #15: SGd1 POLES
PROJECTION = EQUAL AREA
NUMBER OF POINTS = 21

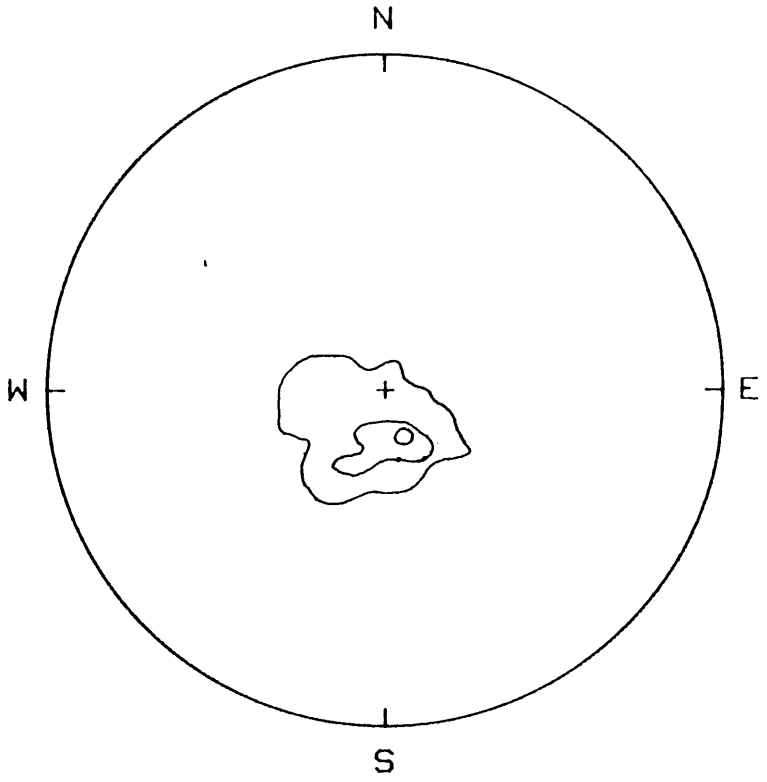

DOMAIN #15: SGd1 CONTOURS
PROJECTION = EQUAL AREA
SCANNING CIRCLE = 1.000%
CONTOURS: 10% 20% 30%

Figure A-22

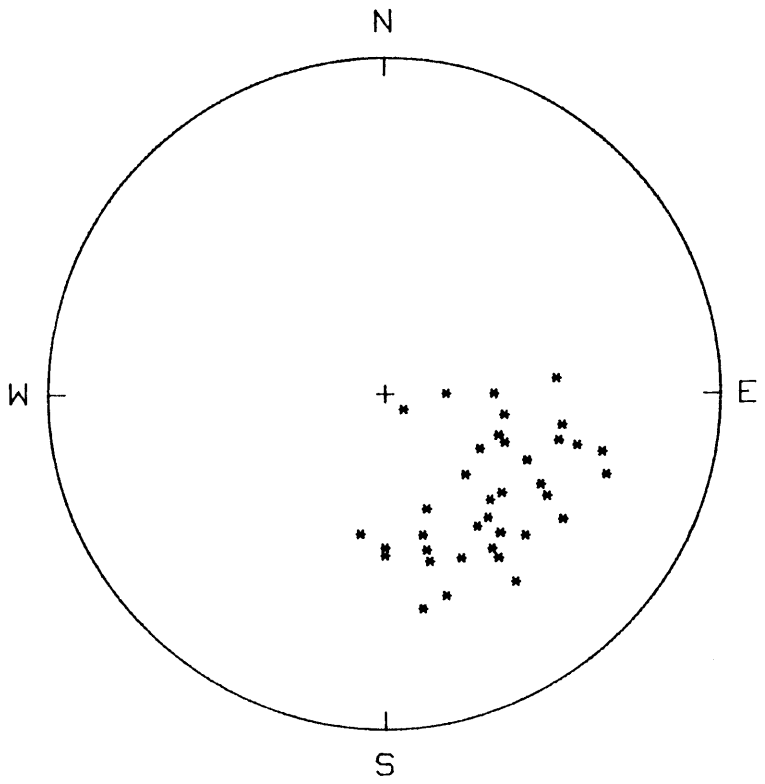

DOMAIN #16: SGd1 POLES
PROJECTION = EQUAL AREA
NUMBER OF POINTS = 39

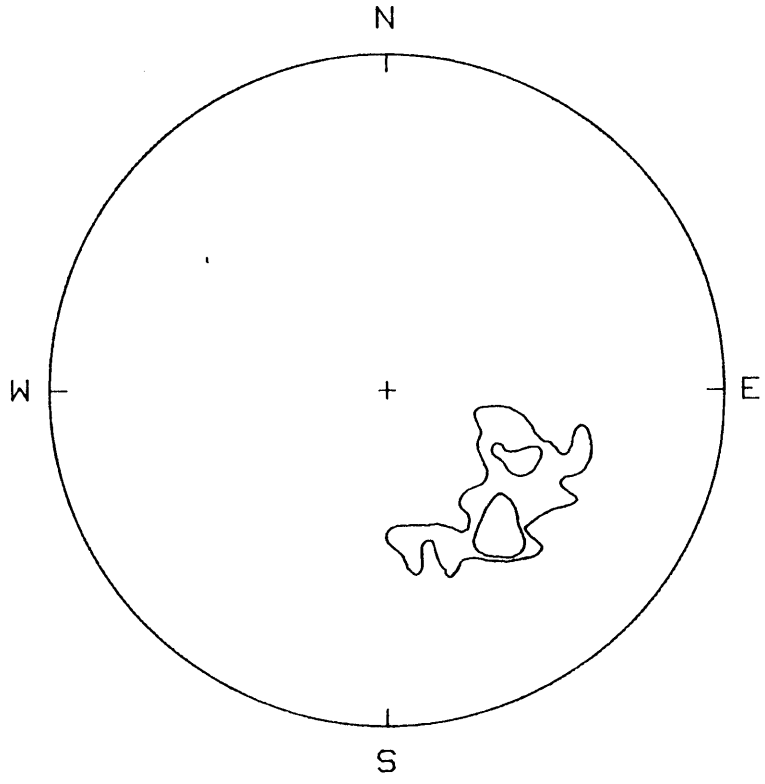

DOMAIN #16: SGd1 CONTOURS
PROJECTION = EQUAL AREA
SCANNING CIRCLE = 1.000%
CONTOURS: 10% 15%

Figure A-23

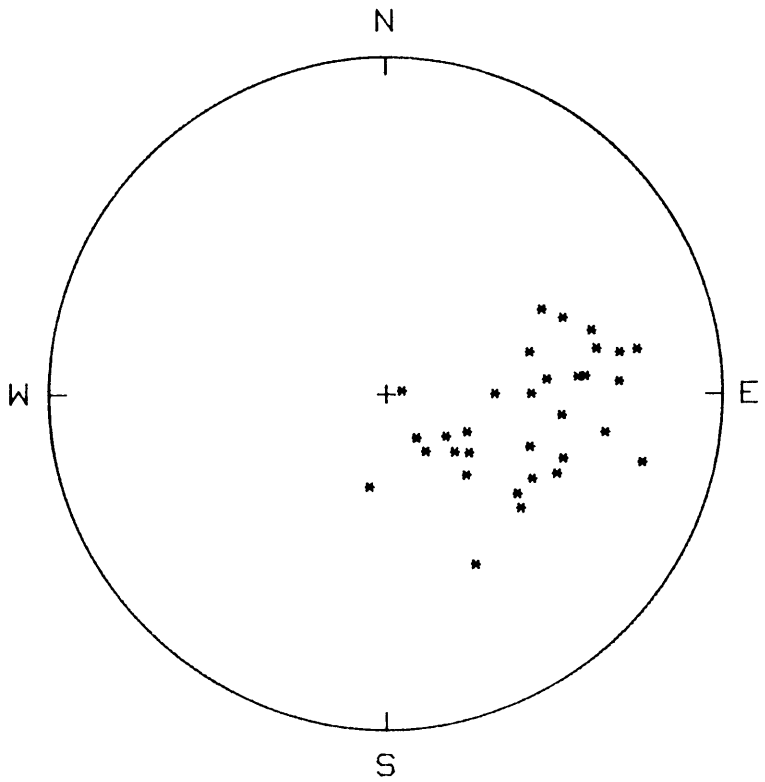

DOMAIN #17: SGd1 POLES
PROJECTION = EQUAL AREA
NUMBER OF POINTS = 32

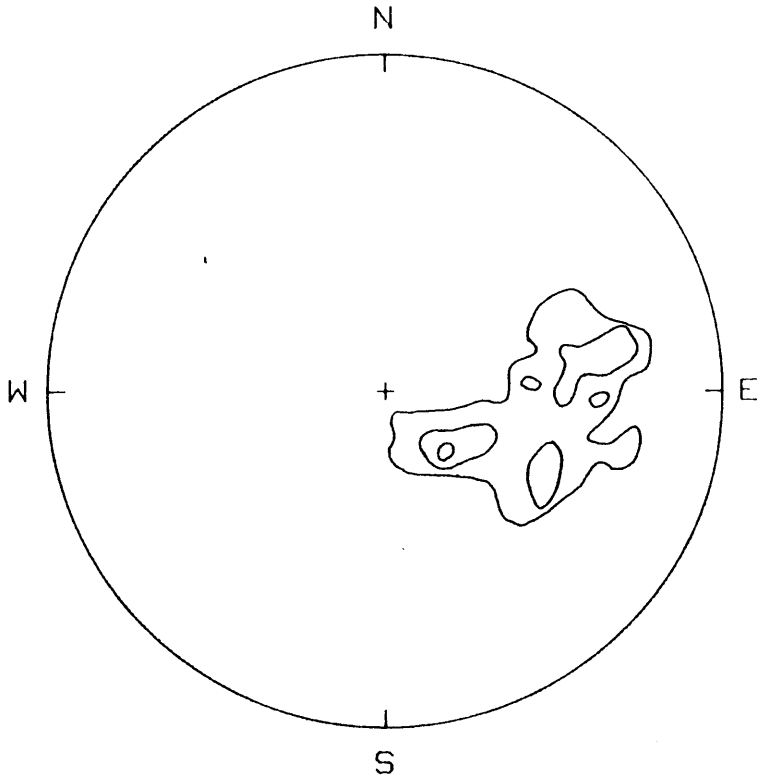

DOMAIN #17: SGd1 CONTOURS
PROJECTION = EQUAL AREA
SCANNING CIRCLE = 1.000%
CONTOURS: 5% 10% 20%

Figure A-24

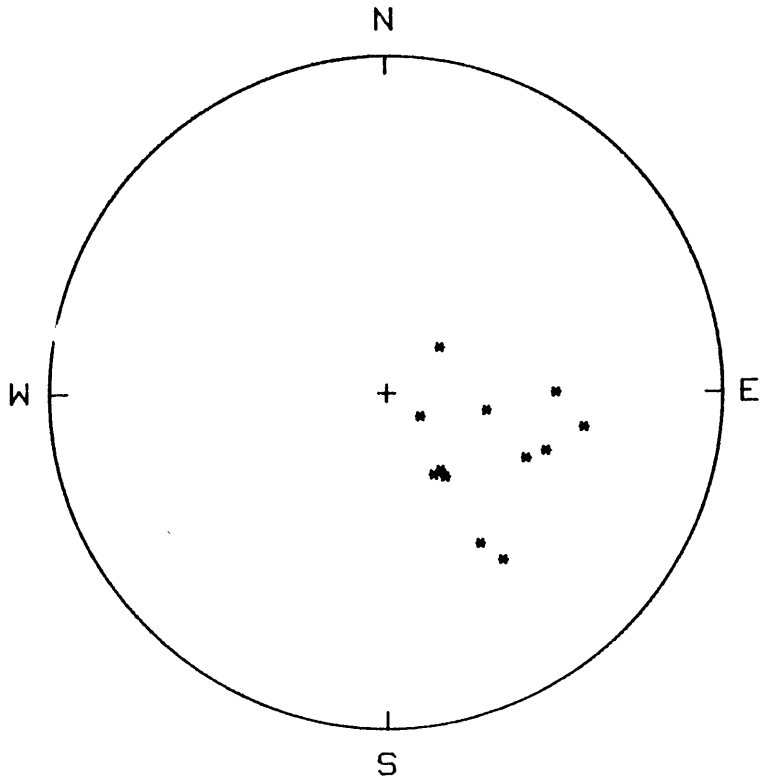

DOMAIN #15: SGd4 POLES
PROJECTION = EQUAL AREA
NUMBER OF POINTS = 12

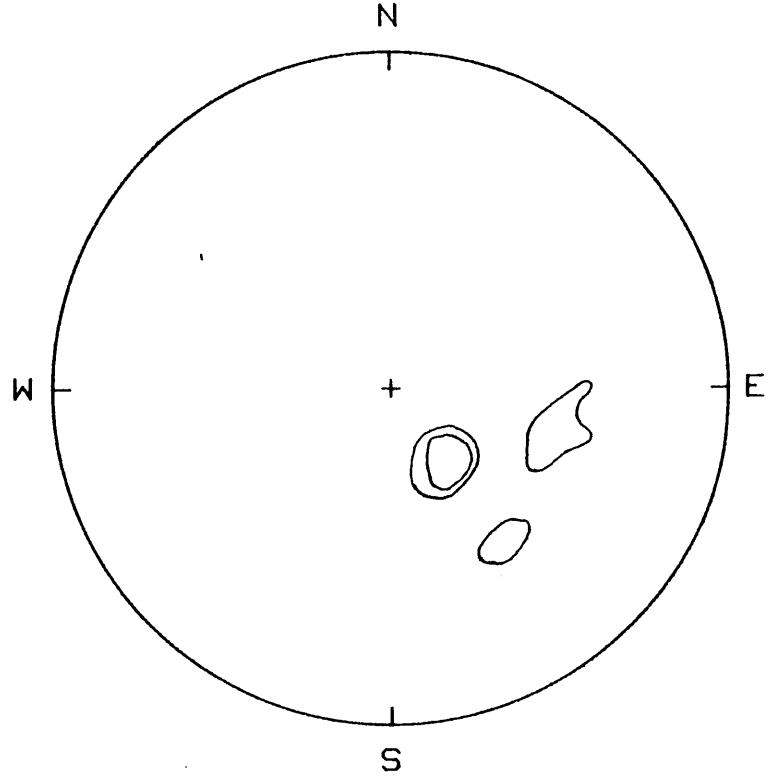

DOMAIN #15: SGd4 CONTOURS
PROJECTION = EQUAL AREA
SCANNING CIRCLE = 1.000%
CONTOURS: 10% 20%

Figure A-25

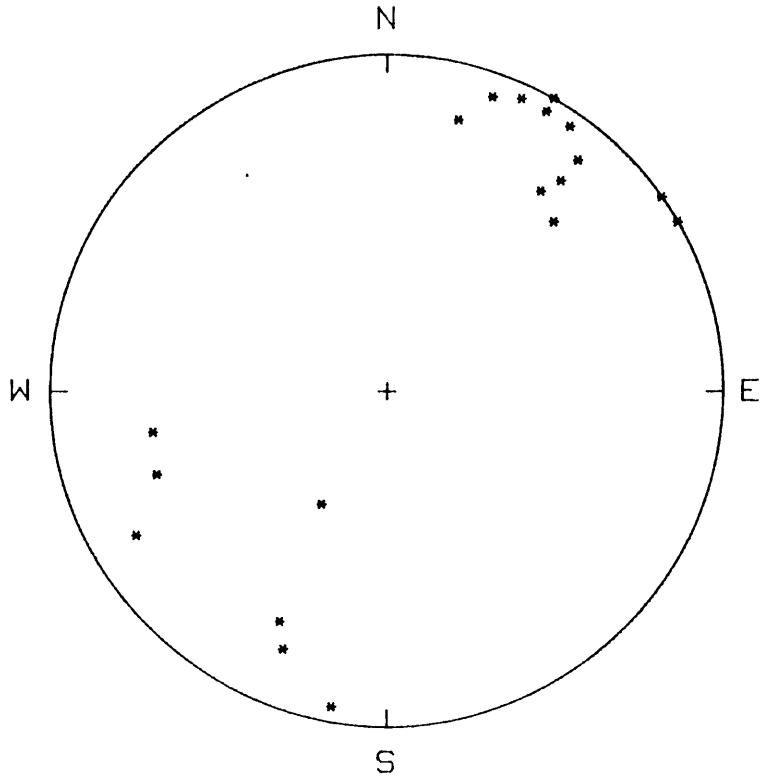

DOMAIN #15: SGd4 FOLDS
PROJECTION = EQUAL AREA
NUMBER OF POINTS = 19

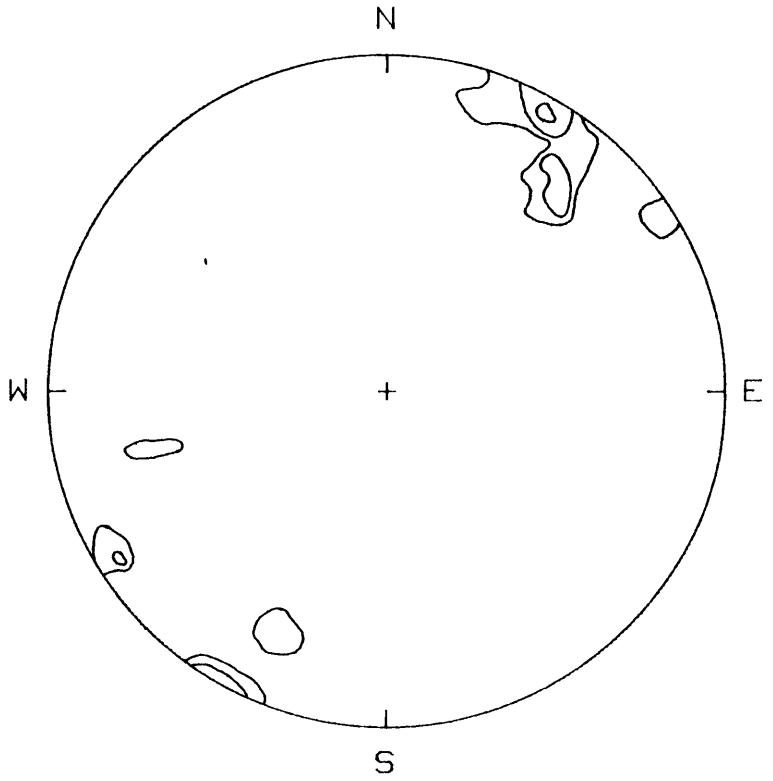

DOMAIN #15: SGd4 CONTOURS
PROJECTION = EQUAL AREA
SCANNING CIRCLE = 1.000%
CONTOURS: 10% 15% 20%

Figure A-26

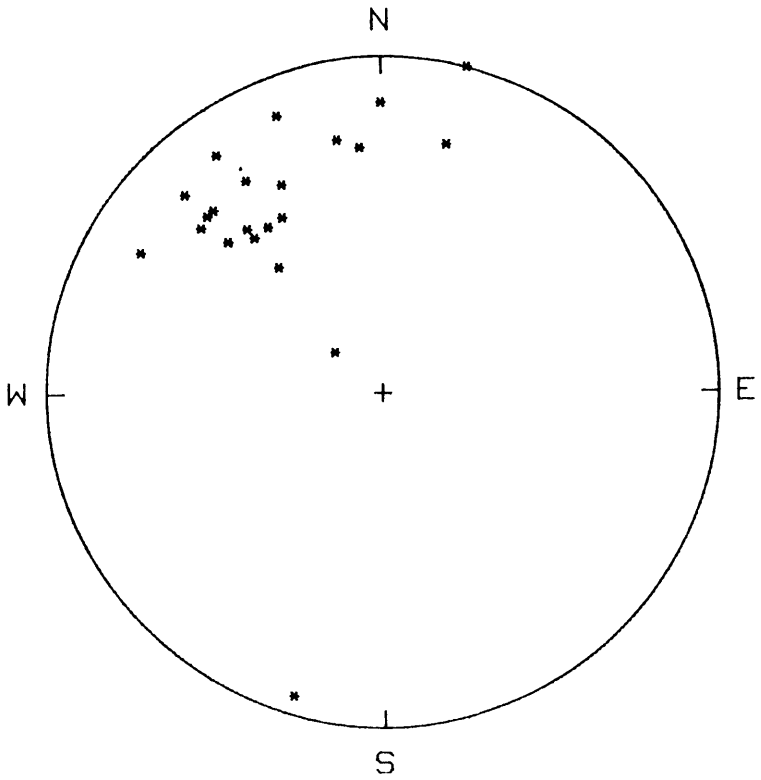

DOMAIN #16: SGd6 FOLDS
PROJECTION = EQUAL AREA
NUMBER OF POINTS = 23

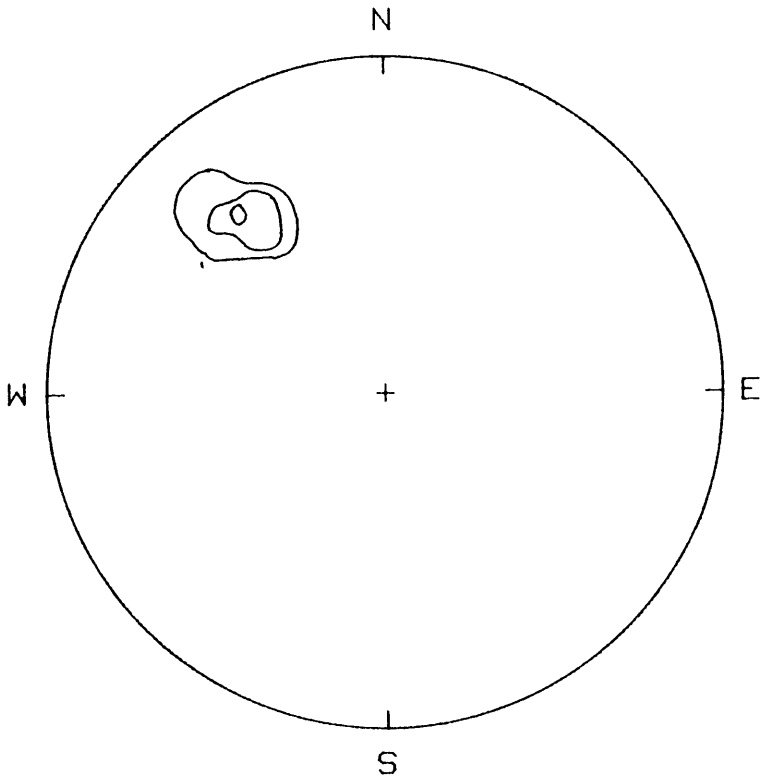

DOMAIN #16: SGd6 CONTOURS
PROJECTION = EQUAL AREA
SCANNING CIRCLE = 1.000%
CONTOURS: 10% 20% 30%

Figure A-27

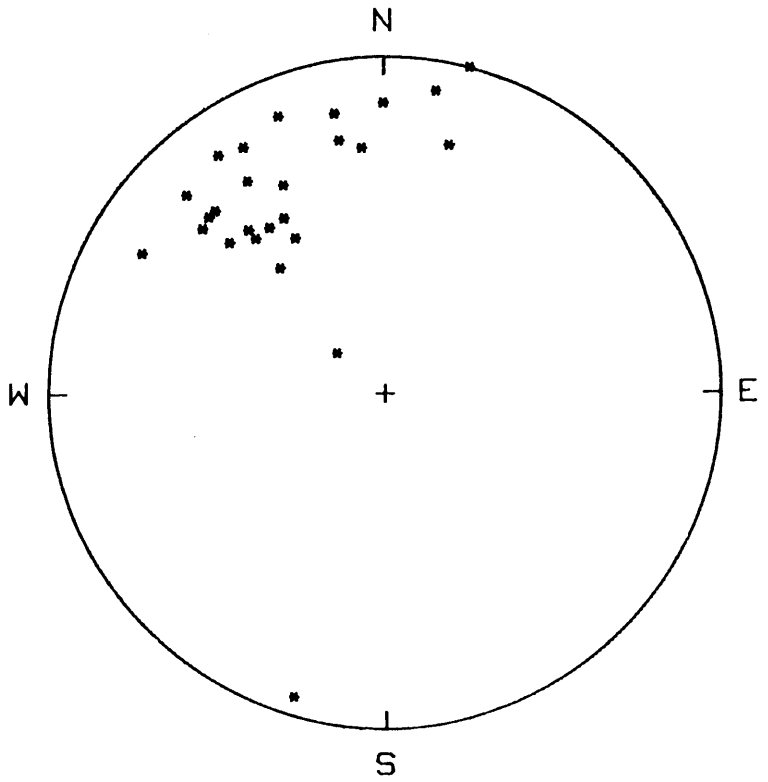

SGd6 FOLDS
PROJECTION = EQUAL AREA
NUMBER OF POINTS = 27

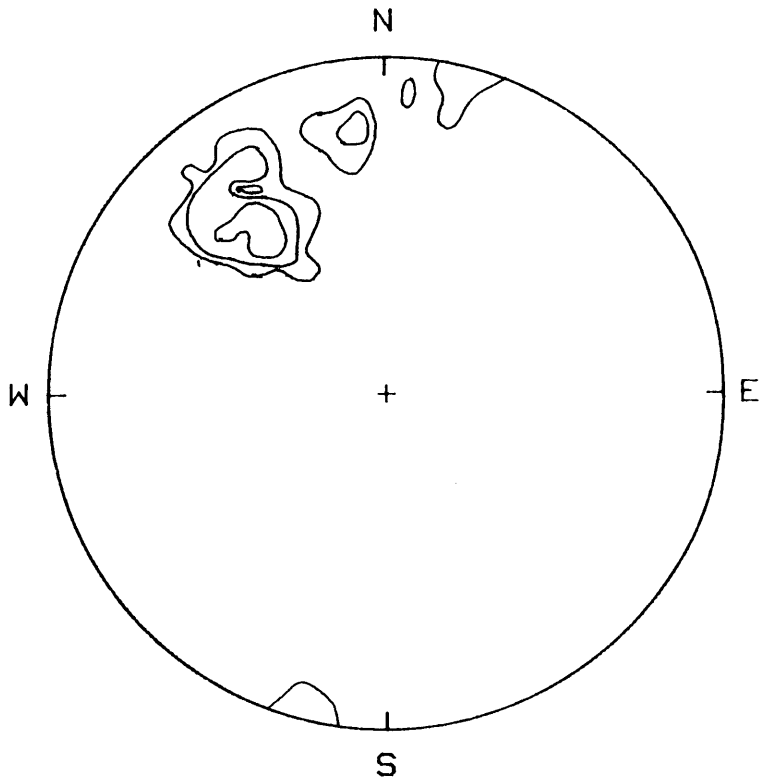

SGd6 FOLD CONTOURS
PROJECTION = EQUAL AREA
SCANNING CIRCLE = 1.000%
CONTOURS: 5% 10% 20%

Figure A-28

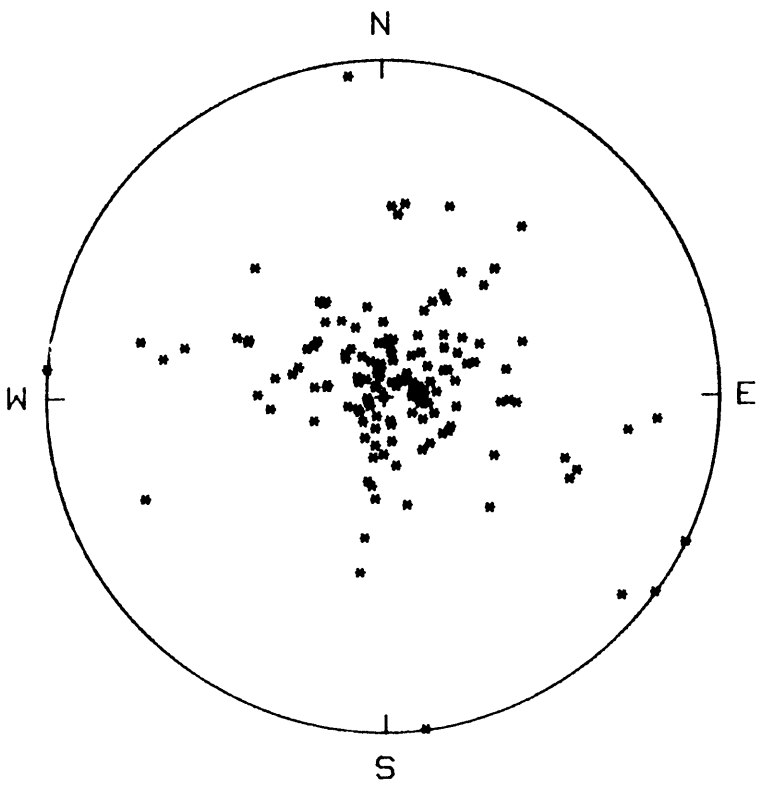

DOMAIN #11: LGd1 POLES
PROJECTION = EQUAL AREA
NUMBER OF POINTS = 148

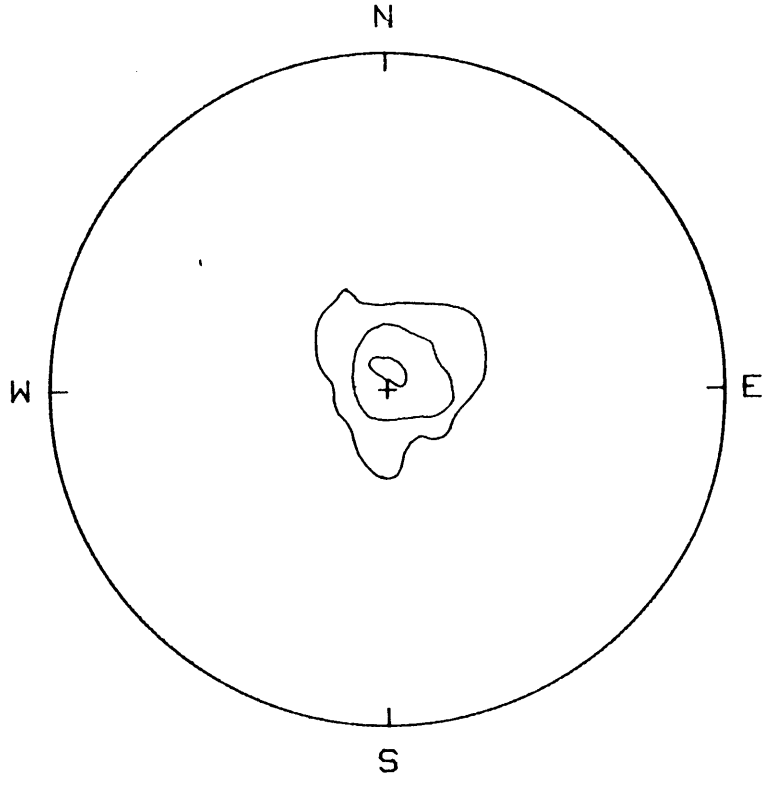

DOMAIN #11: LGd1 CONTOURS
PROJECTION = EQUAL AREA
SCANNING CIRCLE = 1.000%
CONTOURS: 5% 10% 20%

Figure A-29

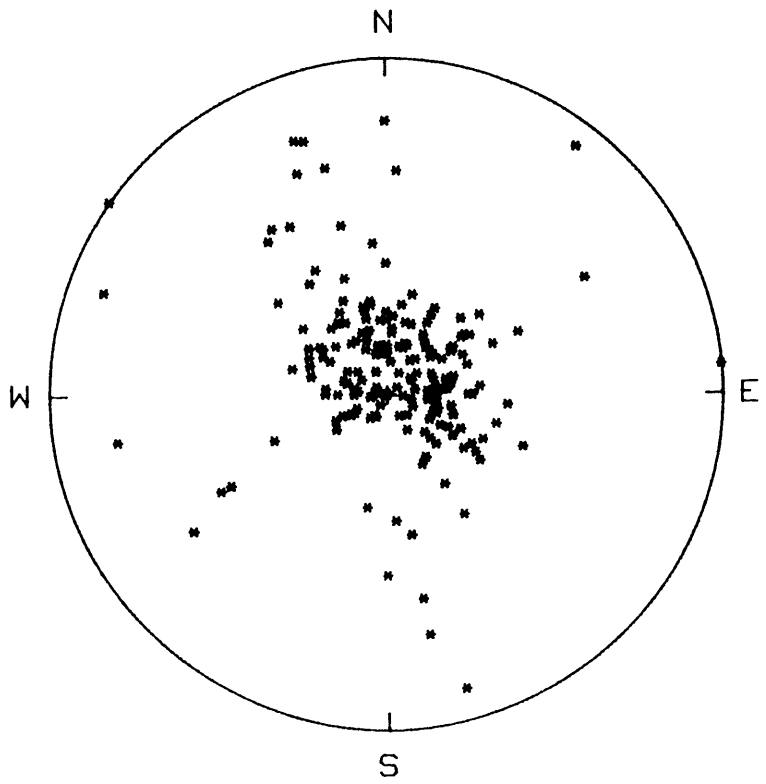

DOMAIN #12: LGd1 POLES
PROJECTION = EQUAL AREA
NUMBER OF POINTS = 212

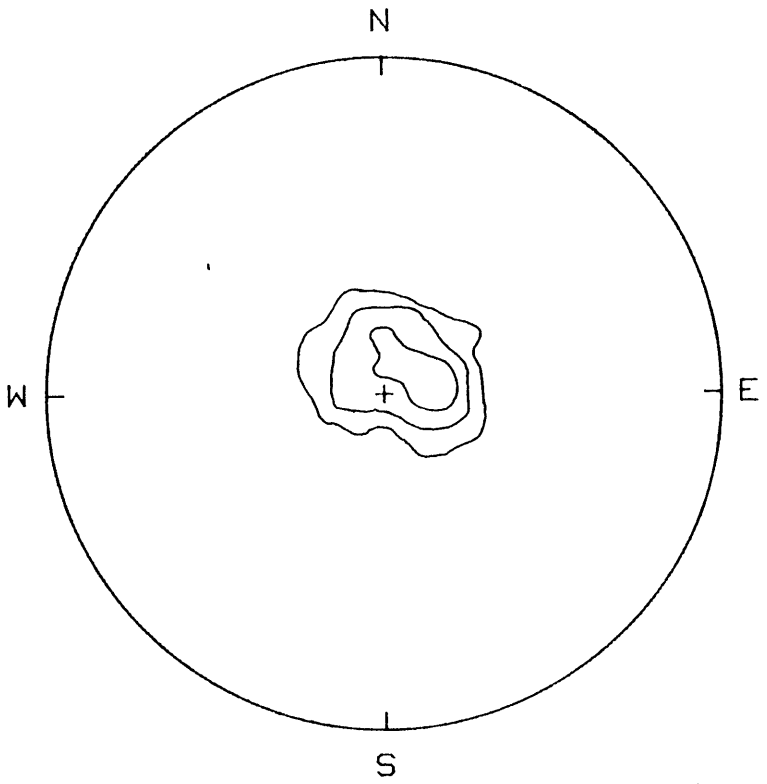

DOMAIN #12: LGd1 CONTOURS
PROJECTION = EQUAL AREA
SCANNING CIRCLE = 1.000%
CONTOURS: 5% 10% 15%

Figure A-30

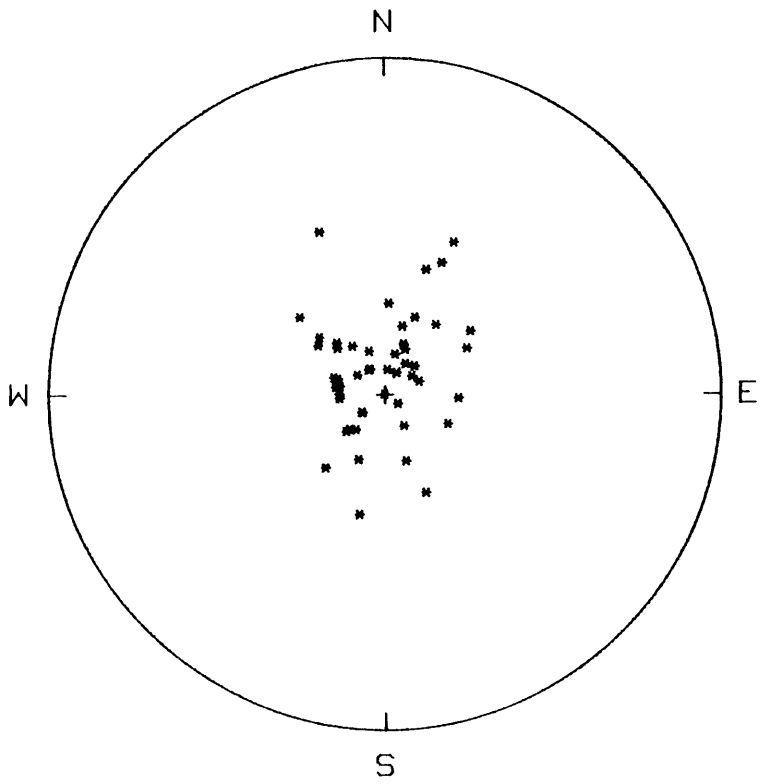

DOMAIN #11: LGd3 POLES
PROJECTION = EQUAL AREA
NUMBER OF POINTS = 50

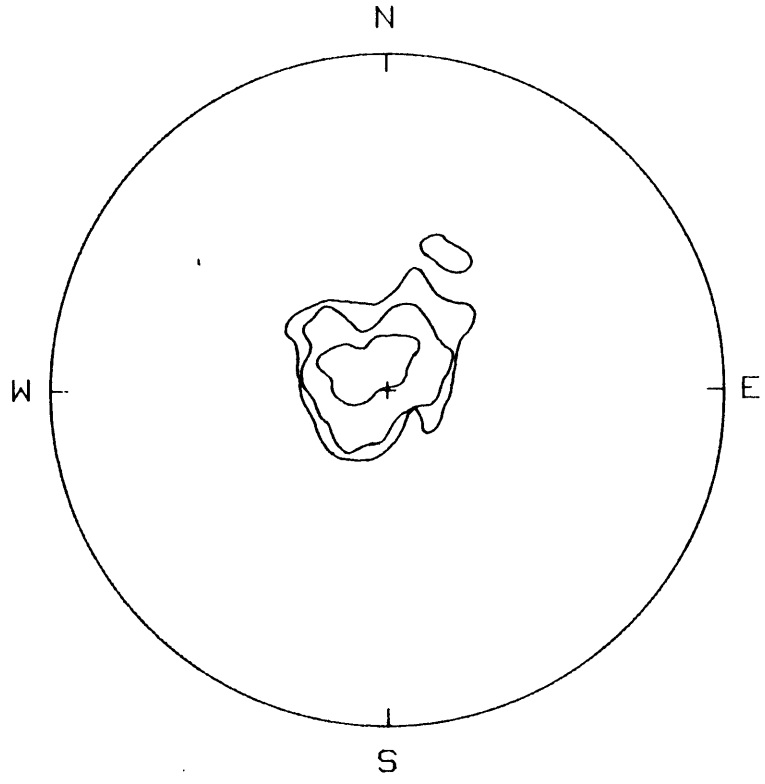

DOMAIN #11: LGd3 CONTOURS
PROJECTION = EQUAL AREA
SCANNING CIRCLE = 1.000%
CONTOURS: 5% 10% 20%

Figure A-31

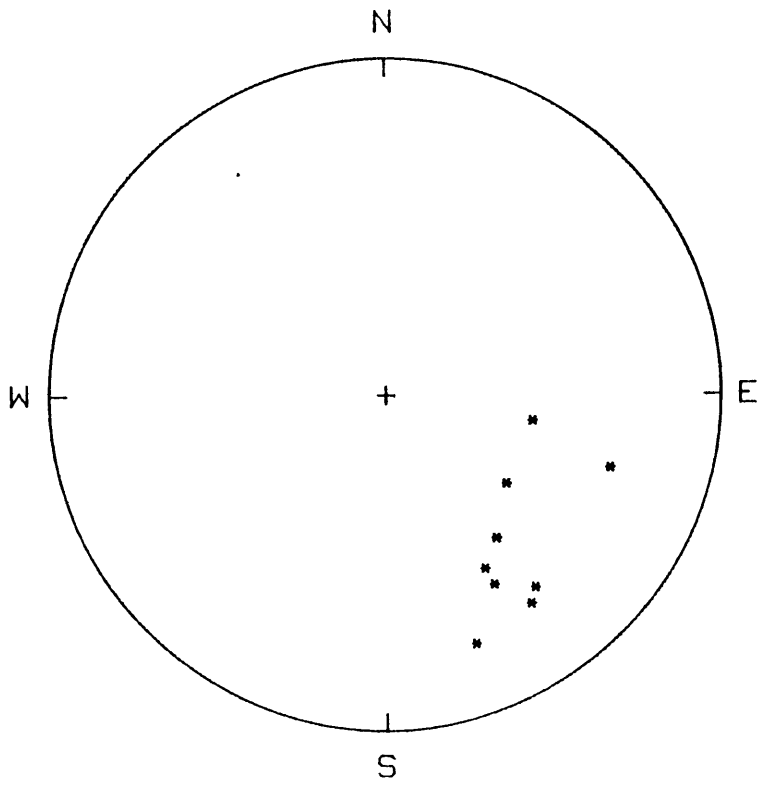

DOMAIN #12: LGd3 POLES
PROJECTION = EQUAL AREA
NUMBER OF POINTS = 10

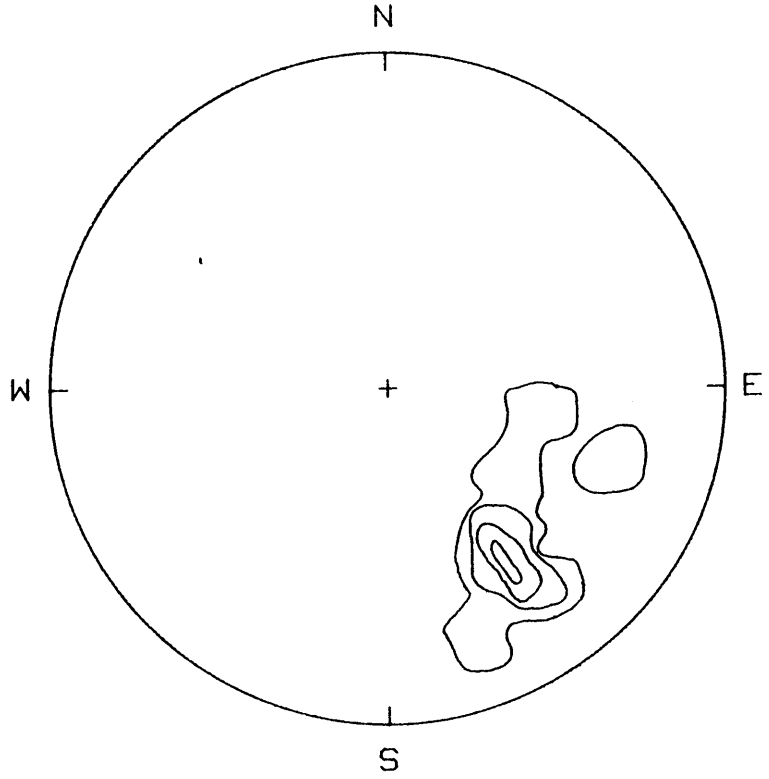

DOMAIN #12: LGd3 CONTOURS
PROJECTION = EQUAL AREA
SCANNING CIRCLE = 1.000%
CONTOURS: 10% 20% 30% 40%

Figure A-32

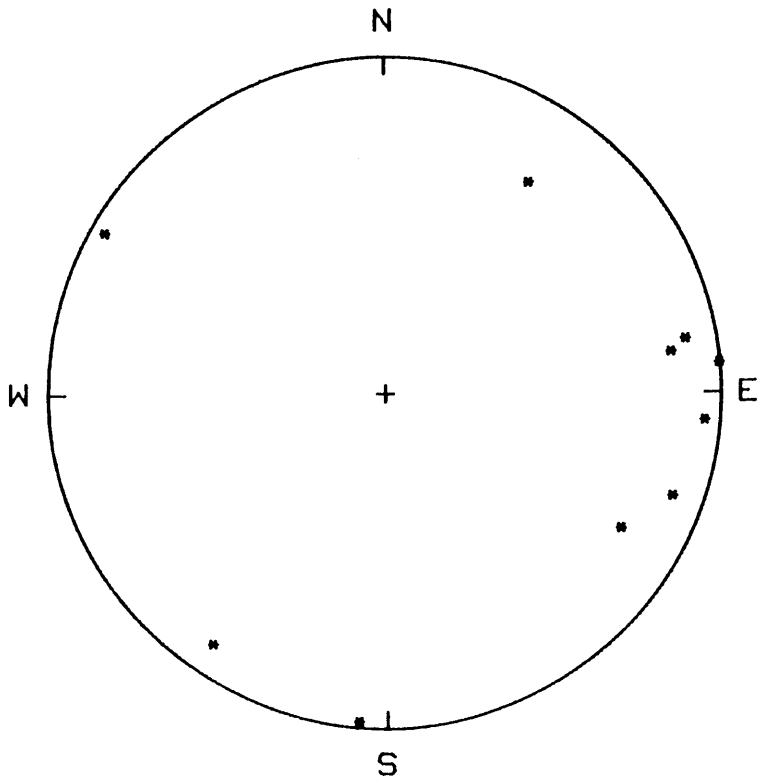

DOMAIN #12: LGd3 FOLDS
PROJECTION = EQUAL AREA
NUMBER OF POINTS = 10

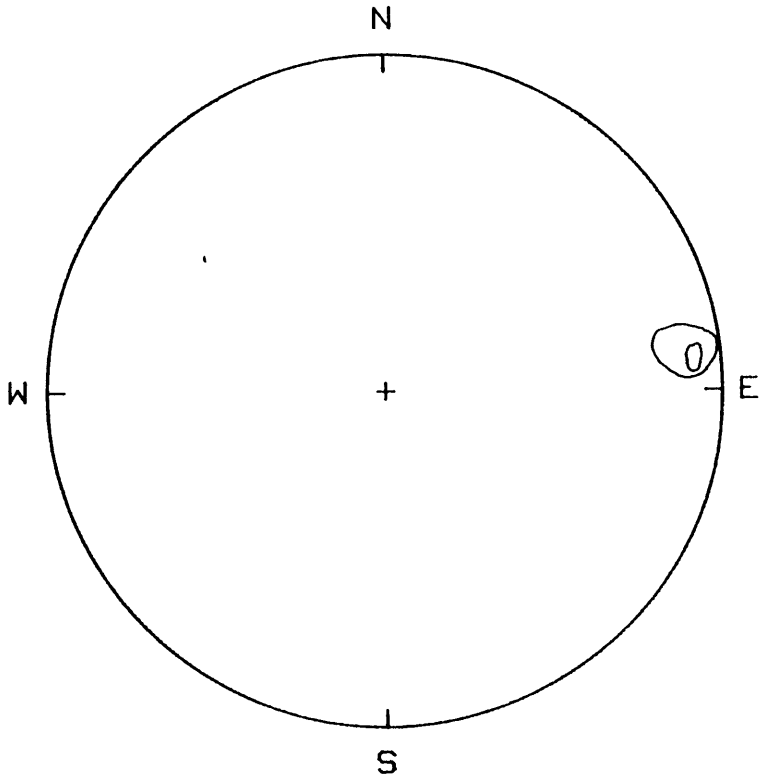

DOMAIN #12: LGd3 CONTOURS
PROJECTION = EQUAL AREA
SCANNING CIRCLE = 1.000%
CONTOURS: 20% 30%

Figure A-33

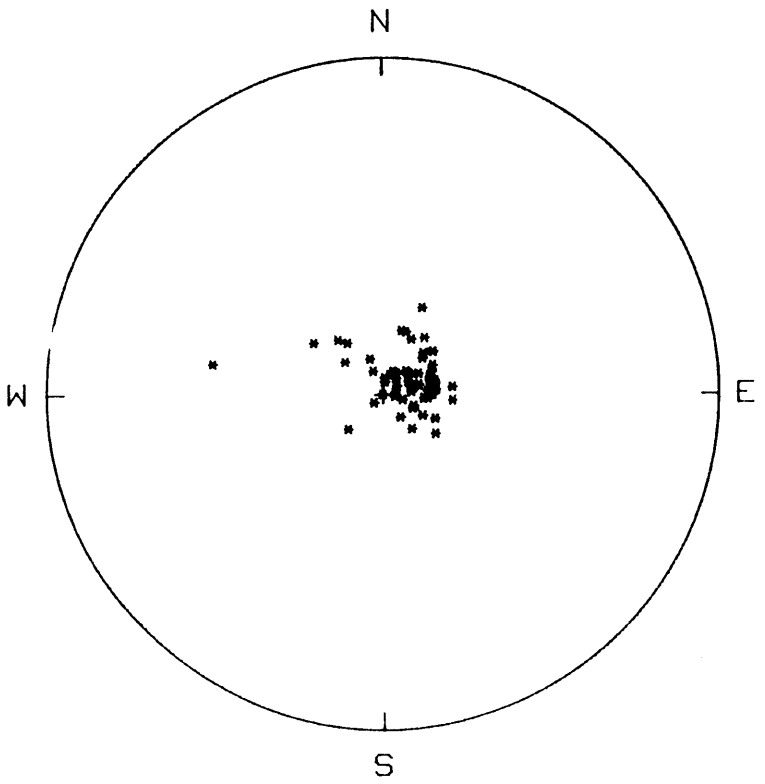

DOMAIN #20: MCd1 POLES
PROJECTION = EQUAL AREA
NUMBER OF POINTS = 63

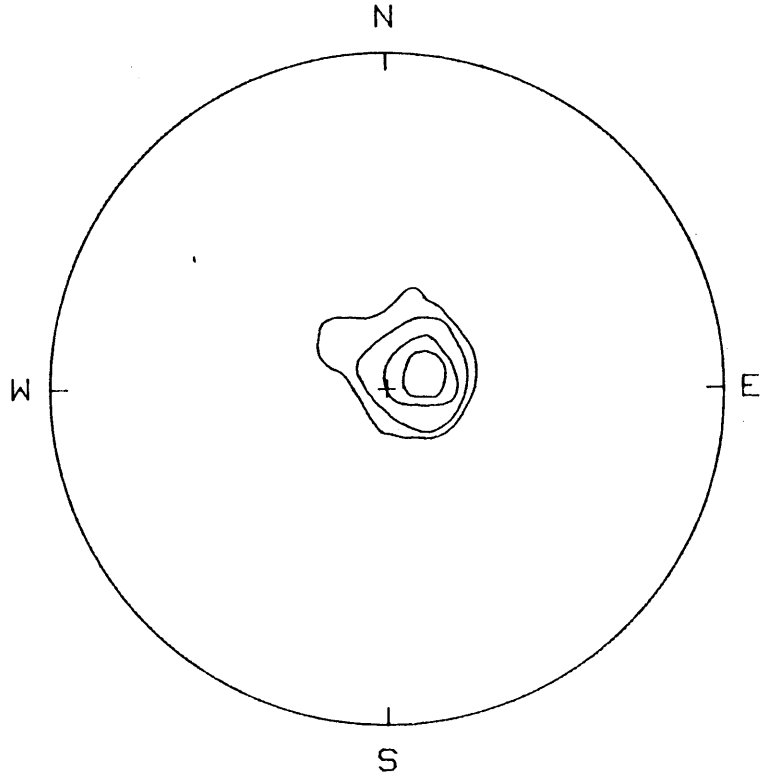

DOMAIN #20: MCd1 CONTOURS
PROJECTION = EQUAL AREA
SCANNING CIRCLE = 1.000%
CONTOURS: 5% 10% 30% 50%

Figure A-34

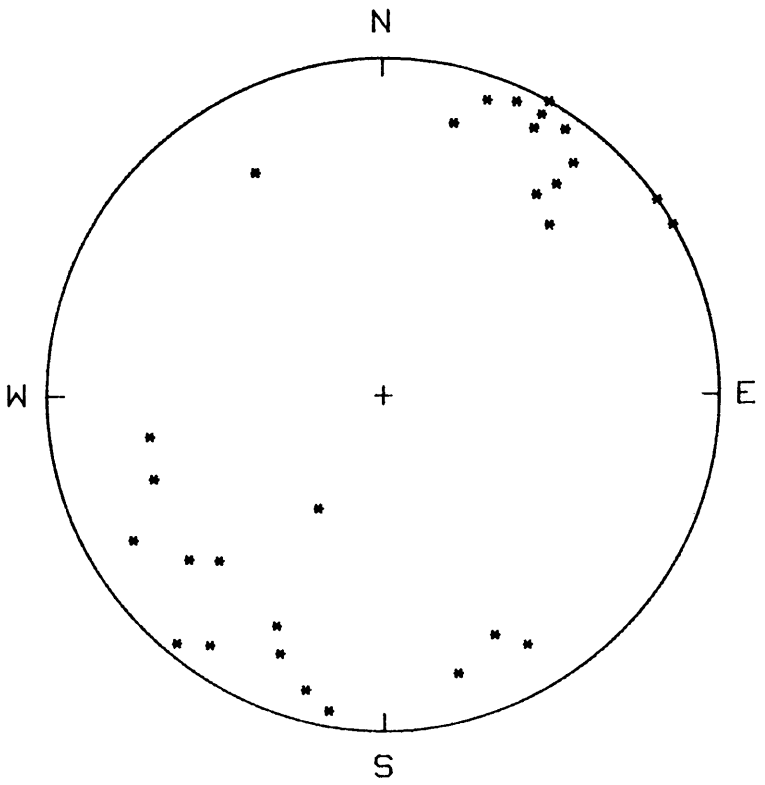

Late D4 FOLDS
PROJECTION = EQUAL AREA
NUMBER OF POINTS = 30

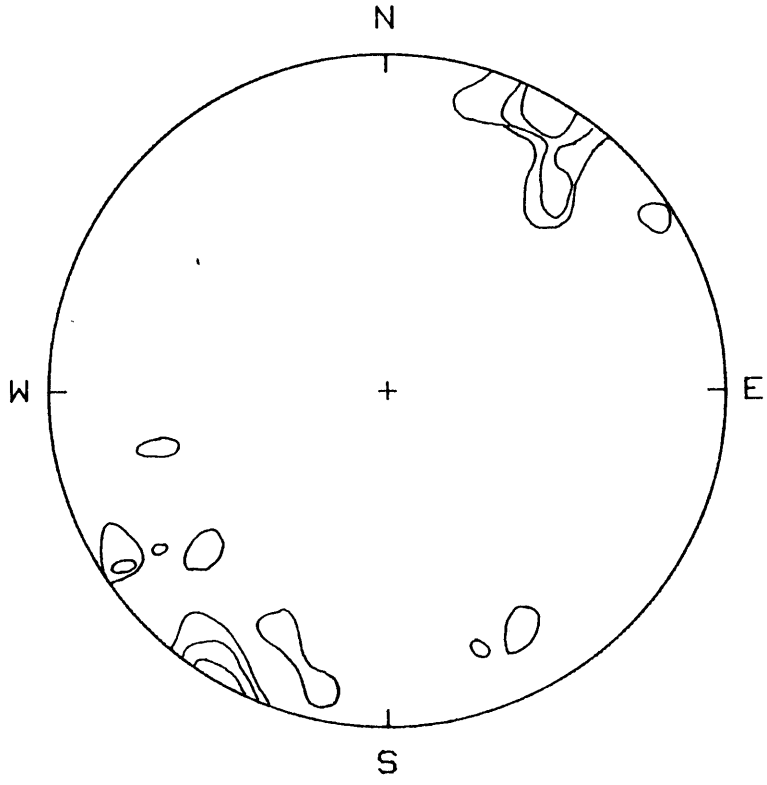

Late D4 FOLD CONTOURS
PROJECTION = EQUAL AREA
SCANNING CIRCLE = 1.000%
CONTOURS: 5% 10% 15%

Figure A-35

APPENDIX B

REPRESENTATIVE MICROPROBE MINERAL ANALYSES

REPRESENTATIVE GARNET MICROPROBE ANALYSES

	85-4G1 (core)	85-4G1 (rim)	84-4F (core)	85-4F (rim)	84-14K (core)
MgO	12.17	6.86	1.76	2.33	1.88
Al_2O_3	22.74	22.21	21.31	21.34	20.25
SiO_2	40.69	39.21	38.33	33.64	37.70
CaO	3.66	9.83	10.85	9.93	6.43
MnO	0.54	0.32	2.11	0.78	1.73
FeO	22.17	22.12	27.88	29.10	33.25
TOTAL	101.97	100.55	102.24	102.10	100.45
	Formula normalized to 12 oxygens				
Mg	1.339	0.780	0.204	0.268	0.130
Al	1.977	1.998	1.949	1.947	1.922
Si	3.002	2.993	2.975	2.991	3.036
Ca	0.289	0.804	0.902	0.823	0.555
Mn	0.034	0.020	0.139	0.051	0.118
Fe	1.368	1.412	1.810	1.884	2.240
TOTAL	8.009	8.008	8.014	8.000	8.002
X_{alm}	0.451	0.468	0.592	0.622	0.736
X_{py}	0.442	0.259	0.067	0.089	0.043
X_{gross}	0.096	0.267	0.295	0.272	0.182
X_{spess}	0.011	0.007	0.455	0.017	0.039
Fe/Fe+Mg	0.505	0.644	0.898	0.875	0.945

REPRESENTATIVE GARNET MICROPROBE ANALYSES

	84-14K (rim)	84-6P (core)	84-6P (rim)	84-8D (core)	84-8D (rim)
MgO	1.98	1.18	1.92	1.39	2.40
Al_2O_3	20.54	21.29	21.41	20.05	20.20
SiO_2	37.99	37.92	38.11	37.74	38.47
CaO	5.84	7.03	7.19	4.36	6.87
MnO	0.08	12.39	4.68	14.48	3.06
FeO	33.96	21.80	27.55	21.96	29.03
TOTAL	100.33	101.60	100.86	100.00	100.05
	Formula normalized to 12 oxygens				
Mg	0.230	0.139	0.227	0.168	0.286
Al	1.938	1.987	1.997	1.912	1.899
Si	3.042	3.004	3.016	3.054	3.068
Ca	0.500	0.597	0.609	0.378	0.587
Mn	0.006	0.831	0.314	0.992	0.207
Fe	2.274	1.444	1.823	1.486	1.936
TOTAL	7.989	8.002	7.985	7.990	7.982
X_{alm}	0.756	0.480	0.613	0.491	0.642
X_{py}	0.076	0.046	0.076	0.055	0.095
X_{gross}	0.166	0.198	0.205	0.125	0.195
X_{spess}	0.002	0.276	0.106	0.328	0.069
Fe/Fe+Mg	0.909	0.913	0.890	0.899	0.871

REPRESENTATIVE GARNET MICROPROBE ANALYSES

	84-8B (core)	84-8B (rim)	84-15S (core)	84-15S (rim)
MgO	1.62	2.34	1.20	2.07
Al_2O_3	19.85	20.36	20.91	21.24
SiO_2	37.77	38.01	37.44	37.94
CaO	6.58	6.34	7.34	4.85
MnO	9.36	5.75	5.23	0.22
FeO	24.81	27.59	29.39	35.37
TOTAL	99.98	100.40	101.51	101.69
	Formula normalized to 12 oxygens			
Mg	0.194	0.279	0.143	0.245
Al	1.887	1.916	1.964	1.983
Si	3.047	3.036	2.985	3.006
Ca	0.569	0.542	0.627	0.411
Mn	0.639	0.389	0.353	0.014
Fe	1.674	1.843	1.960	2.343
TOTAL	8.009	8.005	8.032	8.002
X_{alm}	0.544	0.606	0.636	0.777
X_{py}	0.063	0.091	0.046	0.081
X_{gross}	0.185	0.178	0.203	0.136
X_{spess}	0.208	0.127	0.114	0.005
Fe/Fe+Mg	0.896	0.869	0.933	0.906

REPRESENTATIVE BIOTITE MICROPROBE ANALYSES

	84-14K (matrix)	84-6P (matrix)	84-6P (rim)	84-8D (matrix)	84-8D (rim)
MgO	9.74	12.00	11.59	11.13	11.34
Al_2O_3	17.97	17.16	17.36	16.90	17.07
SiO_2	36.26	38.00	37.41	38.39	38.43
CaO	0.02	0.02	0.06	0.00	0.03
TiO_2	1.63	1.56	1.57	1.62	1.51
MnO	0.04	0.04	0.12	0.17	0.20
FeO	21.26	18.06	18.39	19.08	18.52
Na_2O	0.03	0.05	0.06	0110	0.04
K_2O	8.89	9.57	9.47	7.96	8.92
TOTAL	95.84	96.45	96.05	95.35	96.07
	Formula normalized to 11 oxygens				
Mg	1.103	1.330	1.294	1.242	1.259
Al	1.609	1.504	1.533	1.491	1.499
Si	2.754	2.827	2.803	2.873	2.863
Ca	0.002	0.001	0.005	0.000	0.002
Ti	0.093	0.087	0.088	0.091	0.085
Mn	0.002	0.003	0.008	0.011	0.013
Fe	1.351	1.123	1.152	1.194	1,154
Na	0.004	0.008	0.009	0.015	0.006
K	0.861	0.908	0.905	0.760	0.848
TOTAL	7.780	7.791	7.799	7.677	7.729
Fe/Fe+Mg	0.550	0.458	0.471	0.490	0.478

REPRESENTATIVE BIOTITE MICROPROBE ANALYSES

	84-8B (rim)	84-8B (matrix)	84-15S (rim)	85-15S (matrix)
MgO	12.51	12.23	9.84	10.01
Al_2O_3	16 52	16.66	17.45	18.01
SiO_2	38.49	38.28	36.34	36.46
CaO	0.03	0.00	0.03	0.02
TiO_2	1.43	1.82	1.48	1.37
MnO	0.13	0.11	0.00	0.00
FeO	17.46	18.24	20.94	20.58
Na_2O	0.15	0.10	0.24	0.21
K_2O	9.19	9.12	8.73	9.02
TOTAL	95.91	96.57	95.04	95.68
	Formula normalized to 11 oxygens			
Mg	1.389	1.353	1.122	1.133
Al	1.450	1.457	1.573	1.611
Si	2.866	2.840	2.781	2.767
Ca	0.002	0.000	0.002	0.002
Ti	0.080	0.102	0.085	0.078
Mn	0.008	0.007	0.000	0.000
Fe	1.087	1.132	1.340	1.306
Na	0.021	0.015	0.035	0.031
K	0.873	0.863	0.852	0.873
TOTAL	7.776	7.768	7.791	7.801
Fe/Fe+Mg	0.439	0.455	0.544	0.535

REPRESENTATIVE PLAGIOCLASE MICROPROBE ANALYSES

	84-4GI	84-14K (core)	84-14K (rim)	84-6P (albite)	84-6P (oligo)
Na_2O	4.66	9.42	10.19	10.33	8.82
MgO	0.00	0.00	0.04	0.01	0.04
Al_2O_3	29.90	19.38	20.39	20.66	21.88
SiO_2	52.80	70.90	69.17	69.10	65.71
CaO	12.53	0.00	1.20	1.12	3.38
FeO	0.32	0.00	0.09	0.19	0.00
K_2O	0.00	0.06	0.07	0.10	0.06
TOTAL	100.21	99.76	101.16	101.51	99.88
	Formula normalized to 8 oxygens				
Na	0.409	0.789	0.851	0.861	0.750
Mg	0.000	0.000	0.003	0.001	0.002
Al	1.596	0.986	1.035	1.046	1.131
Si	2.391	3.062	2.979	2.969	2.883
Ca	0.608	0.000	0.056	0.051	0.159
Fe	0.012	0.000	0.003	0.007	0.000
K	0.000	0.003	0.004	0.005	0.003
TOTAL	5.015	4.841	4.931	4.941	4.928
X_{Ca}	0.598	0.000	0.061	0.056	0.174
X_{Na}	0.402	0.996	0.935	0.938	0.822
X_K	0.000	0.004	0.004	0.006	0.004

REPRESENTATIVE PLAGIOCLASE MICROPROBE ANALYSES

	84-8D (core)	84-8D (rim)	84-8B (albite)	84-8B (oligo)	84-15S
Na_2O	7.60	7.96	9.60	5.98	11.71
MgO	0.02	0.01	0.03	0.02	0.02
Al_2O_3	22.12	21.50	20.10	21.83	19.81
SiO_2	66.42	67.07	69.18	69.04	68.34
CaO	3.46	2.94	1.19	3.09	0.28
FeO	0.00	0.00	0.07	0.04	0.20
K_2O	0.05	0.07	0.08	0.08	0.06
TOTAL	99.66	99.55	100.25	100.08	100.40
		Formula normalized to 8 oxygens			
Na	0.644	0.674	0.806	0.499	0.989
Mg	0.001	0.001	0.002	0.001	0.001
Al	1.139	1.107	1.026	1.107	1.017
Si	2.902	2.931	2.998	2.971	2.978
Ca	0.162	0.138	0.055	0.142	0.013
Fe	0.000	0.000	0.002	0.001	0.007
K	0.003	0.004	0.004	0.004	0.003
TOTAL	4.851	4.854	4.894	4.727	5.009
X_{Ca}	0.200	0.169	0.064	0.220	0.013
X_{Na}	0.796	0.826	0.931	0.773	0.984
X_K	0.003	0.005	0.005	0.007	0.003

REPRESENTATIVE MUSCOVITE MICROPROBE ANALYSES

	84-14K	84-6P	84-8D	84-8B	84-15S
MgO	0.98	1.70	1.43	1.30	1.09
Al_2O_3	33.97	31.68	32.77	31.91	33.40
SiO_2	46.83	50.81	51.60	50.83	48.56
CaO	0.03	0.00	0.00	0.00	0.02
TiO_2	0.30	0.51	0.53	0.47	0.31
MnP	0.06	0.03	0.00	0.07	0.00
FeO	1.73	2.85	1.67	3.12	2.26
Na_2O	0.70	0.75	0.79	1.05	1.22
K_2O	10.08	9.94	8.63	7.33	8.42
TOTAL	94.69	98.27	97.42	96.07	95.28
	Formula normalized to 11 oxygens				
Mg	0.097	0.164	0.136	0.126	0.107
Al	2.681	2.410	2.474	2.447	2.597
Si	3.136	3.280	3.305	3.307	3.204
Ca	0.002	0.000	0.000	0.000	0.002
Ti	0.015	0.025	0.026	0.023	0.015
Mn	0.003	0.002	0.000	0.004	0.000
Fe	0.097	0.154	0.090	0.170	0.124
Na	0.091	0.094	0.098	0.132	0.156
K	0.861	0.818	0.705	0.608	0.708
Total	6.984	6.946	6.834	6.817	6.914

REPRESENTATIVE HORNBLENDE MICROPROBE ANALYSES

	T85-4GI	84-4F	84-8B
MgO	15.92	8.97	8.92
Al_2O_3	14.82	13.18	15.33
SiO_2	44.06	43.06	42.64
CaO	12.03	10.91	9.60
TiO_2	0.22	0.79	0.38
MnO	0.00	0.10	0.27
FeO	7.83	18.27	17.69
Na_2O	2.47	2.26	2.86
K_2O	0.25	0.07	0.10
TOTAL	97.59	97.61	97.78
	Formula normalized to 23 oxygens		
Mg	3.403	2.007	1.981
Al	2.505	2.332	2.692
Si	6.319	6.461	6.352
Ca	1.849	1.754	1.532
Ti	0.024	0.089	0.042
Mn	0.000	0.012	0.034
Fe	0.939	2.292	2.203
Na	0.686	0.656	0.827
K	0.045	0.014	0.018
TOTAL	15.769	15.618	15.681
Fe/Fe + Mg	0.216	0.533	0.527

REPRESENTATIVE PYROXENE MICROPROBE ANALYSES

	85-4G1 (enstatite)	85-4G7 (augite)
Na_2O	0.02	0.59
MgO	28.14	15.22
Al_2O_3	0.97	1.98
SiO_2	55.45	53.04
CaO	0.23	22.72
TiO_2	0.04	0.04
Cr_2O_3	0.08	0124
MnO	0.00	0.22
FeO	10.22	6.49
TOTAL	101.17	100.54
	Formula normalized to 8 oxygens	
Na	0.002	0.042
Mg	1.493	0.834
Al	0.041	0.086
Si	1.974	1.950
Ca	0.009	0.895
Ti	0.001	0.001
Cr	0.002	0.007
Mn	0.000	0.007
Fe	0.483	0.200
TOTAL	4.004	4.022
X_{Ca}	0.004	0.464
X_{Mg}	0.752	0.433
X_{Fe}	0.243	0.103

REPRESENTATIVE OLIVINE MICROPROBE ANALYSES

	85-4G1
Na_2O	0.00
MgO	41.11
Al_2O_3	0.04
SiO_2	38.53
CaO	0.02
TiO_2	0.00
Cr_2O_3	0.08
MnO	0.06
FeO	20.93
TOTAL	100.76
	Formula normalized to 4 oxygens
Na	0.000
Mg	1.571
Al	0.001
Si	0.987
Ca	0.000
Ti	0.000
Cr	0.002
Mn	0.001
Fe	0.448
TOTAL	3.011
X_{Mg}	0.778
X_{Fe}	0.222

APPENDIX C: RECALIBRATION OF GARNET-BIOTITE THERMOMETER AND GARNET-PLAGIOCLASE-MUSCOVITE-BIOTITE BAROMETER

The geothermometer:

$$Mg_3Al_2Si_3O_{12} + KFe_3AlSi_3O_{10}(OH)_2 = Fe_3Al_2Si_3O_{12} + KMg_3AlSi_3O_{10}(OH)_2$$

pyrope annite almandine phlogopite

was calibrated by Ferry and Spear (1978). Hodges (unpub. data) re-regressed the experimental data using the technique of York (1969), and obtained the following values for enthalpy, ΔH, and entropy, ΔS:

$$\Delta H = 12716 \text{ cal}$$

$$\Delta S = 4.7 \text{ cal mol}^{-1}\text{K}^{-1}.$$

Similarly, the geobarometer:

$$Fe_3Al_2Si_3O_{12} + Ca_3Al_2Si_3O_{12} + KAl_3Si_3O_{10}(OH)_2$$

almandine grossular muscovite

$$= {}_3CaAl_2Si_2O_8 + KFe_3AlSi_3O_{10}(OH)_2$$

anorthite annite

empirically calibrated by Hodges and Crowley (1985) was re-regressed by Hodges (unpub. data) to yield:

$$\Delta H = 16722 \text{ cal}$$

$$\Delta S = 38.956 \text{ cal mol}^{-1}\text{K}^{-1}.$$

These values for ΔH and ΔS were used to calculate the pressures and temperatures presented in Chapter 4.

APPENDIX D: CALIBRATION OF THE PLAGIOCLASE-GARNET-ORTHOPYROXENE-KYANITE BAROMETER

The reaction:

$$2CaAl_2Si_2O_8 + 2/3Mg_3Al_2Si_3O_{12}$$

anorthite pyrope

$$\Rightarrow 2/3Ca_3Al_2Si_3O_{12} + 2Al_2SiO_5 + Mg_2Si_2O_6 \qquad \text{(D-1)}$$

grossular kyanite enstatite

is a linear sum of the two reactions:

$$3CaAl_2Si_2O_8 \Rightarrow Ca_3Al_2Si_3O_{12} + 2Al_2SiO_5 + SiO_2 \qquad \text{(D-2)}$$

$$1/3Ca_3Al_2Si_3O_{12} + 2/3Mg_3Al_2Si_3O_{12} + SiO_2 \Rightarrow CaAl_2Si_2O_8 + MgSi_2O_6 \qquad \text{(D-3)}$$

Reaction D-2 has been calibrated by Newton ana Haselton (1981), while Newton and Perkins (1982) calibrated reaction D-3.

Molar enthalpy and entropy for reaction D-1 were calculated using the data of Helgeson et al. (1978). Molar volume was calculated using the data of Helgeson et al. (1978) and the relationship of Newton and Haselton (1981) for the grossular component in garnet. The activity-composition relations for anorthite, pyrope, grossular and enstatite are those of Newton and Perkins (1982).

The data for reaction D-1 are:

$$\Delta H = 13352 \text{ cal}$$

$$\Delta S = 36.709 \text{ cal mol}^{-1}\text{K}^{-1}$$

$$\Delta V = 4.5768 - V_{Grossular} \text{ cal bar}^{-1}$$

APPENDIX E1:

^{40}Ar-^{39}Ar HEATING SCHEDULES EFJORD-SINGIS AREA

TEMP C	40AR/ 39AR	37AR/ 39AR	36AR/ 39AR	MOLES 39AR	39AR %TOTAL	%40AR RAD	K/ CA	APPARENT AGE Ma
		T85_2EB		(E-14)			J= .002941	
840	73.14	.0005	.0103	5.0	4.3	95.8	1031.579	338.0 +/- 5.1
915	74.21	.0017	.0002	21.7	18.6	99.9	287.221	355.7 +/- 3.8
975	75.13	.0096	.0010	16.9	14.5	99.6	50.988	358.7 +/- 4.4
1010	74.64	.0001	.0001	20.9	17.9	99.9	4900.000	357.7 +/- 4.0
1080	74.65	.0274	.0003	40.5	34.7	99.8	17.896	357.5 +/- 3.6
FUSE	74.94	.0059	.0010	11.8	10.1	99.6	83.248	358.0 +/- 3.6
TOTAL				116.7	100.0			356.60
PLATEAU AGE			358.0 +/- 2.8					

TEMP C	40AR/ 39AR	37AR/ 39AR	36AR/ 39AR	MOLES 39AR	39AR %TOTAL	%40AR RAD	K/ CA	APPARENT AGE Ma
		T85_2EM		(E-14)			J= .003829	
840	68.25	.0445	.0180	1.1	.7	92.2	11.003	389.3 +/- 22.9
915	62.90	.0212	.0093	3.6	2.1	95.6	23.113	373.7 +/- 4.6
970	60.57	.0018	.0033	61.0	36.3	98.3	265.741	370.6 +/- 4.1
1010	59.80	.0064	.0014	46.9	27.9	99.3	76.598	369.5 +/- 3.6
1080	59.85	.0022	.0019	31.4	18.7	99.0	224.256	368.8 +/- 4.0
FUSE	60.89	.0218	.0049	23.9	14.3	97.6	22.524	369.7 +/- 3.7
TOTAL				167.9	100.0			370.03
PLATEAU AGE			369.7 +/- 3.3					

TEMP C	40AR/ 39AR	37AR/ 39AR	36AR/ 39AR	MOLES 39AR	39AR %TOTAL	%40AR RAD	K/ CA	APPARENT AGE Ma
		T85_4EM		(E-14)			J= .003822	
855	100.34	.0290	.0340	4.7	2.8	90.0	16.896	534.7 +/- 9.9
925	77.82	.0267	.0026	11.6	7.0	99.0	18.352	465.5 +/- 4.6
960	76.18	.0091	.0032	18.3	11.1	98.7	53.846	455.7 +/- 4.2
1000	74.91	.0034	.0024	40.7	24.7	99.0	144.117	450.2 +/- 4.1
1075	75.51	.0058	.0014	55.0	33.3	99.4	84.482	455.0 +/- 4.2
FUSE	80.37	.0563	.0024	34.8	21.1	99.1	8.703	479.4 +/- 4.5
TOTAL				165.1	100.0			462.05

TEMP C	40AR/ 39AR	37AR/ 39AR	36AR/ 39AR	MOLES 39AR	39AR %TOTAL	%40AR RAD	K/ CA	APPARENT AGE Ma
		T85_13BM		(E-14)			J= .004377	
840	156.17	.0514	.0129	5.0	2.5	97.5	9.527	921.7 +/- 9.6
925	68.16	.0328	.0036	37.5	18.6	98.4	14.923	464.3 +/- 4.2
960	65.23	.0225	.0007	16.9	8.4	99.6	21.739	451.6 +/- 4.2
1000	65.32	.0205	.0028	37.1	18.4	98.7	23.944	448.4 +/- 5.1
1070	66.71	.0097	.0013	66.8	33.1	99.4	50.411	459.7 +/- 4.3
FUSE	71.43	.0259	.0013	38.6	19.1	99.4	18.919	488.3 +/- 4.6
TOTAL				201.8	100.0			474.74

TEMP C	40AR/ 39AR	37AR/ 39AR	36AR/ 39AR	MOLES 39AR	39AR %TOTAL	%40AR RAD	K/ CA	APPARENT AGE Ma
		H81_11A		(E-14)			J= .00491	
880	874.20	3.7700	.7727	2.5	4.0	73.9	.1296	2581.1 +/- 30.0
925	458.87	5.1390	.5687	1.8	3.0	63.5	.0950	1605.8 +/- 31.8
960	298.30	6.4820	.5678	1.3	2.1	43.9	.0752	899.5 +/- 40.4
985	178.45	10.3500	.3539	1.3	2.1	41.8	.0470	567.3 +/- 36.3
1010	108.96	11.4680	.1660	2.2	3.6	55.8	.0424	474.9 +/- 21.6
1025	75.18	10.3100	.0722	5.1	8.2	72.7	.0472	431.8 +/- 16.2
1040	61.60	10.2150	.0280	21.8	35.4	87.9	.0476	428.0 +/- 4.2
1050	82.08	9.8850	.0780	3.7	6.0	72.9	.0492	467.5 +/- 17.7
1065	78.75	9.6630	.0908	3.3	5.4	66.9	.0503	417.7 +/- 13.9
1075	76.44	9.5800	.0746	3.7	6.0	72.1	.0508	435.0 +/- 8.3
1085	74.01	9.7770	.0717	4.1	6.6	72.4	.0497	424.1 +/- 11.6
1100	86.62	8.7800	.1099	2.2	3.6	63.3	.0554	432.5 +/- 18.7
1125	77.33	8.2690	.0910	3.0	4.8	66.0	.0589	405.9 +/- 19.7
FUSE	84.51	4.0770	.0889	5.7	9.2	69.3	.1198	457.0 +/- 8.5
TOTAL				61.6	100.0			567.78

_MP C	40AR/ 39AR	37AR/ 39AR	36AR/ 39AR	MOLES 39AR	39AR %TOTAL	%40AR RAD	K/ CA	APPARENT AGE Ma
		T84_19G		(E-14)			J= .0049	
925	118.27	2.2270	.1342	34.6	6.1	66.6	.2197	589.6 +/- 5.5
960	73.12	4.4650	.0598	26.1	4.6	76.3	.1094	437.2 +/- 5.5
975	74.90	5.2620	.0595	23.2	4.1	77.1	.0928	450.9 +/- 5.0
985	72.04	5.8970	.0517	33.6	5.9	79.4	.0827	447.6 +/- 4.2
1000	72.21	6.1900	.0502	43.6	7.7	80.1	.0788	452.0 +/- 4.4
1010	66.82	6.3860	.0344	37.4	6.6	85.5	.0764	447.1 +/- 4.2
1025	65.45	6.3930	.0321	36.4	6.4	86.3	.0763	442.5 +/- 5.1
1040	65.19	6.5550	.0299	25.9	4.6	87.2	.0744	445.3 +/- 5.1
1050	61.92	6.8010	.0204	41.0	7.2	91.1	.0717	442.3 +/- 4.3
1065	62.31	6.8890	.0207	40.6	7.2	91.0	.0708	444.4 +/- 4.2
1075	57.65	6.7380	.0097	152.4	26.9	95.9	.0724	434.5 +/- 3.9
1085	61.03	6.7580	.0190	55.1	9.7	91.7	.0721	439.0 +/- 4.2
1100	89.50	6.7480	.1154	6.4	1.1	62.5	.0722	438.8 +/- 8.4
1125	124.10	6.8560	.2243	3.8	.7	47.0	.0711	455.7 +/- 21.1
FUSE	180.70	6.8130	.4210	6.1	1.1	31.4	.0716	445.1 +/- 8.0
TOTAL				566.1	100.0			450.75

TEMP C	40AR/ 39AR	37AR/ 39AR	36AR/ 39AR	MOLES 39AR	39AR %TOTAL	%40AR RAD	K/ CA	APPARENT AGE Ma
		T85_2A		(E-14)			J= .003392	
890	762.62	2.4212	.6164	6.0	2.0	76.1	.2020	1965.7 +/- 41.0
940	245.44	5.2400	.1298	2.7	.9	84.5	.0931	964.3 +/- 75.1
975	177.24	11.5810	.1411	3.2	1.0	77.0	.0419	691.2 +/- 27.0
00	190.90	18.2150	.1494	5.4	1.8	77.6	.0265	743.1 +/- 10.4
005	179.22	19.8870	.1512	4.6	1.5	75.9	.0243	693.5 +/- 10.5
1010	144.62	21.0460	.0950	6.5	2.1	81.8	.0229	616.7 +/- 8.2
1015	133.44	20.5380	.0988	6.0	2.0	79.3	.0235	561.1 +/- 7.6
1025	121.49	21.2890	.0878	12.0	3.9	80.0	.0226	521.5 +/- 5.9
1030	126.81	20.5924	.1126	4.4	1.4	75.0	.0234	511.6 +/- 6.8
1040	112.51	20.3850	.0781	7.6	2.5	80.9	.0237	492.1 +/- 5.9
1050	103.65	20.7200	.0529	16.4	5.4	86.5	.0233	485.8 +/- 4.6
1065	97.71	20.7165	.0397	31.4	10.3	89.7	.0233	476.0 +/- 4.6
1075	96.77	20.3400	.0405	40.5	13.3	89.3	.0237	470.1 +/- 4.3
1085	93.01	19.5500	.0332	38.2	12.6	91.1	.0247	461.8 +/- 4.5
110	93.42	19.3047	.0396	29.7	9.8	89.1	.0250	454.6 +/- 4.2
120	95.91	19.3230	.0464	17.5	5.8	87.3	.0250	456.9 +/- 4.4
25	97.81	19.8530	.0523	14.2	4.7	85.8	.0243	458.1 +/- 4.6
USE	91.17	20.2220	.0215	57.4	18.9	94.8	.0239	470.1 +/- 4.5
TOTAL				303.8	100.0			520.42

TEMP C	40AR/ 39AR	37AR/ 39AR	36AR/ 39AR	MOLES 39AR	39AR %TOTAL	%40AR RAD	K/ CA	APPARENT AGE Ma
		T85_2B		(E-14)			J= .003431	
880	2050.80	30.9900	1.5020	1.6	.6	78.5	.0154	3419.1 +/- 87.4
975	690.60	13.4200	.7300	1.9	.7	68.9	.0361	1757.9 +/- 35.3
1010	254.50	19.4100	.3378	3.3	1.3	61.4	.0249	783.6 +/- 36.5
1025	189.96	22.5100	.2480	4.5	1.8	62.4	.0214	624.3 +/- 14.5
1040	114.99	22.4600	.0850	9.4	3.7	79.7	.0214	500.7 +/- 7.0
1050	101.39	22.3670	.0658	16.4	6.5	82.6	.0215	462.4 +/- 6.9
1065	93.05	22.0000	.0496	36.6	14.5	86.1	.0219	444.8 +/- 4.4
1075	98.99	21.5700	.0772	65.8	26.1	78.7	.0223	433.6 +/- 4.0
1085	92.28	21.3200	.0580	50.2	19.9	83.3	.0226	428.3 +/- 4.0
1100	99.14	21.8000	.0655	17.4	6.9	82.2	.0221	451.5 +/- 6.0
1110	99.22	22.5050	.0477	15.5	6.1	87.6	.0214	478.0 +/- 5.5
1130	98.99	22.3000	.0422	15.1	6.0	89.2	.0216	484.5 +/- 5.8
FUSE	107.35	22.0290	.0384	14.6	5.8	91.1	.0219	529.4 +/- 5.7
TOTAL				252.3	100.0			488.04

TEMP C	40AR/ 39AR	37AR/ 39AR	36AR/ 39AR	MOLES 39AR	39AR %TOTAL	%40AR RAD	K/ CA	APPARENT AGE Ma
		T85_2D1		(E-14)			J= .003413	
890	365.21	2.3288	.4567	6.8	1.4	63.1	.2100	1048.0 +/- 11.3
940	112.44	1.0083	.0742	9.3	2.0	80.5	.4856	486.1 +/- 6.3
975	95.26	1.9401	.0713	7.4	1.6	78.0	.2522	408.3 +/- 5.4
1000	107.10	3.1908	.1030	8.5	1.8	71.8	.1532	421.2 +/- 6.3
1010	97.82	3.4622	.0715	7.9	1.7	78.7	.1412	421.7 +/- 5.4
1025	92.39	7.0052	.0482	14.1	3.0	85.2	.0696	431.2 +/- 4.9
1040	85.54	9.9061	.0383	18.4	3.9	87.7	.0491	413.8 +/- 4.3
1050	84.79	11.2124	.0381	22.8	4.8	87.7	.0433	411.3 +/- 3.8
1065	81.62	12.2064	.0302	54.1	11.4	90.2	.0398	407.9 +/- 3.7
1075	81.86	12.3580	.0315	60.4	12.7	89.8	.0393	407.2 +/- 3.7
1085	83.15	12.0820	.0368	64.5	13.6	88.1	.0402	405.7 +/- 4.1
1110	80.75	12.1910	.0287	34.2	7.2	90.7	.0398	405.8 +/- 4.1
1120	78.55	12.5660	.0259	25.9	5.5	91.5	.0386	399.1 +/- 3.8
1125	75.42	12.9570	.0165	37.2	7.9	94.9	.0374	397.8 +/- 4.4
FUSE	74.11	13.0658	.0098	102.5	21.6	97.5	.0371	401.1 +/- 3.7
TOTAL		-		473.9	100.0			416.82

TEMP C	40AR/ 39AR	37AR/ 39AR	36AR/ 39AR	MOLES 39AR	39AR %TOTAL	%40AR RAD	K/ CA	APPARENT AGE Ma
		T85_3B1		(E-14)			J= .003032	
890	1943.62	13.3949	1.8467	.8	.2	72.0	.0362	3003.5 +/-190.8
940	667.05	19.6890	.8830	.8	.2	61.1	.0245	1466.7 +/-126.6
975	251.27	20.8695	.4205	1.6	.3	51.2	.0231	602.3 +/- 38.7
990	149.98	24.6950	.1459	5.1	1.0	72.6	.0195	523.0 +/- 14.0
1005	150.17	20.6680	.1604	3.6	.7	69.5	.0233	503.0 +/- 37.6
1015	97.09	11.1500	.0278	27.0	5.5	92.4	.0436	437.4 +/- 4.2
1025	92.09	10.7770	.0203	51.6	10.5	94.4	.0451	425.1 +/- 4.0
1032	89.59	10.6980	.0174	62.1	12.6	95.2	.0454	418.0 +/- 3.9
1040	89.61	10.6220	.0175	63.0	12.7	95.2	.0458	417.8 +/- 3.8
1050	88.63	10.4987	.0154	99.7	20.2	95.8	.0463	416.2 +/- 3.8
1060	94.38	10.9970	.0293	26.5	5.4	91.7	.0442	423.6 +/- 4.0
1080	99.26	13.2030	.0364	10.8	2.2	90.2	.0367	437.2 +/- 5.0
1085	92.48	12.3960	.0181	21.3	4.3	95.3	.0392	430.6 +/- 4.0
1100	89.55	12.4360	.0125	42.2	8.5	97.0	.0390	425.2 +/- 4.0
1120	92.13	12.2142	.0131	45.8	9.3	96.8	.0397	435.4 +/- 4.2
FUSE	96.90	11.5410	.0269	32.1	6.5	92.7	.0421	438.0 +/- 4.3
TOTAL				494.0	100.0			432.06

TEMP C	40AR/ 39AR	37AR/ 39AR	36AR/ 39AR	MOLES 39AR	39AR %TOTAL	%40AR RAD	K/ CA	APPARENT AGE Ma
		T85_3B2		(E-14)			J= .003023	
890	2711.74	9.1388	2.2846	1.2	.9	75.1	.0532	3561.8 +/-131.6
940	2433.45	22.6030	3.1624	.4	.3	61.7	.0213	3112.9 +/-375.0
975	647.81	23.1120	1.2900	.6	.5	41.4	.0208	1086.2 +/-132.4
1000	422.59	36.9378	.7189	1.2	.9	50.4	.0129	917.3 +/- 54.4
1010	343.54	43.6750	.5058	1.3	1.0	57.5	.0109	867.7 +/- 43.9
1025	297.92	38.4257	.4159	1.6	1.2	59.8	.0124	795.8 +/- 34.1
1045	167.18	39.0520	.1290	10.9	8.4	79.1	.0122	622.1 +/- 6.4
1065	142.25	39.7148	.0954	39.7	30.5	82.4	.0120	561.8 +/- 5.3
1075	129.13	39.8260	.0867	34.1	26.1	82.6	.0119	517.9 +/- 4.8
1085	136.16	39.8164	.1116	11.9	9.1	78.1	.0119	516.6 +/- 6.2
1110	173.85	39.3110	.2218	3.3	2.5	64.1	.0121	537.8 +/- 21.4
1120	143.56	38.3680	.1224	4.7	3.6	76.9	.0124	533.2 +/- 9.2
1125	132.99	38.5350	.0882	5.7	4.4	82.7	.0123	531.4 +/- 6.5
1135	143.28	38.8810	.1195	4.1	3.2	77.5	.0122	536.1 +/- 21.5
FUSE	147.58	38.7640	.0675	9.5	7.3	88.6	.0123	616.2 +/- 7.8
TOTAL				130.5	100.0			599.20

TEMP C	40AR/ 39AR	37AR/ 39AR	36AR/ 39AR	MOLES 39AR	39AR %TOTAL	%40AR RAD	K/ CA	APPARENT AGE Ma
		T85_4F		(E-14)			J= .003783	
890	7619.50	10.7500	1.6970	1.0	.7	93.4	.0452	6021.2 +/-146.0
940	1729.00	19.2170	.7170	1.2	.9	87.8	.0251	3466.1 +/- 36.8
975	302.95	22.7890	.1326	5.4	3.8	87.7	.0211	1270.4 +/- 11.7
1000	216.46	23.0470	.0524	28.8	20.6	93.7	.0209	1041.0 +/- 8.2
1010	205.70	23.1940	.0467	24.0	17.1	94.2	.0208	1005.4 +/- 7.8
1025	208.60	23.4470	.0469	14.0	10.0	94.3	.0205	1017.0 +/- 8.2
1030	202.90	24.5600	.0451	9.8	7.0	94.4	.0196	997.4 +/- 8.4
1040	207.96	26.1000	.0455	5.7	4.1	94.5	.0184	1018.5 +/- 9.7
1050	205.90	26.1800	.0471	6.5	4.6	94.3	.0183	1008.5 +/- 8.6
1060	228.89	26.8200	.0946	1.6	1.1	88.7	.0179	1044.4 +/- 16.3
1070	204.30	26.8200	.0619	2.3	1.6	92.1	.0179	985.1 +/- 10.9
1080	216.73	26.3370	.0266	10.4	7.4	97.3	.0182	1074.7 +/- 8.8
1090	217.96	24.2800	.0247	13.4	9.6	97.5	.0198	1079.6 +/- 9.1
1100	205.18	23.4800	.0290	10.9	7.8	96.7	.0205	1024.3 +/- 8.7
1125	211.50	23.6300	.0665	1.5	1.1	91.6	.0204	1005.6 +/- 20.0
FUSE	252.67	23.8400	.2116	3.4	2.4	76.0	.0202	999.0 +/- 16.0
TOTAL				140.0	100.0			1094.71

TEMP C	40AR/ 39AR	37AR/ 39AR	36AR/ 39AR	MOLES 39AR	39AR %TOTAL	%40AR RAD	K/ CA	APPARENT AGE Ma
		T85_28A		(E-14)			J= .004478	
890	1339.51	8.7819	.9742	2.1	.6	78.6	.0554	3153.7 +/- 49.2
940	477.50	13.1750	.6128	8.3	2.1	62.3	.0368	1537.8 +/- 36.1
975	157.59	18.2110	.1795	5.1	1.3	67.3	.0265	708.8 +/- 9.5
1000	116.91	25.1270	.1031	5.2	1.3	75.7	.0191	611.8 +/- 10.5
1005	103.12	23.9140	.0834	6.1	1.6	77.9	.0201	563.4 +/- 16.8
1010	88.95	22.8990	.0472	14.1	3.6	86.4	.0210	541.5 +/- 6.6
1015	84.80	21.5460	.0373	22.4	5.8	89.0	.0224	532.9 +/- 5.4
1025	82.32	20.6870	.0297	39.0	10.1	91.3	.0233	530.7 +/- 5.1
1032	81.47	19.5990	.0299	34.0	8.8	91.1	.0246	524.3 +/- 5.1
1040	82.48	18.4226	.0257	36.5	9.4	92.6	.0262	537.0 +/- 5.2
1045	87.38	17.7847	.0303	22.5	5.8	91.4	.0272	557.8 +/- 7.1
1050	93.63	17.8040	.0474	6.8	1.8	86.5	.0272	565.0 +/- 8.8
1060	96.83	19.3106	.0690	3.7	1.0	80.5	.0250	547.1 +/- 12.9
1080	76.96	19.2070	.0265	12.6	3.3	91.8	.0251	502.2 +/- 5.8
1100	78.97	18.6040	.0297	42.5	11.0	90.7	.0260	508.3 +/- 4.9
1120	75.95	18.2930	.0115	93.3	24.1	97.4	.0264	522.7 +/- 4.6
FUSE	79.18	18.1995	.0182	33.0	8.5	95.0	.0266	530.2 +/- 5.8
TOTAL				387.2	100.0			568.14

TEMP C	40AR/ 39AR	37AR/ 39AR	36AR/ 39AR	MOLES 39AR	39AR %TOTAL	%40AR RAD	K/ CA	APPARENT AGE Ma
		T85_28C		(E-14)			J= .004468	
890	1170.88	6.0672	.7652	2.3	.3	80.7	.0804	2989.0 +/- 23.0
940	414.11	6.0330	.3650	2.3	.3	74.1	.0809	1561.7 +/- 30.1
975	195.42	10.0217	.2337	3.7	.4	65.1	.0485	816.4 +/- 9.1
1000	157.91	18.5336	.1065	10.6	1.3	81.0	.0261	824.7 +/- 10.2
1005	95.34	11.3816	.0976	15.4	1.8	70.7	.0427	478.3 +/- 6.6
1010	73.82	9.1246	.0430	32.9	3.9	83.7	.0533	442.7 +/- 4.3
1015	65.49	8.6362	.0213	72.9	8.7	91.4	.0564	430.1 +/- 4.3
1025	62.53	8.4669	.0140	97.2	11.5	94.4	.0575	424.8 +/- 4.0
1030	64.97	8.4828	.0209	47.9	5.7	91.5	.0574	427.4 +/- 4.3
1040	65.54	8.3582	.0237	37.0	4.4	90.3	.0583	425.6 +/- 4.8
1065	61.49	8.1248	.0110	93.0	11.1	95.7	.0599	423.5 +/- 3.9
1085	62.15	8.6146	.0117	90.8	10.8	95.5	.0565	426.8 +/- 5.9
1110	59.94	8.4555	.0080	159.6	19.0	97.1	.0576	419.4 +/- 3.9
1125	60.86	8.1932	.0086	98.5	11.7	96.9	.0594	424.2 +/- 3.9
FUSE	62.85	8.1097	.0121	77.2	9.2	95.3	.0601	430.1 +/- 4.1
TOTAL				841.2	100.0			443.35

APPENDIX E2:

^{40}Ar-^{39}Ar RELEASE SPECTRA EFJORD-SINIS AREA

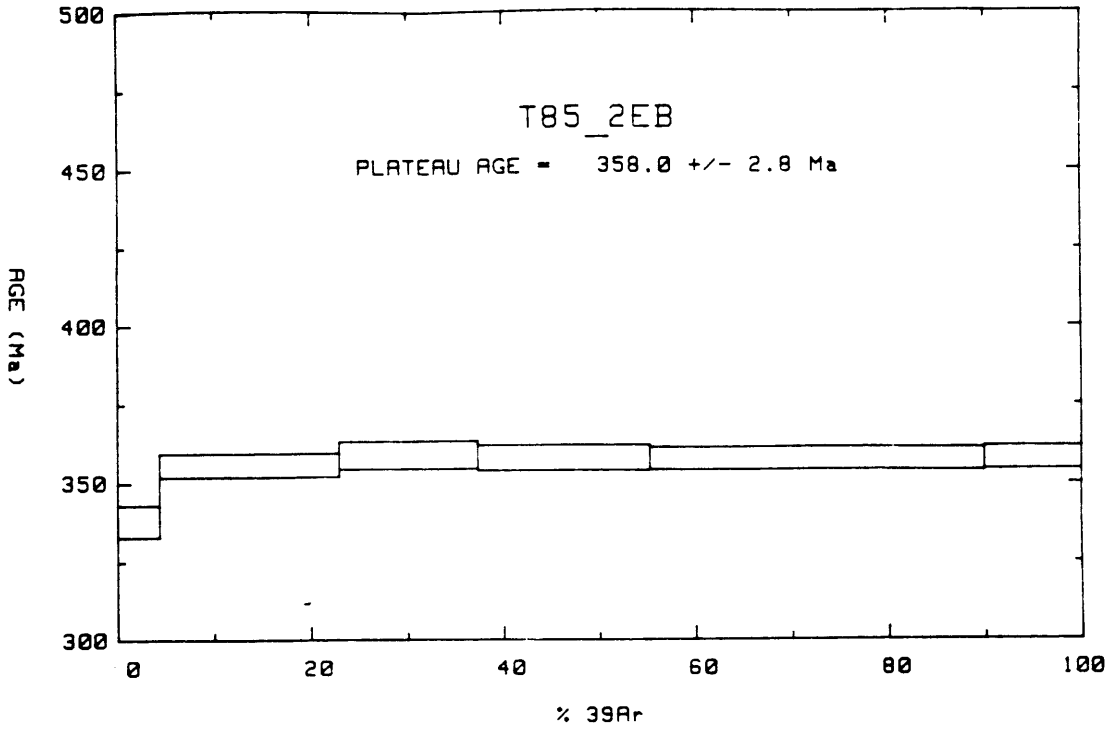
T85_2EB
PLATEAU AGE = 358.0 +/- 2.8 Ma
AGE (Ma)
500
450
400
350
300
0
20
40
60
80
100
% 39Ar

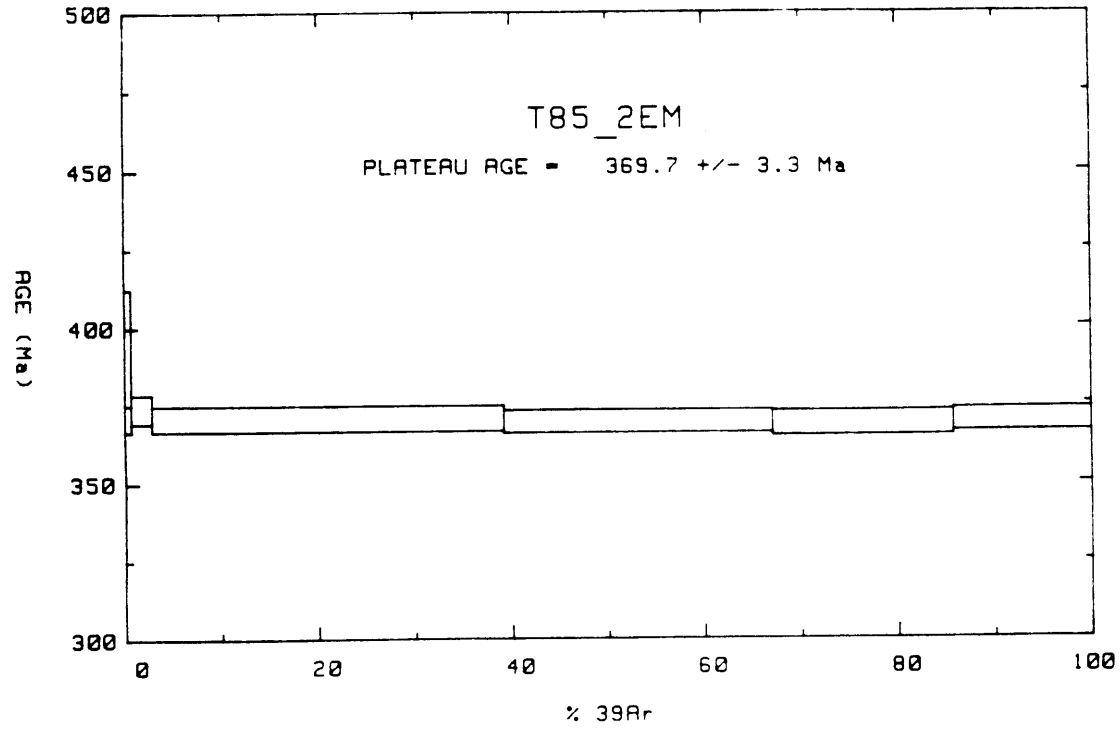
T85_2EM
PLATEAU AGE = 369.7 +/- 3.3 Ma
AGE (Ma)
500
450
400
350
300
0
20
40
60
80
100
% 39Ar

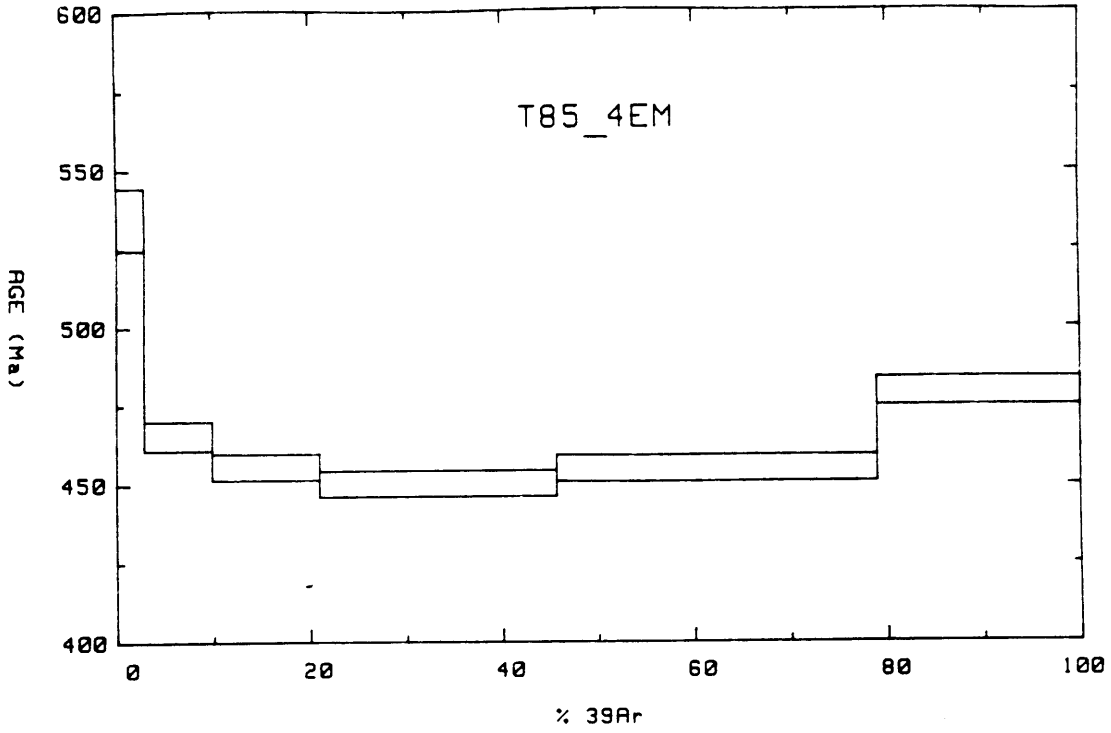
T85_4EM
600
550
500
450
400
AGE (Ma)
0
20
40
60
80
100
% 39Ar

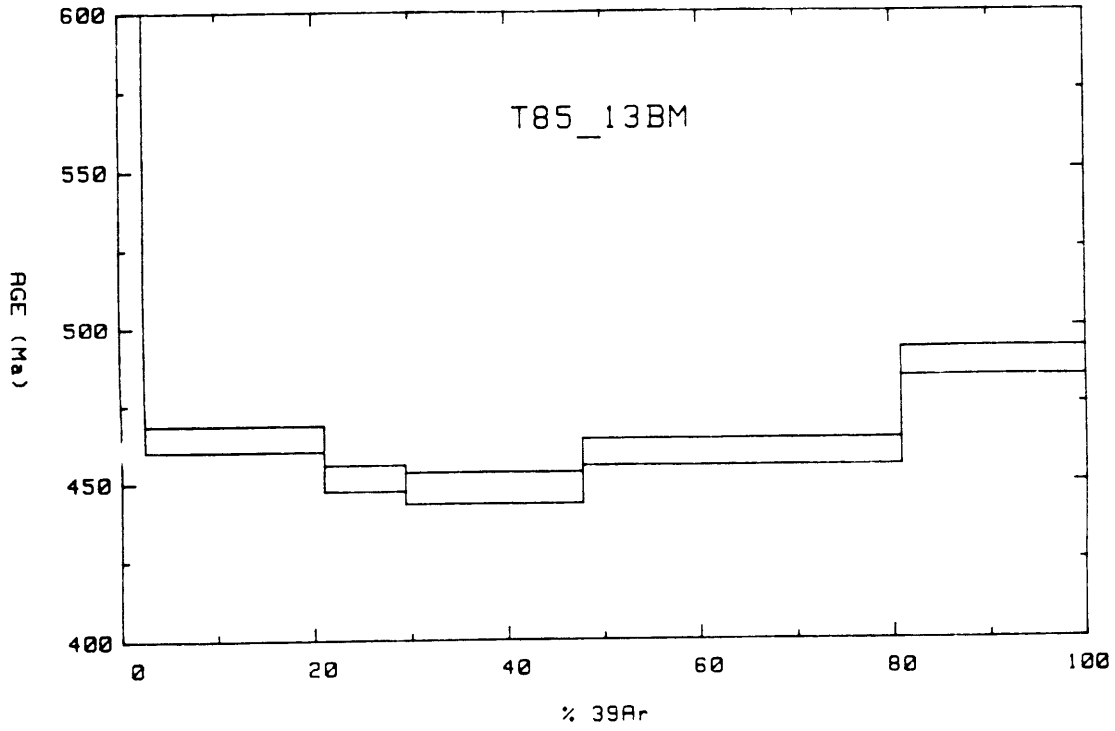
T85_13BM
600
550
500
450
400
AGE (Ma)
0
20
40
60
80
100
% 39Ar

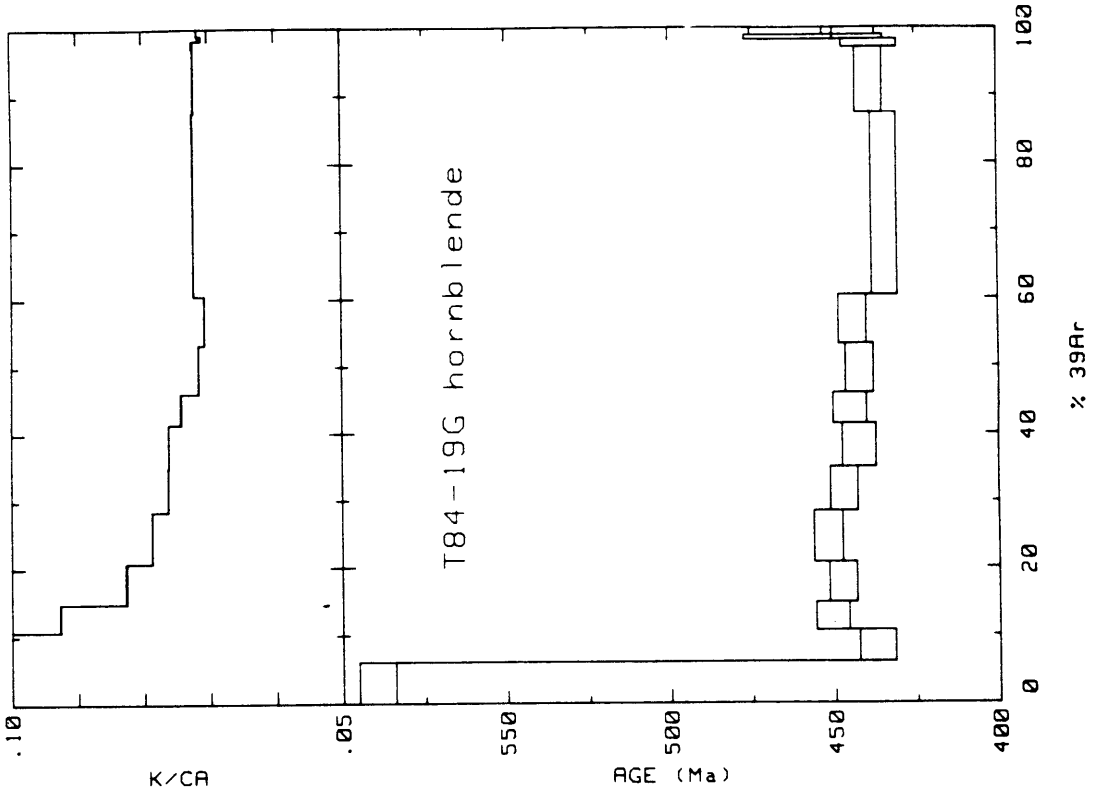
T84-19G hornblende
.10
.05
K/CA
550
500
450
400
AGE (Ma)
0
20
40
60
80
100
% 39Ar

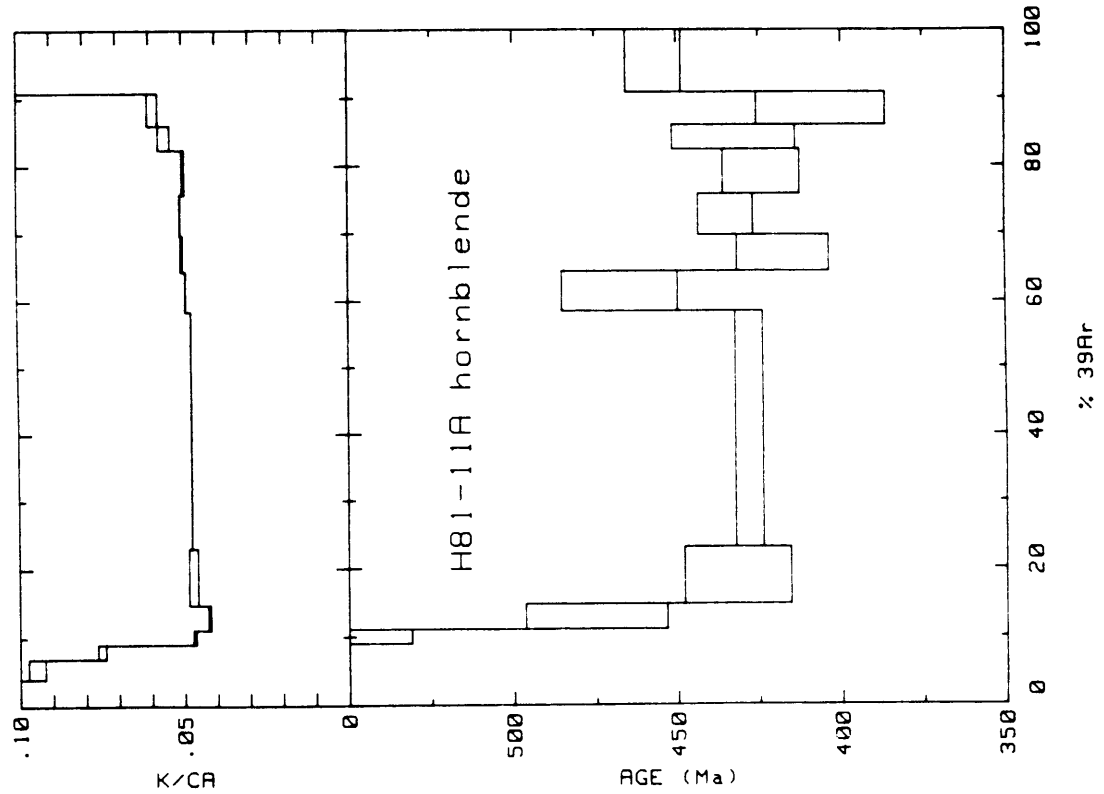
H81-11A hornblende
.10
.05
0
K/CA
500
450
400
350
AGE (Ma)
0
20
40
60
80
100
% 39Ar

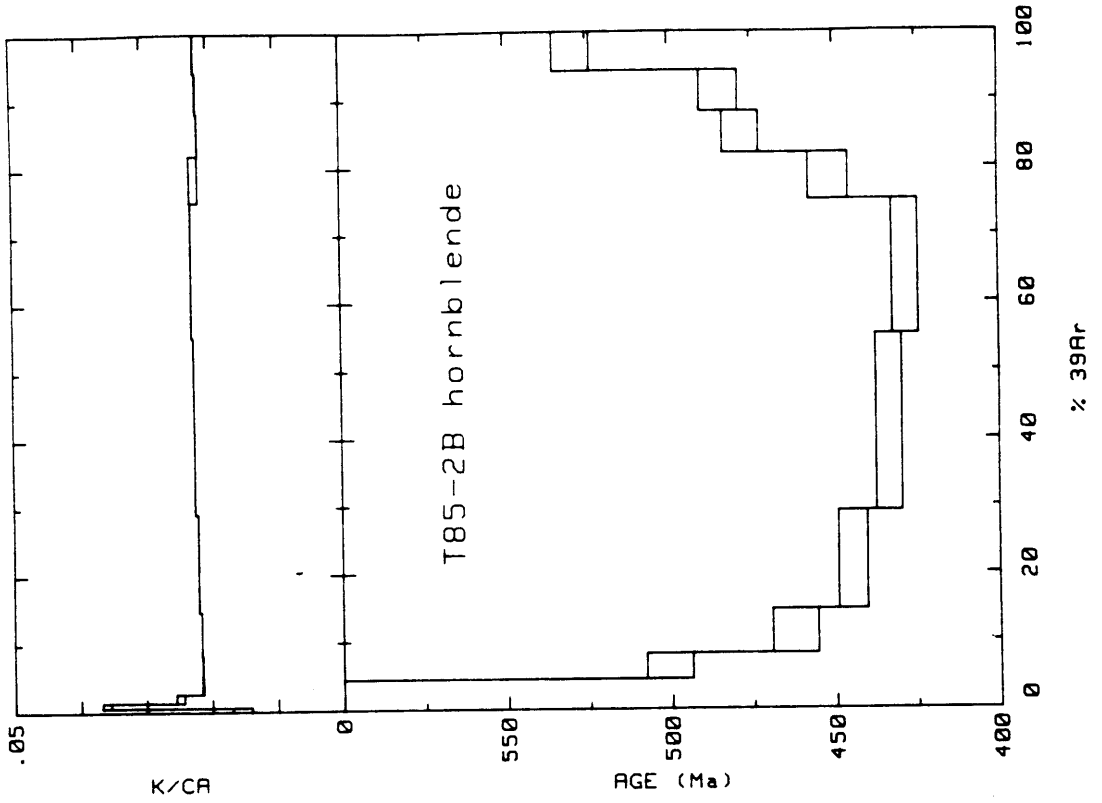
T85-2B hornblende
.05
0
K/CA
550
500
450
400
AGE (Ma)
0
20
40
60
80
100
% 39Ar

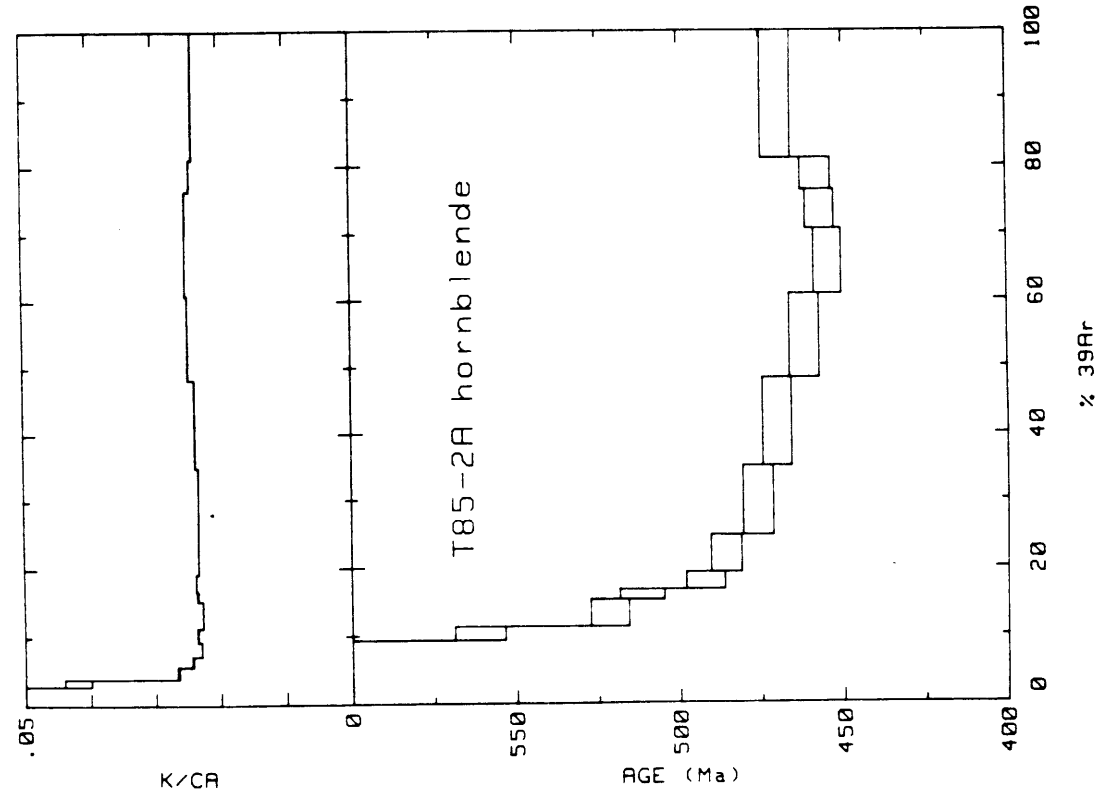
T85-2A hornblende
.05
0
K/CA
550
500
450
400
AGE (Ma)
0
20
40
60
80
100
% 39Ar

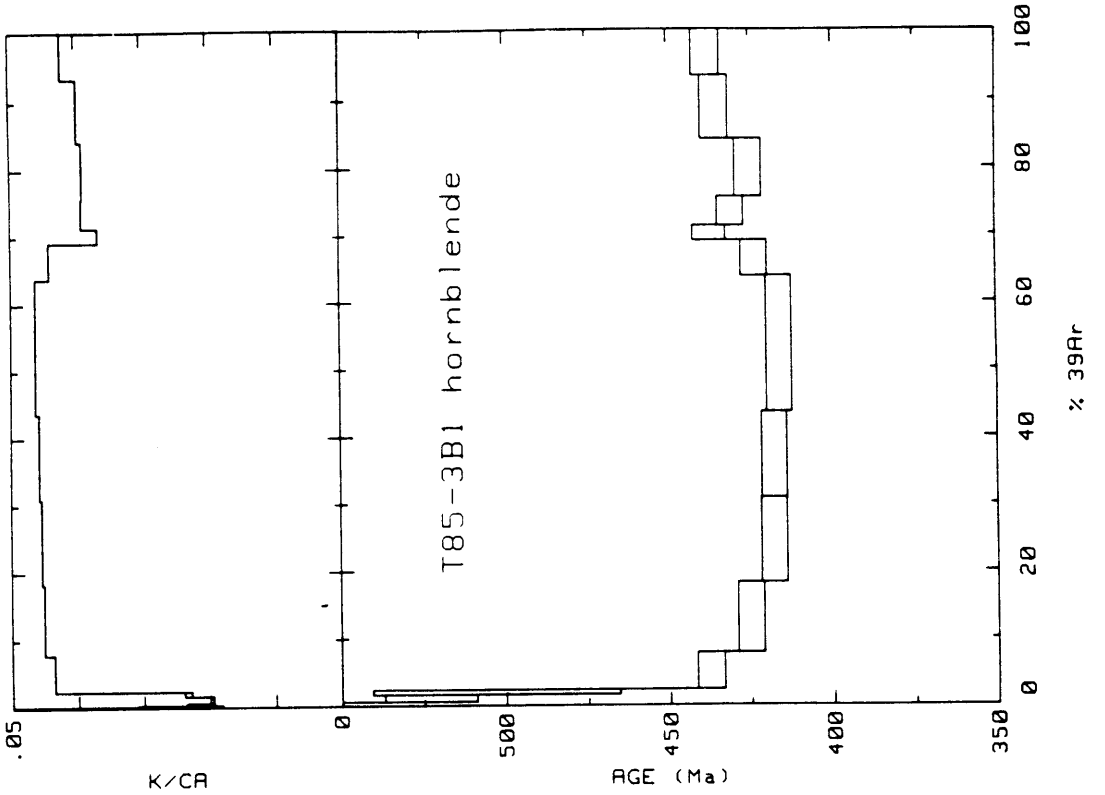
T85-3B1 hornblende
.05
0
K/CA
500
450
400
350
AGE (Ma)
0
20
40
60
80
100
% 39Ar

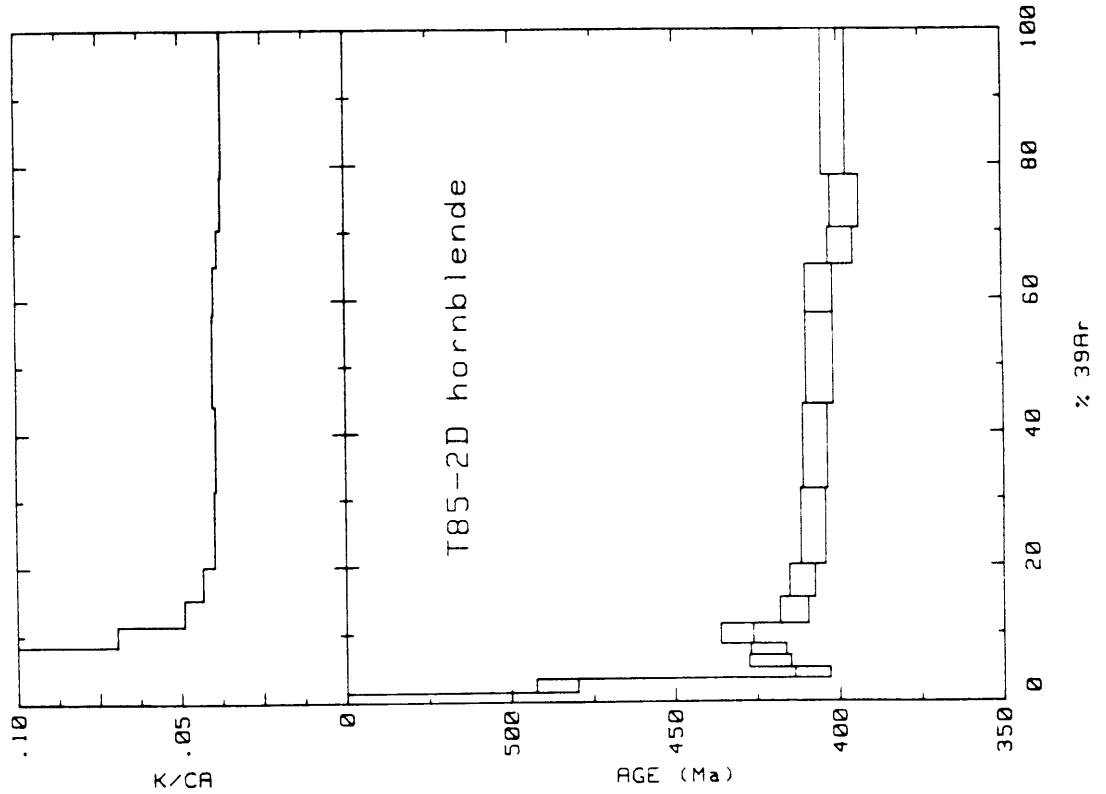
T85-2D hornblende
.10
.05
0
K/CA
500
450
400
350
AGE (Ma)
0
20
40
60
80
100
% 39Ar

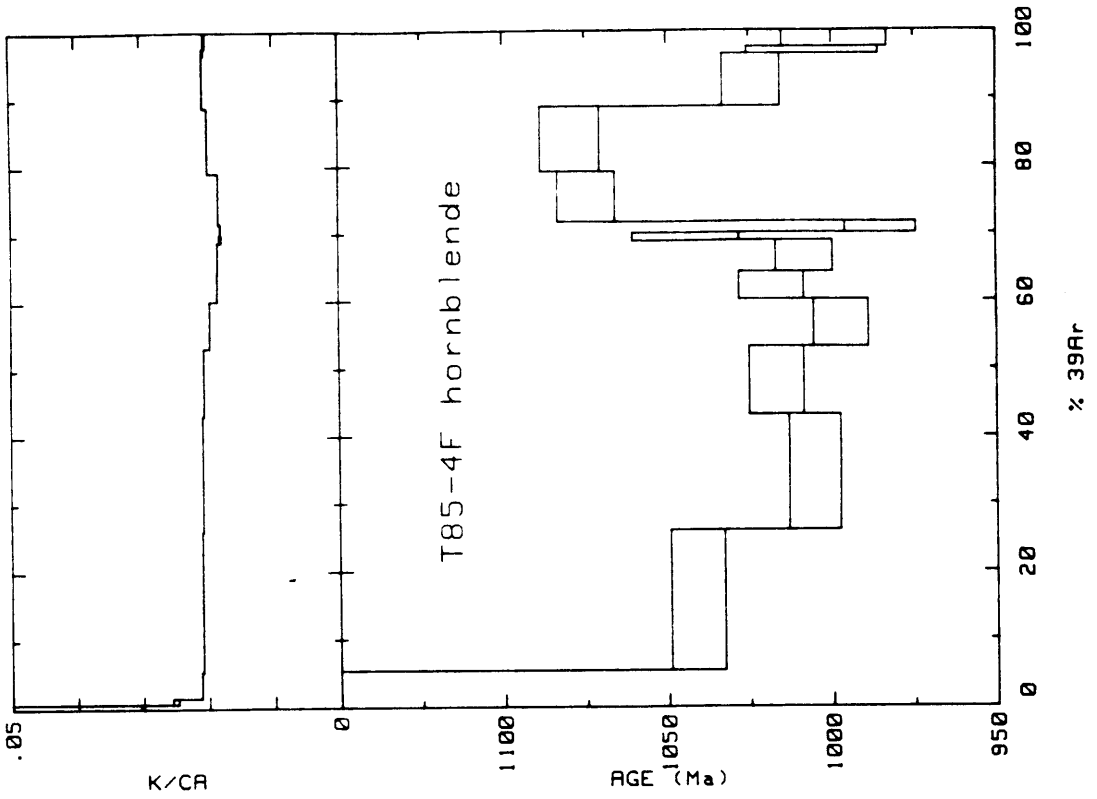
T85-4F hornblende
.05
0
K/CA
1100
1050
1000
950
AGE (Ma)
0
20
40
60
80
100
% 39Ar

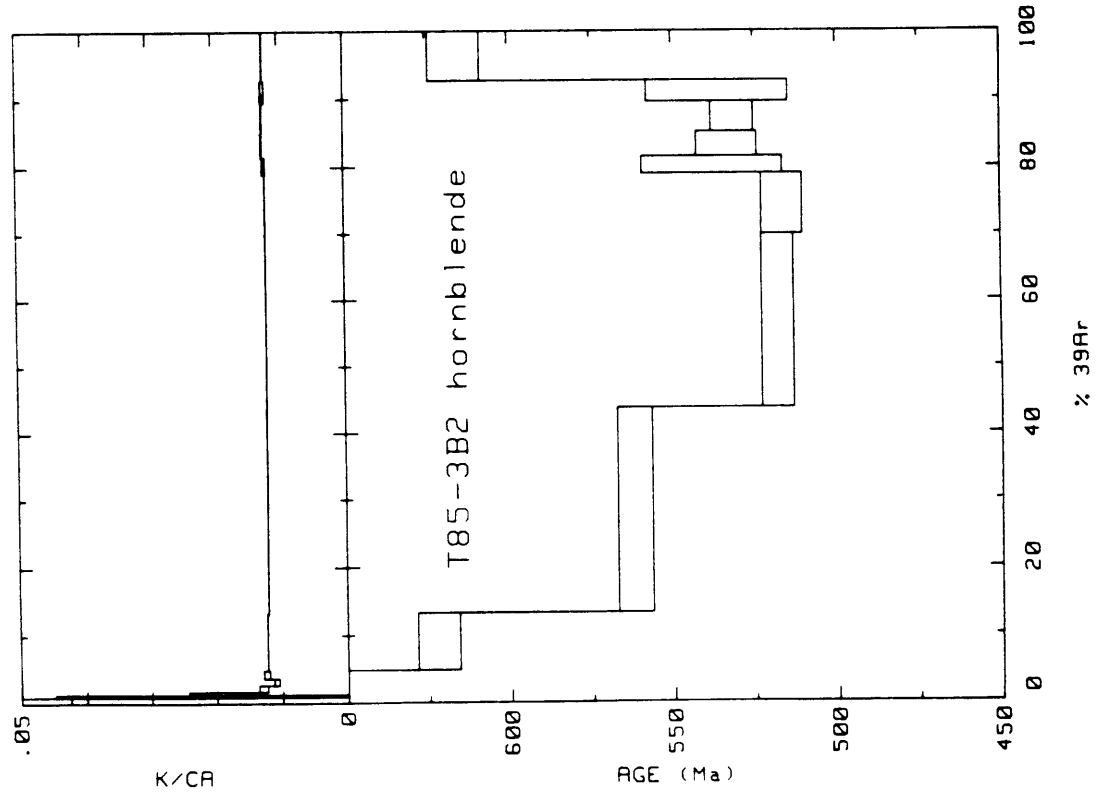
T85-3B2 hornblende
.05
0
K/CA
600
550
500
450
AGE (Ma)
0
20
40
60
80
100
% 39Ar

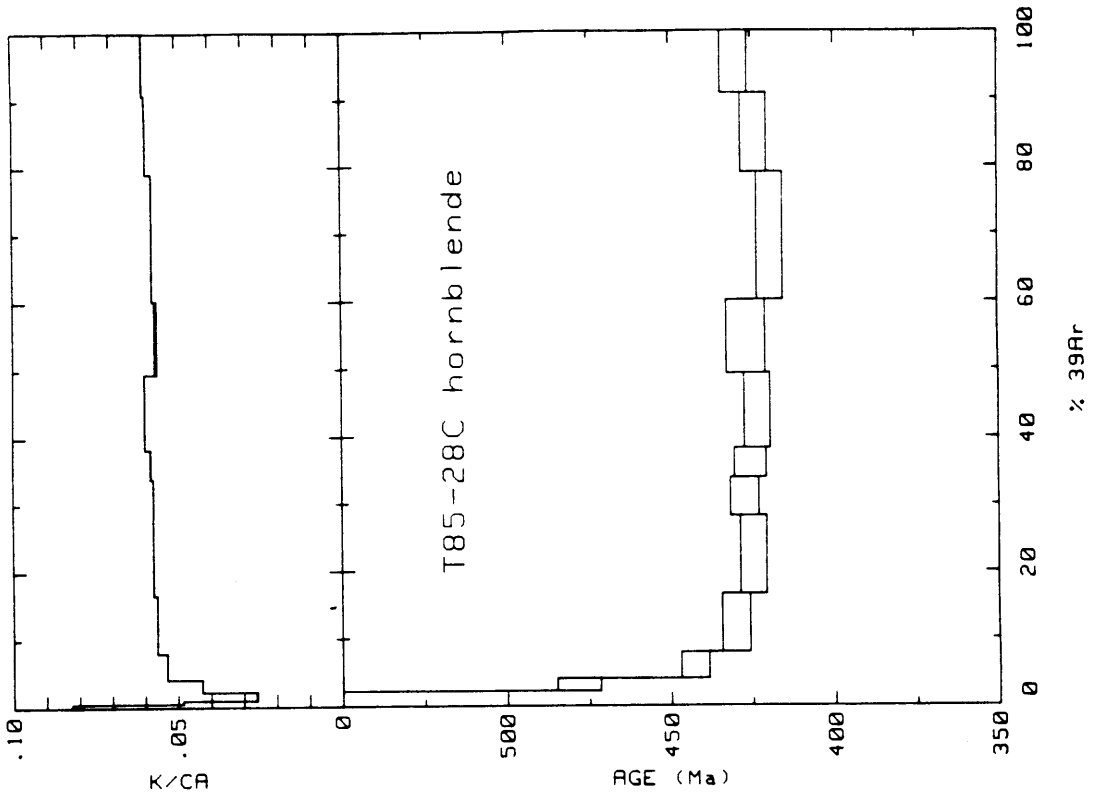
T85-28C hornblende
.10
.05
0
K/CA
500
450
400
350
AGE (Ma)
0
20
40
60
80
100
% 39Ar

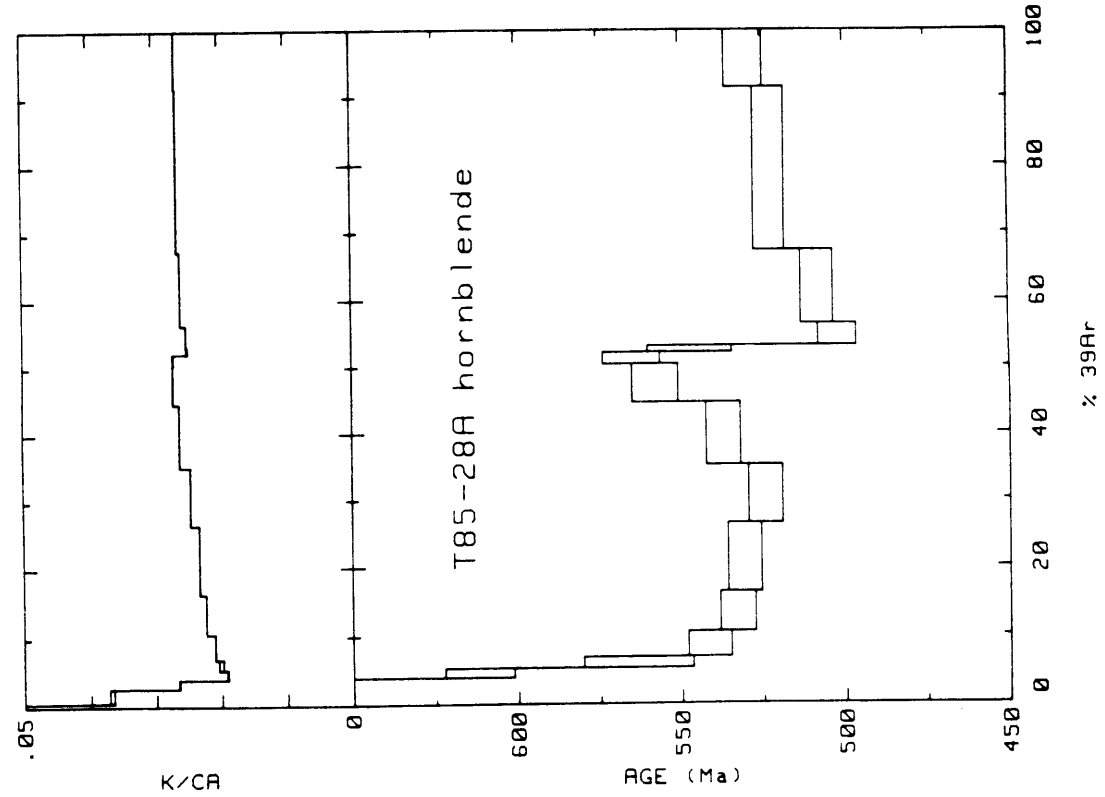
T85-28A hornblende
.05
0
K/CA
600
550
500
450
AGE (Ma)
0
20
40
60
80
100
% 39Ar

APPENDIX E3:

^{40}Ar-^{39}Ar ISOTOPE CORRELATION PLOTS EFJORD-SINIS AREA

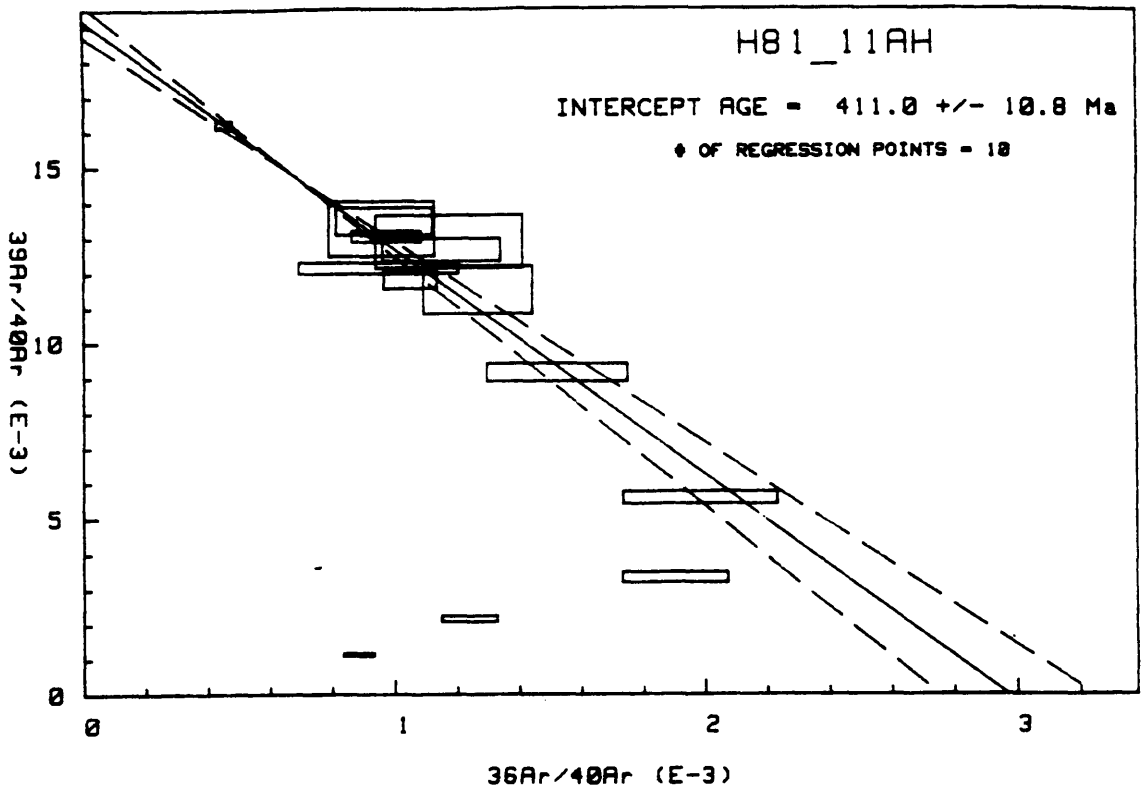
H81_11AH
INTERCEPT AGE = 411.0 +/- 10.8 Ma
OF REGRESSION POINTS = 10
39Ar/40Ar (E-3)
36Ar/40Ar (E-3)
0
5
10
15
0
1
2
3

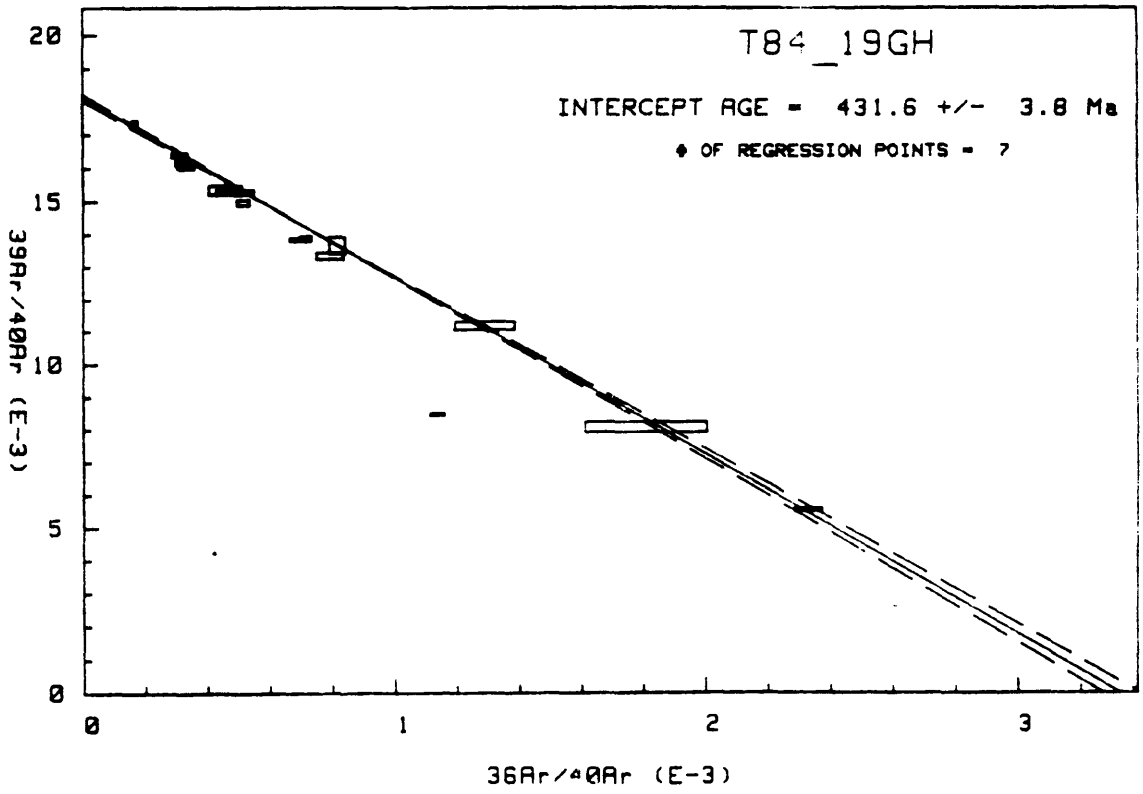
T84_19GH
INTERCEPT AGE = 431.6 +/- 3.8 Ma
OF REGRESSION POINTS = 7
39Ar/40Ar (E-3)
36Ar/40Ar (E-3)
0
5
10
15
20
0
1
2
3

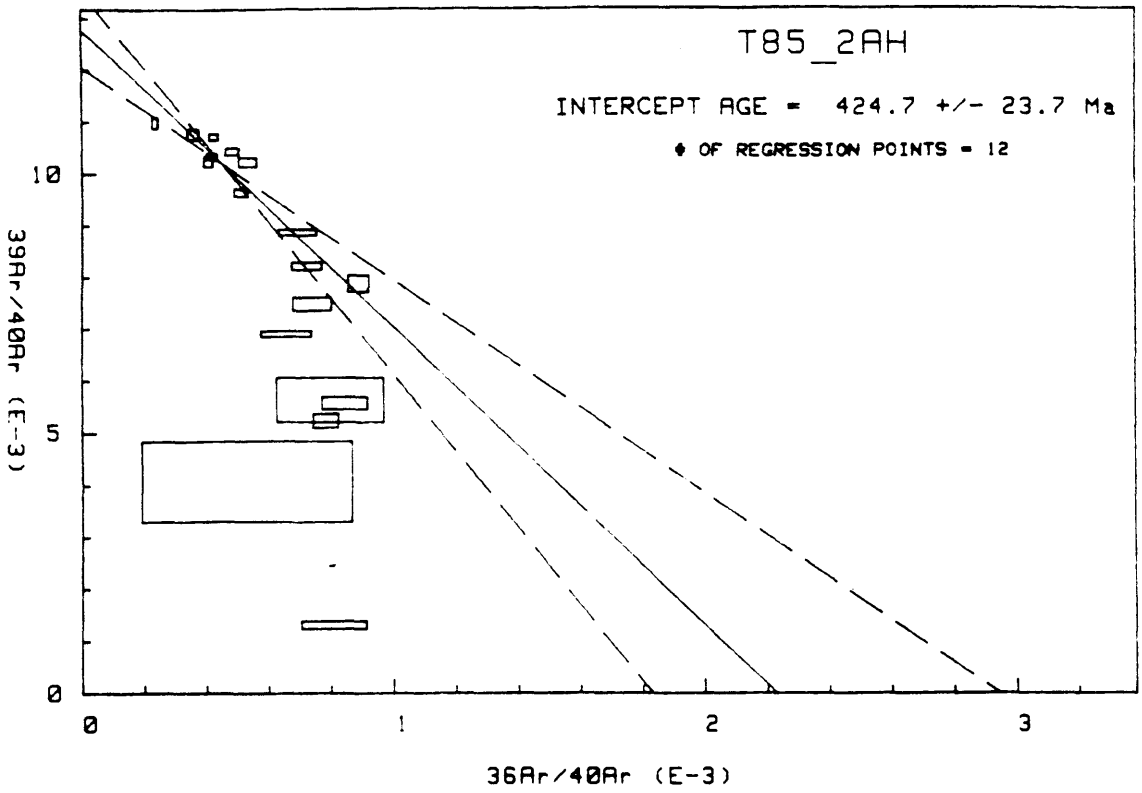
T85_2AH
INTERCEPT AGE = 424.7 +/- 23.7 Ma
OF REGRESSION POINTS = 12
39Ar/40Ar (E-3)
36Ar/40Ar (E-3)
0
5
10
0
1
2
3

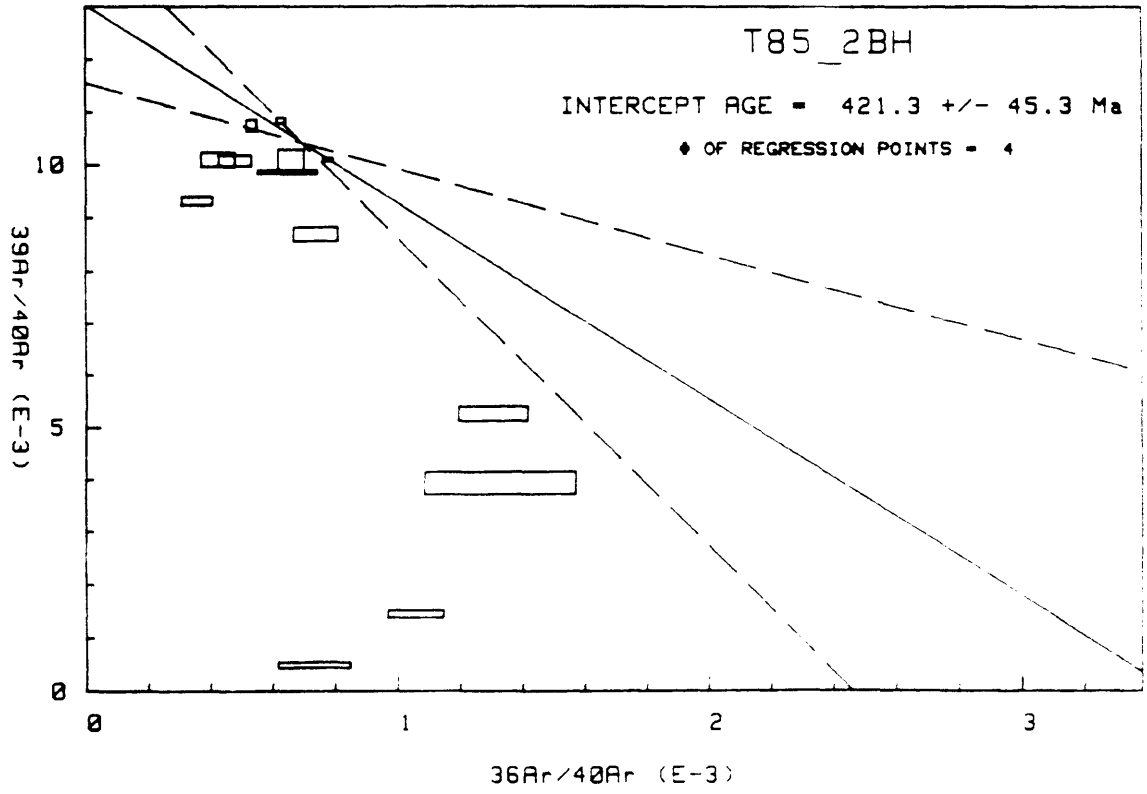
T85_2BH
INTERCEPT AGE = 421.3 +/- 45.3 Ma
OF REGRESSION POINTS = 4
39Ar/40Ar (E-3)
36Ar/40Ar (E-3)
0
5
10
0
1
2
3

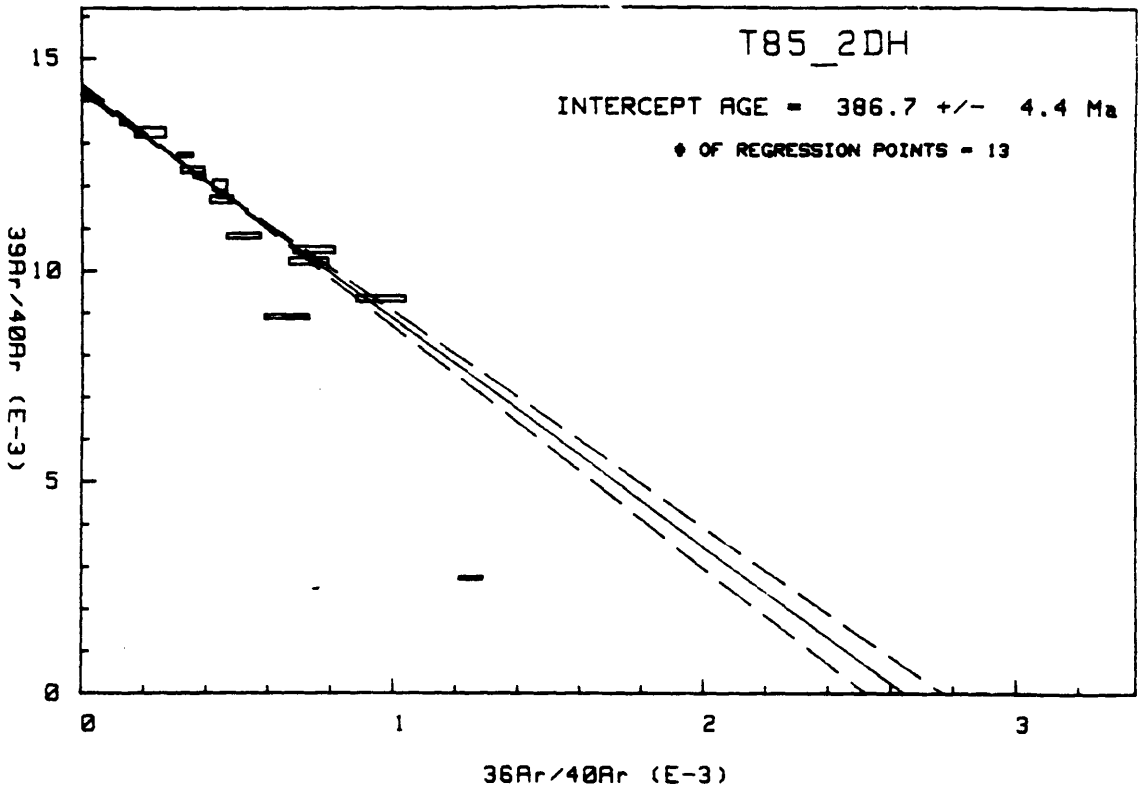
T85_2DH
INTERCEPT AGE = 386.7 +/- 4.4 Ma
OF REGRESSION POINTS = 13
39Ar/40Ar (E-3)
36Ar/40Ar (E-3)
0
5
10
15
0
1
2
3

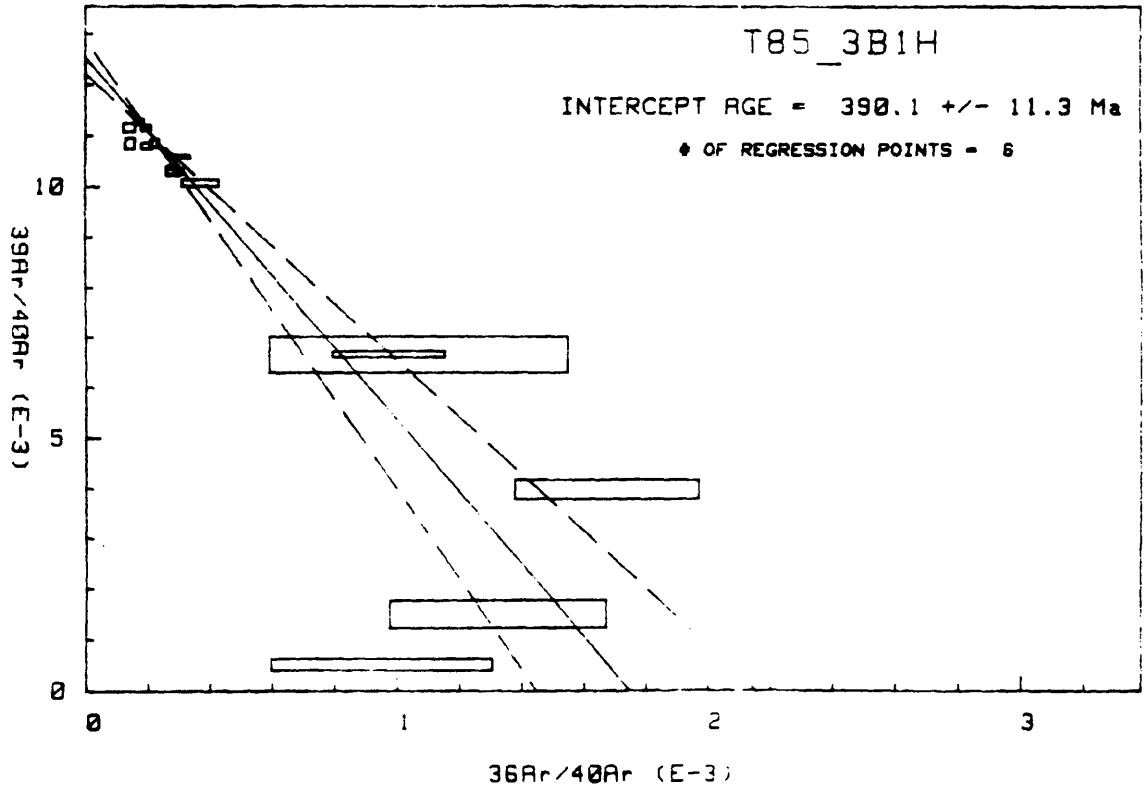
T85_3B1H
INTERCEPT AGE = 390.1 +/- 11.3 Ma
OF REGRESSION POINTS = 6
39Ar/40Ar (E-3)
36Ar/40Ar (E-3)
0
5
10
0
1
2
3

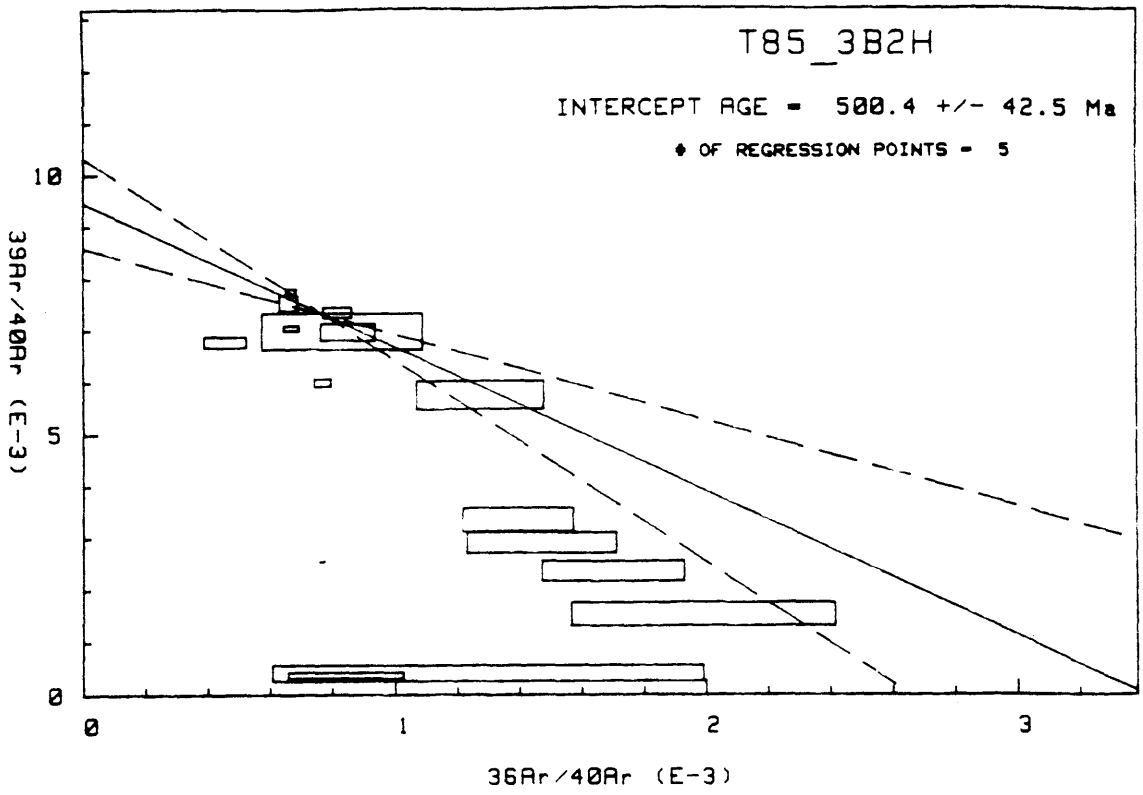
T85_3B2H
INTERCEPT AGE = 500.4 +/- 42.5 Ma
OF REGRESSION POINTS = 5
39Ar/40Ar (E-3)
36Ar/40Ar (E-3)
0
5
10
0
1
2
3

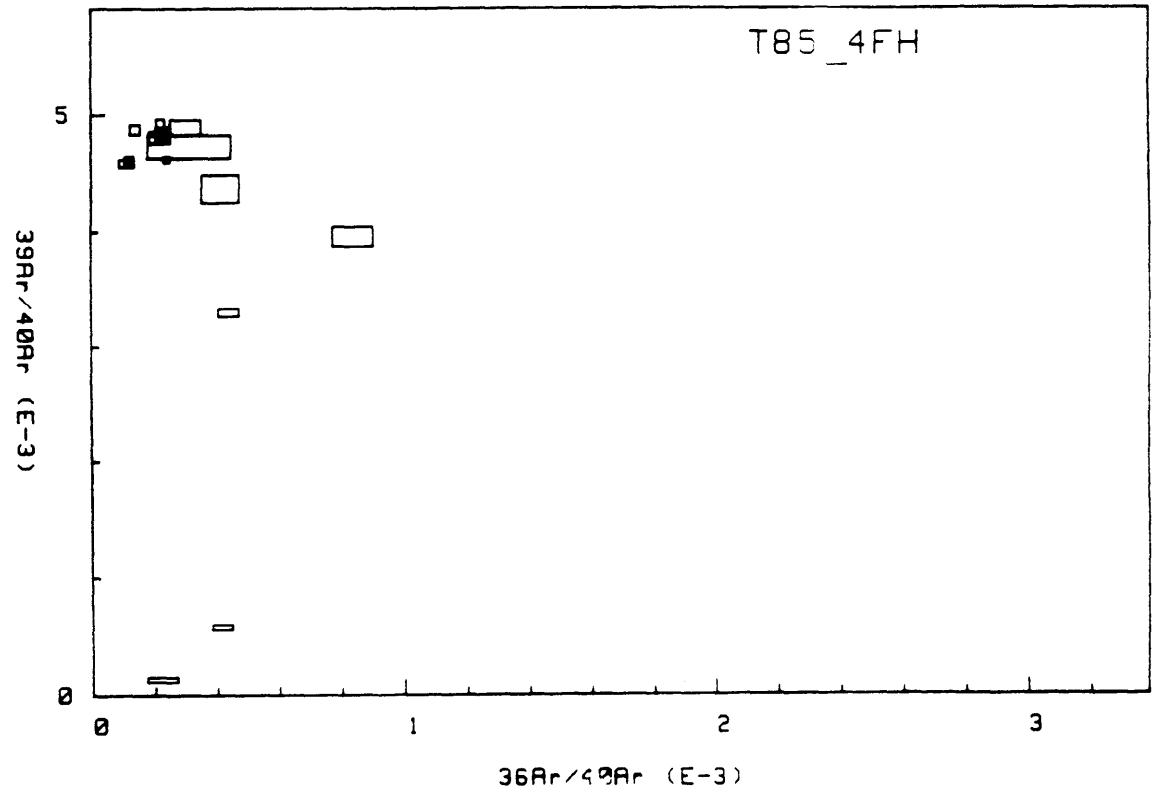
T85_4FH
39Ar/40Ar (E-3)
36Ar/40Ar (E-3)
0
5
0
1
2
3

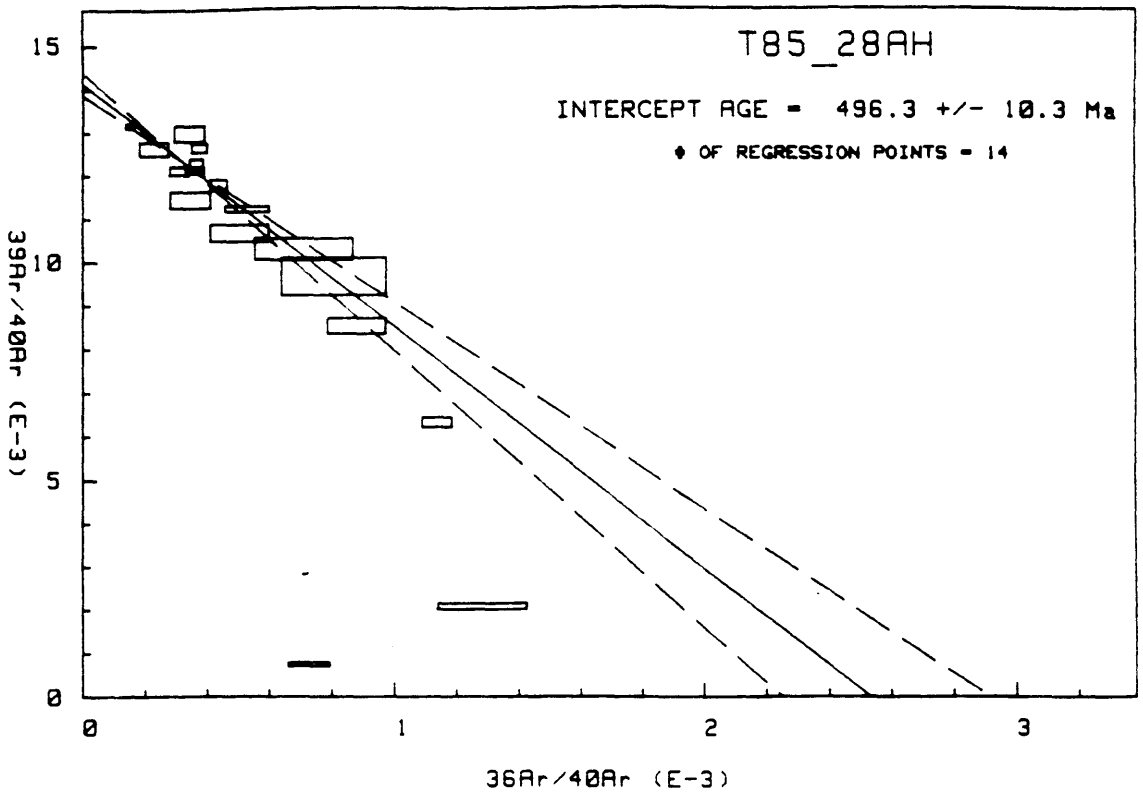
T85_28AH
INTERCEPT AGE = 496.3 +/- 10.3 Ma
OF REGRESSION POINTS = 14
39Ar/40Ar (E-3)
36Ar/40Ar (E-3)
0
5
10
15
0
1
2
3

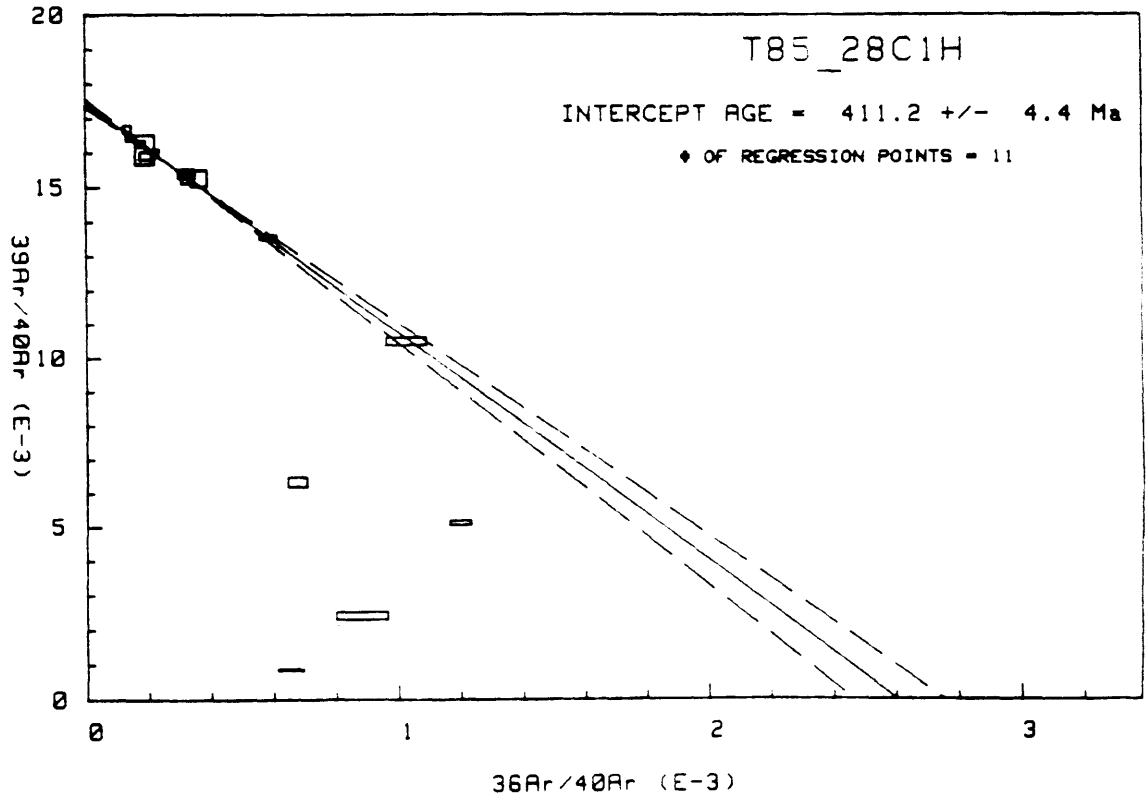
T85_28C1H
INTERCEPT AGE = 411.2 +/- 4.4 Ma
OF REGRESSION POINTS = 11
39Ar/40Ar (E-3)
36Ar/40Ar (E-3)
0
5
10
15
20
0
1
2
3

PLATE 1: GEOLOGIC MAP OF THE SITAS - SINGIS AREA, SWEDEN

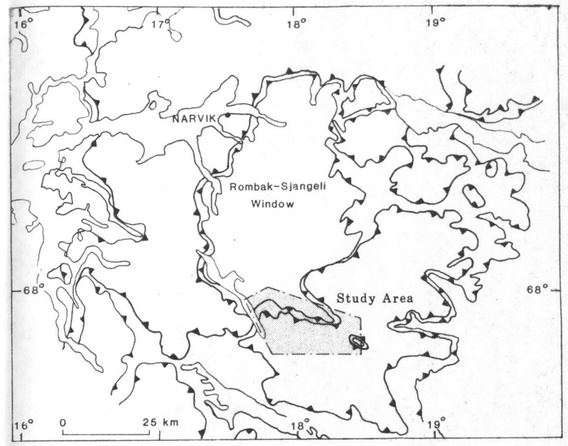

SCALE - 1:50,000

0 1 2 km

N

Geology by Peter G. Tilke

PLATE 2: N60W GEOLOGIC CROSS SECTIONS OF THE SITAS - SINGIS AREA, SWEDEN

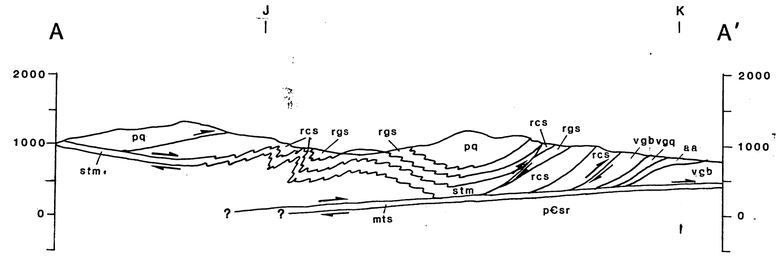

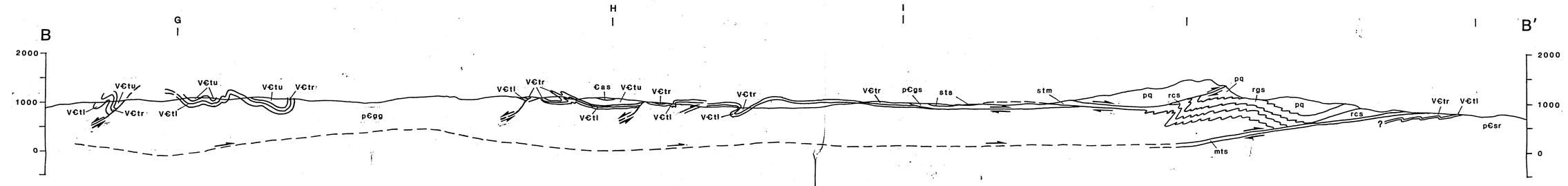

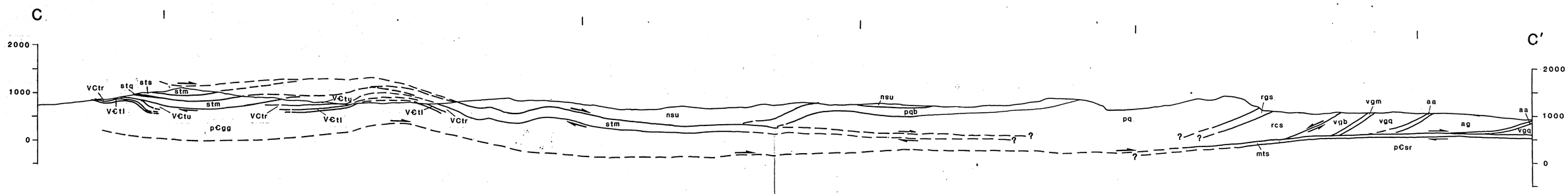

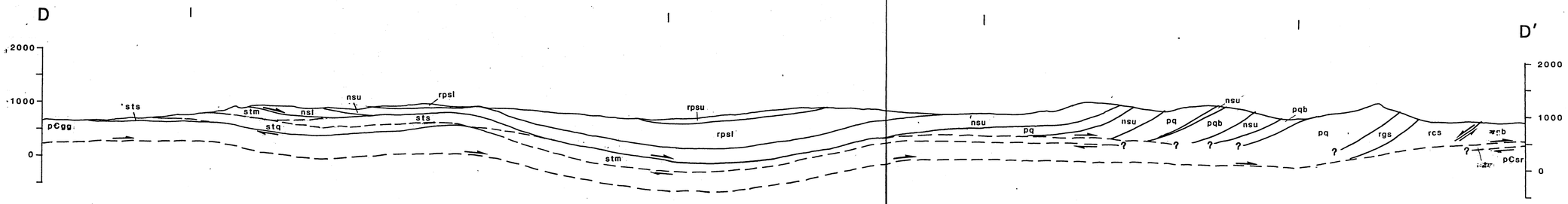

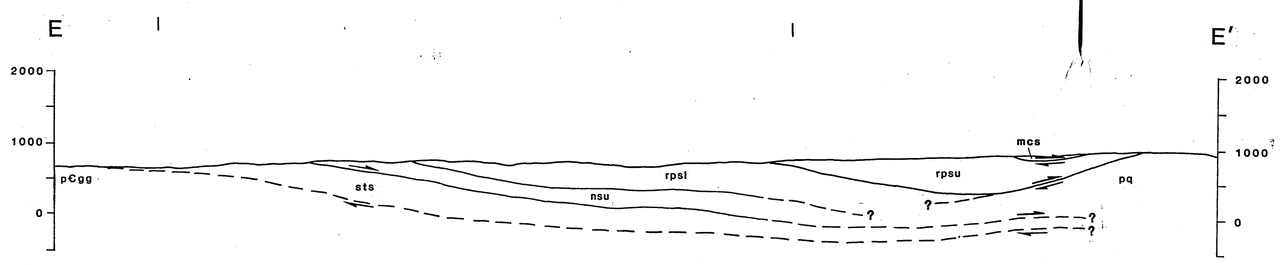

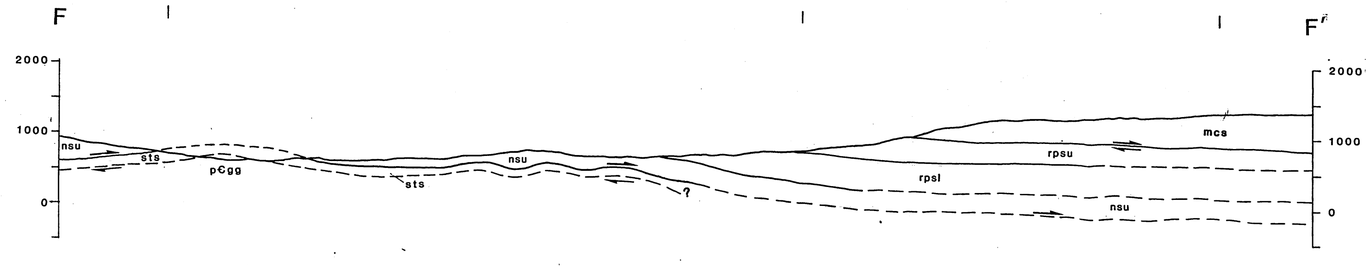

SCALE - 1:50,000

0 1 2 km

NO VERTICAL EXAGGERATION

VERTICAL SCALE: METERS ABOVE SEA LEVEL

PLATE 3: N30E GEOLOGIC CROSS SECTIONS OF THE SITAS - SINGIS AREA, SWEDEN

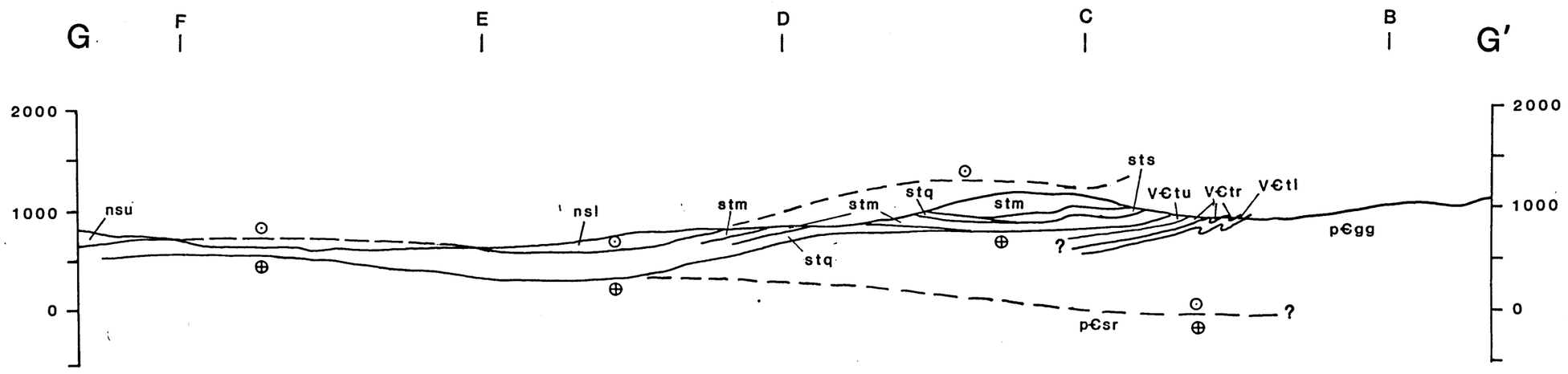

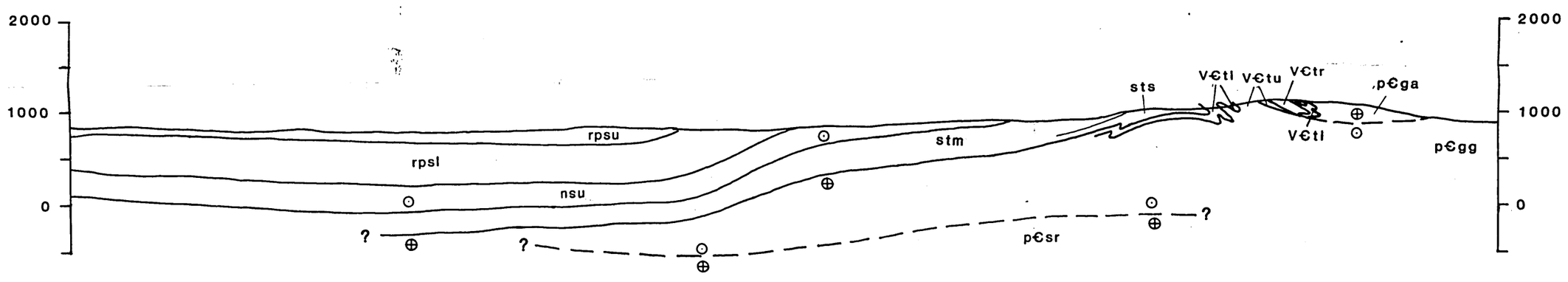

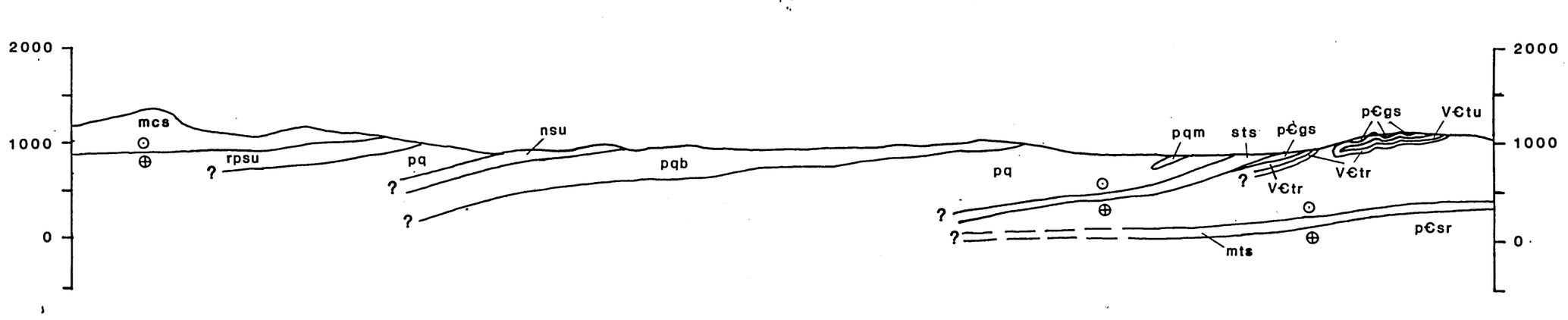

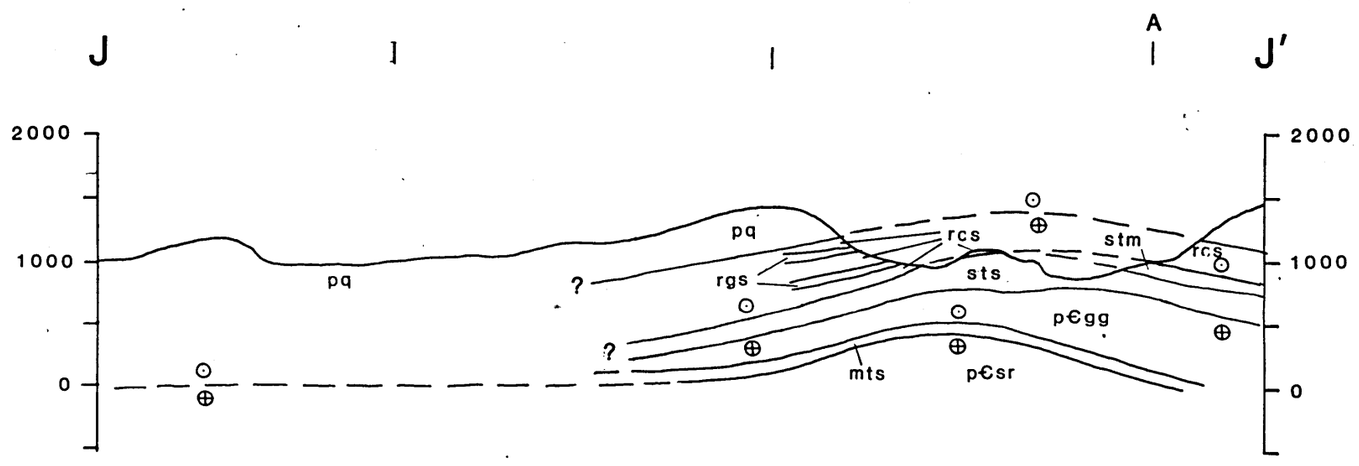

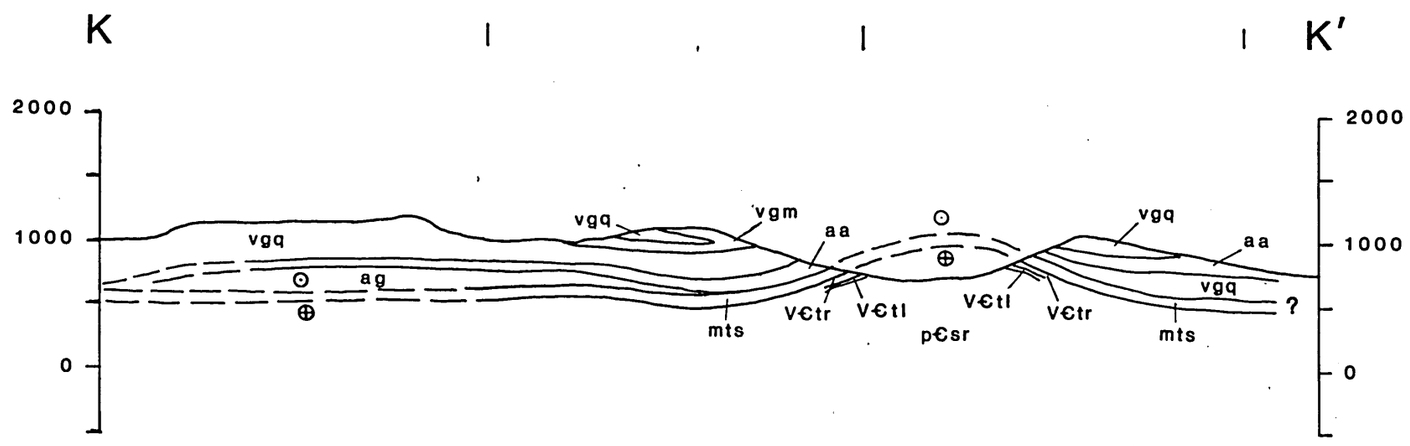

SCALE - 1:50,000

0 1 2 km

NO VERTICAL EXAGGERATION

VERTICAL SCALE: METERS ABOVE SEA LEVEL

PLATE 4: GEOLOGIC MAP OF THE KAISEJAURE AREA

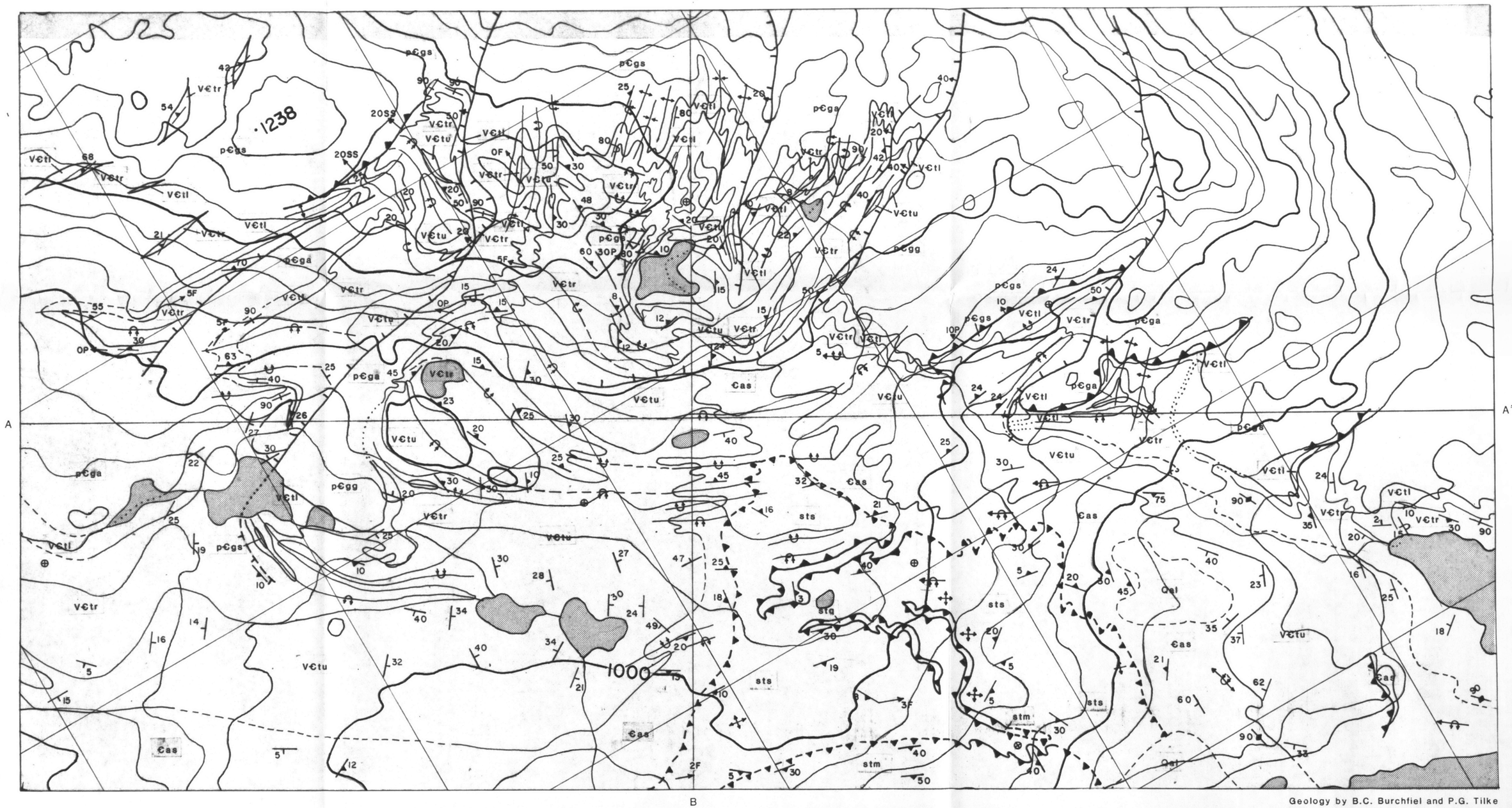

Geology by B.C. Burchfiel and P.G. Tilke

PLATE 5: GEOLOGIC CROSS SECTIONS OF THE KAISEJAURE AREA

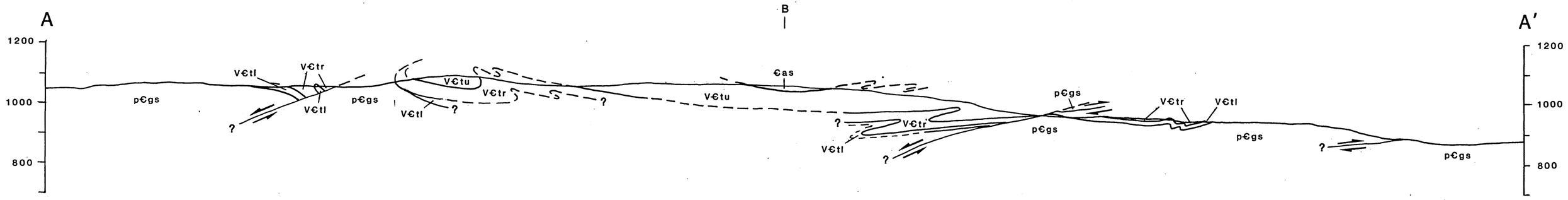

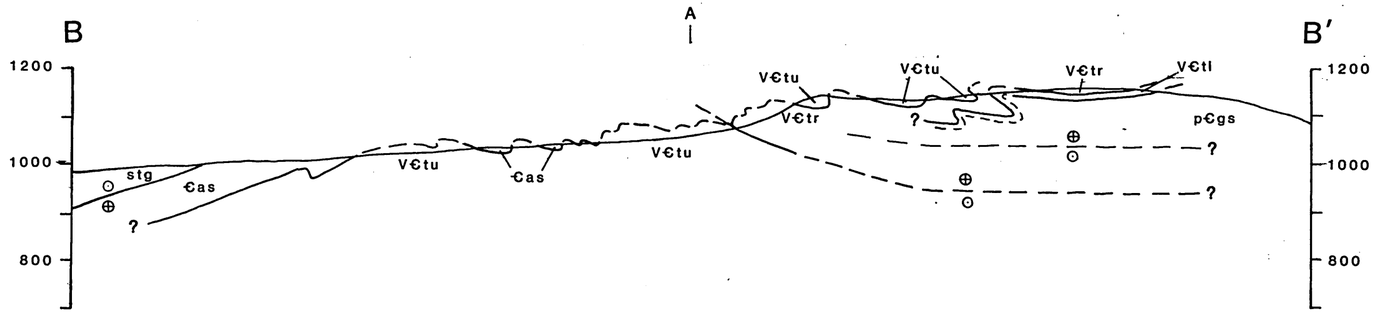

SCALE – 1:10,000

0 250 500 m

NO VERTICAL EXAGGERATION

VERTICAL SCALE: METERS ABOVE SEA LEVEL

PLATE 6: DEFORMATIONAL PHASES AND EVENTS OF THE SITAS-SINGIS AREA

Unit \ Time (Ma)	490	430	410			390	370
Rombak-Sjangeli Window			? RSd1	RSd2	RSd3-RSd5	RSd6	
Singis Window			? SWd1		SWd2		
Storrit Complex		? SCd1	? SCd2	SCd3	SCd4	SCd5	
Matert Thrust		? MTd1			MTd2		
Aurek Assemblage	AAd1		AAd2	AAd3	AAd4		AAd5
Salka Group		SGd1	SGd2	SGd3 ? SGd4	SGd5		SGd6
Litte Group		LGd1	LGd2	LGd3 ?		LGd4	
Maitat Complex	MCd1	MCd2	MCd3 ?				
Event	D1	D2	D3	D4	D5	D6	D7	D8

PLATE 7: TECTONIC MAP OF THE EFJORD – KEBNEKAISE AREA

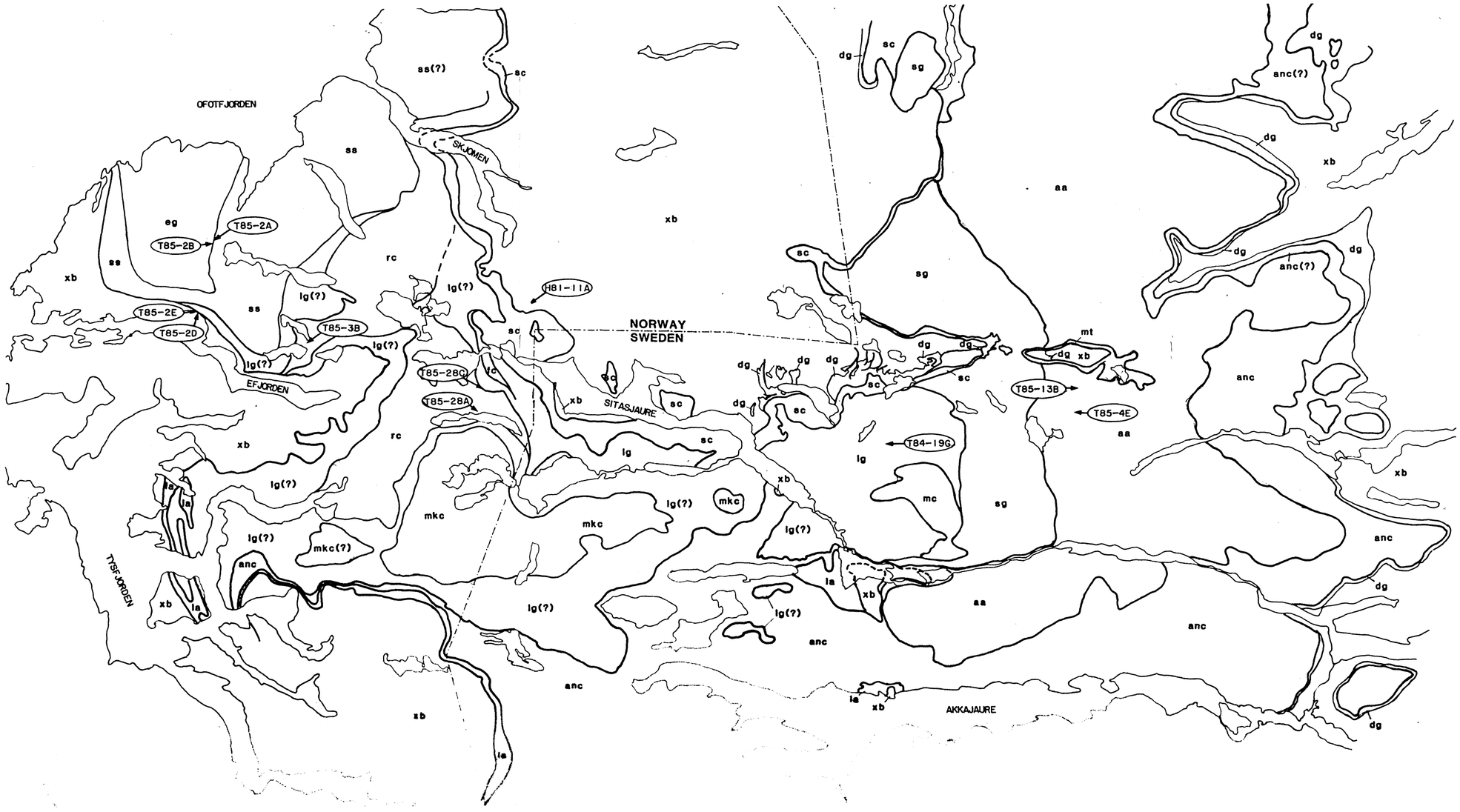

- eg — Evenes (Salangen) Group
- ss — Sjurvatnet Schist
- mkc — Marko Complex
- rc — Rauvatn Complex
- fc — Filfjell Complex
- mc — Maitat Complex
- lg — Litte Group
- sg — Salka Group
- aa — Aurek Assemblage
- anc — Akkajaure Nappe Complex
- sc — Storrit Complex
- mt — Matert shear zone
- la — Lower allochthon
- dg — Dividal Group
- xb — Crystalline basement

SCALE 1:300,000

0 15 km

Ar–Ar sample locality

PLATE 8: EXPLANATION

SYMBOLS

Depositional contact (inferred, concealed)

Thrust fault (overturned, inferred, concealed)

Normal faut (dipping 30, inferred, concealed)

Bedding (overturned)

Primary metamorphic foliation (mylonitic foliation in shear zone rocks)

Axial planar foliation

3F — Intersection lineation or fold axis

3M — Mineral lineation

3P — Stretched pebble lineation

3SS — Slickenside lineation

3 — Tight upright fold

Open anticline

Open syncline

Overturned anticline

Overturned syncline

Synformal anticline

TECTONOSTRATIGRAPHY

Qal	alluvium
mcs	Maitat complex schist
mcm	Maitat complex mafic rocks
rpsu	Rapetjakka schist – upper
rpsl	Rapetjakka schist – lower
rpsc	Rapetjakka schist – calcareous horizon
nsu	Njunjas schist – upper
nsl	Njunjas schist – lower
nsq	Njunjas schist – quartzitic horizon
nsg	Njunjas schist – graphitic horizon
nscs	Njunjas schist – calcareous horizon
pqb	Patta blue-grey quartzite
pqm	Patta quartzite – calcareous schist horizon
pq	Patta quartzite
rgs	Rusjka graphitic schist
rcs	Rusjka calcareous schist
va	Vidja amphibolite
vgb	Vidja biotite gneiss
vgm	Vidja muscovite gneiss
vgq	Vidja quartzofeldspathic gneis
aa	Aurek amphibolite
ago	Aurek olivine gabbro
ags	Aurek gabbro – sheared
ag	Aurek gabbro – massive
stm	Storrit granitic mylonite
stq	Storrit quartzitic mylonite
sts	Storrit mylonitic siltstone
mtg	Matert granitic mylonite
mts	Matert mylonitic siltstone
Cas	Alum shale
V€tu	Tornetrask Formation – upper sandstone member
V€tr	Tornetrask Formation – red and green siltstone member
V€tl	Tornetrask Formation – lower sandstone member
p€gg	Grunfjell granite
p€ga	Grunfjell amphibolite
p€gs	Grunfjell metasediment
p€sr	Singis rhyolite